FLUORESCENT CARBON DOTS AND CARBON NANO-ONIONS:

SYNTHESIS AND MULTIFUNCTIONAL APPLICATION

Submitted by

ANSHU BHATI
(ID.No. 2013RCY9573)

DEPARTMENT OF CHEMISTRY

MALAVIYA NATIONAL INSTITUTE OF TECHNOLOGY

JAIPUR – 302017 (INDIA)

APRIL, 2019

FLUORESCENT CARBON DOTS AND CARBON NANO-ONIONS:

SYNTHESIS AND MULTIFUNCTIONAL APPLICATION

Submitted in

fulfillment of the requirements for the degree of

Doctor of Philosophy
in
Chemistry

By

ANSHU BHATI
(ID.No. 2013RCY9573)

Under the supervision of

DR. SUMIT KUMAR SONKAR
Assistant Professor

DEPARTMENT OF CHEMISTRY

MALAVIYA NATIONAL INSTITUTE OF TECHNOLOGY

JAIPUR – 302017 (INDIA)

APRIL, 2019

MALAVIYA NATIONAL INSTITUTE OF TECHNOLOGY, JAIPUR

Candidate's Declaration

I, **Anshu Bhati,** declare that this thesis titled **"FLUORESCENT CARBON DOTS AND CARBON NANO-ONIONS: SYNTHESIS AND MULTIFUNCTIONAL APPLICATION"** and the work presented in it, are my own. I confirm that:

- This work was done wholly or mainly while in candidature for a research degree at this university.

- Where any part of this thesis has previously been submitted for a degree or any other qualification at this university or any other institution, this has been clearly stated.

- Where I have consulted the published work of others, this is always clearly attributed.

- Where I have quoted from the work of others, the source is always given. With the exception of such quotations, this thesis is entirely my own work.

- I have acknowledged all main sources of help.

- Where the thesis is based on work done by myself, jointly with others, I have made clear exactly what was done by others and what I have contributed myself.

Date: **Anshu Bhati**
                                                                                         ID No. 2013RCY9573
                                                                              Department of Chemistry
                                                                                          MNIT, Jaipur

MALAVIYA NATIONAL INSTITUTE OF TECHNOLOGY, JAIPUR

Supervisor's Certificate

This is to certify that the thesis entitled "**FLUORESCENT CARBON DOTS AND CARBON NANO-ONIONS: SYNTHESIS AND MULTIFUNCTIONAL APPLICATION**" is a bonafide research work carried out under my supervision and guidance in fulfillment of the requirement for the award of the degree of **Doctor of Philosophy** in the Department of CHEMISTRY and Malaviya National Institute of Technology, Jaipur, India. The matter embodied in this thesis is original and has not been submitted to any other University or Institute for the award of any other degree.

Date:

Dr. Sumit Kumar Sonkar
Assistant Professor
Department of Chemistry
MNIT Jaipur

ACKNOWLEDGEMENT

The research work presented in this thesis would not have been possible without the contributions of my close subordinates who always supported me when I needed them the most. I extend my appreciation and devout gratitude to many persons who have helped me throughout the research work and assisted me in accomplishment of this doctoral thesis.

*First and foremost, I would like to express my deep and utmost gratitude to my research supervisor, **Dr. Sumit Kumar Sonkar**, Assistant Professor, MNIT Jaipur for, giving me the opportunity to join as his group as a Ph.D. student, I am greatful for his sincere and selfless support, prompt and useful advice during my research. A person with an amicable, and positive temperament, Sir has always made himself available to clarify my doubts despite his busy schedules and I consider it as a great opportunity to do my doctoral programme under his guidance and to learn from his research expertise. I am very glad and thankful to him for showing constant enthusiasm, patience and positive outlook for research which was always contagious and motivational for me, even during the tough times. His guidance helped me in all the time of research and writing of this thesis. I could not have imagined having a better advisor and mentor for my Ph.D study. I like to thank him for encouraging and giving me freedom of thought during my research and allowing me to grow as an individual.*

*It gives me immense pleasure in acknowledging **Prof. Udaykumar R. Yaragatti**, Director, MNIT Jaipur, for providing necessary laboratory facilities. I am highly grateful to **Dr. Ragini Gupta**, Head of the department, DREC members **Dr. Jyoti Joshi**, **Dr. Rajkumar Joshi** and **Dr. Sumanta Kumar Meher** for their insightful comments and encouragement, but also for the hard question which incented me to widen my research from various perspectives. I express my warm thanks to **Dr. Biman Bandyopadhyay**, **Dr. Pradeep Kumar**, **Dr. Mukesh Jain**, **Dr. Sandeep Chaudhary**, **Dr. Abbas Raja Naziruddin**, and **Dr. Sudhir Kashyap**. I whole-heartedly grateful to **Dr. Sabyasachi Sarkar** and **Dr. Kumud Malika Tripathi** for their valuable suggestions and discussions related to my work. I*

Abstract

A cost effective, facile synthetic methodology for the fabrication of doped carbon dots (CD) and water soluble carbon nano-onions (wsCNO) were described in this thesis. A blue fluorescent nitrogen, phosphorous doped CD were synthesized by microwave charring of imidazole, phosphoric acid and poly ethylene glycol and used them as an efficient photocatalyst material for the reduction of toxic of Cr(VI) into Cr(III) under Sunlight irradiation. For using the red or near infrared fluorescent material as photocatalyst a red fluorescent self-doped CD were synthesized by the microwave charring of *Bougainvillea* leaves extract further a red emitting zinc doped CD were also synthesized by the doping of zinc acetate into the *Bougainvillea* leaves extract to enhance the photoluminescence properties of doped CD. These red fluorescent CD show excitation independent emission in the red region and used as photocatalyst for the degradation of pollutant dye and reduction of toxic metal ions, respectively under the presence of sunlight. wsCNO were synthesized by the traditional pyrolysis of vegetable ghee and pyrolysis of wood wool followed by the acid treatment. The high density surface passivated wsCNO were used as a fluorescent imaging and sensing probe. The wsCNO were also used as fertilizer and the effect of metallic micronutrient concentration, protein content, conductivity, overall dimension on the first generation seeds obtained by the wsCNO treatment were studied.

TABLE OF CONTENTS

ANNEXURE I

LIST OF ABBREVIATIONS

Abbreviated Form	Extended Form
AAS	Atomic Absorption Spectroscopy
AFM	Atomic Force Microscopy
ANOVA	Analysis of Variance
Al	Aluminium
As	Arsenic
B	Boron
Ba	Barium
CD	Carbon Dots
CND	Carbon Nanodiamonds
CNT	Carbon nanotubes
CNP	Carbon nano-particles
CO_2	Carbon di oxide
CSCNT	Cup stacked Carbon Nano Tubes
C. elegans	*Caenorhabditis elegans*
C.aeritinum	*Cicer aeritinum*
CVD	Chemical Vapor Deposition
CdSe	Cadmium Selenide
Cr	Chromium
Cu	Copper
CV	Cyclic Voltammetry
1,4-DHP	1,4-Dihydro-2,6-Dimethylpyridine-3,5-Dicarboxylate
DRS	Diffuses Reflectance Spectroscopy
DPC	Di-Phenyl Carbazide
DMSO	Dimethyl sulphoxide
DI	Deionized water
D_2O	Deuterium Oxide

Abbreviated Form	Extended Form
Na$_2$-EDTA	Disodium Ethylene Diaminetetraacetate
E. coli	*Escherichia coli*
FESEM	Field Emission Scanning Electronic Microscopy
FGS	First Generation Seeds
FNC	Fluorescent Nano-CarbonsDM
FRET	Fluorescence Resonance Energy Transfer
FT-IR	Fourier Transform Infrared
Ge	Germanium
Gd	Gadolinium
GO	Graphene oxide
GQD	Graphene Quantum Dots
HeLa	Human Cervical Cancer Cell Line
HRSEM	High Resolution Scanning Electron Microscopy
h$^+$	Holes
^{1}H NMR	Proton Nuclear Magnetic Resonance Spectroscopy
HRTEM	High-Resolution Transmission Electronic Microscopy
•OH	Hydroxyl Radicals
H$_2$O$_2$	Hydrogen peroxide
Fe	Iron
ICP-MS	Inductively Coupled Plasma Mass spectrometry
Pb	Lead
LOD	Limit of Detection
Li	Lithium
Mg	Magnesium
MRI	Magnetic resonance imaging
Hg	Mercury
MB	Methylene Blue
Mo	Molybdenum

Abbreviated Form	Extended Form
Mn	Manganese
MWCNT	Multiwalled carbon nanotubes
ND	Nano-diamond
NB	Nile Blue
N-CD	N-doped CD
NIR	Near-Infra Red
Ni	Nickel
HNO_3	Nitric Acid
N	Nitrogen
NP-CD	Nitrogen-Phosphorous Doped Carbon Dots
r-Mg-N-CD	Red-Emitting Magnesium-Nitrogen-Embedded Carbon Dots
Rpm	Resolution per minute
$K_2Cr_2O_7$	Potassium Dichromate
p-BZQ	Para-Benzoquinone
Ppm	Part per million
P	Phosphorous+
H_3PO_4	Phosphoric acid
P-CD	Phosphorous Doped CD
PL	Photoluminescence
H^+	Proton
PEG	Poly ethylene glycol
p-XRD	Powder X-ray Diffraction
P.putida	*Pseudomonas putida*
QD	Quantum Dots
QY	Quantum Yield
S	Sulfur
Se	Selenium
Si	Silicon

Abbreviated Form	Extended Form
Ag	Silver
Na	Sodium
SD	Standard Deviation
SAED	Selected Area Energy Diffraction
(±SE)	Standard Error
O_2^-	Superoxide
SWCNT	Single Walled Carbon Nanotubes
Tb	Terbium
t-BA	Tertiary Butyl Alcohol
TiO_2	Titanium dioxide
TEM	Transmission Electronic Microscopy
TGA	Thermo gravimetric Analysis
UCPL	Up-Conversion Photoluminescence
UV-Vis	Ultra-Violet Visible Spectroscopy
wsCNO	Water Soluble Carbon Nano-Onions
wsCNT	Water Soluble Carbon Nanotubes
XPS	X-Ray Photoelectron Spectroscopy
Zn	Zinc
ZnO	Zinc Oxide
ZnS	Zinc Sulfide
Z	Zeta potential in mV
C_{ZnO}-Dots	Zinc Oxide Doped Carbon Dots
eV	Electron volt
Δ	Chemical Shift in Parts Per Million
υ	Wavenumber
Λ	Wavelength

Chapter -1

Introduction

1.1   Introduction

In the past few years, fluorescent nano-carbons (FNC) [1-11], comprising carbon dots (CD) [3, 7, 10, 12], carbon nano-diamonds (CND) [9], carbon nano-onions (CNO) [2, 4, 8, 11, 13], and graphene quantum dots (GQD) [5, 6], have drawn immense interest, particularly for biological cell imaging [3, 10, 14-16] with several benefits in comparison with conventional metal-based quantum dots (QD) [17-19]. In terms of bio-compatibility (non-toxic nature) [3, 10, 20, 21], their high values of quantum yield (QY) [10, 16, 22], combined with their excellent solubility and stability [3, 7, 10], make these an effective fluorescent probe for long-term use for biological purposes [3, 10]. FNC are mostly composed of spherical nano-carbon possessing a high surface area to volume ratio, and have further been utilized for surface passivation purposes via simple surface modification (attaching surface functionalities). Surface modification is mainly achieved via the simple organic chemistry of oxidation, followed by the addition of polymeric [12, 14] and monomeric amines [23] to achieve high QY values, comparable with those of conventional metal based QD [17-19]. Metal-based QD show classical quantum confinement effects in their size-dependent multi-colored emission. Theoretically, in comparison with QD, FNC do not have any defined band gap for fluorescence emission [23] and this is an advantageous property for multi-colored emission from the same nano-carbon [4, 13, 24]. Till now, among the FNC, CD are the widely used nano-carbon because of their simpler synthetic methodologies with easy reproducibility, and the CNO are least explored because of its complicated synthetic procedures. The present thesis has been related to the wet uses of the CD (doped-CD) and CNO. Thus the introduction section have been further divided into two sections; as section (A) covers the synthesis and application of the doped-CD and the section (B) describes the synthesis and application of CNO.

SECTION A

1.2   Carbon Dots

The first report of CD came in year 2006 synthesized from laser ablation of a graphitic target [7]. The as synthesised CD show apparently no fluorescence but when surface passivation of acid treated CD was done with the aminopolyethylene (poly(ethylene glycol), PEG_{1500N}, these surface functionalized CD were excited with increment wavelength they show blue to red shifting in emission as shown in Figure 1.1 [7]. The QY value of CD reached up to the ~ 47% over the separation of the most fluorescent fraction from the as produced CD [25].
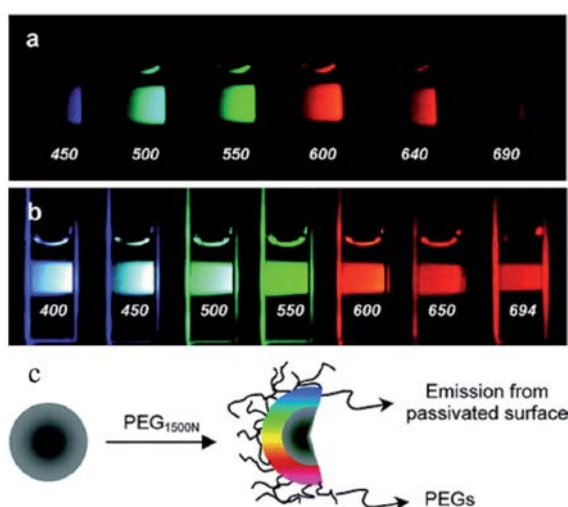
Figure 1.1: Aqueous solution of the functionalized, CD-PEG_{1500N} at different excitation wavelength, as indicated (a) photographic image under different band pass filter; (b) direct photographic image and (c) Schematic representation of surface passivation of CD with PEG_{1500N} [7].

Till now, many top-down and bottom-up synthetic techniques have been explored [26-30] for the easier production of CD. Especially, the cost-effective green synthesis using bio-mass/waste bio-mass as a low cost, compatible and easily available carbon precursor material are in high demand. Low cost carbon precursor includes, the ascorbic acid [31], banana juice [32], candle soot [33], chicken eggs [34], citrate [35], chitosan [36], diesel soot [37], gelatin [38], glucosamine [39], saccharides [40], juices (orange, sugar cane, lemon and strawberry) [41-44], pomelo, and watermelon peel [45, 46]. As synthesized, CD and their functionalized versions have shown immense potential for a wide variety of applications, such as

bio-imaging agents [15, 47], biosensors [27, 30], chemical sensors [48], drug delivery [49], electro-catalysts [50], photocatalyst [29] and photodynamic therapy [51]. Biocompatibility and low-cost synthetic protocols with ease in reproducibility and bio-compatibility make these CD best suited for imaging purposes [3, 10, 14, 15, 47]. It has been widely accepted that the presence of high density surficial defects (defective centers) on FNC is responsible for their tunable multi-colored emission profiles [16]. Emission from the defective centers of surficial defects was first noticed from the single-walled carbon nanotubes (SWCNT) and multi-walled carbon nanotubes (MWCNT) passivated with polymeric amines. The exact mechanism of the tunable PL is still debatable, but the most accepted theory is in the support of generation of electrons and their recombination with the holes as the electron-hole recombination processes. Presently, the two important theories related to mechanism are quantum confinement effect (different size) and the surficial defects generated either by surface functionalization or by doping [52]. As per the general understanding and the literature review, PL properties of CD were strongly affected by the method of synthesis, carbon precursor taken, defects on surface, surface functionalization, on the nature and the percentage of dopant [28, 52].

1.3   Doped-CD

The intrinsic optical properties of CD can be tuned/modulated via the process of doping by heteroatoms (N, S, P and B) with single and co-doping like N-P, N-S, N-B and Mg/N doping [53-60] by taking different carbon and heteroatom precursor. Along with these, the metal doping of Ge, Gd, Si, Se, Tb and Zn were also reported by using their salts [61-64] with the expectations to show some other prominent applications in addition to its conventional ones.

1.3.1   Nitrogen Doping

Nitrogen (N) is a n-type dopant with five valence electrons with the size comparable to C and enhances the optical properties of CD by serving its excess electrons with an upward shifting in fermi level of energy. Studies showed that the limited doping of N, shows the emission in the blue region. The increase in the contents of N-doping shift the emission of CD towards the longer wavelength region, which may be due to the decreasing band gap or the shifting of absorption

towards longer wavelength due to insertion of more non-bonding electrons [52]. A wide range of application was performed by these doped N-CD such as biochemical sensing, photocatalysis, bioimaging, bio-probes and optoelectronic devices [29, 52, 65]. For the fabrication of N-CD, N containing compound were taken as a precursor. Zhang *et al.* reported the N-CD via a solvothermal method using CCl_4 and $NaNH_2$ as a precursor [66] and reported the enhancement of the PL property by tuning the N content. Xu *et al.* also reported the enhancing of PL properties, due to the formation of the new emissive trap on the surface of N-CD by introducing bonding disorder on the hexagonal rings [67]. Ma *et al.* reported a facile synthesis of the highly fluorescent N-CD by the ultra-sonication method using ammonium hydroxide and glucose as a precursor [68]. N-CD show higher photocatalytic efficiency for the degradation of methyl orange and visible light irradiation than non-doped CD. Hydrothermal synthesis of N-CD by taking folic acid as a precursor was reported by the Chen & co-workers [69]. The N-CD show an efficient and selective fluorescent "turn off" sensing of Hg(II) with the detection limit of 0.23mM. Further many green synthesis of N-CD have also been reported like synthesis by grass [70] and pomelo peels [46]. There are few reports also available, stating that by increasing the N content and change in solvent, red emitting N-CD can be synthesized. Sun *et al.* synthesized red emitting N-CD by mixing citric acid and formamide in a microwave reactor for the 1 h at 400 W with a QY of 22.9% [71]. The N-CD showed excitation independent emission at 640 nm, which were used in the bio-imaging and drug delivery. Jiang *et al.* reported the solvothermal synthesis of the red-emitting CD by mixing of p-phenylenediamine in ethanol with QY of 26.1% and used them in imaging [72]. A direct heating at 180°C of citric acid mixed in polyethylenimine and ethylene glycol resulted into formation of CD emitting at 710 nm were reported by Hu *et al.* [73] Some green synthetic precursor were also used for the formation of red emitting N-Doped CD such as by taking the hydrothermal treatment of the pulp free lemon juice in ethanol solution resulted into the red emission at 631 nm of CD (QY 28%) [74].

1.3.2 Phosphorous Doping

Another n-type dopant which has been frequently used to fabricate doped-CD is the Phosphorous (P) from the same group of N. Its size is bigger than C atoms so it produces substitutional defects in the carbon mass and serves as an n-type donor. The research related to the doping of P by taking the precursors having the P, like phosphoric acid [75], triphenylphosphine [76], monosodium phosphate [54], and phosphorous tribromide [77]. The increase in PL properties can be ascribed as concomitance of the isolated sp^2 cluster with the defect sites increase the band gap and show enhanced fluorescence compared to a single cluster. They also suggested that while increasing the P content due to insertion of P into the sp^2 cluster, the isolation enhanced which ultimately result in the enhancement of the fluorescence.

1.3.3 Boron Doping

Unlike the N and P, Boron (B) is an electron deficient element with three valence electrons, so act as a p-type carrier as a dopant, so introducing the B into carbon frame work has also been used to tune the optical and electronic properties. Shan *et al.* reported a facile one pot solvothermal synthesis of B-doped CD taking BBr_3 as B source and hydroquinone as C source [56]. The blue fluorescent B-doped CD show a higher QY of 14.8% than that of non-doped CD (3.4%). The enhanced fluorescence may be attributed to the strong electron withdrawing nature of B (an e$^-$ deficient atom). Sadhanala *et al.* synthesized B-doped CD via a simple hydrothermal route taking boric acid and sucrose as precursor [78]. They reported the increased QY value from 0.5 to 2% after doping.

1.3.4. Doping with more than one element as a dopant

Along with the doping with single element some researchers used the doping of more than one elements as a dopant to explore its multiple applications. Han *et al.* synthesized single doped (B, N, P, S) and multiple element doped-CD (B & N, N & P, N & S) by the flame combustion technique using boric acid (for B), pyrrole (for N), tri-phenyl phosphine (for P) and tert. dodecylmercaptan (for S) precursor [76]. They found that B, N doped-CD shows highest catalytic activity towards oxygen reduction reaction among the all other doped-CD. Gong *et al.* synthesized N, P doped-CD by acidic oxidation of pumpkin by phosphoric acid [59]. A green

fluorescent N, P doped-CD show excitation-dependent emission with QY value of 9.42%. A large stoke shift (125 nm) was observed in N, P-doped CD with good reversibility and the effect of auto-fluorescence also be avoided in biological system. N, P doped-CD of QY 23.5% were synthesized by hydrothermal treatment of adenosine-5-triphosphate [79]. The synthesized N, P doped-CD show high biocompatibility, wide response range, rapid response time and high sensitivity, these all properties makes these N, P doped-CD an efficient probe for the in vivo sensing of reactive N and O species and for the bioimaging. Xu *et al.* hydrothermally synthesized N, P doped-CD by using diammonium phosphate and sodium citrate and used these in the Hg(II) sensing [80]. Gong *et al.* reported the synthesis of N, P doped-CD by simple heating taking the glucose, ethylene diamine and concentrated phosphoric acid as a precursor and used them in bioimaging and nano-carrier of anticancer drug doxorubicin. Li *et al.* synthesized N, P doped-CD by microwave using N-phosphonomethyl aminodiacetic acid and ethylenediamine and used them in imaging purpose [81]. Chandra *et al.* reported the hydrothermal synthesis of N, P doped-CD by taking di-ammonium hydrogen phosphate and citric acid as precursor and applied them as intercellular Fe(III) sensor and also in imaging purpose [82] based on the above reports it might be stated that the optical properties of CD were significantly affected by the synergic effect of dopant elements.

1.3.5   Metal Doping

In addition to above discussed elements from the P-block, metals even also also been used as dopant such as Ge, Gd, Se, Si, Tb, Zn etc. for changing the electrochemical, and optical properties of CD [61-64, 83]. Ge-doped CD were developed using bis-(2-carboxyethylgermanium(IV)sesquioxide) and citric acid precursor via a carbonization at 200°C for 15 min. [61]. The Ge-doped CD shows excitation independent blue emission with good photostability, high biocompatibility, high intracellular delivery efficiency and stability and were used for the Hg(II) sensing. Bourlinos *et al.* synthesized Gd-doped CD via a simple pyrolysis at 200°C in presence of oxygen by taking tris (hydroxymethyl) aminomethane mixed with gadopentetic acid and betaine hydrochloride [84] and being used for the medical purpose mainly in MRI. In another report Gong *et al.* fabricated Gd-doped CD by a

microwave assisted method using gadolinium(III) oxide sucrose [85]. The synthesized green emitting Gd-doped CD with QY 3.4% also show a good T1 contrast image for MRI. When CNP were first oxidized and then reduced by the NaHSe in a hydrothermal, the yellow emitted Se-doped CD were synthesized.[63] Qian *et al.* synthesized Si doped-CD using silicon tetrachloride and hydroquinone by a solvothermal process with QY of 19.2% [63]. The Si-doped-CD were used for multifunctional sensing of Fe(III), H_2O_2 and melamine. A blue emitting Tb-doped CD were also synthesized by taking a mixture of terbium(III)nitrate and citric acid and heated up to 190°C[62] and were used for the selective sensing of 2,4,6-trinitrophenol. A yellow fluorescent Zn-doped CD was reported via a solvothermal route by mixing citric acid and zinc chloride in toluene and used them in multifunctional application [86]. Similarly, Sun *et al.* reported the ZnO-doped and ZnS-doped CD as shown in Figure 1.2 [22]. Anilkumar *et al.* reported a high QY of ~78% for the ZnS doped CD and 70% for the TiO_2 doped CD by separating the most fluorescent fraction from the bulk [87].
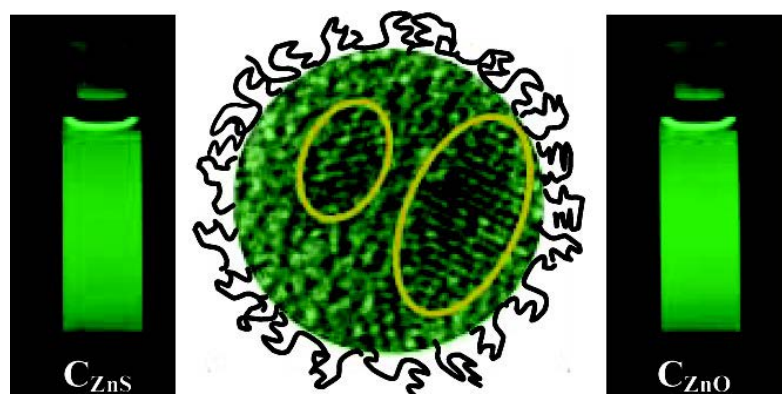
Figure 1.2: Schematic representation of metal doping in the Carbon core and photographic image of aqueous solution of C_{ZnS} and C_{ZnO} dots under 450 nm excitation [22].

1.4   Application of CD

1.4.1   Bioimaging application of CD

Sun *et al.* in their study showed the potential bio-imaging prospects of CD on unicellular (prokaryotic, primitive type cells) *Escherichia coli (E.coli)* cells and on human Caco-2 cells[7] by showing internalization of these CD in the model organism. The internalized CD (passivated with polyamines) was further sustained

by MCF-7 cells (human breast cancer cells) and was studied by two-photon luminescence microscopy [14] Regarding the *in vivo* biocompatibility of CD compared with commercially supplied CdSe/ZnS QD on mice was performed by Yang *et al.*, and showed the non-toxic and competitive fluorescence imaging performance of CD with commercially supplied CdSe/ZnS QD [16]. CD were intravenously injected into mice for whole-body circulation. Results suggest that the intravenously injected CD were primarily excreted via urine, an excretion pathway has been reported for PEGylated nanoparticles, especially for very small particles like the ones used here. Tao *et al.* synthesized CD with diameter of 3-4 nm from the mixed acid treatment of the SWCNT/MWCNT/graphite [88]. The yellow light emitting CD showed excitation dependent emission up to NIR region. They used CD as *in vivo* imaging probe in mice and this CD exhibit non-toxicity towards the mice. The *in vivo* imaging inside the mice by CD were shown in Figure 1.3.
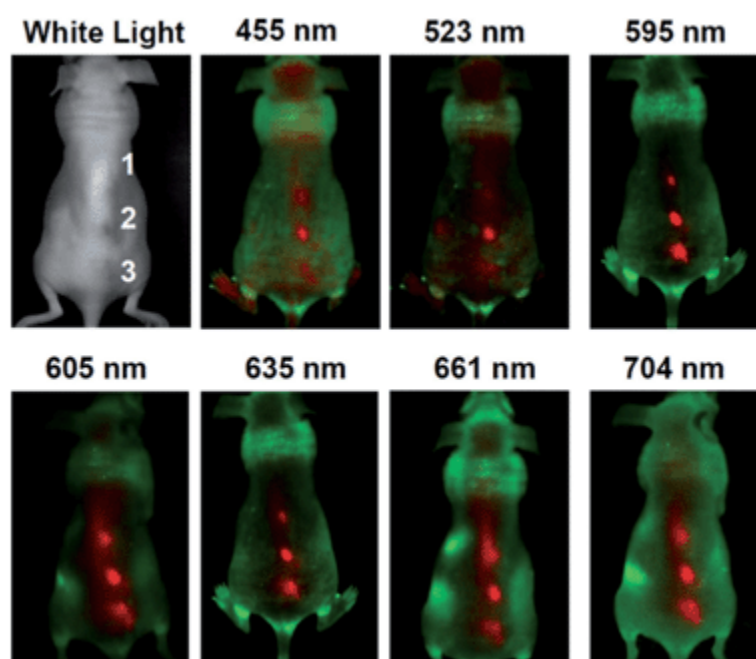
Figure 1.3: *In vivo* fluorescence imaging of CD injected into mice upon excitation at different wavelength, red fluorescence show the presence of CD while green was the auto fluorescence [88].

The functionalized CD can be used in the drug delivery and diagnosis of diseases due to its high biocompatibility and water solubility. Li *et al.* reported the targeting of cancer cells by the functionalization of CD with transferrin (a

glycoprotein) CD [89]. They claimed that this modified CD were largely entered into the human cervical cell lines (HeLa cells) [89]. The imaging effect was more pronounced for modified CD than unmodified CD.

1.4.2 Sensing application of CD

With their enormous properties CD were used as an efficient biosensor for the detection of phosphate, glucose, cholesterol, metal ions, pH and DNA in, enzymes, proteins, cells and even in pathogenic bacteria [26, 27, 52, 90]. Moreover, apart from sensing of biomolecules and heavy metal ions few reports are also available for anions detection like fluoride with a better detection limit [52]. Most of the nano-carbon PL sensors are based on fluorescence turn-off and quenching mechanism is still not clearly elucidated. Shen *et al.* reported a non-enzymatic blood glucose sensor using boronic acid functionalized CD via a fluorescence turn off mechanism [91]. The author reported the mechanism of sensing based on the quenching of fluorescence by the interaction of cis-diol group of glucose molecule with the boronic acid present on the surface of CD with detection limit of 1.5mM. They also checked the detection of glucose inside human serum. Tripathi *et al.* isolated CD from the diesel exhaust soot and further the acid functionalized CD, were used for the fluorescence "turn-off-on" cholesterol sensing [92]. The sensing mechanism was explained on the basis of interaction between MB, CD and cholesterol. Initially, MB interacted with CD which led to the quenching of fluorescence emission. When cholesterol molecules comes in the proximity of the CD-MB, the MB molecules immediately react with cholesterol molecules and thus resulted fluorescence "turn on" as shown in Figure 1.4. Since, the doping is recognized to enhance the PL property so doped-CD were also widely used in the fluorescence sensing of heavy metal ion such as Fe(III), Hg(II), Pb(II), Cr(VI), Ag(I), Cu(II) and Zn(II) with a good detection limit. Doped-CD were also used as a fluorescence detector of DMSO, H_2O_2, glucose molecule, dopamine, catechol, amoxicillin, pyridine, micro RNA, temperature and pH [93].
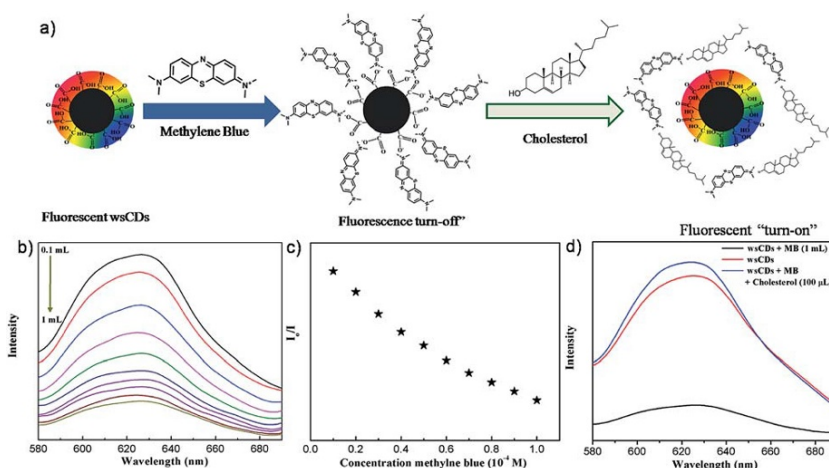
Figure 1.4: (a) Schematic illustration for the mechanism of fluorescence "turn-off-on" based detection of cholesterol via interaction of CD with MB and cholesterol molecules, respectively; (b) fluorescence spectra showing quenching on stepwise addition of 0.1 mL aqueous solutions of MB; (c) a relationship between I_o/I and MB concentration; (d) fluorescence "turn on" on adding cholesterol due to removal of surficial MB molecules from the wsCD [92].

1.4.3 Photocatalytic removal of pollutant from waste water by CD

With the development of textile industries and urbanization contamination of wastewater with toxic organic dyes and heavy metal ions are common causing environmental damage. Organic dyes are acutely toxic, highly stable towards biodegradation and cause extensive concerns to the environment and human health due to mutagenic and genotoxic nature. Various remarkable milestone have been already established for the remediation of wastewater with photocatalysis technique due to its high efficiency and sustainability. Photocatalysis is the acceleration of photo-induced reactions with catalyst. These catalyst accelerate the light adsorption due to their characteristic physiochemical properties and thus retarded the recombination of photo-induced e^- and their corresponding h^+, these e^- and h^+ either directly or by producing some radicals accelerated the photoreaction. Recently, the use of infinite source of light, Sunlight as a source in a photocatalytic reaction makes photocatalysis more sustainable and closer to routine application. An ideal photocatalyst is that which is able to use the complete UV-Vis-NIR range of spectrum. Still a photocatalyst which utilizes the whole red/NIR/IR spectrum of light are needed to be discovered [29, 65].
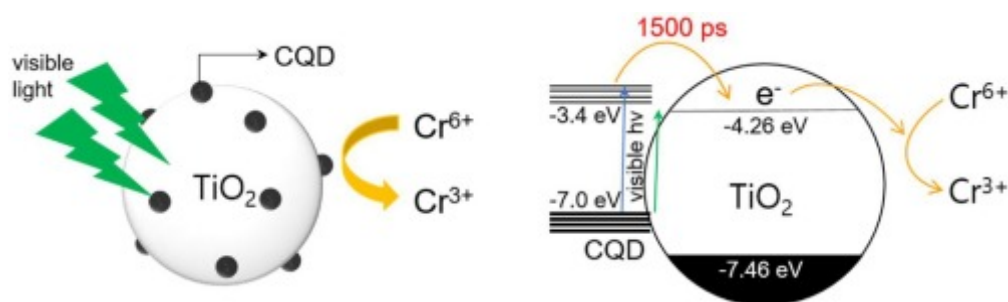
Figure 1.5: Schematic representation for the mechanism photocatalytic reduction of Cr(VI) under the visible light irradiation by CQD -TiO$_2$ nanocomposites [94].

For the enhancement in the photocatalytic ability insertion of hetero atom tunes the electronic structure of CD. N-CD were reported as a photocatalyst for the degradation of methyl orange (MO) under visible light irradiation [68]. They reported that enhanced photocatalytic ability of N-CD was due to higher capacitance of N-CD which formed by insertion of N electrons and thus the electronic structure of N-CD were changed. These changes enhance binding with ions and capacitance of N-CD. Wu *et al*. synthesized Cu-N-doped CD and used them as efficient photocatalyst for oxidation of 1,4-DHP [95]. They also reported that the doping increases the photocatalytic efficiency 3.5 times higher than the undoped-CD due to increase e$^-$ accepting and donating ability of CD by insertion of Cu-N into CD. Choi *et al.* reported a facile synthesis of CD-TiO$_2$ composites for the effective photoreduction of toxic Cr(VI) under visible light irradiation [94]. The transfer of photo-induced e$^-$ from CD to TiO$_2$ nanoparticles with a time of 1500ps and the overall mechanism for photoreduction is shown in Figure 1.5. The composites show 8.6 times higher photoreduction ability than TiO$_2$ nanoparticles. CD-Si hybrid nanoparticles were also reported for the photocatalytic reduction of Cr(VI) under visible light irradiation [96].

The thesis describes a facile, cost effective and simple methodology for the synthesis of doped-CD. Blue and red light emitting doped-CD were synthesized and used as an efficient photocatalyst for the aqueous phase reduction of toxic metal ion Cr(VI) into Cr(III) and the photodegradation of pollutant organic dye as MB.

SECTION B

1.5   Carbon Nano-onions (CNO)

CNO, were discovered in 1992 by Ugarte as a new carbon nanomaterials while transforming the fullerene to CNT, and named these graphitic multi-shelled as CNO [97]. The formation of CNO was observed during the (Transmission electron microscopy) TEM analysis, where Ugarte found that when high energy electron beam (10 times more intense than usually used) irradiated on the carbon soot there is formation of a concentric graphitic shell. The formation of a concentric graphitic shells was explained as the high radiation beam was irradiated on the carbon soot, to minimize the strain hexagonal lattice added some pentagon and to remove the dangling bonds they become curled as the high beam radiations provided the structural fluidity (more the curvature more the pentagons). The HRTEM and structures of CNO shown in Figure 1.6 [98].
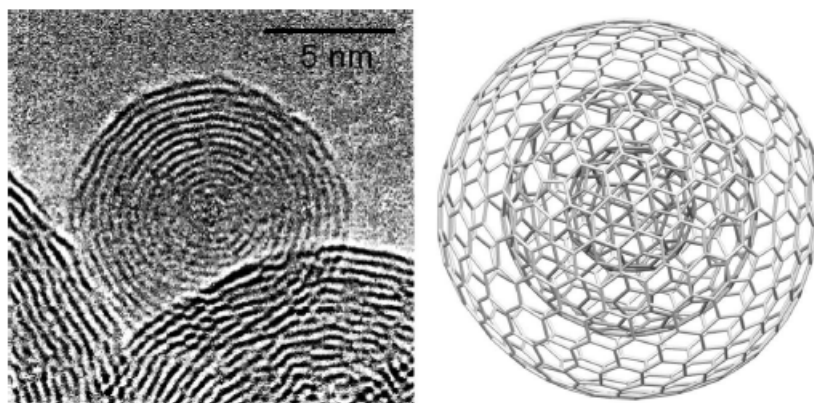
Figure 1.6: HRTEM image (left) and structure (right) of CNO [98].

Presently CNO are an emerging class of quasi spherical nano-carbon, which typically consists of successive layer of graphene around a filled or hollow core and they offer a high aspect ratio and conductivity [8]. Morphologically, graphitic structures of CNO are in between fullerene and graphitic nanotubes having closed graphitic shells which are placed on one on another [4, 99, 100]. So far, less attention have been given to CNO even though the prospective applications have already discussed. CNO exhibited the characteristic, onion-like morphology and small domains of graphitic sp^2 carbons with localization of the p orbital electrons and dangling bond defects in the periphery [8]. As a consequence, it could be envisioned as an enclosed graphitic shell with excellent optical and electrochemical

properties that render them a potential nanomaterial for industrial, biomedical and electronic applications [8, 101-103]. From the time of their discovery [97] until the present date, only a limited number of synthetic methods for CNO have been available and it can be synthesized mainly by using high energy techniques. Such as the arc-discharge method, in which two graphite electrodes are arced under water for the synthesis of CNO on the water surface [99]. Annealing of nano-diamond for 1.5 h at a temperature range of $500–1400^0$ C under vacuum[104] and electron transfer in a nano-diamond at 200 keV has also been used [105]. Another method is the thermal reduction of glycerine and magnesium at 650^oC for 12 h in an autoclave [106]. CVD has also been used and involves methane and depositing CNO on a silicon surface [107]. Hou *et al.* used the catalytic synthetic method by using nickel as a catalyst in the counter flow diffusion of flames of ethylene, methane and nitrogen [108]. Han *et al.* reported the thermal treatment of copper(II) chloride dihydrate and calcium carbide in an autoclave at 600^oC for 10 h for synthesis of CNO[109] and via the flame pyrolysis of naphthalene [110]. Besides this, a very easy and cost effective method was also reported using the pyrolysis technique over waste wood known as "wood wool" [4,13,101]. Among all the reported methods, annealing of nano-diamond and arc discharge has been the most commonly used methods until now. So far CNO have shown significant potential in the field of lithium ion batteries [109] as supercapacitor electrodes [100], capacitors [111], optical limiters [112], catalysis, [113,114] sensing [28], tribology [115,116], fuel cells [117], and terahertz shielding [118].

1.6   Application of CNO

1.6.1   Bioimaging application of CNO

The lesser exploration of CNO in biological science could be due to its typical synthesis process and non-solubility in the aqueous medium. Recently, Ghosh *et al.* documented an excellent report on the novel optical bioimaging technique by the water-soluble version of CNO as wsCNO. Like CD, wsCNO passivated with the heavy extent of the carboxylic group makes them glowed throughout the visible domain making wsCNO as another alternative of bio-imaging. The oral ingestion of non-toxic fluorescent probe of wsCNO are capable of imaging the full life cycle of alive *Drosophila melongator* (commonly known as

fruit flies) from its egg stage to adulthood even at the concentration of 4 ppm solution. They synthesized the wsCNO by the pyrolysis of the waste product commonly known as wood wool with the aim to control the low cost of the fluorescent probe. In contrast to costly, time-consuming conventionally used techniques such as the real-time X-ray and MRI for biomedical diagnosis, the feeding experiment is as simple as to mix the optimized fluorescent probe with food model which is going to be analysed just like the spoon feeding of a young sapling. Not only will the fruit-fly but some others models also take their food as they did in routine life and start glowing. The most important prospect of this feeding experiment is that fluorescent fruit flies did not show any toxic effects upon withdrawal of the nanoparticles from their food, they excreted the fluorescing material and continued to proliferate to the next generation, demonstrating a return to their normal lives, without causing the loss of life of analysed animal. Figure 1.7 presents the representative images of the life cycle, from egg to complete adulthood of *Drosophila melanogaster* viewed under three different filters and merged multicolour images.
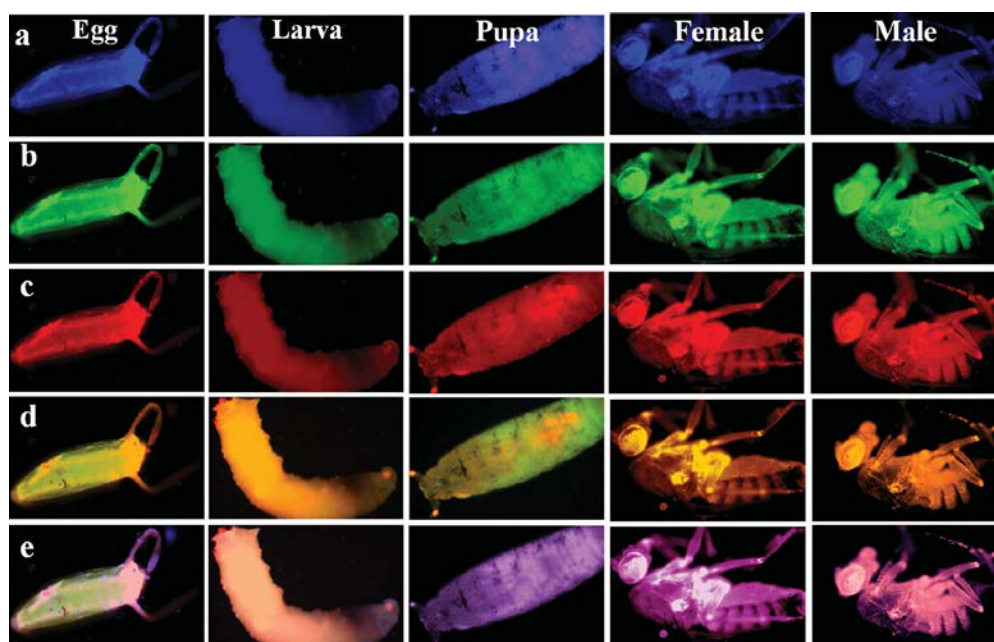
**Figure 1.7:** Different developmental stages of *Drosophila melanogaster* from egg to adult fly under different band-pass filters: (a) 385 nm; (b) 488 nm; (c) 561 nm. (d) Merged image of 488/561 nm band-pass filters; (e) Merged image of 385/488/561 nm band-pass filters. For imaging larval to adult stages, movements of the living objects were controlled by anaesthetization using diethyl ether vapor [13].

Another report from the same group shows the potential high fluorescence prospects in the food web of two different model organisms from an entirely different class. First one is unicellular, *E. coli* (prokaryotic) and the other one is higher multicellular organism (eukaryotic) as *Caenorhabditis elegans* (*C. elegans*). Here also a simple spoon feeding experiment was done, as firstly, wsCNO fed to *E. coli* and *E. coli* cells start glowing throughout the visible domain without showing any toxic effect. Subsequently, the *E. coli* are fed to *C. elegans* and the intestinal duct of these *C. elegans* were analyzed. The results do not reflect any toxic effect of wsCNO on the growth of these organisms suggesting new avenues in nano toxicology research and biomedical application including drug delivery. This non-toxic, fluorescent aspects of wsCNO investigated between two different classes of organisms could be expected a high impact in the field of biological imaging. Giordani *et al*. used pristin-CNO and covalently bind them with boron difluoride azadipyrromethene [2]. This functionalized CNO were used for NIR fluorescence imaging of HeLa Kyoto cells. They also done a comparative study of these functionalized CNO with the similarly functionalized CNT and found that CNO were less toxic and showed efficient cellular uptake compare to CNT. The same group also reported that when CNO were functionalized with highly fluorescent borondipyrromethenes dye, this functionalized CNO can use for the high resolution fluorescence imaging of the MCF-7 human breast cancer cells [119] in both the reports CNO show efficient cellular uptake via the endocytosis with no cytotoxicity. Dubey *et al.* reports a simple gram scale synthesis of CNO via simple pyrolysis of camphor and polystyrene foam and the obtained carbon soot was further soxhlet purified and acid treated to obtain the water solubility and used them for imaging of *E. coli* cells [102].

1.6.2 CNO for sensing of bio-molecules and metal ions

CNO were used sensing of biomolecules and metal ions. Luszczyn *et al*. covalently functionalized CNO with biomolecule and used as a biosensor by avitin–biotin interactions with good biocompatibility [120]. Sensing phenomena done via the surface plasmon resonance spectroscopy and here, CNO work as linking layer between the sensor gold surface and biomolecule. CNO were also used for the heavy

metal detection and serve for environment remediation [121]. Surface oxidized CNO can be work as adsorbent for the different heavy metals like Cd(II), Cu(II), Ni(II), Pb(II) and Zn(II) and show 10 times higher sensing efficiency than the C_{60}. Recently, Tripathi *et al.* synthesized green light emitting CNO from the primitive CVD method by taking flaxseed oil as carbon precursor as shown in Figure 1.8 [11]. They used the wsCNO for the fast sensing of Al(III) ions with a detection limit of 0.27μM even in a high ionic concentration and same were used in the photocatalytic degradation of MB.
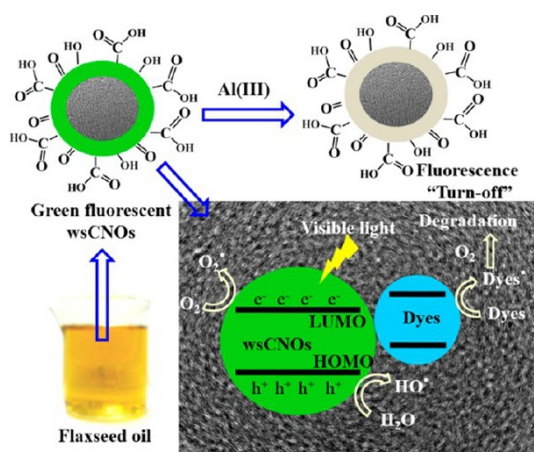
Figure 1.8: A schematic representation of application of CNO in sensing of Al(III) and photodegradation of MB [11].

1.6.3 CNO as the plant growth promoters

Sonkar *et al.* monitored the full life cycle stages from seed to seed with an increase in the overall productivity of gram plants, when treated with wsCNO (obtained from wood waste known as "wood wool") [101]. The 10 days old saplings grown under laboratory conditions were transplanted to natural soil having the standard composition of C and N to complete their entire full cycle as displayed in Figure 1.9a. The positive effects of wsCNO in treated plants were shown in the increased productivity of plants in terms of getting more number of fruits (gram seeds) (Figure 1.9b and c) per plant. wsCNO were found embedded inside the tracheal elements of xylem vessels of treated plants and no such sign of wsCNO presence was observed in control plants as observed by microscopic studies. The overall growth of gram plants was attributed to increased water conduction properties of plants with the transport of micronutrients. Oxidative treatment of

carbon generated by pyrolysis of wood wool caused heavy loss of the graphitic plane. The surface carboxylate groups can directly attach different types of cationic micronutrients via the formation of ion pairs and can smoothly interact with the anionic micronutrient ions via the formation of hydrogen bonds [122, 123]. These negative surfaces act somewhat like a storage house for nutrients, possibly controlling their sustained release. Such interactions boost the facile transport and distribution of the essential micro- and other nutrients inside the xylem[28].
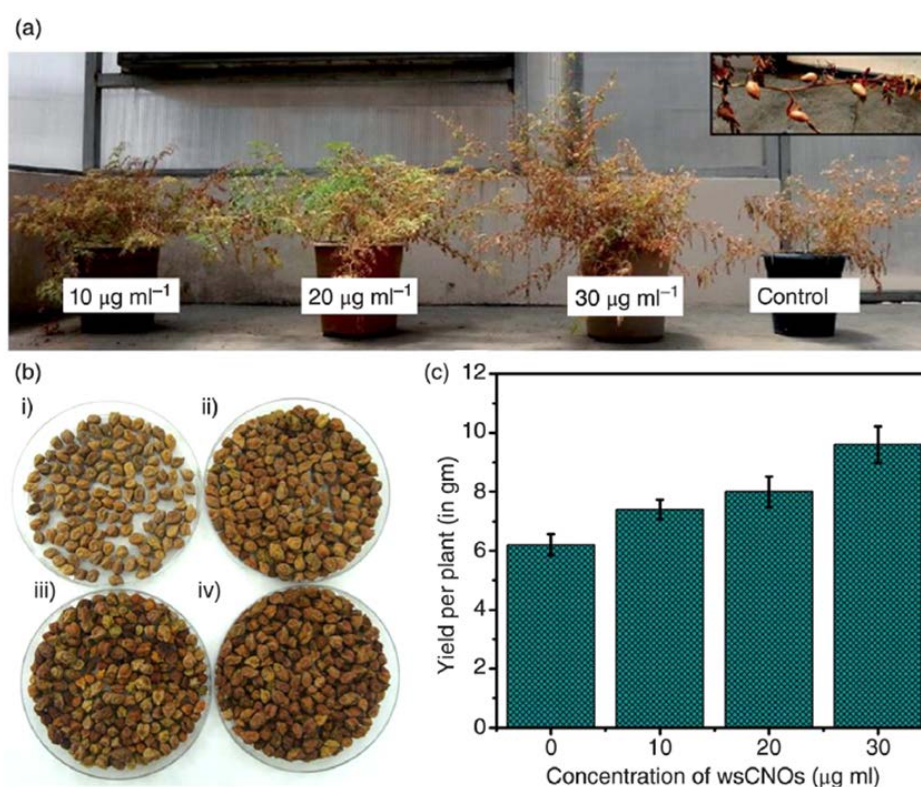
Figure 1.9: (a) Phenotypes of 4 month old treated plants (10, 20, and 30 μg ml^{-1}) in comparison with control, just before harvesting (inset shows image of fruits). (b) Phenotypes of gram seeds (fruits) after harvesting (i) control; (ii-iv) under varying concentrations of wsCNO (0, 10, 20, and 30 μg ml^{-1}), respectively; (c) histogram illustrating weight of fruits per plant [101].

Herein, this thesis described a facile, low cost, simple methodology for the synthesis of CNO from the traditional pyrolysis of vegetable ghee and pyrolysis of wood wool. The as prepared CNO were soxhelet purified and acid treated to obtaining the water solubility. The wsCNO show excitation independent emission covering range upto NIR region. wsCNO were used in imaging, sensing and as a

growth stimulator. The effcet on overall dimensions, yield per plant, protein content, and metallic micronutrient concentration of FGS obtained from the wsCNO treated plant were studied.

1.7   Scope of the work

The present thesis described a simple, low-cost fabrication methodology for the synthesis of the doped-CD and wsCNO and their multifunctional applications. Doped-CD worked as an efficient photocatalyst material for the photoreduction of the toxic metal ion (Cr(VI) to Cr(III)) and the photodegradation of toxic organic dye as MB. wsCNO were used as imaging and sensing probe, as well being used as fertilizer for the gram plants. The newer outcomes, concerning the potential wet applications of doped-CD and wsCNO have been investigated and the results are presented in the subsequent chapters.

1.8   References

1.   Kozák, O., Sudolská, M., Pramanik, G., Cígler, P., Otyepka, M., Zbořil, R., Photoluminescent Carbon Nanostructures. *Chem Mater* **2016,** *28* (12), 4085- 4128.

2.   Giordani, S., Bartelmess, J., Frasconi, M., Biondi, I., Cheung, S., Grossi, M., Wu, D., Echegoyen, L., O'Shea, D. F., Nir Fluorescence Labelled Carbon Nano-Onions: Synthesis, Analysis and Cellular Imaging. *J Mater Chem B* **2014,** *2* (42), 7459-7463.

3.   Luo, P. G., Sahu, S., Yang, S.-T., Sonkar, S. K., Wang, J., Wang, H., LeCroy, G. E., Cao, L., Sun, Y.-P., Carbon "Quantum" Dots for Optical Bioimaging. *J. Mater. Chem. B* **2013,** *1* (16), 2116- 2127.

4.   Sonkar, S. K., Ghosh, M., Roy, M., Begum, A., Sarkar, S., Carbon Nano- Onions as Nontoxic and High-Fluorescence Bioimaging Agent in Food Chain-an in Vivo Study from Unicellular *E. Coli* to Multicellular *C. Elegans*. *Mater Express* **2012,** *2* (2), 105-114.

5.   Shen, J., Zhu, Y., Yang, X., Li, C., Graphene Quantum Dots: Emergent Nanolights for Bioimaging, Sensors, Catalysis and Photovoltaic Devices. *Chem.Commun* **2012,** *48*, 3686-3699.

6.   Kim, S., Hwang, S. W., Kim, M.-K., Shin, D. Y., Shin, D. H., Kim, C. O., Yang, S. B., Park, J. H., Hwang, E., Choi, S.-H., Ko, G., Sim, S., Sone, C., Choi, H. J., Bae, S., Hong, B. H., Anomalous Behaviors of Visible Luminescence from Graphene Quantum Dots: Interplay between Size and Shape. *ACS Nano* **2012,** *6* (9), 8203-8208.

7.   Sun, Y.-P., Zhou, B., Lin, Y., Wang, W., Fernando, K. A. S., Pathak, P., Meziani, M. J., Harruff, B. A., Wang, X., Wang, H., Luo, P. G., Yang, H., Kose, M. E., Chen, B., Veca, L. M., Xie, S.-Y., Quantum-Sized Carbon Dots for Bright and Colorful Photoluminescence. *J Am Chem Soc* **2006,** *128* (24), 7756-7757.

8.   Bartelmess, J., Giordani, S., Carbon Nano Onions (Multi Layer Fullerenes) : Chemistry and Applications *Beilstein J. Nanotechnol.* **2014,** *5*, 1980-1998.

9.   Chang, Y.-R., Lee, H.-Y., Chen, K., Chang, C.-C., Tsai, D.-S., Fu, C.-C., Lim, T.-S., Tzeng, Y.-K., Fang, C.-Y., Han, C.-C., Chang, H.-C., Fann, W.,

Mass Production and Dynamic Imaging of Fluorescent Nanodiamonds. *Nature Nanotechnol* **2008,** *3*, 284.

10. Luo, P. G., Yang, F., Yang, S.-T., Sonkar, S. K., Yang, L., Broglie, J. J., Liu, Y., Sun, Y.-P., Carbon-Based Quantum Dots for Fluorescence Imaging of Cells and Tissues. *RSC Adv* **2014,** *4*, 10791–10807.

11. Tripathi, K. M., Tran, T. S., Kim, Y. J., Kim, T., Green Fluorescent Onion-Like Carbon Nanoparticles from Flaxseed Oil for Visible Light Induced Photocatalytic Applications and Label-Free Detection of Al(III) Ions. *ACS Sustainable Chem Eng* **2017,** *5* (5), 3982-3992.

12. Wang, X., Cao, L., Yang, S.-T., Lu, F., Meziani, M. J., Tian, L., Sun, K. W., Bloodgood, M. A., Sun, Y.-P., Bandgap-Like Strong Fluorescence in Functionalized Carbon Nanoparticles. *Angew. Chem.* **2010,** *122*, 5310-5314.

13. Ghosh, M., Sonkar, S. K., Saxena, M., Sarkar, S., Carbon Nano-Onions for Imaging the Life Cycle of Drosophila Melanogaster. *Small* **2011,** *7*, 3170-3177.

14. Cao, L., Wang, X., Meziani, M. J., Lu, F., Wang, H., Luo, P. G., Lin, Y., Harruff, B. A., Veca, L. M., Murray, D., Xie, S.-Y., Sun, Y.-P., Carbon Dots for Multiphoton Bioimaging. *J. Am. Chem. Soc.* **2007,** *129* (37), 11318-11319.

15. Yang, S.-T., Cao, L., Luo, P. G., Lu, F., Wang, X., Wang, H., Meziani, M. J., Liu, Y., Qi, G., Sun, Y.-P., Carbon Dots for Optical Imaging in Vivo. *J Am Chem Soc* **2009,** *131* (32), 11308-11309.

16. Yang, S.-T., Wang, X., Wang, H., Lu, F., Luo, P. G., Cao, L., Meziani, M. J., Liu, J.-H., Liu, Y., Chen, M., Huang, Y., Sun, Y.-P., Carbon Dots as Nontoxic and High-Performance Fluorescence Imaging Agents. *J Phys Chem C* **2009,** *113* (42), 18110-18114.

17. Hardman, R., A Toxicologic Review of Quantum Dots: Toxicity Depends on Physicochemical and Environmental Factors. *Environ Health Perspect.* **2006,** *114* (2), 165–172.

18. Geys, J., Nemmar, A., Verbeken, E., Smolders, E., Ratoi, M., Hoylaerts, M. F., Nemery, B., Hoet, P. H. M., Acute Toxicity and Prothrombotic Effects of Quantum Dots: Impact of Surface Charge. *Environ Health Perspect.* **2008,** *16* (12), 1607–1613.

19. Rossetti, R., Brus, L., Electron-Hole Recombination Emission as a Probe of Surface Chemistry in Aqueous Cadmium Sulfide Colloids. *J Phys Chem* **1982,** *86* (23), 4470-4472.

20. Shen, L., Zhang, L., Chen, M., Chen, X., Wang, J., The Production of Ph-Sensitive Photoluminescent Carbon Nanoparticles by the Carbonization of Polyethylenimine and Their Use for Bioimaging. *Carbon* **2013,** *55*, 343-349.

21. Roy, P., Chen, P.-C., Periasamy, A. P., Chen, Y.-N., Chang, H.-T., Photoluminescent Carbon Nanodots: Synthesis, Physicochemical Properties and Analytical Applications. *Materials Today* **2015,** *18* (8), 447-458.

22. Sun, Y.-P., Wang, X., Lu, F., Cao, L., Meziani, M. J., Luo, P. G., Gu, L., Veca, L. M., Doped Carbon Nanoparticles as a New Platform for Highly Photoluminescent Dots. *J Phys Chem C* **2008,** *112* (47), 18295-18298.

23. LeCroy, G. E., Sonkar, S. K., Yang, F., Veca, L. M., Wang, P., TackettII, K. N., Yu, J.-J., Vasile, E., Qian, H., Liu, Y., Luo, P. G., Sun, Y.-P., Toward Structurally Defined Carbon Dots as Ultracompact Fluorescent Probes. *ACS Nano* **2014,** *8* (5), 4522-4529.

24. Das, S. K., Liu, Y., Yeom, S., Kim, D. Y., Richards, C. I., Single-Particle Fluorescence Intensity Fluctuations of Carbon Nanodots. *Nano Letters* **2014,** *14* (2), 620-625.

25. Sun, C., Zhang, Y., Kalytchuk, S., Wang, Y., Zhang, X., Gao, W., Zhao, J., Cepe, K., Zboril, R., Yu, W. W., Rogach, A. L., Down-Conversion Monochromatic Light-Emitting Diodes with the Color Determined by the Active Layer Thickness and Concentration of Carbon Dots. *J Mater Chem C* **2015,** *3* (26), 6613-6615.

26. Li, H., Kang, Z., Liu, Y., Lee, S.-T., Carbon Nanodots: Synthesis, Properties and Applications. *J Mater Chem* **2012,** *22* (46), 24230-24253.

27. Wang, Y., Zhu, Y., Yu, S., Jiang, C., Fluorescent Carbon Dots: Rational Synthesis, Tunable Optical Properties and Analytical Applications. *RSC Adv* **2017,** *7* (65), 40973-40989.

28. N., B. S., A., B. G., Luminescent Carbon Nanodots: Emergent Nanolights. *Angew Chem Int Ed* **2010,** *49* (38), 6726-6744.

29. Zhijie, Z., Tingting, Z., Xiaoming, L., Jiayue, X., Haibo, Z., Progress of Carbon Quantum Dots in Photocatalysis Applications. *Part. Part. Syst. Char.* **2016,** *33* (8), 457-472.

30. Zhao, A., Chen, Z., Zhao, C., Gao, N., Ren, J., Qu, X., Recent Advances in Bioapplications of C-Dots. *Carbon* **2015,** *85*, 309-327.

31. Jia, X., Li, J., Wang, E., One-Pot Green Synthesis of Optically Ph-Sensitive Carbon Dots with Upconversion Luminescence. *Nanoscale* **2012,** *4* (18), 5572-5575.

32. De, B., Karak, N., A Green and Facile Approach for the Synthesis of Water Soluble Fluorescent Carbon Dots from Banana Juice. *RSC Adv* **2013,** *3* (22), 8286-8290.

33. Haipeng, L., Tao, Y., Chengde, M., Fluorescent Carbon Nanoparticles Derived from Candle Soot. *Angew Chem Int Ed* **2007,** *46* (34), 6473-6475.

34. Jing, W., Cai-Feng, W., Su, C., Amphiphilic Egg-Derived Carbon Dots: Rapid Plasma Fabrication, Pyrolysis Process, and Multicolor Printing Patterns. *Angew Chem Int Ed* **2012,** *51* (37), 9297-9301.

35. Yang, Z., Xu, M., Liu, Y., He, F., Gao, F., Su, Y., Wei, H., Zhang, Y., Nitrogen-Doped, Carbon-Rich, Highly Photoluminescent Carbon Dots from Ammonium Citrate. *Nanoscale* **2014,** *6* (3), 1890-1895.

36. Yang, Y., Cui, J., Zheng, M., Hu, C., Tan, S., Xiao, Y., Yang, Q., Liu, Y., One-Step Synthesis of Amino-Functionalized Fluorescent Carbon Nanoparticles by Hydrothermal Carbonization of Chitosan. *Chem Commun* **2012,** *48* (3), 380-382.

37. Tripathi, K. M., Sonker, A. K., Sonkar, S. K., Sarkar, S., Pollutant Soot of Diesel Engine Exhaust Transformed to Carbon Dots for Multicoloured Imaging of E. Coli and Sensing Cholesterol. *RSC Adv.* **2014,** *4*, 30100-30107.

38. Liang, Q., Ma, W., Shi, Y., Li, Z., Yang, X., Easy Synthesis of Highly Fluorescent Carbon Quantum Dots from Gelatin and Their Luminescent Properties and Applications. *Carbon* **2013,** *60*, 421-428.

39. Liu, S., Zhao, N., Cheng, Z., Liu, H., Amino-Functionalized Green Fluorescent Carbon Dots as Surface Energy Transfer Biosensors for Hyaluronidase. *Nanoscale* **2015,** *7* (15), 6836-6842.

40. Li, Y., Zhong, X., Rider, A. E., Furman, S. A., Ostrikov, K., Fast, Energy-Efficient Synthesis of Luminescent Carbon Quantum Dots. *Grren Chem* **2014,** *16* (5), 2566-2570.

41. Sahu, S., Behera, B., Maiti, T. K., Mohapatra, S., Simple One-Step Synthesis of Highly Luminescent Carbon Dots from Orange Juice: Application as Excellent Bio-Imaging Agents. *Chem Commun* **2012,** *48* (70), 8835-8837.

42. Huang, H., Lv, J.-J., Zhou, D.-L., Bao, N., Xu, Y., Wang, A.-J., Feng, J.-J., One-Pot Green Synthesis of Nitrogen-Doped Carbon Nanoparticles as Fluorescent Probes for Mercury Ions. *RSC Adv* **2013,** *3* (44), 21691-21696.

43. Mehta, V. N., Jha, S., Kailasa, S. K., One-Pot Green Synthesis of Carbon Dots by Using Saccharum Officinarum Juice for Fluorescent Imaging of Bacteria (Escherichia Coli) and Yeast (Saccharomyces Cerevisiae) Cells. *Mater. Sci. Eng.: C* **2014,** *38*, 20-27.

44. Ding, H., Ji, Y., Wei, J.-S., Gao, Q.-Y., Zhou, Z.-Y., Xiong, H.-M., Facile Synthesis of Red-Emitting Carbon Dots from Pulp-Free Lemon Juice for Bioimaging. *J. Mater. Chem. B* **2017,** *5* (26), 5272-5277.

45. Zhou, J., Sheng, Z., Han, H., Zou, M., Li, C., Facile Synthesis of Fluorescent Carbon Dots Using Watermelon Peel as a Carbon Source. *Mater. Lett.* **2012,** *66* (1), 222-224.

46. Lu, W., Qin, X., Liu, S., Chang, G., Zhang, Y., Luo, Y., Asiri, A. M., Al-Youbi, A. O., Sun, X., Economical, Green Synthesis of Fluorescent Carbon Nanoparticles and Their Use as Probes for Sensitive and Selective Detection of Mercury (II) Ions. *Anal. Chem.* **2012,** *84* (12), 5351-5357.

47. Hola, K., Zhang, Y., Wang, Y., Giannelis, E. P., Zboril, R., Rogach, A. L., Carbon Dots-Emerging Light Emitters for Bioimaging, Cancer Therapy and Optoelectronics. *Nano Today* **2014,** *9* (5), 590-603.

48. Guo, Y., Wang, Z., Shao, H., Jiang, X., Hydrothermal Synthesis of Highly Fluorescent Carbon Nanoparticles from Sodium Citrate and Their Use for the Detection of Mercury Ions. *Carbon* **2013,** *52*, 583-589.

49. Wang, Q., Huang, X., Long, Y., Wang, X., Zhang, H., Zhu, R., Liang, L., Teng, P., Zheng, H., Hollow Luminescent Carbon Dots for Drug Delivery. *Carbon* **2013,** *59*, 192-199.

50. Zhu, C., Zhai, J., Dong, S., Bifunctional Fluorescent Carbon Nanodots: Green Synthesis Via Soy Milk and Application as Metal-Free Electrocatalysts for Oxygen Reduction. *Chem Commun* **2012,** *48* (75), 9367-9369.

51. Peng, H., Jing, L., Xiansong, W., Zhe, W., Chunlei, Z., Meng, H., Kan, W., Feng, C., Zhiming, L., Guangxia, S., Daxiang, C., Xiaoyuan, C., Light-Triggered Theranostics Based on Photosensitizer-Conjugated Carbon Dots for Simultaneous Enhanced-Fluorescence Imaging and Photodynamic Therapy. *Adv Mater* **2012,** *24* (37), 5104-5110.

52. Park, Y., Yoo, J., Lim, B., Kwon, W., Rhee, S. W., Improving the Functionality of Carbon Nanodots: Doping and Surface Functionalization. *J Mater Chem A* **2016,** *4* (30), 11582-11603.

53. Yu, J., Xu, C., Tian, Z., Lin, Y., Shi, Z., Facilely Synthesized N-Doped Carbon Quantum Dots with High Fluorescent Yield for Sensing Fe(III). *New J Chem* **2016,** *40* (3), 2083-2088.

54. Sarkar, S., Das, K., Ghosh, M., Das, P. K., Amino Acid Functionalized Blue and Phosphorous-Doped Green Fluorescent Carbon Dots as Bioimaging Probe. *RSC Adv.* **2015,** *5* (81), 65913-65921.

55. Hu, Y., Yang, J., Tian, J., Jia, L., Yu, J.-S., Waste Frying Oil as a Precursor for One-Step Synthesis of Sulfur-Doped Carbon Dots with Ph-Sensitive Photoluminescence. *Carbon* **2014,** *77*, 775-782.

56. Shan, X., Chai, L., Ma, J., Qian, Z., Chen, J., Feng, H., B-Doped Carbon Quantum Dots as a Sensitive Fluorescence Probe for Hydrogen Peroxide and Glucose Detection. *Analyst* **2014,** *139* (10), 2322-2325.

57. Wang, C., Sun, D., Zhuo, K., Zhang, H., Wang, J., Simple and Green Synthesis of Nitrogen-, Sulfur-, and Phosphorus-Co-Doped Carbon Dots with Tunable Luminescence Properties and Sensing Application. *RSC Adv* **2014,** *4* (96), 54060-54065.

58. Li, F., Liu, C., Yang, J., Wang, Z., Liu, W., Tian, F., Mg/N Double Doping Strategy to Fabricate Extremely High Luminescent Carbon Dots for Bioimaging. *RSC Adv* **2014,** *4* (7), 3201-3205.

59. Gong, X., Lu, W., Liu, Y., Li, Z., Shuang, S., Dong, C., Choi, M. M. F., Low Temperature Synthesis of Phosphorous and Nitrogen Co-Doped Yellow Fluorescent Carbon Dots for Sensing and Bioimaging. *J Mater Chem B* **2015,** *3* (33), 6813-6819.

60. Sun, D., Ban, R., Zhang, P.-H., Wu, G.-H., Zhang, J.-R., Zhu, J.-J., Hair Fiber as a Precursor for Synthesizing of Sulfur- and Nitrogen-Co-Doped Carbon Dots with Tunable Luminescence Properties. *Carbon* **2013,** *64*, 424-434.

61. Yuan, Y. H., Li, R. S., Wang, Q., Wu, Z. L., Wang, J., Liu, H., Huang, C. Z., Germanium-Doped Carbon Dots as a New Type of Fluorescent Probe for Visualizing the Dynamic Invasions of Mercury(Ii) Ions into Cancer Cells. *Nanoscale* **2015,** *7* (40), 16841-16847.

62. Qian, Z., Shan, X., Chai, L., Ma, J., Chen, J., Feng, H., Si-Doped Carbon Quantum Dots: A Facile and General Preparation Strategy, Bioimaging Application, and Multifunctional Sensor. *ACS App Mater Interfaces* **2014,** *6* (9), 6797-6805.

63. Yang, S., Sun, J., Li, X., Zhou, W., Wang, Z., He, P., Ding, G., Xie, X., Kang, Z., Jiang, M., Large-Scale Fabrication of Heavy Doped Carbon Quantum Dots with Tunable-Photoluminescence and Sensitive Fluorescence Detection. *J Mater Chem A* **2014,** *2* (23), 8660-8667.

64. Cheng, J., Wang, C.-F., Zhang, Y., Yang, S., Chen, S., Zinc Ion-Doped Carbon Dots with Strong Yellow Photoluminescence. *RSC Adv* **2016,** *6* (43), 37189-37194.

65. Wang, R., Lu, K.-Q., Tang, Z.-R., Xu, Y.-J., Recent Progress in Carbon Quantum Dots: Synthesis, Properties and Applications in Photocatalysis. *J. Mater. Chem. A.* **2017,** *5* (8), 3717-3734.

66. Zhang, Y.-Q., Ma, D.-K., Zhuang, Y., Zhang, X., Chen, W., Hong, L.-L., Yan, Q.-X., Yu, K., Huang, S.-M., One-Pot Synthesis of N-Doped Carbon

Dots with Tunable Luminescence Properties. *J Mater Chem* **2012,** *22* (33), 16714-16718.

67. Yang, X., Ming, W., Yang, L., Xi-Zeng, F., Xue-Bo, Y., Xi-Wen, H., Yu-Kui, Z., Nitrogen-Doped Carbon Dots: A Facile and General Preparation Method, Photoluminescence Investigation, and Imaging Applications. *Chem-European J* **2013,** *19* (7), 2276-2283.

68. Ma, Z., Ming, H., Huang, H., Liu, Y., Kang, Z., One-Step Ultrasonic Synthesis of Fluorescent N-Doped Carbon Dots from Glucose and Their Visible-Light Sensitive Photocatalytic Ability. *New J Chem* **2012,** *36* (4), 861-864.

69. Zhang, R., Chen, W., Nitrogen-Doped Carbon Quantum Dots: Facile Synthesis and Application as a "Turn-Off" Fluorescent Probe for Detection of Hg(II) Ions. *Biosens Bioelectron* **2014,** *55*, 83-90.

70. Sen, L., Jingqi, T., Lei, W., Yingwei, Z., Xiaoyun, Q., Yonglan, L., M., A. A., O., A.-Y. A., Xuping, S., Hydrothermal Treatment of Grass: A Low-Cost, Green Route to Nitrogen-Doped, Carbon-Rich, Photoluminescent Polymer Nanodots as an Effective Fluorescent Sensing Platform for Label-Free Detection of Cu(Ii) Ions. *Adv Mater* **2012,** *24* (15), 2037-2041.

71. Sun, S., Zhang, L., Jiang, K., Wu, A., Lin, H., Toward High-Efficient Red Emissive Carbon Dots: Facile Preparation, Unique Properties, and Applications as Multifunctional Theranostic Agents. *Chem. Mater.* **2016,** *28* (23), 8659-8668.

72. Jiang, K., Sun, S., Zhang, L., Lu, Y., Wu, A., Cai, C., Lin, H., Red, Green, and Blue Luminescence by Carbon Dots: Full-Color Emission Tuning and Multicolor Cellular Imaging. *Angew. Chem. Int. Ed.* **2015,** *54* (18), 5360-5363.

73. Hu, S., Trinchi, A., Atkin, P., Cole, I., Tunable Photoluminescence across the Entire Visible Spectrum from Carbon Dots Excited by White Light. *Angew. Chem. Int. Ed.* **2015,** *54* (10), 2970-2974.

74. Ding, H., Ji, Y., Wei, J.-S., Gao, Q.-Y., Zhou, Z.-Y., Xiong, H.-M., Facile Synthesis of Red-Emitting Carbon Dots from Pulp-Free Lemon Juice for Bioimaging. *J. Mater. Chem. B* **2017,** *5* (26), 5272-5277.

75. Chandra, S., Das, P., Bag, S., Laha, D., Pramanik, P., Synthesis, Functionalization and Bioimaging Applications of Highly Fluorescent Carbon Nanoparticles. *Nanoscale* **2011,** *3* (4), 1533-1540.

76. Han, Y., Tang, D., Yang, Y., Li, C., Kong, W., Huang, H., Liu, Y., Kang, Z., Non-Metal Single/Dual Doped Carbon Quantum Dots: A General Flame Synthetic Method and Electro-Catalytic Properties. *Nanoscale* **2015,** *7* (14), 5955-5962.

77. Zhou, J., Shan, X., Ma, J., Gu, Y., Qian, Z., Chen, J., Feng, H., Facile Synthesis of P-Doped Carbon Quantum Dots with Highly Efficient Photoluminescence. *RSC Adv* **2014,** *4* (11), 5465-5468.

78. Sadhanala, H. K., Nanda, K. K., Boron-Doped Carbon Nanoparticles: Size-Independent Color Tunability from Red to Blue and Bioimaging Applications. *Carbon* **2016,** *96*, 166-173.

79. Gong, Y., Yu, B., Yang, W., Zhang, X., Phosphorus, and Nitrogen Co-Doped Carbon Dots as a Fluorescent Probe for Real-Time Measurement of Reactive Oxygen and Nitrogen Species inside Macrophages. *Biosens Bioelectron* **2016,** *79*, 822-828.

80. Xu, Q., Li, B., Ye, Y., Cai, W., Li, W., Yang, C., Chen, Y., Xu, M., Li, N., Zheng, X., Street, J., Luo, Y., Cai, L., Synthesis, Mechanical Investigation, and Application of Nitrogen and Phosphorus Co-Doped Carbon Dots with a High Photoluminescent Quantum Yield. *Nano Research* **2017**, 1.

81. Li, H., Shao, F.-Q., Zou, S.-Y., Yang, Q.-J., Huang, H., Feng, J.-J., Wang, A.-J., Microwave-Assisted Synthesis of N,P-Doped Carbon Dots for Fluorescent Cell Imaging. *Microchimica Acta* **2016,** *183* (2), 821-826.

82. Chandra, S., Dipranjan, L., Arindam, P., Angshuman, R. C., Parimal, K., Kumar, S. S., Synthesis of Highly Fluorescent Nitrogen and Phosphorus Doped Carbon Dots for the Detection of Fe(III) Ions in Cancer Cells. *Luminescence* **2016,** *31* (1), 81-87.

83. Chen, B. B., Liu, Z. X., Zou, H. Y., Huang, C. Z., Highly Selective Detection of 2,4,6-Trinitrophenol by Using Newly Developed Terbium-Doped Blue Carbon Dots. *Analyst* **2016,** *141* (9), 2676-2681.

84. Bourlinos, A. B., Bakandritsos, A., Kouloumpis, A., Gournis, D., Krysmann, M., Giannelis, E. P., Polakova, K., Safarova, K., Hola, K., Zboril, R., Gd(III)-Doped Carbon Dots as a Dual Fluorescent-Mri Probe. *J Mater Chem* **2012,** *22* (44), 23327-23330.

85. Gong, N., Wang, H., Li, S., Deng, Y., Chen, X. a., Ye, L., Gu, W., Microwave-Assisted Polyol Synthesis of Gadolinium-Doped Green Luminescent Carbon Dots as a Bimodal Nanoprobe. *Langmuir* **2014,** *30* (36), 10933-10939.

86. Mykhailiv, O., Zubyk, H., Plonska-Brzezinska, M. E., Carbon Nano-Onions: Unique Carbon Nanostructures with Fascinating Properties and Their Potential Applications. *Inorganica Chim Acta* **2017,** *468*, 49-66.

87. Anilkumar, P., Wang, X., Cao, L., Sahu, S., Liu, J.-H., Wang, P., Korch, K., Tackett Ii, K. N., Parenzan, A., Sun, Y.-P., Toward Quantitatively Fluorescent Carbon-Based "Quantum" Dots. *Nanoscale* **2011,** *3* (5), 2023-2027.

88. Huiquan, T., Kai, Y., Zhen, M., Jianmei, W., Youjiu, Z., Zhenhui, K., Zhuang, L., In Vivo NIR Fluorescence Imaging, Biodistribution, and Toxicology of Photoluminescent Carbon Dots Produced from Carbon Nanotubes and Graphite. *Small* **2012,** *8* (2), 281-290.

89. Li, Q., Ohulchanskyy, T. Y., Liu, R., Koynov, K., Wu, D., Best, A., Kumar, R., Bonoiu, A., Prasad, P. N., Photoluminescent Carbon Dots as Biocompatible Nanoprobes for Targeting Cancer Cells *in Vitro*. *J Phys Chem C* **2010,** *114* (28), 12062-12068.

90. Jelinek, R., Carbon-Dots in Sensing Applications. In *Carbon Quantum Dots: Synthesis, Properties and Applications*, Springer International Publishing: Cham, 2017; pp 71-91.

91. Shen, P., Xia, Y., Synthesis-Modification Integration: One-Step Fabrication of Boronic Acid Functionalized Carbon Dots for Fluorescent Blood Sugar Sensing. *Anal Chem* **2014,** *86* (11), 5323-5329.

92. Tripathi, K. M., Sonker, A. K., Sonkar, S. K., Sarkar, S., Pollutant Soot of Diesel Engine Exhaust Transformed to Carbon Dots for Multicoloured

Imaging of E. Coli and Sensing Cholesterol. *RSC Adv.* **2014,** *4* (57), 30100-30107.

93. Atabaev, T., Doped Carbon Dots for Sensing and Bioimaging Applications: A Minireview. *Nanomaterials* **2018,** *8* (5), 342.

94. Choi, D., Ham, S., Jang, D.-J., Visible-Light Photocatalytic Reduction of Cr(VI) Via Carbon Quantum Dots-Decorated TiO_2 Nanocomposites. *J Enviorn Chem Eng* **2018,** *6* (1), 1-8.

95. Wenting, W., Liying, Z., Weiyu, F., Jizhong, S., Xiaoming, L., Zhongtao, L., Ruiqin, W., Jinqiang, Z., Jingtang, Z., Mingbo, W., Haibo, Z., Cu–N Dopants Boost Electron Transfer and Photooxidation Reactions of Carbon Dots. *Angew Chem* **2015,** *127* (22), 6640-6644.

96. Liu, Y., Ma, Y.-j., Liu, C.-y., Zhang, Z.-y., Yang, W.-d., Nie, S.-d., Zhou, X.-h., The Effective Removal of Cr(VI) Ions by Carbon Dot–Silica Hybrids Driven by Visible Light. *RSC Adv* **2016,** *6* (72), 68530-68537.

97. Ugarte, D., Curling and Closure of Graphitic Networks under Electron-Beam Irradiation. *Nature* **1992,** *359*, 707.

98. Ugarte, D., Onion-Like Graphitic Particles. *Carbon* **1995,** *33* (7), 989-993.

99. Sano, N., Wang, H., Alexandrou, I., Chhowalla, M., Teo, K. B. K., Amaratunga, G. A. J., Iimura, K., Properties of Carbon Onions Produced by an Arc Discharge in Water. *J Appl Phys* **2002,** *92* (5), 2783-2788.

100. Plonska-Brzezinska, M. E., Brus, D. M., Molina-Ontoria, A., Echegoyen, L., Synthesis of Carbon Nano-Onion and Nickel Hydroxide/Oxide Composites as Supercapacitor Electrodes. *RSC Adv* **2013,** *3* (48), 25891-25901.

101. Sonkar, S. K., Roy, M., Babara, D. G., Sarkar, S., Water Soluble Carbon Nano-Onions from Wood Wool as Growth Promoters for Gram Plants. *Nanoscale* **2012,** *4* (24), 7670-7675.

102. Dubey, P., Tripathi, K. M., Sonkar, S. K., Gram Scale Synthesis of Green Fluorescent Water- Soluble Onion-Like Carbon Nanoparticles from Camphor and Polystyrene Foam. *RSC Adv.* **2014,** *4*, 5838-5844.

103. Zeiger, M., Jackel, N., Mochalin, V. N., Presser, V., Review: Carbon Onions for Electrochemical Energy Storage. *J Mater Chem A* **2016,** *4* (9), 3172-3196.

104. Zou, Q., Wang, M. Z., Li, Y. G., Lv, B., Zhao, Y. C., HRTEM and Raman Characterisation of the Onion-Like Carbon Synthesised by Annealing Detonation Nanodiamond at Lower Temperature and Vacuum. *J. Exper. Nanosci.* **2010,** *5* (6), 473-487.

105. Qin, L.-C., Iijima, S., Onion-Like Graphitic Particles Produced from Diamond. *Chem Phys Lett* **1996,** *262* (3), 252-258.

106. Du, J., Liu, Z., Li, Z., Han, B., Sun, Z., Huang, Y., Carbon Onions Synthesized Via Thermal Reduction of Glycerin with Magnesium. *Mater Chem Phys* **2005,** *93* (1), 178-180.

107. Shoji, F., Feng, Z., Kono, A., Nagai, T., Spherical Carbon Particle Growth in a Methane Plasma. *Appl Phys Lett* **2006,** *89* (17), 171504.

108. Hou, S.-S., Chung, D.-H., Lin, T.-H., High-Yield Synthesis of Carbon Nano-Onions in Counterflow Diffusion Flames. *Carbon* **2009,** *47* (4), 938-947.

109. Han, F.-D., Yao, B., Bai, Y.-J., Preparation of Carbon Nano-Onions and Their Application as Anode Materials for Rechargeable Lithium-Ion Batteries. *J Phys Chem C* **2011,** *115* (18), 8923-8927.

110. Choucair, M., Stride, J. A., The Gram-Scale Synthesis of Carbon Onions. *Carbon* **2012,** *50*, 1109-1115.

111. Portet, C., Yushin, G., Gogotsi, Y., Electrochemical Performance of Carbon Onions, Nanodiamonds, Carbon Black and Multiwalled Nanotubes in Electrical Double Layer Capacitors. *Carbon* **2007,** *45* (13), 2511-2518.

112. Georgakilas, V., Guldi, D. M., Signorini, R., Bozio, R., Prato, M., Organic Functionalization and Optical Properties of Carbon Onions. *J Am Chem Soc* **2003,** *125* (47), 14268-14269.

113. Nicolas, K., I., M. N., V., R. V., Michael, S., Gerhard, M., V., B. Y., L., K. V., Robert, S., The Catalytic Use of Onion-Like Carbon Materials for Styrene Synthesis by Oxidative Dehydrogenation of Ethylbenzene. *Angew Chem Int Ed* **2002,** *41* (11), 1885-1888.

114. Su, D., Maksimova, N. I., Mestl, G., Kuznetsov, V. L., Keller, V., Schlögl, R., Keller, N., Oxidative Dehydrogenation of Ethylbenzene to Styrene over Ultra-Dispersed Diamond and Onion-Like Carbon. *Carbon* **2007,** *45* (11), 2145-2151.

115. Hirata, A., Igarashi, M., Kaito, T., Study on Solid Lubricant Properties of Carbon Onions Produced by Heat Treatment of Diamond Clusters or Particles. *Trbol Int* **2004,** *37* (11), 899-905.

116. Joly-Pottuz, L., Bucholz, E. W., Matsumoto, N., Phillpot, S. R., Sinnott, S. B., Ohmae, N., Martin, J. M., Friction Properties of Carbon Nano-Onions from Experiment and Computer Simulations. *Tribol Lett* **2009,** *37* (1), 75.

117. Xu, B., Yang, X., Wang, X., Guo, J., Liu, X., A Novel Catalyst Support for Dmfc: Onion-Like Fullerenes. *J. Power Sour.* **2006,** *162* (1), 160-164.

118. Liu, L., Das, A., Megaridis, C. M., Terahertz Shielding of Carbon Nanomaterials and Their Composites – a Review and Applications. *Carbon* **2014,** *69*, 1-16.

119. Bartelmess, J., De Luca, E., Signorelli, A., Baldrighi, M., Becce, M., Brescia, R., Nardone, V., Parisini, E., Echegoyen, L., Pompa, P. P., Giordani, S., Boron Dipyrromethene (BODIPY) Functionalized Carbon Nano-Onions for High Resolution Cellular Imaging. *Nanoscale* **2014,** *6* (22), 13761-13769.

120. Joanna, L., E., P.-B. M., Amit, P., T., D. A., Agneta, S., T., S. D., Beata, K.-S., Krzysztof, W., Luis, E., Small Noncytotoxic Carbon Nano-Onions: First Covalent Functionalization with Biomolecules. *Chem- European J* **2010,** *16* (16), 4870-4880.

121. Seymour, M. B., Su, C., Gao, Y., Lu, Y., Li, Y., Characterization of Carbon Nano-Onions for Heavy Metal Ion Remediation. *J Nanopart Res* **2012,** *14* (9), 1087.

122. Wang, X., Han, H., Liu, X., Gu, X., Chen, K., Lu, D., Multi-Walled Carbon Nanotubes Can Enhance Root Elongation of Wheat (Triticum Aestivum) Plants. *J Nanopart Res* **2012,** *14*.

123. Saxena, M., Maity, S., Sarkar, S., Carbon Nanoparticles in 'Biochar' Boost Wheat (Triticum Aestivum) Plant Growth *RSC Adv.* **2014,** *4* (75), 399948-399954.

Chapter-2

Sunlight-Induced Photoreduction of Cr(VI) to Cr(III) by Fluorescent Nitrogen-Phosphorus Doped Carbon Dots
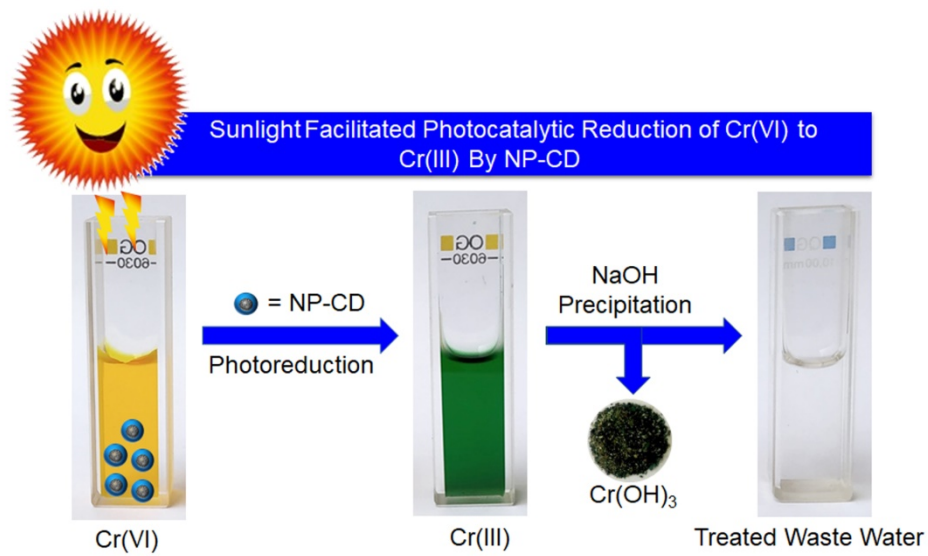
2.1 Introduction

Doping is a well-established method for articulating the optical and electrical properties of carbon nanoparticles since their discovery [1-4]. Many reports are available stating that the doped-CD show remarkable results in terms of better quantum yield over the blue-green [5] and red [6, 7] region of the visible spectrum along with its novel applications. Few groups have reported the doping of nitrogen (N) and phosphorus (P) to form nitrogen-phosphorous doped carbon dots (NP-CD), using hydrothermal [8-10], solvothermal [11] and microwave [12-15] assisted methods with the different precursor materials. NP-CD used for several applications such as for sensing Hg^{2+} [10], as a nano-carrier of anticancer drug [16], imaging purpose [8, 12-14, 16], oxygen reduction [17], intercellular Fe^{3+} sensor [8], fluorescence sensing of living cells [13] and in the flourescence sensing of reactive oxygen and nitrogen species [9]. Presently, the doping of the CD are used to articulate its potential properties, with a huge expectation of the exploration of its newer prospects. For instance, in the field of water treatment [18, 19] via aqueous phase photocatalysis [6, 7, 20], which has been barely investigated. As per the general understanding, the heavy-metal-ion contamination in water is a severe threat, which indeed demands a viable, sustainable approach for its efficient sensing followed by its removal. For the same, sunlight-induced photocatalysis can be considered as a promising approach for the photodegradation of environmental pollutants [21, 22]. The fabrication of novel nano-structured-materials with unique physical/chemical properties along with high efficiency towards the photocatalysis are the crucial step and required much attention [6, 7, 23, 24].

Beyond the conventional existing applications of CD, the present work investigate a newer perspective of NP-CD, using the natural sunlight for photoreduction of toxic Cr(VI) to Cr(III), followed by precipitation of Cr(III) salt. The toxic non-biodegradable [25] pollutant Cr(VI) is a well-known by-product of many industrial processes, like electroplating, paint making, leather tanning, and others, was discarded in the wastewater [26]. Cr(VI) is continuously damaging the aquatic system and shows devastating consequences [27]. Compared to the Cr(VI), Cr(III) is less toxic and can easily be precipitated out or adsorbed by the already existing methods [28]. So the conversion of Cr(VI) to Cr(III) followed by its simple

precipitation is always in high demand. Nevertheless, it could be a sustainable approach, if the same can be performed under the presence of natural sunlight [6, 7, 23, 24].

2.2   Experimental

2.2.1   Materials and reagents

All chemical reagents were of analytical grade and used without further purification.

2.2.2   Instrumentation

Perkin Elmer Lambda 35 spectrometer used for the UV-Vis absorption spectra. Fluoromax 4C.L. System were used for the Fluorescence spectrometry analyses in aqueous solutions, ESCA$^+$ omicron nanotechnology oxford instrument were used for the XPS measurements. Bruker Vertex 70 FT-IR spectrophotometer were used for the recording of FTIR spectra using KBr pellets. The morphology of the NP-CD were studied by the Tecnai 20 G2 300 kV, STWIN model transmission electron microscope. HRTEM analyses were done at 300 kV acceleration voltage.

2.2.3   Synthesis of NP-CD

The NP-CD were synthesized from the pool of the mixed reagents containing 3 g of imidazole, 10 mL phosphoric acid and 10 mL polyethylene glycol (molecular weight ~ 400g/mol) in a 100 mL beaker. A domestic microwave oven at 560 watts power was used to carbonize the mixture after 10 minutes sonication. The transparent solution containing (imidazole, phosphoric and polyethylene glycol), now turned into the dark brown solution. The supernatant was then centrifuged at 6000 rpm for 15 minutes to obtain a clear solution collected and dried on the water bath to obtain NP-CD. Further, the as-synthesized NP-CD get neutralized with the ammonia solution to remove the excess phosphoric acid followed by repetitively washing with DI water. The synthetic procedure for the formation of different CD was the same only the difference in the starting materials, Such as in CD (only PEG was used), in the case of N-CD (imidazole + PEG) and for P-CD (phosphoric acid + PEG) was used under the similar conditions used for the fabrication of NP-CD. The QY of the NP-CD calculated by the given formula.

$$Q = Q_r * \frac{I}{I_r} * \frac{A_r}{A} * \frac{\cap^2}{\cap^2{}_r}$$

Where Q is the QY, I is the measured integrated emission intensity, ∩ is the refractive index of the solvent and A is the optical density. The subscript "r" refers to the reference standard with known QY. Herein the quinine sulphate was dissolved in 0.1M H2SO4 as the reference standard with a known QY of 0.54.

2.2.4 Photocatalytic Activity Measurement

The photocatalytic activity of NP-CD were investigated by the reduction of the synthetic contaminated water from its orange colored Cr(VI) to green colored Cr(III) in aqueous solution under direct irradiation of sunlight. A stock solution of 2000 ppm Cr(VI) was prepared dissolving 1.42 gm potassium dichromate in the 250 mL of DI water. The lower concentration of the Cr(VI) was prepared by diluting the stock solution. In a typical process, 3.5 mg of the NP-CD were mixed in the 50 mL of different Cr(VI) solutions and sonicated for 30 minutes to obtain the adsorption-desorption equilibrium, afterwards the solution were kept into the sunlight irradiation for the photoreduction. To study the kinetic rate of the photocatalytic reduction, we collected the 2 mL of the samples at the time interval of 10 minutes. The obtained samples were centrifuged and further diluted. The diluted solution was treated with DPC assay [6, 29, 30] to detect the Cr(VI) concentration at 540 nm in the UV-Vis spectrophotometer. The treated clean water after removal of Cr(III) were evaporated and thus the regeneration of NP-CD which was used in the next cycle.

2.3 Results and discussion

A single-step process presented here describe the facile synthesis of the NP-CD from the pool of imidazole (source of nitrogen (N)), phosphoric acid (source of phosphorus (P)) and polyethylene glycol (source of carbon (C)), via the simplest method of microwave charring for ~ 4 minutes. The as-synthesized blue fluorescent NP-CD utilized for the aqueous phase photoreduction of Cr(VI) to Cr(III) under the presence of natural sunlight. Compared to artificial light, natural sunlight shows its significant contribution towards the photoreduction of the Cr(VI) to Cr(III) concerning the time required for the photoreduction is shown in Table 1, which also includes synthesis time for the fabrication of nano-carbons in comparison with the

existing reports. Furthermore, the Cr(III) was also precipitated out by the NaOH solution to get treated water from the synthetic contaminated water.
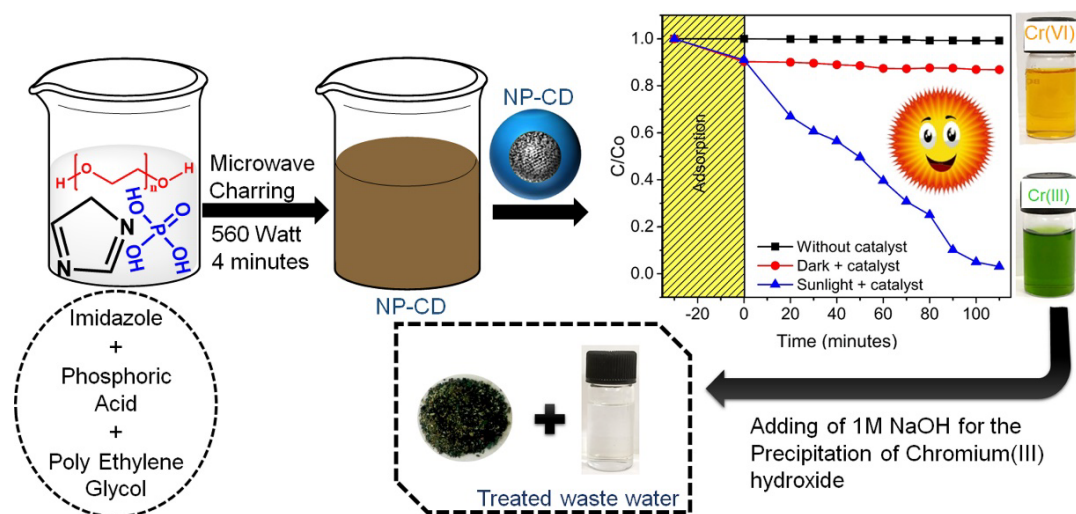
Scheme 2.1: A Schematic representation showing the microwave assisted-facile synthesis and application of NP-CD for aqueous phase photoreduction of Cr(VI) to Cr(III), under the influence of sunlight followed by the precipitation of Cr(III) into its green colored hydroxide salt.

2.3.1 Spectroscopic characterization

The absorption spectrum, (Figure 2. 1 (a)) shows peaks at ~ 210 nm and ~ 270 nm that correspond to the transitions associated with π-π* (C=C) and n-π* (C=N/P), respectively. The photographic images of the NP-CD in daylight and under the UV light illumination are shown in Figure 2.1 (b). The blue emitting NP-CD show the excitation wavelength dependent flurorescence emission (Figure 2. 1 (c)), situated mostly between the blue-green region (~ 360 nm to ~ 540 nm) of the visible spectrum, having the highest emission intensity at ~ 443 nm (excited at 380 nm), and possesing a quantum yield value of ~ 15 % [31]. In addition, the photostability of NP-CD was investigated for 5 hours at the excitation wavelength of 380 nm and it shows good photostability (Figure 2. 1(d)) without any apperent loss in the emission intensity.
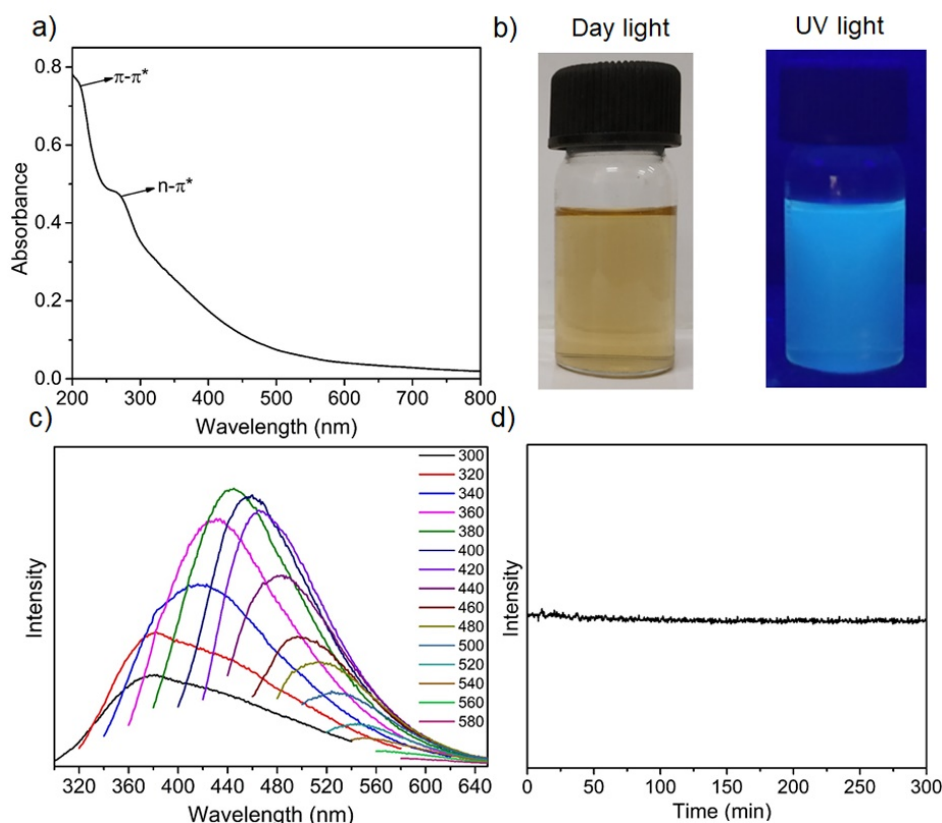
Figure 2.1: (a) UV-Vis spectrum; (b) photographic image in day light and UV light; (c) excitation dependent fluorescence emission spectra (excited from 300 nm to 580 nm with the increment of 20 nm towards the higher wavelength) and (d) photostability at 380nm excitation for 5 h of NP-CD.

2.3.2 XPS and FT-IR Analysis

The possible identification of the surface functionalities [32, 33] of the NP-CD was carried out by XPS and FTIR. XPS spectrum of NP-CD (Figure 2. 2 (a)) shows the signature peaks associated with four elements; carbon (C1s), oxygen (O1s), nitrogen (N1s), and phosphorus (P2p and P2s) at ~ 284.4 eV, ~ 532.1 eV, ~ 399.8eV, ~ 132.6 and ~ 188 eV, respectively. The inset of Figure 2. 2(a) shows a tabular data for the elemental composition from the XPS survey scan. Figure 2. 2 (b-e) shows the high-resolution short scanned XPS spectra of C1s, N1s, P2p, and O1s respectively after deconvulation. Short scanned C1s analysis after deconvulation as displayed in Figure 2. 2 (b), showing the presence of six different peaks located at 283.4 eV, 284.2 eV, 284.8eV, 285.6eV, 286.2eV and 288 eV corresponding to the presence of different binding states of carbon as C=C, C-C, C-N/P, C-O, C=N and C=O, respectively [34, 35]. After deconvulation short scan of N1s show three major peaks at 398.9, 400.6eV and 402 eV corresponding to the C=N-C (pyridinic N), C-N-H (pyrollic N), and C=N (graphitic N), respectively

(Figure 2. 2(c)). Similarly, The P2p short scan after deconvulation shows two peaks at 134.5 eV and 133.5 eV corresponding to the presence of the P-O and P-C, respectively (Figure 2. 2(d)) [9]. The short scan for O1s region after deconvulation shows the presence of three major peaks at 532.9 eV, 532.3 eV and 531.1 eV corresponding to the presence of C=O/C=N, C-O and O-N/P, respectively (Figure 2. 2(e)) [36]. FTIR results (Figure 2. 2 (f)) show a broad band from 3484-3200 cm-1 corresponding to the N-H (sharp end) and O-H stretching vibrations.[12, 16, 37] The doublet at ~ 2925 and ~ 2873 cm-1 correspond to the C-H stretching vibrations. [37] The medium band at ~ 1745 cm-1 and ~ 1643 cm-1 correspond to C=O and C=C stretching vibrations. The medium band at ~ 1456 cm-1 and ~ 1351 cm-1 correspond to C=N and C-N stretching vibrations, respectively.[37-39] The medium and sharp peaks ~ 1068 cm-1 and ~ 940 cm-1 correspond to the C-O, P-O-C stretching vibrations. The bands between ~ 600 cm-1 to ~ 500 cm^{-1} correspond to the aromatic stretching [12, 16, 17, 38, 40] along with presence of the signature peaks of -P-O-C- and =N-C- confirming the doping of N and P in the NP-CD. The presence of different type of functional groups confirmed by the FTIR spectra of NP-CD were also in accordance with binding suggested by the XPS spectra. Additionally, to understand the distribution of the different elements especially, the N and P within the carbonized matrix of NP-CD. We did a XPS analysis concerning the percentage composition of the different elements at three different places in the same sample and presented the data in the form of standard error as C (52.85 ± 0.36)%, O (30.23 ± 0.13)%, N (5.55 ± 0.06)%, P (11.36 ± 0.33)%
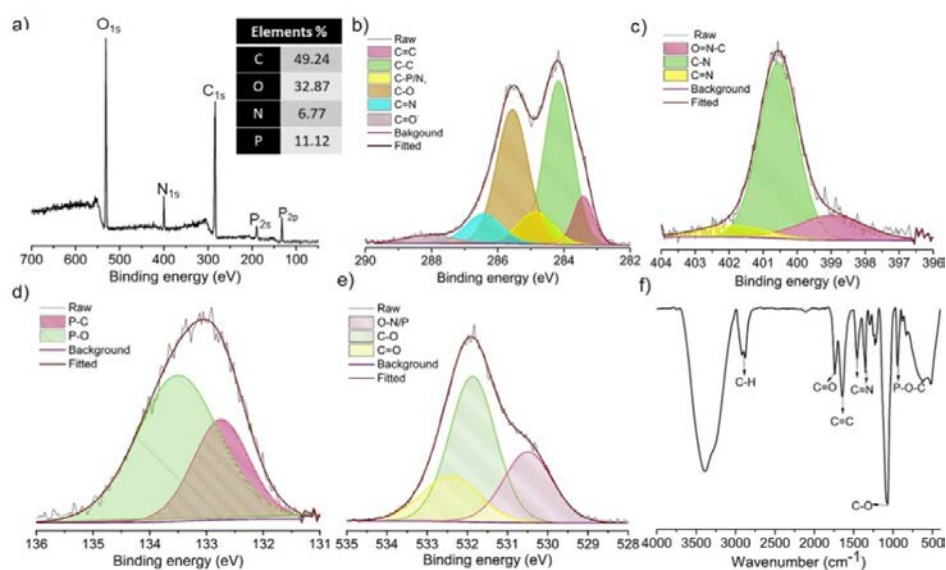
Figure 2.2: (a) XPS survey scan of NP-CD with its corresponding short scan of; (b) C1s; (c) N1s; (d) P2p and (e) O1s; (f) FTIR spectra

2.3.3 Microscopic analysis

Transmission electron microscopy (TEM) was used to observe the morphology of NP-CD, (Figure 2. 3). The TEM image of NP-CD (Figure 2. 3 a), shows well dispersed spherical particles with the corresponding size distribution analysis in Figure 2. 3(b). Gaussian fitting of the size distribution curve shows that the average size of the NP-CD is 9.5 nm with the standard deviation of 3.3 nm. The High-resolution TEM (HRTEM) image in Figure 2. 3(c) shows the graphitic fringes encircled with the yellow circles. Figure 2. 3 (d) is the HRTEM image of NP-CD, which shows the interplanar layers of the graphitic carbon of 0.22 nm
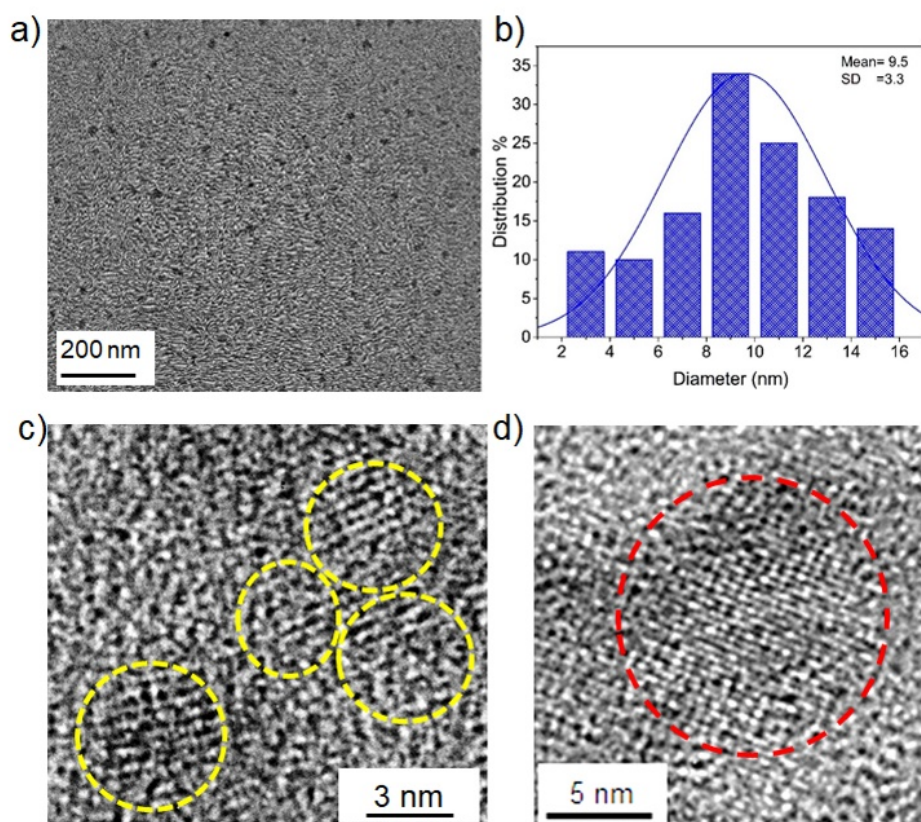

Figure 2.3: (a) TEM image of NP-CD; and (b) its corresponding size distribution; (c) HRTEM image of NP-CD highlightes with yellow circles showing the arrangements of graphitic packing as interplanar fringes; (d) HRTEM image showing the interplanar arrangements of NP-CD.

2.3.4   Sunlight Induced Photocatalytic Reduction of Cr (VI)

Using the potassium dichromate as a source of Cr(VI) to prepare the synthetic contaminated water, NP-CD were used here for the aqueous phase photocatalytic reduction of Cr(VI) to Cr(III) under the influence of natural sunlight. The important prospect of the present finding ascribed towards the photoreduction of variable concentrations of Cr(VI) (10 ppm to 2000 ppm) to its respective Cr(III) using the same dose of the photocatalyst. The effects of NP-CD and sunlight on photocatalysis were shown in the Figure 2.4(a). The adsorption-desorption equilibrium was attained via sonicating for 30 minutes in the daylight (Figure 2.4 (a-b)) and afterwards the Cr(VI) was kept under the sunlight, and after every 10 minutes the photo reduced solutions were collected for the UV-Vis analysis. The residual Cr(VI) concentrations after the photoreduction were investigated by the UV-Vis spectrometer at 540 nm wavelength with the help of di-phenyl carbazide (DPC) assay [6, 29, 30]. In the absence of NP-CD (black line-Figure 2.4 (a)) and the sunlight (red line-Figure 2.4 (a)), there was almost negligible changes in the initial concentration of Cr(VI). While after the addition of the NP-CD in the presence of sunlight (blue line-Figure 2.4 (a)) almost complete photoreduction of the Cr (VI) (400 ppm) had been achieved within the ~ 110 minutes. Additionally, the same Figure 2.4 (a) shows that NP-CD exhibited only ~ 10 % of adsorption. The quantitative evaluation of Cr(VI) reduction by NP-CD was performed using different concentrations (10, 50, 100, 400, 1000, 2000 ppm) of Cr (VI) with the same catalyst dose(0.07mg mL-1) just by increasing the sunlight irradiation time. The continuous decrease in the initial concentration of Cr(VI) represented as C/Co with the time under the sunlight irradiation is shown in Figure 2.4 (b). The photocatalytic reduction of Cr(VI) by NP-CD follows pseudo-first-order kinetics with a significant R^2 value (Figure 2.4(c)). The rate constant and it's corresponding half-life for different Cr(VI) concentration were shown in Figure 2.4 (d). The plausible mechanism for the photocatalytic Cr(VI) reduction by NP-CD, has been displayed in Figure 2.4(e). Under the influence of sunlight irradiation, holes and electrons are generated in the valence and conduction bands of NP-CD (equation (i)). Further, the photo induced holes react with water molecules to generate highly reactive H+ (as shown in equation (ii)). The photo induced electrons were initially reacting with the

Cr(VI) present near the periphery of the NP-CD as shown in equation (iii). These highly reactive protons and electrons cumulatively reduce Cr(VI) to Cr(III) as shown in equation (iv). The overall mechanism is showing schematically to understand the plausible reason for the photocatalytic reduction of toxic Cr(VI) to less toxic Cr(III). Nevertheless to state about the requirement of the acidic pH, as with the increase in pH towards basic side decreases the photoreduction efficiency of NP-CD [41]. The Cr(III) has been separated from the water by the precipitation in the form of the hydroxides of Cr(III) after the addition of NaOH solution [42].
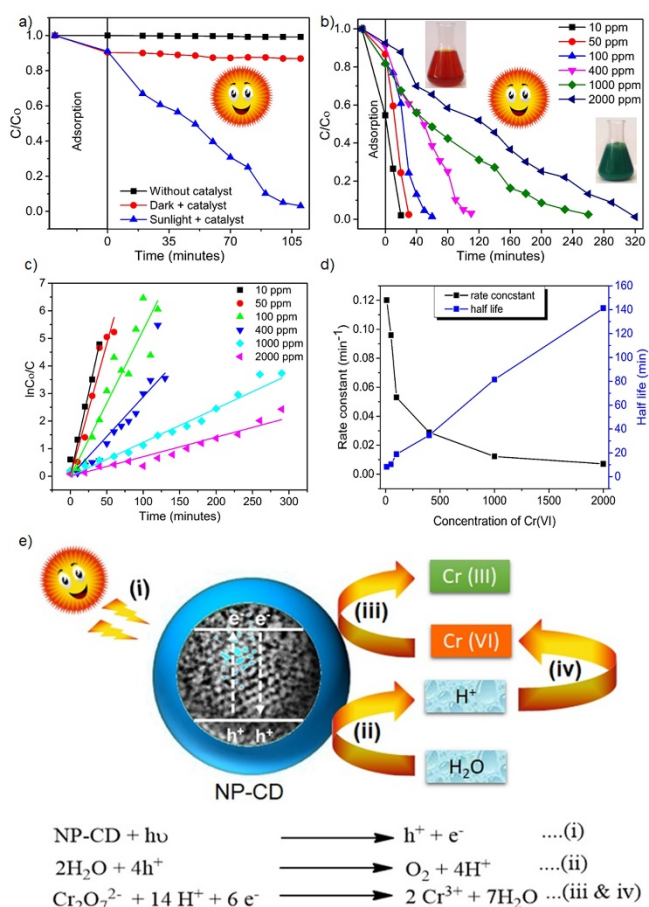

Figure 2.4: (a) Plot of (C/Co) for the photoreduction of the 400 ppm of Cr(VI) by NP-CD under the different condition; b) Plot of (C/Co) for Cr(VI) photoreduction by NP-CD under different concentrations of Cr(VI); c) pseudo-first-order linear fit data with different concentration of Cr(VI); (d) rate constant and half-life graph for the different concentration of Cr (VI) and e) schematic representation of plausible reaction mechanism of photocatalytic reduction of Cr(VI) to Cr(III) under the sunlight irradiation by NP-CD.

2.3.5   Effect of the dopants of N, P on the photoreduction ability of NP-CD towards Cr(VI)

To investigate the effect of N and P content on the photoreduction ability of NP-CD, a control set of experiments was performed using single dopant material such as only N and only P charred with the same amount of polyethylene glycol (control sample) under the similar experimental conditions as being used for the synthesis of NP-CD. Figure 2.5 (a) shows the prominent effect of combined doping of N-P compared to the un-doped (CD) and singly doped CD as (N-CD and P-CD). As well as, the effect of the amount of the reactant has also been investigated on the photoreduction efficiency by changing the reactant concentration to optimize the reaction conditions and obtain the maximum efficiency of photocatalyst. Figure 2. 5 (b-d) shows the effect of varying concentration of each reactant compared to the control (NP-CD). From the Figure 2.5 (b-d) it was concluded that the reactant mixture of 3 g imidazole, 10 mL phosphoric acid and 10 mL polyethylene glycol was the best composition for the fabrication of NP-CD for its potential application in photocatalytic reduction of Cr(VI) to Cr(III). Additionally, under the sunlight irradiation, Figure 2.5(e) shows the extent of photocatalyst loading on the photoreduction efficiency of NP-CD and as expected it was found that on increasing the catalyst dose the rate of the photoreduction becomes faster compared to the lower dose for the same concentrations of Cr(VI) (400 ppm) [43]. When the dose was 0.14 mg mL^{-1} the time required for 400 ppm Cr(VI) reduction was 20 minutes while at 0.07 mg mL^{-1} the time required for photocatalytic reduction was 110 minutes. For the present finding a moderate amount of photocatalyst was being used (0.07 mg mL-1). The NP-CD worked as a stable photocatalyst as observed by its recyclability upto six cycles which shows 98% efficiency for the 400 ppm Cr(VI), is demonstrated in Figure 2. 5(f).
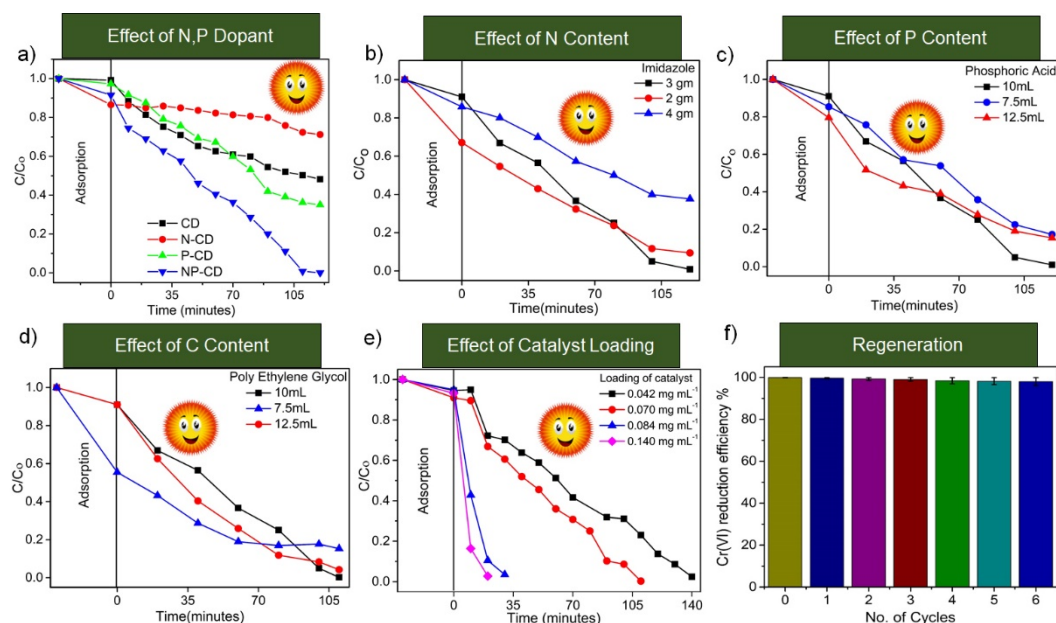
Figure 2.5: a) Effect of the reactant contents of N and P on the working efficiency of the CD; b) effect of imidazole; (c) effect of phosphoric acid; (d) and the effect of polyethylene glycol; e) effect of catalyst loading; f) the photocatalytic performance up to six cycles by the recycling test on the photoreduction efficiency of NP-CD on the 400ppm Cr(VI) under the sunlight irradiation.

2.3.6. Effect of interfering ions and real sample analysis

Further, to explore the possibilities of NP-CD in practical application, the photoreduction ability of NP-CD has been examined in the presence of many other interfering ions. Experimentally separate solutions of the 100 ppm of different interfering[44] ions (as chloride (Cl^-), sulphate (SO_4^{2-}), nitrate (NO_3^-), phosphate (PO_4^{3-}), ferrous (Fe^{2+}) and calcium (Ca^{2+})) along with a mixture that contains all the different interfering ions [44], were mixed into the solutions of 400 ppm Cr(VI) under the similar experimental conditions as discussed above. All the experiment carried out at the dose of photocatalyst (0.07mg mL^{-1}) in 120 minute of sunlight irradiation. After performing the interference study, a minimal decrease in the reduction efficiency of NP-CD observed as shown in Figure 2.6 (a), with different interfering ions and their corresponding mixture compared with the control set containing 400 ppm Cr(VI) solution without any interfering ion. The NP-CD shows an effective and efficient photocatalysis as the 100 ppm concentration of all the interfering ions and its corresponding mixtures does not affect the photoreduction

abilities of NP-CD. Concerning the environmental application, we collected practical lab waste sample from MNIT Jaipur containing Cr(VI) ion which was confirmed by DPC assay. After collecting the sample, we performed the same experiment with same dose of NP-CD (0.07 mg mL-1) under natural sunlight. We took the photo reduced sample after every 20 minute for UV-vis analysis by the DPC assay at a wavelength 540 nm. From UV-vis analysis, we observed that the initial concentration of Cr(VI) in unknown sample was 156 ppm. A ~99 % photoreduction of Cr(VI) to Cr(III) observed in 100 minutes. A plot of C/Co verses time is displayed in Figure 2.6 (b) showing photoreduction of lab waste sample under natural sunlight. The sample without catalyst is termed as control (red line) and with catalyst NP-CD is termed as control-NP-CD (black line).
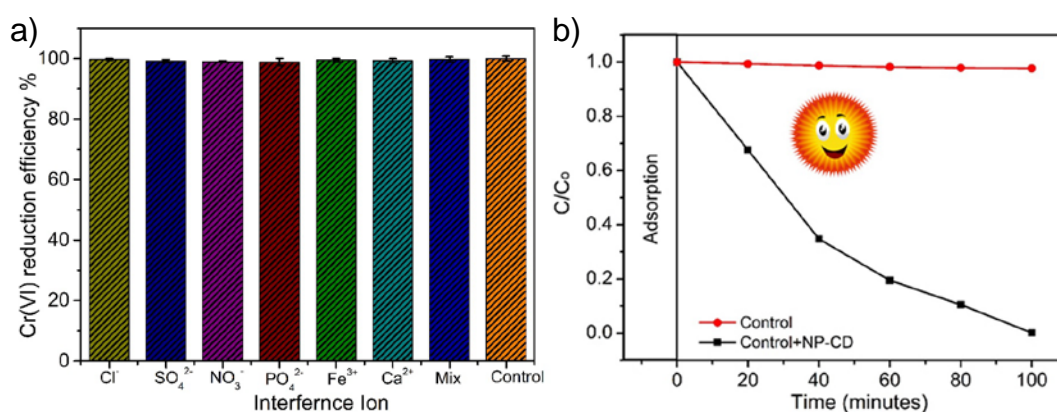
Figure 2.6: (a) Photoreduction efficiency of NP-CD under the different presence of the interfering ions Cl^-, SO_4^{2-}, NO_3^-, PO_4^{3-}, Fe^{2+} and Ca^{2+} along with its mixture which contains 100 ppm of each the interfering ion under the presence of sunlight and (b) Plot of (C/Co) for the photoreduction of industrial sample without NP-CD (red line) and with NP-CD (black line) under the natural sunlight

2.4 Conclusion

The present chapter briefs about the synthesis and exploration of NP-CD as an efficient material for aqueous phase photocatalytic reduction of Cr(VI) to Cr(III) under the influence of natural sunlight. Moreover, the less toxic Cr(III) was removed from the treated water using a simple process of precipitation. The ease in the recyclability along with no apparent loss in the catalytic efficiency could hold a very large, prosperous future of these NP-CD in the field of photocatalytic water

remediation. The structural characteristic of NP-CD could further provide significant potential as priority materials to execute many hidden applications towards the removal of various toxic inorganic and organic pollutants from the wastewater.

2.5   References

[1]   Sun, Y.-P., Zhou, B., Lin, Y., Wang, W., Fernando, K. A. S., Pathak, P., Meziani, M. J., Harruff, B. A., Wang, X., Wang, H., Luo, P. G., Yang, H., Kose, M. E., Chen, B., Veca, L. M., Xie, S.-Y., Quantum-Sized Carbon Dots for Bright and Colorful Photoluminescence. J.Am.Chem.Soc. 2007, 128 (24), 7756-7757.

[2]   Park, Y., Yoo, J., Lim, B., Kwon, W., Rhee, S. W., Improving the Functionality of Carbon Nanodots: Doping and Surface Functionalization. J Mater Chem A 2016, 4 (30), 11582-11603.

[3]   Wang, R., Lu, K.-Q., Tang, Z.-R., Xu, Y.-J., Recent Progress in Carbon Quantum Dots: Synthesis, Properties and Applications in Photocatalysis. J.Mater. Chem. A 2017, 5 (8), 3717-3734.

[4]   Zhijie, Z., Tingting, Z., Xiaoming, L., Jiayue, X., Haibo, Z., Progress of Carbon Quantum Dots in Photocatalysis Applications. Part. Part. Syst. Char. 2016, 33 (8), 457-472.

[5]   Wang, Y., Zhu, Y., Yu, S., Jiang, C., Fluorescent Carbon Dots: Rational Synthesis, Tunable Optical Properties and Analytical Applications. RSC Adv. 2017, 7 (65), 40973-40989.

[6]   Khare, P., Bhati, A., Anand, S. R., Gunture, Sonkar, S. K., Brightly Fluorescent Zinc-Doped Red-Emitting Carbon Dots for the Sunlight-Induced Photoreduction of Cr(VI) to Cr(III). ACS Omega 2018, 3 (5), 5187-5194.

[7]   Bhati, A., Anand, S. R., Gunture, Garg, A. K., Khare, P., Sonkar, S. K., Sunlight-Induced Photocatalytic Degradation of Pollutant Dye by Highly Fluorescent Red-Emitting Mg-N-Embedded Carbon Dots. ACS Sustainable Chem. Eng. 2018.

[8]   Chandra, S., Dipranjan, L., Arindam, P., Angshuman, R. C., Parimal, K., Kumar, S. S., Synthesis of Highly Fluorescent Nitrogen and Phosphorus Doped Carbon Dots for the Detection of Fe^{3+} Ions in Cancer Cells. Luminescence 2016, 31 (1), 81-87.

[9]   Gong, Y., Yu, B., Yang, W., Zhang, X., Phosphorus, and Nitrogen Co-Doped Carbon Dots as a Fluorescent Probe for Real-Time Measurement of

Reactive Oxygen and Nitrogen Species inside Macrophages. Biosens. Bioelectron. 2016, 79, 822-828.

[10] Xu, Q., Li, B., Ye, Y., Cai, W., Li, W., Yang, C., Chen, Y., Xu, M., Li, N., Zheng, X., Street, J., Luo, Y., Cai, L., Synthesis, Mechanical Investigation, and Application of Nitrogen and Phosphorus Co-Doped Carbon Dots with a High Photoluminescent Quantum Yield. Nano Research 2017, 1.

[11] Wu, H., Mi, C., Huang, H., Baofu, H., li, J., Xu, S., Solvothermal Synthesis of Green-Fluorescent Carbon Nanoparticles and Their Application, 2012.

[12] Li, H., Shao, F.-Q., Zou, S.-Y., Yang, Q.-J., Huang, H., Feng, J.-J., Wang, A.-J., Microwave-Assisted Synthesis of N,P-Doped Carbon Dots for Fluorescent Cell Imaging. Microchim. Acta 2016, 183 (2), 821-826.

[13] Liu, R., Zhao, J., Huang, Z., Zhang, L., Zou, M., Shi, B., Zhao, S., Nitrogen and Phosphorus Co-Doped Graphene Quantum Dots as a Nano-Sensor for Highly Sensitive and Selective Imaging Detection of Nitrite in Live Cell. Sens. Actuators, B 2017, 240, 604-612.

[14] Ananthanarayanan, A., Wang, Y., Routh, P., Sk, M. A., Than, A., Lin, M., Zhang, J., Chen, J., Sun, H., Chen, P., Nitrogen and Phosphorus Co-Doped Graphene Quantum Dots: Synthesis from Adenosine Triphosphate, Optical Properties, and Cellular Imaging. Nanoscale 2015, 7 (17), 8159-8165.

[15] Sun, X., Brückner, C., Lei, Y., One-Pot and Ultrafast Synthesis of Nitrogen and Phosphorus Co-Doped Carbon Dots Possessing Bright Dual Wavelength Fluorescence Emission. Nanoscale 2015, 7 (41), 17278-17282.

[16] Gong, X., Zhang, Q., Gao, Y., Shuang, S., Choi, M. M. F., Dong, C., Phosphorus and Nitrogen Dual-Doped Hollow Carbon Dot as a Nanocarrier for Doxorubicin Delivery and Biological Imaging. ACS Appl Mater & Interfaces 2016, 8 (18), 11288-11297.

[17] Li, R., Wei, Z., Gou, X., Nitrogen and Phosphorus Dual-Doped Graphene/Carbon Nanosheets as Bifunctional Electrocatalysts for Oxygen Reduction and Evolution. ACS Catalysis 2015, 5 (7), 4133-4142.

[18] Tripathi, K. M., Singh, A., Myung, Y., Kim, T., Sonkar, S. K., Sustainable Nanocarbons as Potential Sensor for Safe Water. In Nanotechnology for Sustainable Water Resources, 2018; pp 141-176.

[19]   Tripathi, K. M., Gupta, N. R., Sonkar, S. K., Nano-Carbons from Pollutant Soot: A Cleaner Approach toward Clean Environment. In Smart Materials for Waste Water Applications, 2016; Vol. 1, pp 127-154.

[20]   Han, M., Zhu, S., Lu, S., Song, Y., Feng, T., Tao, S., Liu, J., Yang, B., Recent Progress on the Photocatalysis of Carbon Dots: Classification, Mechanism and Applications. Nano Today 2018, 19, 201-218.

[21]   Liu, S., Hu, Q., Qiu, J., Wang, F., Lin, W., Zhu, F., Wei, C., Zhou, N., Ouyang, G., Enhanced Photocatalytic Degradation of Environmental Pollutants under Visible Irradiation by a Composite Coating. Environmental Science & Technology 2017, 51 (9), 5137-5145.

[22]   Ameta, R., Benjamin, S., Ameta, A., Ameta, S., Photocatalytic Degradation of Organic Pollutants: A Review, 2012.

[23]   Khare, P., Singh, A., Verma, S., Bhati, A., Sonker, A. K., Tripathi, K. M., Sonkar, S. K., Sunlight-Induced Selective Photocatalytic Degradation of Methylene Blue in Bacterial Culture by Pollutant Soot Derived Nontoxic Graphene Nanosheets. ACS Sustainable Chem. Eng. 2018, 6 (1), 579-589.

[24]   Bhati, A., Singh, A., Tripathi, K. M., Sonkar, S. K., Sunlight-Induced Photochemical Degradation of Methylene Blue by Water-Soluble Carbon Nanorods. Int J Photoenergy 2016, 2016, 8.

[25]   Omole, M. A., K'Owino, I. O., Sadik, O. A., Palladium Nanoparticles for Catalytic Reduction of Cr(VI) Using Formic Acid. Appl. Catal., B 2007, 76 (1), 158-167.

[26]   Yang, Y., Wang, G., Deng, Q., Ng, D. H. L., Zhao, H., Microwave-Assisted Fabrication of Nanoparticulate Tio2 Microspheres for Synergistic Photocatalytic Removal of Cr(VI) and Methyl Orange. ACS Appl Mater & Interfaces 2014, 6 (4), 3008-3015.

[27]   Abdullah, H., Kuo, D.-H., Facile Synthesis of N-Type (Agin)Xzn2(1– X)S2/P-Type Ag2s Nanocomposite for Visible Light Photocatalytic Reduction to Detoxify Hexavalent Chromium. ACS Appl Mater & Interfaces 2015, 7 (48), 26941-26951.

[28]   Ma, H.-L., Zhang, Y., Hu, Q.-H., Yan, D., Yu, Z.-Z., Zhai, M., Chemical Reduction and Removal of Cr(VI) from Acidic Aqueous Solution by

Ethylenediamine-Reduced Graphene Oxide. J Mater Chem 2012, 22 (13), 5914-5916.

[29]   Verma, N. K., Khare, P., Verma., N., Synthesis of Iron-Doped Resorcinol Formaldehyde-Based Aerogels for the Removal of Cr(VI) from Wate. Green Process Synth 2015, 4 (1), 37-46.

[30]   Khare, P., Yadav, A., Ramkumar, J., Verma, N., Microchannel-Embedded Metal–Carbon–Polymer Nanocomposite as a Novel Support for Chitosan for Efficient Removal of Hexavalent Chromium from Water under Dynamic Conditions. Chem. Eng. J. 2016, 293 (Supplement C), 44-54.

[31]   Crosby, G. A., Demas, J. N., Measurement of Photoluminescence Quantum Yields. Review. J Phys Chem 1971, 75 (8), 991-1024.

[32]   Nxumalo, E., Coville, N., Nitrogen Doped Carbon Nanotubes from Organometallic Compounds: A Review, 2010.

[33]   Zikalala, S. A., Kuvarega, A. T., Mamba, B. B., Mhlanga, S. D., Nxumalo, E. N., The Effect of Synthetic Routes on the Physicochemical Properties and Optical Response of N-Doped Titania–Oxidized Carbon Nanotube Nanohybrids. Materials Today Chemistry 2018, 10, 1-18.

[34]   Tripathi, K. M., Bhati, A., Singh, A., Gupta, N. R., Verma, S., Sarkar, S., Sonkar, S. K., From the Traditional Way of Pyrolysis to Tunable Photoluminescent Water Soluble Carbon Nano-Onions for Cells Imaging and Selective Sensing of Glucose. RSC Adv. 2016, 6, 37319-37340.

[35]   Tripathi, K. M., Bhati, A., Singh, A., Sonker, A. K., Sarkar, S., Sonkar, S. K., Sustainable Changes in the Contents of Metallic Micronutrients in First Generation Gram Seeds Imposed by Carbon Nano-Onions: A Life Cycle Seed to Seed Study. ACS Sustainable Chem. Eng., 2017, 5 (4), 2906–2916.

[36]   Zheng, B., Liu, T., Paau, M. C., Wang, M., Liu, Y., Liu, L., Wu, C., Du, J., Xiao, D., Choi, M. M. F., One Pot Selective Synthesis of Water and Organic Soluble Carbon Dots with Green Fluorescence Emission. RSC Advances 2015, 5 (15), 11667-11675.

[37]   Song, Z., Quan, F., Xu, Y., Liu, M., Cui, L., Liu, J., Multifunctional N,S Co-Doped Carbon Quantum Dots with Ph- and Thermo-Dependent Switchable

Fluorescent Properties and Highly Selective Detection of Glutathione. Carbon 2016, 104, 169-178.

[38] Sun, D., Ban, R., Zhang, P.-H., Wu, G.-H., Zhang, J.-R., Zhu, J.-J., Hair Fiber as a Precursor for Synthesizing of Sulfur- and Nitrogen-Co-Doped Carbon Dots with Tunable Luminescence Properties. Carbon 2013, 64, 424-434.

[39] Dong, Y., Pang, H., Yang, H. B., Guo, C., Shao, J., Chi, Y., Li, C. M., Yu, T., Carbon-Based Dots Co-Doped with Nitrogen and Sulfur for High Quantum Yield and Excitation-Independent Emission. Angew. Chem.Int.Ed 2013, 52 (30), 7800-7804.

[40] Lin, Z., Waller, G., Liu, Y., Liu, M., Wong, C.-P., Facile Synthesis of Nitrogen-Doped Graphene Via Pyrolysis of Graphene Oxide and Urea, and Its Electrocatalytic Activity toward the Oxygen-Reduction Reaction. Adv. Energy Mater. 2012, 2 (7), 884-888.

[41] Shao, D., Wang, X., Fan, Q., Photocatalytic Reduction of Cr(Vi) to Cr(Iii) in Solution Containing Zno or Zsm-5 Zeolite Using Oxalate as Model Organic Compound in Environment. Microporous and Mesoporous Materials 2009, 117 (1), 243-248.

[42] Zhong, Y., Qiu, X., Chen, D., Li, N., Xu, Q., Li, H., He, J., Lu, J., Flexible Electrospun Carbon Nanofiber/Tin(Iv) Sulfide Core/Sheath Membranes for Photocatalytically Treating Chromium(VI)-Containing Wastewater. ACS Appl Mater & Interfaces 2016, 8 (42), 28671-28677.

[43] Shirzad-Siboni, M., Farrokhi, M., Darvishi Cheshmeh Soltani, R., Khataee, A., Tajassosi, S., Photocatalytic Reduction of Hexavalent Chromium over Zno Nanorods Immobilized on Kaolin. Ind. Eng. Chem. Res 2014, 53 (3), 1079-1087.

[44] Djellabi, R., Ghorab, M. F., Photoreduction of Toxic Chromium Using Tio2-Immobilized under Natural Sunlight: Effects of Some Hole Scavengers and Process Parameters. Desalination and Water Treatment 2015, 55 (7), 1900-1907.

Chapter-3
Sunlight-Induced Photocatalytic Degradation of Pollutant Dye by Highly Fluorescent Red-Emitting Mg-N-Embedded Carbon Dots
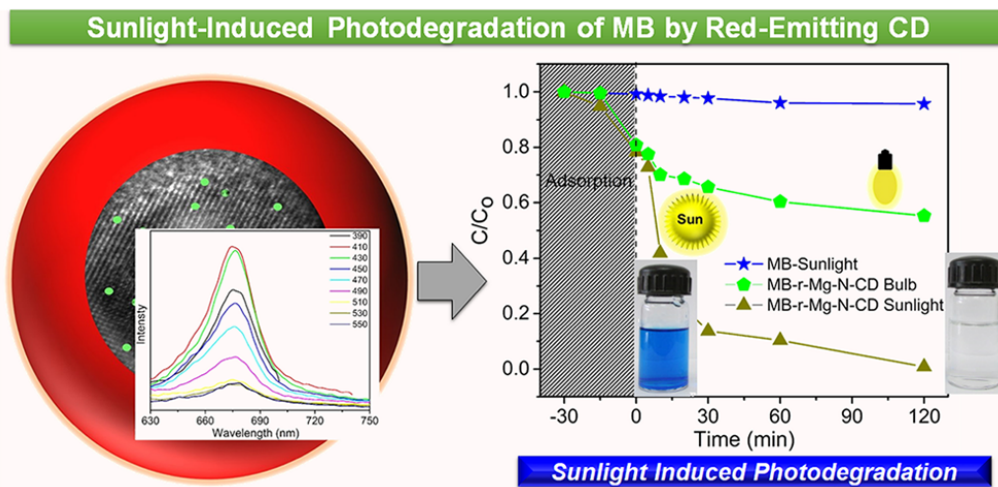
3.1 Introduction

Presently, advances to explore the nontoxic-biocompatible probes8 working in the long-wavelength region of the spectrum (red and NIR) for the *in vivo* photoluminescent imaging have gained a lot of interest [1]. These probes are expected to enable safer in-depth imaging of cells, tissues and organs. The red and NIR regions constitutes the most suitable part of the spectrum that showed minimally intrusive absorption and self-fluorescence from the biological samples [2,3]. For this, significant efforts are already being taken for developing the highly fluorescent semiconductor QD and organic dyes as a fluorescent probe for bioimaging applications [4,5]. However, the long-known biological constraint for the use of QD is its lower solubility and toxicity as well as the photobleaching effects associated with the fluorescent organic dyes, which certainly limit their long-term uses for biological applications [6,7]. Concerning the biocompatibility, photostability and the high competitive QY values of highly photoluminescent probes, CD [8,9] and GQD [10,11] can be a better alternative [12-19]. Nevertheless, along with being explored everywhere, including the few reports on its photocatalytic applications [20−39]. The red and NIR emission of CD/GQD can be further explored on the basis of surface modifications and choosing a different carbon precursor [40−44]. A few groups have investigated the synthesis of red emitting CD/GQD, based on hydrothermal [45−47], solvothermal [48] and microwave [49−51] assisted methods using different synthetic precursor materials. These precursor materials have included o-phenyldiamine and phosphoric acid [52], thiourea and citric acid [53], lemon pulp [46], mango leaves [49] and they have been used these red-emitting CD/GQD for the multipurpose applications [46−51,53−55]. The most common observation noted for the emission in the higher-wavelength region in the published reports [40,45−49,51,53−57] was the influence of the incorporation/doping of heteroatoms [48,51−54,57].

The present finding describes in this chapter related to an easier approach for the fabrication of water-soluble red emitting magnesium nitrogen embedded cabon dots termed as "r-Mg-N-CD" from the leaves of a readily available ornamental plant named *Bougainvillea*. Importantly, the newer perspective concerning the use of red-

emitting synthesized r-Mg-N-CD has been experimentally explored as a potential photocatalyst material, for the photodegradation of pollutant organic dye named MB.

3.2   Experimental Section

3.2.1   Materials and Reagents

All chemical reagents of analytical grade and used without further purification.

3.2.2   Instrumentation

TEM, XPS, FTIR and UV-Vis instrumentation were same as described in Chapter 2.The topography and thickness of r-Mg-N-CD were analyzed by using a Pico SPM (Molecular Imaging) AFM. Spectroscopy: PL spectrometry analyses in aqueous solutions were conducted at room temperature with a PerkinElmer LS55 spectrophotometer. fluorescence microscopy: The optical images of r-Mg-N-CD were analyzed with a Leica inverted microscope (Leica DM 2500, Leica microscopy system Ltd.) under 562 nm band-pass filters. ^{1}H NMR measurements were recorded on a JEOL ECS-400 (operating at 400 MHz, in D_2O solvent).

3.2.3   Synthesis of r-Mg-N-CD

r-Mg-N-CD were synthesized from *Bougainvillea* plants via a green synthesis process. The young plant leaves, mostly from the 3–5th internode of the younger green branches, were taken and washed repeatedly with DI water in order to remove soluble impurities and were kept at room temperature (±30°C) for evaporation of DI water. The fresh leaves were chopped into ∼1 cm size and blended with a hand blender after these blended leaves (∼10 g) were mixed in 100 mL of ethanol/water (1:1) solution for 10 min at 40°C kept on sonication. The extract of leaves was carbonized for 15 min at 90% power (1400 W) in a domestic microwave oven. The as-produced sample was sonicated followed by high-speed centrifugation at ∼7000 rpm for 30 min. Further, the supernatant solution transferred to a glass Petri dish and dried on water bath to yield the powdered sample. The dried powder sample was named as r-Mg-N-CD having the quantitative yield of ∼70% (with respect to as-prepared bulk sample), possessing the QY of ∼40%. The

photographic image of r-Mg-N-CD taken in the ethanol/water solution (1:1) [49]. For the control, the photodegradation efficiency of leaf extract (as a control test) compared with r-Mg-N-CD sample was checked and its photodegradation efficiency was found to be ineffective over the same time-period. The QY was measured with reference to NB. QY of r-Mg-N-CD were determined by using NB [58]. The QY of the NB is 0.27 [59].

3.2.4   Photocatalytic Activity Measurement

The photocatalytic activity of r-Mg-N-CD samples was determined by the degradation of MB, a heteropolyaromatic dye, in aqueous solution under direct sunlight. A stock solution of MB with a concentration of 20 mg L^{-1} was prepared in DI water for photocatalytic degradation. In a typical process, 150 mg of r-Mg-N-CD were added in 50 mL of prepared MB solution and stirred for 30 min in the dark to reach the adsorption and desorption equilibration. The solutions were then exposed to direct sunlight. During the photocatalytic tests, fixed amounts of the photoreacted solution were taken at time intervals of 30 min. The collected solution centrifuged and the supernatant collected in a quartz cuvette for determining MB concentration in the supernatant by using UV–vis absorbance spectroscopy at wavelength 664 nm. Further, these samples dried to carry out the ^{1}H NMR analysis to distinguish the degraded products formed. The r-Mg-N-CD regenerated by initial washing with dil.HCl followed by repeatedly washing with DI water till the pH of solution become neutral.

3.3   Results and Discussion

A simple synthesis of r-Mg-N-CD is presented schematically in Scheme 3.1. The two-step synthetic process involved the extraction of *Bougenvillea* leaves extract into the mixture of ethanol/water (1:1), followed by the charring step in the domestic microwave. As-synthesized r-Mg-N-CD showed excitation-independent red emission profile located at ∼678 nm. Apart from the routine biocompatible imaging [40,46,48,49,55,57] and sensing applications [49,51,54] as shown in Table 3.1, herein these red emitting r-Mg-N-CD are used for the photocatalytic aqueous phase degradation of MB. Under the influence of natural sunlight, r-Mg-N-CD showing faster (∼6 times) rate of photodegradation of MB (in comparison to the

artificial light of a 100 W tungsten bulb). The as-obtained r-Mg-N-CD showed its significant expression, related to the excitation independent red emissions with high QY of ~40% (on separation reached up to ~48%) and an excellent photostability. The high values of QY with emission at the longer wavelength (~678 nm) made this material comparative to the already existing red-emitting QD [60].

Table 3.1. Comparative Table Showing Synthesis and Application of Existing Red-Emitting CD/GQD

Source	Method	Synthesis condition	Diameter	Excitation (λ_{ex} nm)	Emission [λ_{em} nm)	QY (%)	Application	Ref.
Citric acid / Formamide	Microwave chemical reactor	1 h (400 W) 160°C	4.0	540 Independent	640	22.9	Imaging, Drugs Delivery	[50]
p-phenylenediamine / ethanol	Solvothermal	12 h 180°C	10.0	365	604	26.1	Imaging	[48]
Urea / phenylenediamine/ Water	Hydrothermal	10 h 160°C	2.6	510 Independent	625	35	Imaging	[45]
citric acid / polyethylenimine / ethylene glycol	Heating	180°C	5–11	355 Independent	710	--	--	[52]
pulp-free lemon juice / ethanol	Solvothermal	10 h 190°C	4.6	533 Independent	631	28	Bioimaging	[46]
2,5-diaminobenzenesulfonic acid / 4-aminophenylboronic acid Hydrochloride / water	Hydrothermal	8 h 180°C	2.4 ± 0.6	500 Independent	600	5.4	Sensing of Fe^{3+} Imaging	[54]
citric acid /thiourea / acetone	Hydrothermal	8h 160°C	4.42 ± 0.67	560 Dependent	594	29-22	Imaging Biocompatibility	[53]

| Source	Method	Synthesis condition	Diameter	Excitation (λ_{ex} nm)	Emission [λ_{em} nm)	QY (%)	Application	Ref.
p-phenylenediamine / phosphorus acid / water	Hydrothermal	24h 180°C	2.4	530 Independent	620	10	Latent fingerprint	[47]
Mango leaves / ethanol	Microwave Oven	5 min 900 W	2-8	400 Independent	680	--	Bioimaging/ sensing study	[49]
p-phenylenediamine/ Ethanol/ water	Microwave	1h 800 W	2.2-6.5	480 Independent	615	15	Sensing Imaging	[51]
Dried VCX-72 carbon black/ HNO$_3$	Ultrasonic cell crusher	24 h 10 min 950 W	3.9, 9.5	445 nm	622	--	Imaging	[40]
Ascorbic acid/ oleylamine	Heating	4h 280°C	3-8 nm	400-550 nm Dependent	625	~ 14	Imaging	[55]
Paraphenylenediamine/ Ethanol/ water	Microwave-assisted	60 min 900 W	~6 nm	380	630	50	Luminescence Imaging	[66]
Bougainvillea leaves extract	Microwave-assisted	15 min 1260 W	~16-18	420	678	40	Photocatalytic degradation	This work
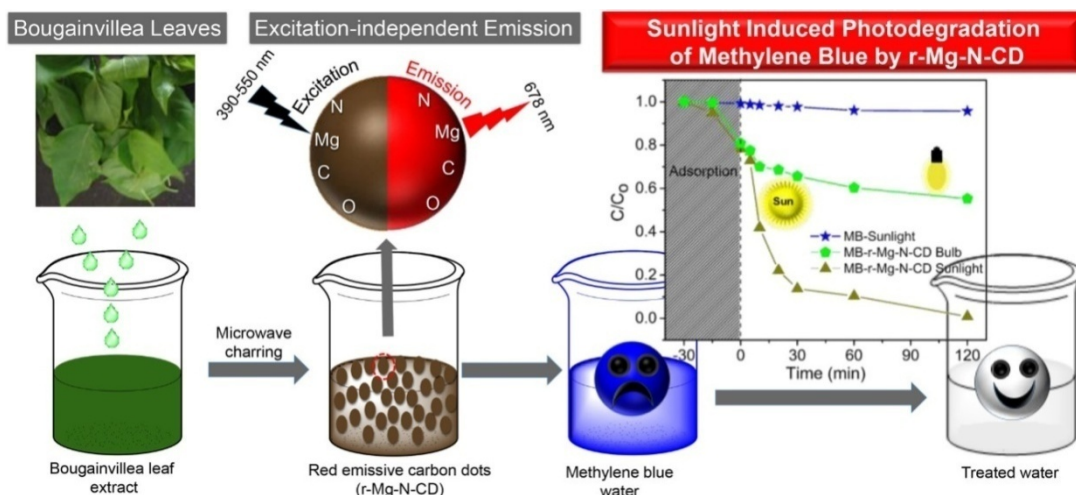
Scheme 3.1. Schematic Diagram Showing the Simple Synthesis of r-Mg-N-CD and Its Application in Sunlight-Induced Photodegradation of MB

3.3.1 Microscopic Analysis

The surface morphology and the internal characterization of the graphitic arrangement of r-Mg-N-CD analyzed by TEM, HRTEM and AFM. Figure 3.1a shows the TEM images of segregated fraction of r-Mg-N-CD as separated from the bulk (as produced sample) by the 30 min sonication followed by high-speed centrifugation. The TEM image (Figure 3.1a) of r-Mg-N-CD show the well-dispersed particles. Figure 3.1b shows the Gaussian fitting size distribution curves of its corresponding TEM images, possess a size distribution of ∼4–18 nm with an average diameter of 10.9 ± 2.8 nm. The internal structural characterization of the r-Mg-N-CD were displayed by the HRTEM images in Figure 3.1c, d. Figure 3.1c shows the two different arrangements of graphitic packing as interplanar fringes within the same sphere (circled as red). Figure 3.1d, displayed the zoomed image of Figure 3.1c, which supports the observation of two different phases of the arrangements of Mg and C with different interplanar distance ∼0.15 and 0.22 nm, respectively [61]. Figure 3.1e shows the topographic AFM image of the r-Mg-N-CD and Figure 3.1f representing the height profile analysis of the Figure 3.1e.
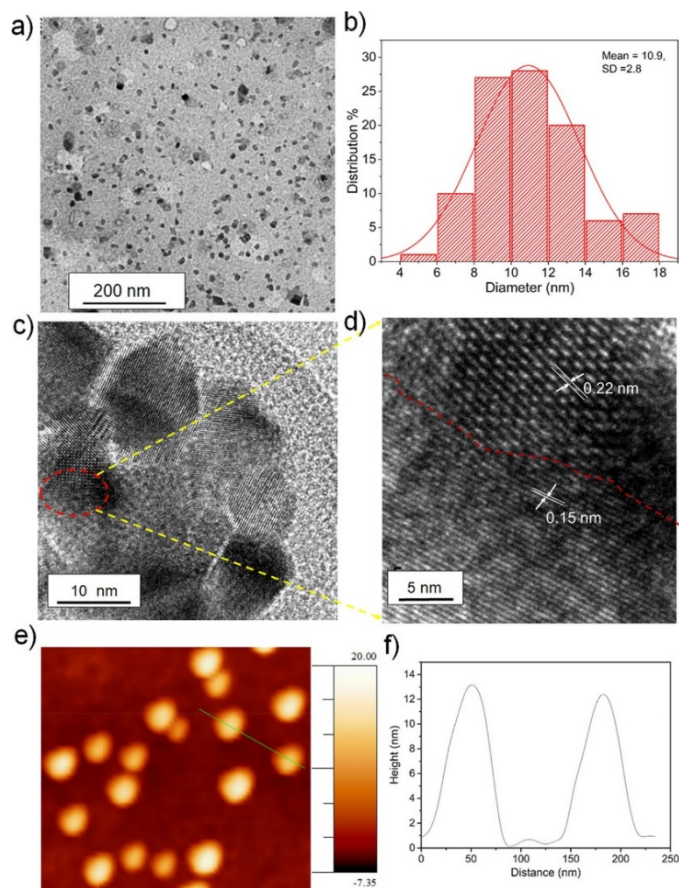
Figure 3.1: (a) TEM image of r-Mg-N-CD; (b) its corresponding size distribution; (c) HRTEM image of r-Mg-N-CD; (d) zoomed image of (c); (e) AFM image of the r-Mg-N-CD and; (f) corresponding height profile image.

3.3.2. Optical Properties: Absorbance and Fluorescence Analysis

The optical behavior of r-Mg-N-CD investigated by UV–visible and fluorescence spectroscopy as illustrated in Figure 3.2a–d. The UV–vis (Figure 3.2a) of the r-Mg-N-CD shows the four different absorption peaks at ~270, ~325, ~420 and ~674 nm, which are due to the presence of diverse and several complicated surface functional states. The absorption peak located at ~270 nm corresponds to C=C bonds (π–π* transitions) and the peaks at 325 and 420 nm were due to n−π* transition, which may be generated because of the presence of C=O or C=N associated with the graphitic framework of r-Mg-N-CD [47,53]. The absorbance peak at higher wavelength ~674 nm arises because of charge transfer between the metal–ligand bonding. Figure 3.2b shows the most prominent aspect of r-Mg-N-CD as its excitation independent red fluorescence, which can be ascribed to the

incorporation/doping of heteroatoms [47,56]. Herein, this can be explained based on embedding of Mg–N within the graphitic carbon framework of CD. Figure 3.2c displays the excellent stability of r-Mg-N-CD toward a photobleaching experiment performed for 5 h at the continuous irradiation at 420 nm excitation. Figure 3.2d displayed the fluorescence images of r-Mg-N-CD (by evaporating a dilute aqueous solution) on the glass slide under the red band-pass filter of 562 nm.
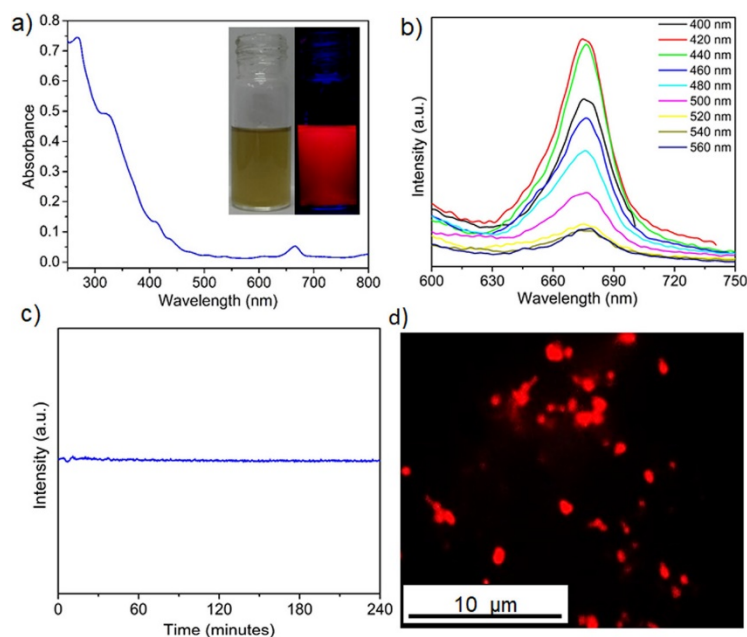

Figure 3.2: (a) UV–vis spectra, inset of (a) digital photographic image of the r-Mg-N-CD irradiated under daylight (left) and under UV light (right); (b) excitation independent fluorescence emission spectra of r-Mg-N-CD (excited from 400 to 560 nm with the increment of 20 nm toward the higher wavelength; (c) photostability of r-Mg-N-CD under 5 h of continuous 420 nm excitation wavelength and (d) fluorescence microscopic images of r-Mg-N-CD at 562 nm band pass filter.

3.3.3 FT-IR and XPS:

The presence of complex surface functionalities of r-Mg-N-CD, investigated using the FT-IR and XPS. The FT-IR spectra (Figure 3.3a) of r-Mg-N-CD shows the several stretching vibrations associated with bonded hydrogen as O–H (3401–3200 cm^{-1} (broad)), $=$C–H and $-$C–H at, 3035 cm^{-1} (weak) and 2923 and 2859 cm^{-1} (weak, doublet). A few merged peaks of C$=$O and C$=$C stretching vibrations were found at 1728 and 1624 cm^{-1}, respectively. The merged peaks at 1400 cm^{-1} arise because of unsymmetrical stretching vibrations of $-$CH$_2$ group and aryl C–N

stretching vibrations, respectively, confirming the embedding of nitrogen. The merged peaks at 1114 and 1067 cm^{-1} correspond to the −C–O– stretching and −CH bending vibrations, respectively. Importantly, a peak situated at ∼516 cm^{-1} was due to the metal–ligand bending vibrations (confirming the presence of Mg) [62]. The embedding of Mg and N in r-Mg-N-CD were confirmed by XPS analysis and described in Figure 3.3b–g. A survey XPS scan confirms the existence of the C, N, O and Mg, within the r-Mg-N-CD. The XPS survey scan showed the peaks at 284.0, 531.4, 399.1, 56 and 89 eV associated with the presence of C$_{1s}$ (76.7%), O$_{1s}$ (11.4%), N$_{1s}$ (6.9%), Mg$_{2p}$(2.9%) and Mg$_{2s}$ (2.1%) as displayed in Figure 3.3b,c where Figure 3.3c is the zoomed image of Figure 3.3b showing the presence of Mg$_{2p}$ and Mg$_{2s}$. Moreover, the high-resolution XPS spectra over the deconvolution showed the presence of different metal-binding sites of C, N and O. The high-resolution XPS short scan of C$_{1s}$ as shown in Figure 3.3d on deconvolution displays the several C-binding sites at 282.5 eV (C–Mg), 283.4 eV (C=C), 284.1 eV (C–C), 285.1 eV (C–O/N), 286.5 eV (C=O) and 291.5 eV (π–π* satellite). Similarly, for the others, the O$_{1s}$ deconvolution shows different binding with C and Mg at 528.9 eV (O–Mg), 531.2 eV (C–O) and 532.9 eV (C=O) (Figure 3.3e) [63]. The deconvolution of N$_{1s}$ show peaks at 397.1 eV (Mg–N), 398.2 eV (pyrrolic N), 399.2 eV (pyridinic N) and 400.5 eV (graphitic N) (Figure 3.3f) [47]. Figure 3.3g showed the deconvolution peaks of Mg$_{2p}$ at 49.3 eV (Mg–O) and 47.3 eV (Mg–C) [64, 65].
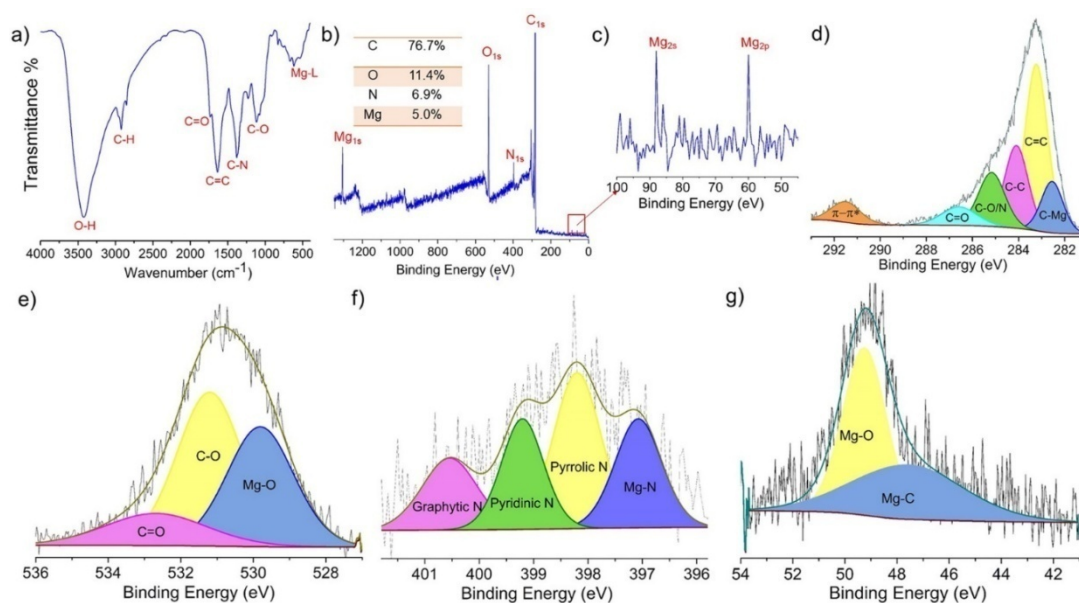
Figure 3.3: (a) FTIR spectra; (b) Survey scan of r-Mg-N-CD; (c) zoomed image of; (b) and its corresponding short scan; (d) C$_{1s}$; (e) O$_{1s}$; (f) N$_{1s}$ and (g) Mg$_{2p}$.

### 3.3.4 Sunlight-Induced Photocatalytic Degradation of MB

The presented finding deals with the newer application of r-Mg-N-CD, used for the photodegradation of MB under the influence of natural sunlight, apart from the long-known conventional applications of CD [40,45−49,51,53,54,57]. The significant influence of the sustainable sunlight can be better explained by a comparative analysis using an artificial light (100 W tungsten bulb). The continuous decrease in the concentration of MB by the r-Mg-N-CD interaction under the influence of the different sources of light plotted as the relative change in the concentration of the MB with a function of time (Figure 3.4a). As shown in Figure 3.4a, the results indicate that the as-synthesized r-Mg-N-CD under the 120 min of sunlight irradiation achieves the highest photocatalytic activity (99.1%), compared with the 100 W tungsten bulb (45%). As a control, the degradation efficiency of MB alone was also checked under the presence of sunlight and showed no significant change. The same figure also includes the data of the experiment that was performed in the dark. Therefore, comparing the result as shown in Figure 3.4a explicitly indicates the significant influence of sunlight on the aqueous-phase photodegradation of MB by r-Mg-N-CD. Figure 3.4b shows the corresponding rate constant values obtained from fitting the experimental data with the Langmuir–Hinshelwood model for the apparent first-order kinetics model and $t_{1/2}$ values obtained for MB degradation at different condition using r-Mg-N-CD. The small value of $t_{1/2}$ under the sunlight indicates the high photocatalytic activity of r-Mg-N-CD with high values of the rate constant for the photodegradation of MB, compared with other conditions (dark and in the light of 100 W tungsten bulb). The interaction of r-Mg-N-CD under irradiation with different light sources investigated by UV–vis DRS [35,67−69]. Figure 3.4c shows the absorption edge near ∼673 nm, which corresponds to the band gap of r-Mg-N-CD. Figure 3.4d shows the Tauc plots (($\alpha h\upsilon)^2$ vs hυ) and indicates the measured band gap for r-Mg-N-CD were 1.45 eV, whereas their values decreased when sensitized with 100 W bulb light (1.42 eV) and 1.38 eV sunlight[70]. The experimental observation (Figure 3.4d) based on diffuse reflectance are consistent with the photodegradation rate constant and $t_{1/2}$ values as shown Figure 3.4b. That shows the decrease in band gap, particularly toward an efficient visible light range enhanced the photocatalysis process for MB degradation.
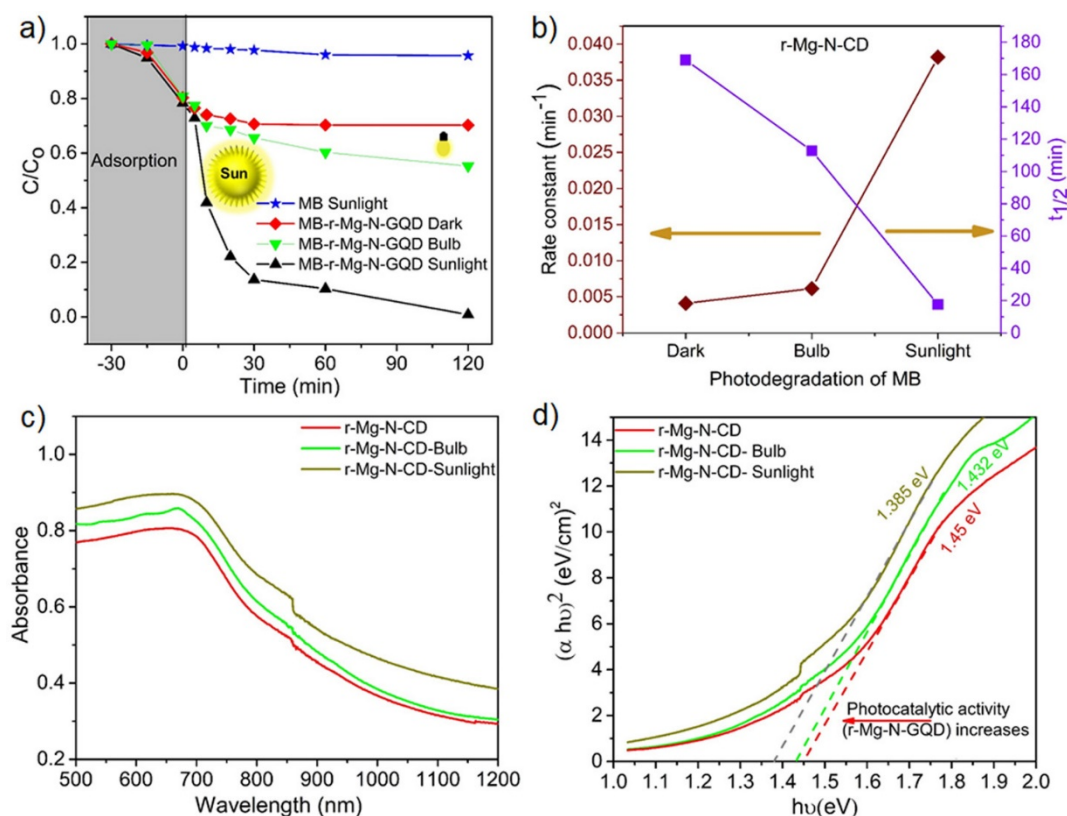
Figure 3.4: (a) Plot of (C/C$_o$) for MB photodegradation by r-Mg-N-CD under different condition; (b) Comparative data of first order rate constant and half-life ($t_{1/2}$) in minutes obtained from experimental data; UV−vis diffuse reflectance absorption spectra (c) and Tauc plots ($\alpha h\upsilon$)^2 versus photo energy (hυ) (d) of r-Mg-N-CD in different light sources.

Further, the most valuable prospect regarding the plausible degradation mechanism of the MB by r-Mg-N-CD under the presence of sunlight can be easily explained on the basis of the trapping experiment (Figure 3.5a–d). In aqueous medium, a photocatalyst under sunlight irradiation generates three types of reactive species as superoxide, holes and hydroxyl radicals, which are responsible for photodegradation of the organic compounds [28,43,71−74]. To understand the specific roles of reactive species, the trapping experiment (including the control set (0.0 mM concentration of scavengers)) was performed using three different types of scavengers: like the p-BZQ as a scavenger for the trap of O$_2^-$; Na$_2$-EDTA for the trapping of h$^+$; and t-BA for the trapping of HO· radicals as shown in (Figure 3.7a–c) respectively [43,71-73]. The molar concentration of the scavengers varied from 0.0, 0.5, 1.0 and 5 mM in an aqueous system of MB-r-Mg-N-CD, as shown in

Figure 3.7. Figure 3.7a shows that the photodegradation activity significantly reduced by ~55% in the presence of 0.5 mM of p-BZQ. However, in the same Figure 3.5b, c), the photocatalytic efficiency was reduced ~by 25% (Figure 3.5b, c) in the presence of Na_2-EDTA and t-BA having the same concentration of scavenger as 0.5 mM, advocating the relatively strong influence of superoxide radicals in the process of photodegradation. Although from Figure 3.5d, it was notable to observe that on further increasing the concentration of respective scavenger, a marginal decrement was noticed for MB degradation by r-Mg-N-CD in sunlight. Therefore, the data supports that holes and hydroxyl radicals also participate with superoxide for MB degradation; however, it is relatively less dominant than that of superoxide. Overall, the superoxide radicals are not solely responsible toward the complete breakdown of the MB, nevertheless, its influence is more prominent compared with the other two reactive species.
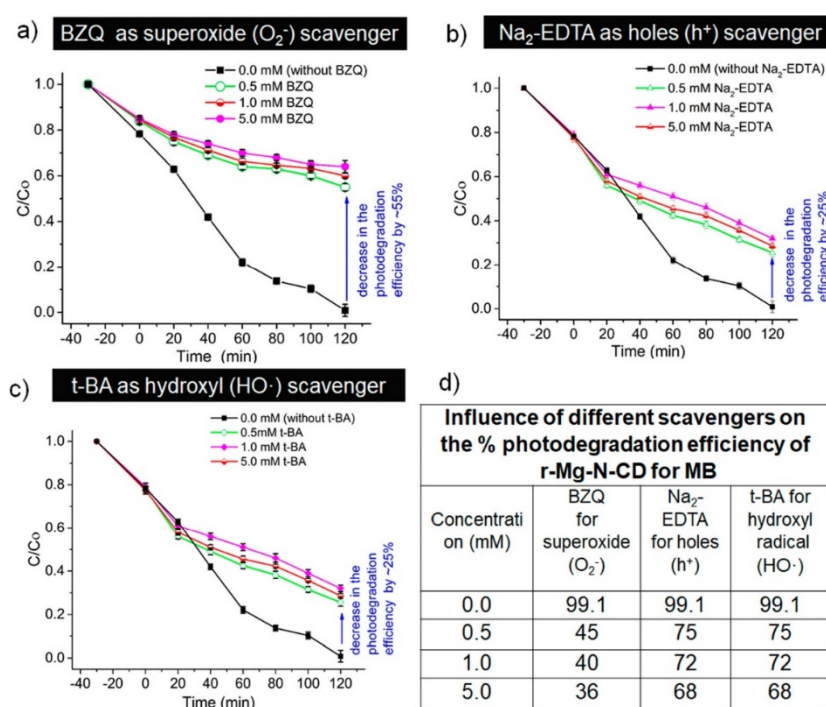
Figure 3.5: Influence on the photodegradation efficiency of MB is shown by trapping the different reactive species in the presence of scavengers; (a) benzoquinone (p-BZQ) for superoxide; (b) Na_2-EDTA for holes; (c) (t-BA) for hydroxyl including error bars and; (d) tabular image shows the overall influence on photodegradation of MB at different concentration of the scavengers including control (0 mM of scavenger).

The plausible photoreaction mechanism steps and pathways for the photodegradation are schematically shown in Figure 3.6a. That describes a long-known theory regarding the uses of surface functionalities regarding surface defects [75,76] located over the surface of r-Mg-N-CD were being utilized here for the capturing of photo excited electrons (highlighted as path I). Photoexcitation of electrons in the graphitic phase of r-Mg-N-CD retards the electron−hole pair recombination and generates the reactive oxygen radicals as shown in path II as reaction intermediates on the surface of r-Mg-N-CD. The generated oxygen radical species further react with water to form hydroxyl radical as shown in path III. The MB molecules adsorbed on the r-Mg-N-CD surface react with active oxygen species (hydroxyl radicals) and holes generated on the r-Mg-N-CD surface as shown in path IV−V and decomposed into smaller hydrocarbons as discussed in detail by NMR analysis in the next section. To check the utility and stability of the photocatalyst, recycling study was carried out as displayed in Figure 3.6b and showed a loss of ~38% in the photodegradation efficiency of the photocatalyst material after the use of four cycles.
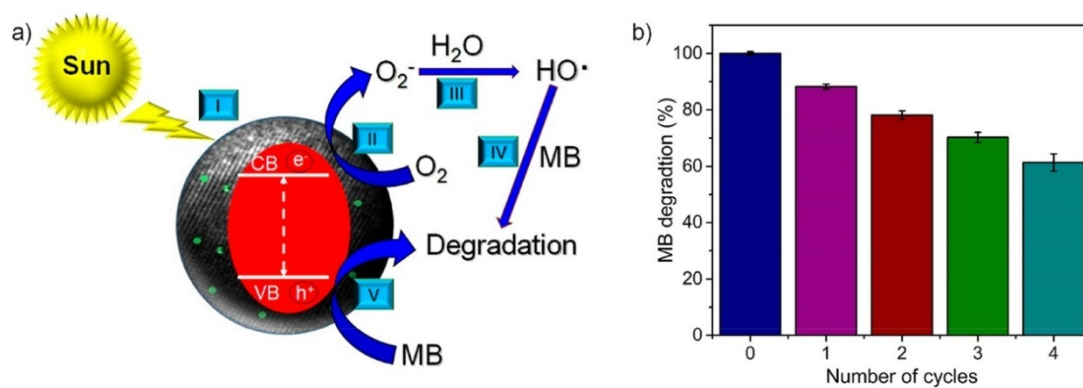

Figure 3.6: (a) Schematic representation of mechanism of photodegradation of MB by r-Mg-N-CD showing several possible pathways (I–V) for dye degradation and; (b) photocatalyst performance of r-Mg-N-CD up to 4 cycles of recycling testing with standard error bar.

3.3.5   Photodegradation Analysis of MB by NMR Spectroscopy

A ^{1}H NMR analysis showing the complete degradation of the aromatic frame of MB (Figure 3.7a) described in Figure 3.7. A comparative NMR analysis of (i) MB; (ii) r-Mg-N-CD and (iii) MB-r-Mg-N-CD (supernatant of r-Mg-N-CD

interacted with MB after the 180 min sunlight irradiation was shown in Figure 3.7b–d. The simplest ^{1}H NMR of MB showed the existence of four different types of protons, appeared at different δ values and were labeled as Ha, Hb, Hc and Hd (Figure 3.7a) in the structural formula of MB. The δ values of MB (for 12 protons) were further divided into two different regions; an aliphatic (for six protons) and an aromatic region (having three separate chemical shift values). To analyze the possible degraded product of MB by r-Mg-N-CD from the pool of MB-r-Mg-N-CD, under the influence of sunlight, the samples collected after the 180 min. As collected samples centrifuged at high speed and the supernatant, containing the photodegraded products dried on a water bath for the NMR analysis [43,74]. Figure 3.7b (i) shows ^{1}H NMR of the six aliphatic protons (Ha) (s) of MB at the δ value of 2.96 ppm. On the other side, six aromatics protons Hb, Hc and Hd showed signals at three different δ value, (two protons as Hb (s) at 6.56 ppm and two protons as Hc (d) at 6.79 to 6.91 ppm and for the last two protons as Hd at 6.98 to 7.00 ppm. For the ^{1}H NMR spectra of r-Mg-N-CD Figure 3.7 (b (ii)), several proton signals were noticed in the aliphatic region (at 1.26,2.19,2.82,2.97,3.55 and 3.70 ppm) in addition to the few aromatic protons (at 6.83,6.91,7.40,8.03,8.78 and 9.08 ppm), supporting the presence of complex surface functionalities as discussed earlier in the section of FT-IR and XPS analysis. The photodegraded products of MB-r-Mg-N-CD after 180 minutes of the sunlight irradiation as shown in Figure 3.7b (iii) confirmed the degradation. Figure 3.7b further zoomed to two different regions: aliphatic (Figure 3.7c) and aromatic (Figure 3.7d), which showed complete degradation of the aromatic framework of MB. As there is no significant character of degraded molecules left in the supernatant water sample that shows the protons signal. Figure 3.7e shows the photographic image of vials containing the MB (before the photodegradation) and clear solution (after the photodegradation).
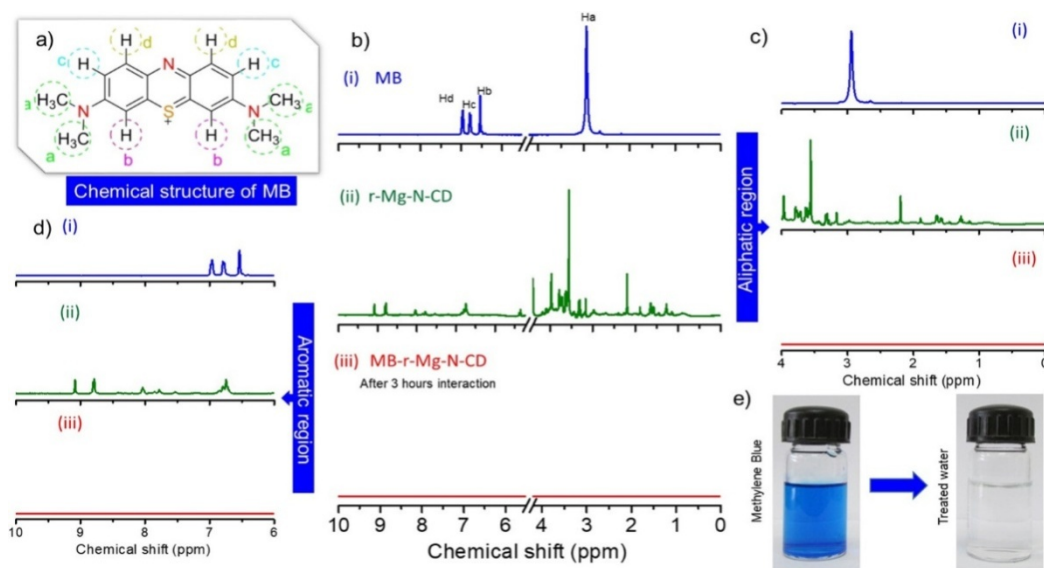
Figure 3.7: (a) Chemical structure of MB showing the different protonic environment; (b) ^{1}H NMR spectra of the photodegradation of MB while interacting with r-Mg-N-CD; (i) ^{1}H NMR of MB; (ii) ^{1}H NMR of r-Mg-N-CD; and (iii) ^{1}H NMR of MB with r-Mg-N-CD after 180 min of sunlight irradiation; (c) Zoomed image of panel; (b) showing the ^{1}H NMR spectra (between 4 ppm to 0 ppm); (d) Zoomed image of Figure 3.7b showing the ^{1}H NMR spectra (between 10 ppm to 6 ppm) and; (e) Effect of r-Mg-N-CD in sunlight on MB blue color (left side blue vial) to colorless (transparent solution in right vial).

3.4   Conclusion

The present finding describes in this chapter discusses the possibilities for fabricating low-cost, high-quantum-yield, red-emitting r-Mg-N-CD in an environment-friendly (without using any externally added chemical reagent). Red-emitting r-Mg-N-CD were used as a novel photocatalytic material for the aqueous phase photodegradation of MB under the presence sunlight. The vast potential of sunlight explored was compared with an artificial tungsten bulb by the use of r-Mg-N-CD, which showed many folds of increase in the rate of photodegradation under the influence of sunlight. Higher in value of QY, solubility in aqueous media and emission in the red wavelength region along with the ability to photodegrade the pollutant dyes within the ~120 min of sunlight irradiation, makes r-Mg-N-CD a potential nanomaterial for its applications in the field of aqueous-phase photodegradation. As well, the embedded Mg can also been replaced from some other metal for enhancing its optical properties [77].

3.5 References

1. Pansare, V. J.; Hejazi, S.; Faenza, W. J.; Prud'homme, R. K. Review of Long-Wavelength Optical and NIR Imaging Materials: Contrast Agents, Fluorophores and Multifunctional Nano Carriers. *Chem. Mater.* **2012**,*24* (5), 812– 827.

2. Amiot, C.; Xu, S.; Liang, S.; Pan, L.; Zhao, J. Near-Infrared Fluorescent Materials for Sensing of Biological Targets. *Sensors* **2008**, *8* (5), 3082.

3. Hong, G.; Antaris, A. L.; Dai, H. Near-infrared Fluorophores for Biomedical Imaging. *Nat. Biomed. Eng.***2017**, *1*, 0010.

4. Luo, S.; Zhang, E.; Su, Y.; Cheng, T.; Shi, C. A Review of NIR Dyes in Cancer Targeting and Imaging.*Biomaterials* **2011**, *32* (29), 7127– 7138.

5. Wang, Y.; Hu, R.; Lin, G.; Roy, I.; Yong, K.-T. Functionalized Quantum Dots for Biosensing and Bioimaging and Concerns on Toxicity. *ACS Appl. Mater. Interfaces* **2013**, *5* (8), 2786– 2799.

6. Hardman, R. A Toxicologic Review of Quantum Dots: Toxicity Depends on Physicochemical and Environmental Factors. *Environ. Health Perspect.* **2006**, *114* (2), 165– 172.

7. Resch-Genger, U.; Grabolle, M.; Cavaliere-Jaricot, S.; Nitschke, R.; Nann, T. Quantum Dots Versus Organic Dyes as Fluorescent Labels. *Nat. Methods* **2008**, *5* (9), 763– 775.

8. Luo, P. G.; Sahu, S.; Yang, S.-T.; Sonkar, S. K.; Wang, J.; Wang, H.; LeCroy, G. E.; Cao, L.; Sun, Y.-P.Carbon "Quantum" Dots For Optical Bioimaging. *J. Mater. Chem. B* **2013**, *1* (16), 2116– 2127.

9. Luo, P. G.; Yang, F.; Yang, S.-T.; Sonkar, S. K.; Yang, L.; Broglie, J. J.; Liu, Y.; Sun, Y.-P. Carbon-Based Quantum Dots for Fluorescence Imaging Of Cells And Tissues. *RSC Adv.* **2014**, *4*, 10791– 10807.

10. Shen, J.; Zhu, Y.; Yang, X.; Li, C. Graphene Quantum Dots: Emergent Nanolights For Bioimaging, Sensors, Catalysis and Photovoltaic Devices. *Chem. Commun.* **2012**, *48* (31), 3686– 3699.

11. Cho, H.-H.; Yang, H.; Kang, D. J.; Kim, B. J. Surface Engineering of Graphene Quantum Dots and Their Applications as Efficient Surfactants. *ACS Appl. Mater. Interfaces* **2015**, *7* (16), 8615– 8621.

12. Li, L.-L.; Ji, J.; Fei, R.; Wang, C.-Z.; Lu, Q.; Zhang, J.-R.; Jiang, L.-P.; Zhu, J.-J. A Facile Microwave Avenue to Electrochemiluminescent Two-Color Graphene Quantum Dots. *Adv. Funct. Mater.* **2012**, *22*, 2971– 2979.

13. Sun, Y.-P.; Zhou, B.; Lin, Y.; Wang, W.; Fernando, K. A. S.; Pathak, P.; Meziani, M. J.; Harruff, B. A.;Wang, X.; Wang, H.; Luo, P. G.; Yang, H.; Kose, M. E.; Chen, B.; Veca, L. M.; Xie, S.-Y. Quantum-Sized Carbon Dots for Bright and Colorful Photoluminescence. *J. Am. Chem. Soc.* **2006**, *128* (24), 7756– 7757.

14. LeCroy, G. E.; Sonkar, S. K.; Yang, F.; Veca, L. M.; Wang, P.; Tackett, K. N.; Yu, J.-J.; Vasile, E.; Qian, H.;Liu, Y.; Luo, P. G.; Sun, Y.-P. Toward Structurally Defined Carbon Dots as Ultracompact Fluorescent Probes.*ACS Nano* **2014**, *8* (5), 4522– 4529.

15. Wang, X.; Cao, L.; Yang, S.-T.; Lu, F.; Meziani, M. J.; Tian, L.; Sun, K. W.; Bloodgood, M. A.; Sun, Y.-P.Bandgap-Like Strong Fluorescence in Functionalized Carbon Nanoparticles. *Angew. Chem., Int. Ed.* **2010**,*49*, 5310– 5314.

16. Baker, S. N.; Baker, G. A. Luminescent Carbon Nanodots: Emergent Nanolights. *Angew. Chem., Int. Ed.***2010**, *49* (38), 6726– 6744.

17. Li, H.; He, X.; Liu, Y.; Huang, H.; Lian, S.; Lee, S.-T.; Kang, Z. One-Step Ultrasonic Synthesis of Water-Soluble Carbon Nanoparticles with Excellent Photoluminescent Properties. *Carbon* **2011**, *49* (2), 605– 609.

18. Zheng, M.; Xie, Z.; Qu, D.; Li, D.; Du, P.; Jing, X.; Sun, Z. On–Off–On Fluorescent Carbon Dot Nanosensor for Recognition of Chromium(VI) and Ascorbic Acid Based on the Inner Filter Effect. *ACS Appl. Mater. Interfaces* **2013**, *5* (24), 13242– 13247.

19. Li, K.; Liu, W.; Ni, Y.; Li, D.; Lin, D.; Su, Z.; Wei, G. Technical Synthesis And Biomedical Applications Of Graphene Quantum Dots. *J. Mater. Chem. B* **2017**, *5* (25), 4811– 4826.

20. Hola, K.; Zhang, Y.; Wang, Y.; Giannelis, E. P.; Zboril, R.; Rogach, A. L. Carbon dots—Emerging light emitters for bioimaging, cancer therapy and optoelectronics. *Nano Today* **2014**, *9* (5), 590– 603.

21.   Hutton, G. A. M.; Reuillard, B.; Martindale, B. C. M.; Caputo, C. A.; Lockwood, C. W. J.; Butt, J. N.;Reisner, E. Carbon Dots as Versatile Photosensitizers for Solar-Driven Catalysis with Redox Enzymes. *J. Am. Chem. Soc.* **2016**, *138* (51), 16722– 16730.

22.   Margraf, J. T.; Strauss, V.; Guldi, D. M.; Clark, T. The Electronic Structure of Amorphous Carbon Nanodots.*J. Phys. Chem. B* **2015**, *119* (24), 7258– 7265.

23.   Rizzo, C.; Arcudi, F.; Đorđević, L.; Dintcheva, N. T.; Noto, R.; D'Anna, F.; Prato, M. Nitrogen-Doped Carbon Nanodots-Ionogels: Preparation, Characterization and Radical Scavenging Activity. *ACS Nano* **2018**, *12*, 1296.

24.   Strauss, V.; Margraf, J. T.; Dolle, C.; Butz, B.; Nacken, T. J.; Walter, J.; Bauer, W.; Peukert, W.; Spiecker, E.;Clark, T.; Guldi, D. M. Carbon Nanodots: Toward a Comprehensive Understanding of Their Photoluminescence. *J. Am. Chem. Soc.* **2014**, *136* (49), 17308– 17316.

25.   Huang, X.; Yang, L.; Hao, S.; Zheng, B.; Yan, L.; Qu, F.; Asiri, A. M.; Sun, X. N-Doped Carbon Dots: A Metal-Free Co-Catalyst on Hematite Nanorod Arrays Toward Efficient Photoelectrochemical Water Oxidation. *Inorg. Chem. Front.* **2017**, *4* (3), 537– 540.

26.   Liu, S.; Tian, J.; Wang, L.; Zhang, Y.; Qin, X.; Luo, Y.; Asiri, A. M.; Al-Youbi, A. O.; Sun, X. Hydrothermal Treatment Of Grass: A Low-Cost, Green Route to Nitrogen-Doped, Carbon-Rich, Photoluminescent Polymer Nanodots as an Effective Fluorescent Sensing Platform For Label-Free Detection of Cu(II) Ions. *Adv. Mater.* **2012**, *24* (15), 2037– 41.

27.   Lu, W.; Qin, X.; Liu, S.; Chang, G.; Zhang, Y.; Luo, Y.; Asiri, A. M.; Al-Youbi, A. O.; Sun, X. Economical, Green Synthesis of Fluorescent Carbon Nanoparticles and Their Use as Probes for Sensitive and Selective Detection Of Mercury(II) Ions. *Anal. Chem.* **2012**, *84* (12), 5351– 7.

28.   Zhang, S.; Gao, H.; Liu, X.; Huang, Y.; Xu, X.; Alharbi, N. S.; Hayat, T.; Li, J. Hybrid 0D-2D Nanoheterostructures: In Situ Growth of Amorphous Silver Silicates Dots on g-C3N4 Nanosheets for Full-Spectrum Photocatalysis. *ACS Appl. Mater. Interfaces* **2016**, *8* (51), 35138– 35149.

29.   Ming, H.; Ma, Z.; Liu, Y.; Pan, K.; Yu, H.; Wang, F.; Kang, Z. Large Scale Electrochemical Synthesis of High Quality Carbon Nanodots and Their Photocatalytic Property. *Dalton Trans* **2012**, *41* (31), 9526– 9531.

30.   Safavi, A.; Sedaghati, F.; Shahbaazi, H.; Farjami, E. Facile Approach To The Synthesis of Carbon Nanodots and Their Peroxidase Mimetic Function in Azo Dyes Degradation. *RSC Adv.* **2012**, *2* (19), 7367– 7370.

31.   Hu, S.; Wei, Z.; Chang, Q.; Trinchi, A.; Yang, J. A Facile and Green Method Towards Coal-Based Fluorescent Carbon Dots With Photocatalytic Activity. *Appl. Surf. Sci.* **2016**, *378*, 402– 407.

32.   Zhang, H.; Zhao, L.; Geng, F.; Guo, L.-H.; Wan, B.; Yang, Y. Carbon Dots Decorated Graphitic Carbon Nitride as An Efficient Metal-Free Photocatalyst For Phenol Degradation. *Appl. Catal., B* **2016**, *180*, 656–662.

33.   Zhang, Y.; Park, M.; Kim, H. Y.; Ding, B.; Park, S.-J. A Facile Ultrasonic-Assisted Fabrication of Nitrogen-Doped Carbon Dots/Biobr Up-Conversion Nanocomposites for Visible Light Photocatalytic Enhancements.*Sci. Rep.* **2017**, *7*, 45086.

34.   Atchudan, R.; Edison, T. N. J. I.; Perumal, S.; Karthik, N.; Karthikeyan, D.; Shanmugam, M.; Lee, Y. R.Concurrent Synthesis Of Nitrogen-Doped Carbon Dots for Cell Imaging and Zno@Nitrogen-Doped Carbon Sheets for Photocatalytic Degradation Of Methylene Blue. *J. Photochem. Photobiol., A* **2018**, *350*, 75– 85.

35.   Zhang, S.; Yang, H.; Huang, H.; Gao, H.; Wang, X.; Cao, R.; Li, J.; Xu, X.; Wang, X. Unexpected Ultrafast and High Adsorption Capacity Of Oxygen Vacancy-Rich Wox/C Nanowire Networks for Aqueous Pb^{2+} And Methylene Blue Removal. *J. Mater. Chem. A* **2017**, *5* (30), 15913– 15922.

36.   Qin, X.; Lu, W.; Asiri, A. M.; Al-Youbi, A. O.; Sun, X. Green, Low-Cost Synthesis of Photoluminescent Carbon Dots By Hydrothermal Treatment Of Willow Bark And Their Application As An Effective Photocatalyst For Fabricating Au Nanoparticles-Reduced Graphene Oxide Nanocomposites For Glucose Detection. *Catal. Sci. Technol.* **2013**, *3* (4), 1027– 10350.

37.   Liu, S.; Tian, J.; Wang, L.; Luo, Y.; Sun, X. One-Pot Synthesis Of CuO Nanoflower-Decorated Reduced Graphene Oxide And Its Application To

Photocatalytic Degradation Of Dyes. *Catal. Sci. Technol.* **2012**, *2* (2),339– 344.

38.   Cheng, N.; Tian, J.; Liu, Q.; Ge, C.; Qusti, A. H.; Asiri, A. M.; Al-Youbi, A. O.; Sun, X. Au-Nanoparticle-Loaded Graphitic Carbon Nitride Nanosheets: Green Photocatalytic Synthesis and Application toward the Degradation of Organic Pollutants. *ACS Appl. Mater. Interfaces* **2013**, *5* (15), 6815– 6819.

39.   Tian, J.; Cheng, N.; Liu, Q.; Xing, W.; Sun, X. Cobalt Phosphide Nanowires: Efficient Nanostructures for Fluorescence Sensing of Biomolecules and Photocatalytic Evolution of Dihydrogen from Water under Visible Light. *Angew. Chem., Int. Ed.* **2015**, *54* (18), 5493– 5497.

40.   Gao, T.; Wang, X.; Yang, L.-Y.; He, H.; Ba, X.-X.; Zhao, J.; Jiang, F.-L.; Liu, Y. Red, Yellow and Blue Luminescence by Graphene Quantum Dots: Syntheses, Mechanism and Cellular Imaging. *ACS Appl. Mater. Interfaces* **2017**, *9* (29), 24846– 24856.

41.   Nurunnabi, M.; Khatun, Z.; Reeck, G. R.; Lee, D. Y.; Lee, Y.-k. Near Infra-Red Photoluminescent Graphene Nanoparticles Greatly Expand Their Use In Noninvasive Biomedical Imaging. *Chem. Commun.* **2013**, *49*(44), 5079– 5081.

42.   Tripathi, K. M.; Sonker, A. K.; Sonkar, S. K.; Sarkar, S. Pollutant Soot Of Diesel Engine Exhaust Transformed To Carbon Dots For Multicoloured Imaging Of E. Coli And Sensing Cholesterol. *RSC Adv.***2014**, *4*, 30100– 30107.

43.   Li, L.; Zhang, R.; Lu, C.; Sun, J.; Wang, L.; Qu, B.; Li, T.; Liu, Y.; Li, S. In Situ Synthesis Of NIR-Light Emitting Carbon Dots Derived From Spinach For Bio-Imaging Applications. *J. Mater. Chem. B* **2017**, *5* (35),7328– 7334.

44.   Arcudi, F.; Đorđević, L.; Prato, M. Synthesis, Separation and Characterization of Small and Highly Fluorescent Nitrogen - Doped Carbon NanoDots. *Angew. Chem., Int. Ed.* **2016**, *55* (6), 2107– 2112.

45.   Ding, H.; Yu, S.-B.; Wei, J.-S.; Xiong, H.-M. Full-Color Light-Emitting Carbon Dots with a Surface-State-Controlled Luminescence Mechanism. *ACS Nano* **2016**, *10* (1), 484– 491.

46.   Ding, H.; Ji, Y.; Wei, J.-S.; Gao, Q.-Y.; Zhou, Z.-Y.; Xiong, H.-M. Facile Synthesis Of Red-Emitting Carbon Dots From Pulp-Free Lemon Juice For Bioimaging. *J. Mater. Chem. B* **2017**, *5* (26), 5272– 5277.

47.   Chen, J.; Wei, J.-S.; Zhang, P.; Niu, X.-Q.; Zhao, W.; Zhu, Z.-Y.; Ding, H.; Xiong, H.-M. Red-Emissive Carbon Dots for Fingerprints Detection by Spray Method: Coffee Ring Effect and Unquenched Fluorescence in Drying Process. *ACS Appl. Mater. Interfaces* **2017**, *9* (22), 18429– 18433.

48.   Jiang, K.; Sun, S.; Zhang, L.; Lu, Y.; Wu, A.; Cai, C.; Lin, H. Red, Green and Blue Luminescence by Carbon Dots: Full-Color Emission Tuning and Multicolor Cellular Imaging. *Angew. Chem., Int. Ed.* **2015**, *54* (18),5360– 5363.

49.   Kumawat, M. K.; Thakur, M.; Gurung, R. B.; Srivastava, R. Graphene Quantum Dots from Mangifera indica: Application in Near-Infrared Bioimaging and Intracellular Nanothermometry. *ACS Sustainable Chem. Eng.***2017**, *5* (2), 1382– 1391.

50.   Sun, S.; Zhang, L.; Jiang, K.; Wu, A.; Lin, H. Toward High-Efficient Red Emissive Carbon Dots: Facile Preparation, Unique Properties and Applications as Multifunctional Theranostic Agents. *Chem. Mater.* **2016**,*28* (23), 8659– 8668.

51.   Wang, C.; Jiang, K.; Wu, Q.; Wu, J.; Zhang, C. Green Synthesis of Red-Emitting Carbon Nanodots as a Novel "Turn-on" Nanothermometer in Living Cells. *Chem. - Eur. J.* **2016**, *22* (41), 14475– 14479.

52.   Hu, S.; Trinchi, A.; Atkin, P.; Cole, I. Tunable Photoluminescence Across the Entire Visible Spectrum from Carbon Dots Excited by White Light. *Angew. Chem., Int. Ed.* **2015**, *54* (10), 2970– 2974.

53.   Miao, X.; Yan, X.; Qu, D.; Li, D.; Tao, F. F.; Sun, Z. Red Emissive Sulfur, Nitrogen Codoped Carbon Dots and Their Application in Ion Detection and Theraonostics. *ACS Appl. Mater. Interfaces* **2017**, *9* (22), 18549–18556.

54.   Liu, Y.; Duan, W.; Song, W.; Liu, J.; Ren, C.; Wu, J.; Liu, D.; Chen, H. Red Emission B, N, S-co-Doped Carbon Dots for Colorimetric and Fluorescent Dual Mode Detection of Fe3+ Ions in Complex Biological Fluids and Living Cells. *ACS Appl. Mater. Interfaces* **2017**, *9* (14), 12663– 12672.

55.   Ali, H.; Bhunia, S. K.; Dalal, C.; Jana, N. R. Red Fluorescent Carbon Nanoparticle-Based Cell Imaging Probe. *ACS Appl. Mater. Interfaces* **2016**, *8* (14), 9305– 9313.

56.   Ke, C.-C.; Yang, Y.-C.; Tseng, W.-L. Synthesis of Blue-, Green-, Yellow- and Red-Emitting Graphene-Quantum-Dot-Based Nanomaterials with Excitation-Independent Emission. *Part. Part. Syst. Char.* **2016**, *33*(3), 132– 139.

57.   Yi, G.; Peng, Y.; Gao, Z. Strong Red-Emitting near-Infrared-to-Visible Upconversion Fluorescent Nanoparticles. *Chem. Mater.* **2011**, *23* (11), 2729– 2734.

58.   Würth, C.; Grabolle, M.; Pauli, J.; Spieles, M.; Resch-Genger, U. Relative and absolute determination of fluorescence quantum yields of transparent samples. *Nat. Protoc.* **2013**, *8*, 1535.

59.   Sens, R.; Drexhage, K. H. Fluorescence quantum yield of oxazine and carbazine laser dyes. *J. Lumin.* **1981**, *24–25*, 709– 712.

60.   Song, W.-S.; Yang, H. Efficient White-Light-Emitting Diodes Fabricated from Highly Fluorescent Copper Indium Sulfide Core/Shell Quantum Dots. *Chem. Mater.* **2012**, *24* (10), 1961– 1967.

61.   Linehan, K.; Doyle, H. Size controlled synthesis of carbon quantum dots using hydride reducing agents. *J. Mater. Chem. C* **2014**, *2* (30), 6025– 6031.

62.   Choudhary, R.; Koppala, S.; Swamiappan, S. Bioactivity studies of calcium magnesium silicate prepared from eggshell waste by sol–gel combustion synthesis. *J. As Cer Soc.* **2015**, *3* (2), 173– 177.

63.   Tripathi, K. M.; Singh, A.; Bhati, A.; Sarkar, S.; Sonkar, S. K. Sustainable Feasibility of the Environmental Pollutant Soot to Few- Layer Photoluminescent Graphene Nanosheets for Multifunctional Applications. *ACS Sustainable Chem. Eng.* **2016**, *4* (12), 6399– 6408.

64.   Pareek, K.; Zhang, Q.; Rohan, R.; Cheng, H. Highly selective carbon dioxide adsorption on exposed magnesium metals in a cross-linked organo-magnesium complex. *J. Mater. Chem. A* **2014**, *2* (33), 13534–13540.

65.   Wu, P.-Y.; Jiang, Y.-P.; Zhang, Q.-Y.; Jia, Y.; Peng, D.-Y.; Xu, W. Comparative study on arsenate removal mechanism of MgO and MgO/TiO2 composites: FTIR and XPS analysis. *New J. Chem.* **2016**, *40* (3), 2878–2885.

66.   Pramanik, A.; Jones, S.; Pedraza, F.; Vangara, A.; Sweet, C.; Williams, M. S.; Ruppa-Kasani, V.;Risher, S. E.; Sardar, D.; Ray, P. C. Fluorescent, Magnetic Multifunctional Carbon Dots for Selective Separation, Identification and Eradication of Drug-Resistant Superbugs. *ACS Omega* **2017**, *2* (2), 554–562.

67.   Pan, X.; Yi, Z. Graphene Oxide Regulated Tin Oxide Nanostructures: Engineering Composition, Morphology, Band Structure and Photocatalytic Properties. *ACS Appl. Mater. Interfaces* **2015**, *7* (49), 27167– 27175.

68.   Zhao, Y.; Zhang, Y.; Liu, A.; Wei, Z.; Liu, S. Construction of Three-Dimensional Hemin-Functionalized Graphene Hydrogel with High Mechanical Stability and Adsorption Capacity for Enhancing Photodegradation of Methylene Blue. *ACS Appl. Mater. Interfaces* **2017**, *9* (4), 4006– 4014.

69.   Umrao, S.; Sharma, P.; Bansal, A.; Sinha, R.; Singh, R. K.; Srivastava, A. Multi-layered graphene quantum dots derived photodegradation mechanism of methylene blue. *RSC Adv.* **2015**, *5* (64), 51790– 51798.

70.   Yu, H.; Irie, H.; Hashimoto, K. Conduction Band Energy Level Control of Titanium Dioxide: Toward an Efficient Visible-Light-Sensitive Photocatalyst. *J. Am. Chem. Soc.* **2010**, *132* (20), 6898– 6899.

71.   Li, F.-t.; Wang, Q.; Ran, J.; Hao, Y.-j.; Wang, X.-j.; Zhao, D.; Qiao, S. Z. Ionic liquid self-combustion synthesis of BiOBr/Bi24O31Br10 heterojunctions with exceptional visible-light photocatalytic performances. *Nanoscale* **2015**, *7* (3), 1116– 1126.

72.   Tao, T.-X.; Dai, J.-S.; Yang, R.-C.; Xu, J.-B.; Chu, W.; Wu, Z.-C. Synthesis, characterization and photocatalytic properties of BiOBr/amidoxime fiber composites. *Mater. Sci. Semicond. Process.* **2015**, *40*,344– 350.

73.   Zhang, B.; Zhang, D.; Xi, Z.; Wang, P.; Pu, X.; Shao, X.; Yao, S. Synthesis of Ag2O/NaNbO3 p–n junction photocatalysts with improved visible light photocatalytic activities. *Sep. Purif. Technol.* **2017**, *178*, 130– 137.

74.   Singh, A.; Khare, P.; Verma, S.; Bhati, A.; Sonker, A. K.; Tripathi, K. M.; Sonkar, S. K. Pollutant Soot for Pollutant Dye Degradation: Soluble Graphene Nanosheets for Visible Light Induced Photodegradation of Methylene Blue. *ACS Sustainable Chem. Eng.* **2017**, *5* (10), 8860– 8869.

75.   Khare, P.; Singh, A.; Verma, S.; Bhati, A.; Sonker, A. K.; Tripathi, K. M.; Sonkar, S. K. Sunlight-Induced Selective Photocatalytic Degradation of Methylene Blue in Bacterial Culture by Pollutant Soot Derived Nontoxic Graphene Nanosheets. *ACS Sustainable Chem. Eng.* **2018**, *6* (1), 579– 589.

76.   Bhati, A.; Singh, A.; Tripathi, K. M.; Sonkar, S. K. Sunlight-Induced Photochemical Degradation of Methylene Blue by Water-Soluble Carbon Nanorods. *Int. J. Photoenergy* **2016**, *2016*, Article ID 2583821.

77.   Khare, P.; Bhati, A.; Anand, S. R.; Gunture; Sonkar, S. K. Brightly Fluorescent Zinc-Doped Red-Emitting Carbon Dots for the Sunlight-Induced Photoreduction of Cr(VI) to Cr(III). *ACS Omega* **2018**, *3* (5), 5187–5194.

Chapter-4

Red-Emitting Fluorescent Zinc-Doped Carbon Dots used for the Photoreduction of Cr(VI) to Cr(III) under Sunlight Irradiation
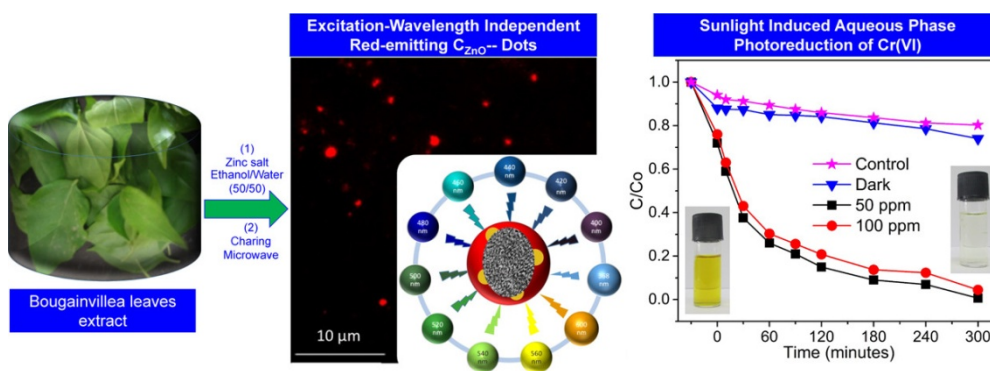
4.1   Introduction

CD/GQD are potent material for applications including bioimaging [1-8]. These imaging application were earlier done in blue –green region but red and NIR region [9-13] seems to lesser harmful for biological entities[14,15]. Only few reports are available for red emitting CD/GQD.[16-22]   Sun *et al.* report the synthesis of metal-doped green fluorescent ZnO and ZnS-doped/-decorated CD by the doping of zinc acetate on the surface of CD via hydrolysis by NaOH and precipitation with Na_2S, respectively [23]. Cheng *et al.* report the synthesis of yellow fluorescent C_{ZnO}-Dots via a one-step hydrothermal synthesis by mixing citric acid and zinc chloride in toluene and used them in bifunctional photonic crystal films, fluorescent microfibers and patterns [24]. Xu *et al.* synthesized blue-light-emitting C_{ZnO}-Dots by mixing sodium citrate and zinc chloride via the hydrothermal method and used them as a biosensor [25]. ZnO/graphene quasi-core shell QD were synthesized by Son *et al.*, who used them in white-light-emitting diodes [26]. Apart from the above-mentioned applications, CD and doped-CD are used in the field of sensing (gas [27], heavy metals [28−30], microbes [31,32] etc.), optical displays [33], tunable photoluminescence [4,34], biocompatibility [33] and competitive QY values [7] and in the field of bioimaging (presently being explored in the red and NIR regions) [9−13]. Based on their vast levels of applicative sustainability CD/doped-CD can be expected to show their potential toward world's most serious concern, that is, contamination of water [35] which increases at a very high rate because of the increase in world population and industrialization. A huge amount of wastewater is discharged routinely which contains a large amount of heavy inorganic metal ions and organic compounds generally known as dyes that subsequently degraded the overall environmental and human health. Few reports are available for the photodegradation of the organic dyes by the waste derived nano-carbons [36−39]. The removal of heavy metals from wastewater has been carried out by different techniques [40−44]. Red-emitting CD can be a significant material, simply because of their lower working levels of energy which can be used for the applications related to water treatment.

Under the influence of sunlight, this chapter describes a new prospect of using red-emitting zin oxide doped carbon dots (C$_{ZnO}$-Dots) apart from their routine application. Concerning its successful usage for the aqueous-phase photoreduction of 100 ppm of Cr(VI) in dichromate water. The as-obtained C$_{ZnO}$-Dots showed excellent solubility and stability in aqueous media along with excellent photostability and exhibited excitation-independent red emissions with high QY (~50%). The most significant prospect of the present finding is the utilization of C$_{ZnO}$-Dots as a novel photocatalyst material for the aqueous-phase photo-reduction of 100 ppm Cr(VI).

4.2 Experimental Section

4.2.1 Materials and Reagents

All chemical reagents were of analytical grade, procured from Merck India and used without further purification.

4.2.2 Instrumentation

TEM, fluorescence microscopy, XPS, FTIR, UV-Vis and fluorescence spectroscopy instrumentation were same as described in Chapter 2 and 3. Cyclic Voltammetry (CV): the CV studies (K-Lyte 1.2 model of Kanopy Techno Solution Pvt. Ltd.) were performed using a three-electrode cell in sunlight; a glassy carbon electrode was used as the working electrode, Pt wire and Ag/AgCl (in 0.1 M KCl) electrodes were used as counter and reference electrodes, respectively. The scan rate was 10 mV/sec and the resting potential has been 1.15 V to start the scan to sweep till -0.8V maintaining the scan window between +1.15 V to −0.8V (vs Ag/AgCl) using 0.1M KCl as supporting electrolyte. 100 ppm K$_2$Cr$_2$O$_7$ as probe was added with the photocatalyst.

4.2.3 Synthesis of C$_{ZnO}$-Dots

C$_{ZnO}$-Dots were synthesized using *Bougainvillea* plant leaves as pristine materials via the green synthesis process. Prior to use, the leaves were cleaned with DI water to remove soluble impurities and were dried at ~30°C. Next, an extract of leaves was obtained by blending the chopped leaves (~1 cm-sized pieces) using a hand blender. After this, the extract (~10 g) was mixed in 100 mL of ethanol/water

mixture [(1:1) (V/V)] solution. Zinc acetate by the 10 wt % of the extract was added into the solution and sonicated for another 10 min. The final mixture was then carbonized at 90% power of a domestic microwave oven of 1400 W for 10 min. The mixture was collected and centrifuged at ~6000 rpm for 30 min. The residual supernatant solution was transferred to a Petri dish and dried on a water bath. The dried powder was named as red color-emitting C_{ZnO}-Dots. The QY was measured [7] for both the samples, as prepared and highly centrifuged sample separated 11000 rpm centrifuge with reference to NB [45,46]. The photographic image was taken in the ethanol:water (1:1) solution as shown in the inset of Figure 4.2(b) [12]. A control sample without zinc doping was prepared under conditions similar to those for C_{ZnO}-Dots from the same plant leaves.

4.2.4 Photocatalytic Activity Measurement

The photocatalytic activity of the C_{ZnO}-Dot samples was determined by the photoreduction of Cr(VI) in aqueous dichromate solution under direct sunlight. A stock solution of $K_2Cr_2O_7$ containing 100 ppm of Cr(VI) was prepared in DI water for photocatalytic reduction, 1.414 g wt of $K_2Cr_2O_7$ was dissolved in 250 mL DI water to make 1000 ppm of Cr(VI) and further concentration were made by dilution. In a typical process, 150 mg of C_{ZnO}-Dots was added in 50 mL of the prepared Cr(VI) solution and was stirred for 30 min in the dark to attain the adsorption/desorption equilibration. The solutions were then exposed to direct sunlight. During the photocatalytic test, a fixed amount of the photoreacted solution was collected at a fixed time interval of 30 min. The collected solution was centrifuged and the supernatant solution was analyzed for the concentration of Cr(VI) and a pink color was obtained on mixing with the standard DPC assay [47]. The photocatalyst were regenerated by initial washing with 0.1M ascorbic acid and then repeatedly washing with DI water till the yellow color of supernatant solution disappear.

4.3   Results and Discussion

The simple methodology illustrated in Scheme 4.1 presents a low-cost fabrication approach for the synthesis of surface-passivated, brightly fluorescent

zinc-oxide-decorated, red-emitting C_{ZnO}-Dots showing excitation-independent red emission at ~661 nm, with excellent photostability and high QY.
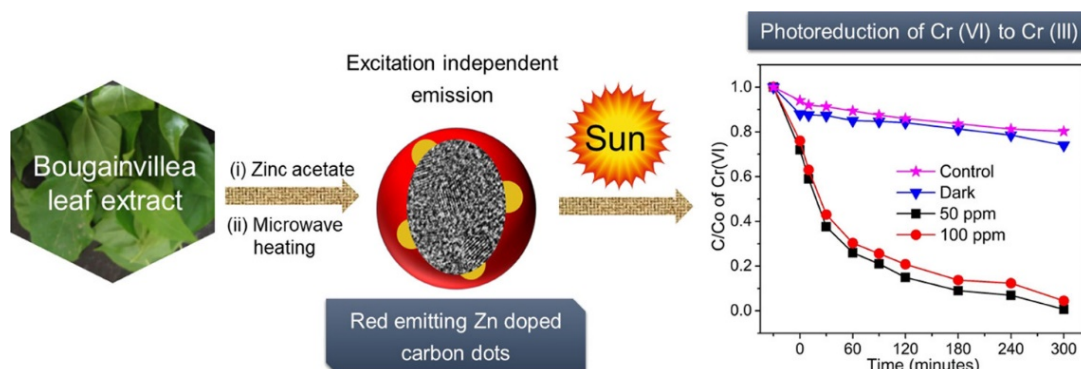

Scheme 4.1 Schematic representation and illustration showing the simple synthesis and the application of red-emitting C_{zno}-dots in the aqueous-phase photoreduction of Cr(VI) to Cr(III), under the influence of sunlight.

4.3.1 Microscopic Analysis

The morphology of C_{ZnO}-Dots was analyzed by TEM and HRTEM. Figure 4.1a shows the TEM image of C_{ZnO}-Dots with well-dispersed particles. Inset of Figure 4.1a shows the photographic image of C_{ZnO}-Dots. The average size of C_{ZnO}-Dots is ~2–6 nm as observed from the size distribution shown in Figure 4.1b. Figure 4.1c displays the HRTEM image of C_{ZnO}-Dots showing the presence of graphitic dots of different shapes and sizes (red circles) and the inset of Figure 4.1c shows SAED, confirming the polycrystalline characteristic of the sample. Figure 4.1d shows XRD spectrum of C_{ZnO}-Dots, confirming the doping of zinc in C_{ZnO}-Dots. The 2θ at 27.6°, 30°, 33.04°, 39.6°, 43.36° and 44.94° is compared with the JCPDS of PDF card number 00-021-1486 for ZnO and that at 23.8° for graphitic carbon.
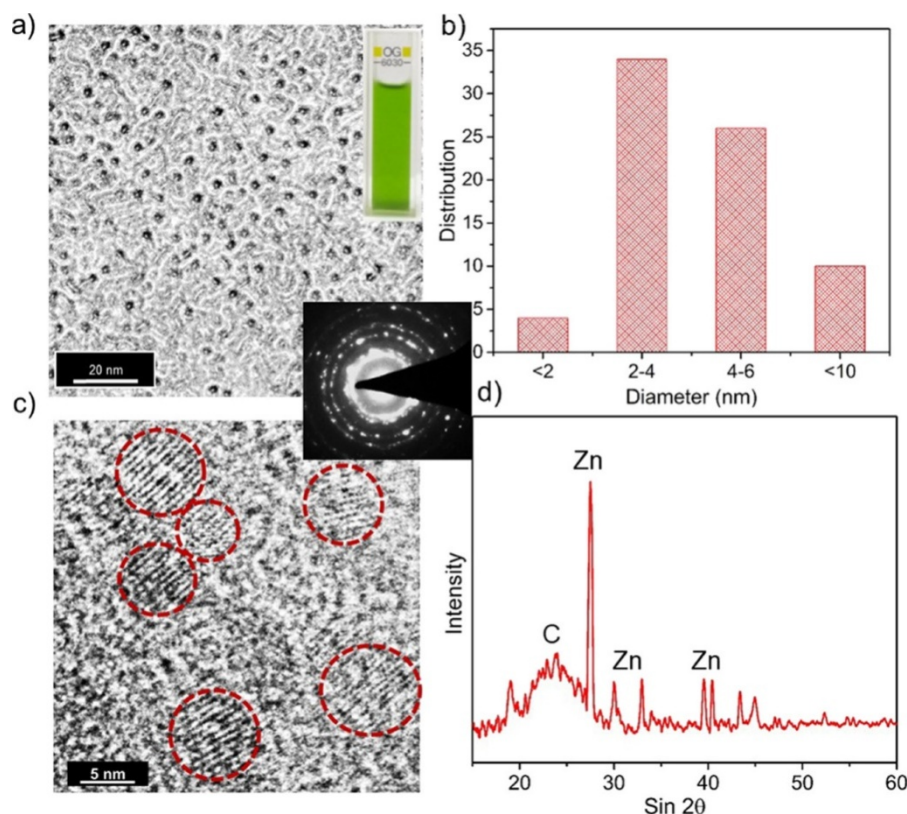
Figure 4.1: (a) TEM image showing well-dispersed C_{ZnO}-Dots; inset of (a) photographic image of the C_{ZnO}-Dots in the daylight; (b) corresponding size distribution; (c) HRTEM image marked with red circles showing C_{ZnO}-Dots with graphitic fringes; the inset of (c) shows the SAED pattern and (d) powder XRD spectrum of the C_{ZnO}-Dots sample.

4.3.2 UV–visible and XPS Analysis

The absorption spectrum of C_{ZnO}-Dots versus the control sample (without ZnO-doped) is shown in Figure 4.2a. Both the C_{ZnO}-Dots and the control samples showed almost similar absorption characteristics except for an increase in the absorption peak intensities at their respective wavelength. As observed, the C_{ZnO}-Dots exhibited a higher absorption intensity compared to the control samples (the hyperchromic effect) and the highest intensity peak at 430 nm corresponds to n−π* compared to other peaks. The inset of Figure 4.2a shows the photographic image of the control samples and C_{ZnO}-Dots in daylight clearly show the changes in the color of the solution after the doping of ZnO. The shift toward the lower wavelength and higher intensity of absorption peaks supports the doping of ZnO within the carbogenic surface of the control sample to yield highly emissive red-emitting C_{ZnO}-Dots. The surface attachment of the zinc material as a dopant in C_{ZnO}-Dots was

investigated by the XPS analysis, as described in Figure 4.2(b–e). The XPS survey scan shows the peaks at 284.8, 532.8, 1024 and 1045 eV associated with the presence of C_{1s} (81.0%), O_{1s} (13.4%) and Zn_{2p} (5.6%), as displayed in Figure 4.2b, confirming the existence of C, O and Zn, within the C_{ZnO}-Dots. Moreover, the high-resolution XPS spectra over the deconvolution showed the presence of different binding sites for C, Zn and O as displayed in Figure 4.2(c–e). The high-resolution XPS short scan of C_{1s} deconvolution displayed several C-binding sites at 282.6 (C–Zn), 283.6 (C=C), 284.5 (C–C), 285.2 (C–O), 286.1 (C=O) and 288.4 eV (COO–) [48,49] (Figure 4.2c). The short scans of Zn are shown in Figure 4.2d. Similarly, for the O_{1s} deconvolution, different binding sites for C and Zn are shown in Figure 4.2e at 529.5 (O–Zn), 530.9 (C–O), 531.8 (C=O) and 532.9 eV (COO$^-$). [50]
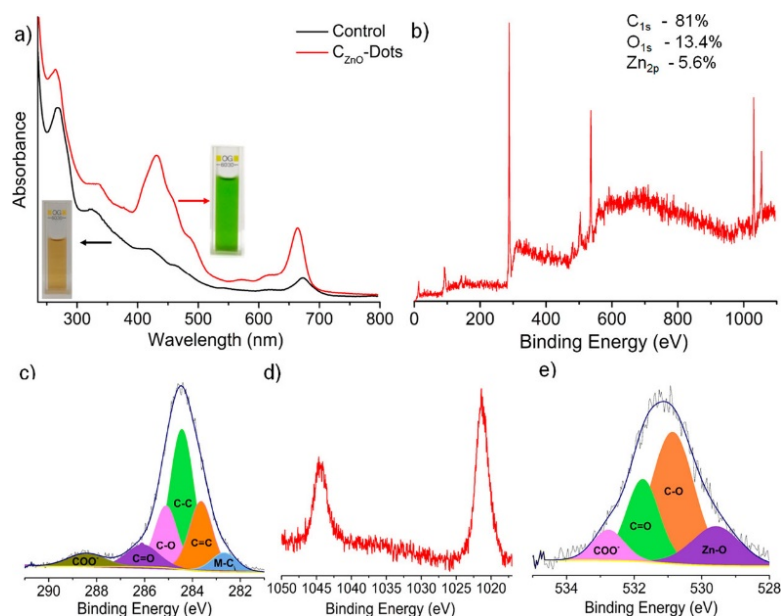
Figure 4.2: (a) UV–vis spectra of the control and C_{ZnO}-Dots; the insets of (a) show the photographic images of the control and C_{ZnO}-Dots in daylight; (b) survey scan of C_{ZnO}-Dots; and its corresponding short scans of (c) C_{1s}, (d) Zn_{2p} and (e) O_{1s}.

Figure 4.3 shows the optical property of C_{ZnO}-Dots via fluorescence spectroscopy. Figure 4.3a shows almost similar characteristic fluorescence spectra for C_{ZnO}-Dots and the control sample. The C_{ZnO}-Dots exhibited a relatively higher fluorescent intensity with a slight blue shift (~17 nm) in the fluorescence spectra compared to the control. The emissive fluorescence spectra are in accordance with the observations noticed in the absorption studies (Figure 4.2a). The brightly fluorescent and prominent aspect concerning the excitation-independent red-emitting C_{ZnO}-Dots is shown in Figure 4.3b. The inset of Figure 4.3b displays the

photographic image of C_{ZnO}-Dots under UV light illumination. Regarding the excitation-independent red emission of C_{ZnO}-Dots can be explained based on documented reports ascribed because of the incorporation/doping of heteroatoms [51,52]. Figure 4.3c displays the optical fluorescence microscopy image of C_{ZnO}-Dots with a 562 nm band-pass filter and Figure 4.3d shows the excellent photostability of C_{ZnO}-Dots toward a photobleaching experiment performed for 5 h at continuous irradiation with excitation at 430 nm. The QY of the as-prepared C_{ZnO}-Dots was ~50% (compared to NB) and this can be increased up to ~72% by centrifuging it on high rpm (11000) for the isolation of most fluorescent fraction. All the photoreduction experiments were carried out by using the as prepared C_{ZnO}-Dots.

4.3.3 C_{ZnO}-Dots in Photocatalytic Reduction of Cr(VI) to Cr(III)

The sunlight-induced photocatalytic activity of C_{ZnO}-Dots was assessed for the aqueous-phase photoreduction of the toxic Cr(VI). The continuous decrease in the concentration of Cr(VI) (in terms of C/C_0) as shown in Figure 4.4a under the influence of sunlight was determined by the absorption analysis at the 540 nm wavelength by following the DPC assay [43]. Prior to the photoreduction experiment, 3 mg mL^{-1} of C_{ZnO}-Dots was mixed in a 100 ppm Cr(VI) stock solution and stirred continuously in the dark for 30 min, to achieve the adsorption–desorption equilibrium. The adsorption data (Figure 4.4a) for C_{ZnO}-Dots in the dark (black line) and sunlight (red line) including the control (blue line) showed that only 27% of Cr(VI) reduction was achieved in the 300 min dark condition. Moreover, the photocatalytic influence of sunlight in the presence of C_{ZnO}-Dots showed the highest reduction of Cr(VI) (~99%) in 300 min, which was 75.7% higher as compared to the control sample. The increase in photoreduction efficiency for C_{ZnO}-Dots could be attributed to the high catalytic activity of ZnO that facilitates the reduction in recombination of photogenerated charge carriers [53]. Moreover, another plausible reason for the high photocatalytic activity of C_{ZnO}-Dots for Cr(VI) reduction is ascribed to their high adsorption values. C_{ZnO}-Dots showed a higher Cr(VI) adsorption efficiency (~25%, red line) compared to that of the control (~8%, blue line), as shown in Figure 4.4a, which can significantly enhance the availability of Cr(VI) at the active sites of the used catalyst material as C_{ZnO}-Dots. During the

process of photocatalysis, the photogenerated electrons from the photocatalyst can readily access surface-adsorbed Cr(VI) ions and thereby stimulate the reduction process [reduce Cr(VI) to Cr(III)] [54,55].
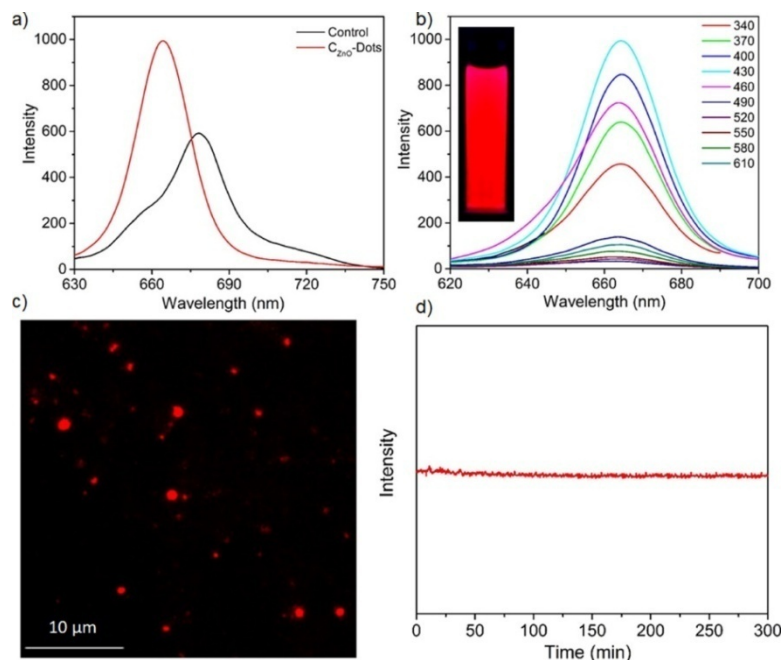

Figure 4.3: (a) Fluorescence spectra of C$_{ZnO}$-Dots and the control sample; (b) Fluorescence spectra excited at different wavelength for C$_{ZnO}$-Dots; the inset of (b) shows the photographic image of C$_{ZnO}$-Dots under UV light in a UV chamber; (c) Fluorescence imaging of C$_{ZnO}$-Dots under the excitation of a 562 nm band-pass filter; and (d) photostability of C$_{ZnO}$-Dots excited continuously at 430 nm wavelength for 5 h
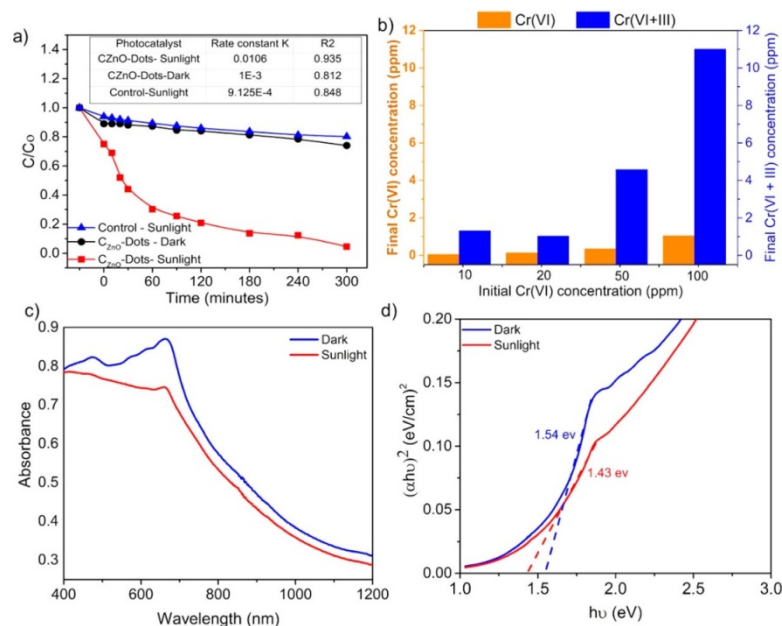
Figure 4.4: (a) Plot of Cr(VI) photoreduction [(C/C_0)] by C_{ZnO}-Dots under different conditions; the inset of (a) shows the comparative data of first-order rate constant and correlation coefficient obtained from fitting the experimental data; (b) the final concentration of Cr(VI) and Cr(VI + III) in the aqueous phase after photoreduction at different initial Cr(VI) concentration based on UV−vis and AAS analysis. (c) UV−vis absorption spectra and (d) Tauc plots of $(\alpha h\upsilon)^2$ vs photo energy ($h\upsilon$) of C_{ZnO}-Dots in the dark and sunlight-exposed samples.

The experimental data are well-fitted with a first-order kinetic model and the rate constant values as well as the correlation coefficient are shown in the inset of Figure 4.4a. However, the experimental data do not fit well with the zero-order and second-order models. Figure 4.4b shows the percentage of Cr(VI) and Cr(VI + III) remaining in the aqueous phase after the photoreduction process at different initial Cr(VI) concentration (10,20,50 and 100 ppm) as determined from UV–vis and AAS, respectively. To further investigate the influence of sunlight irradiation on C_{ZnO}-Dots, the change in the band gap value was analyzed by using the DRS compared to that in the dark [56−58]. Figure 4.4c shows the absorption edge near ~661 nm, which corresponds to the band gap of C_{ZnO}-Dots. Figure 4.4d shows the Tauc's plot [$(\alpha h\upsilon)^2$ vs $h\upsilon$] [59]; the band gap for C_{ZnO}-Dots was 1.54 eV while their values decreased to 1.43 eV when sensitized with sunlight. The results show that the band gap energy decreases and particularly shifts toward an efficient visible light range that enhanced the photocatalysis process for Cr(VI) reduction. The high rate

constant values under sunlight irradiation as discussed earlier (Figure 4.4a) are consistent with the experimental observation based on diffuse reflectance. Furthermore, the effects of percentage (%) doping and the amount of photocatalyst (C_{ZnO}-Dots) loading had been studied to understand their effects on the rate of photoreduction. A separate study was performed by varying the experimental conditions related to the percentage doping of zinc (Figure 4.5a) and the amount of catalyst (Figure 4.5b). The results are shown in Figure 4.5, which illustrates that the maximum photoreduction [100 ppm Cr(VI)] under the influence of sunlight was obtained at 3 mg/mL amount of C_{ZnO}-Dots when they were doped with 10 wt % Zn salt as a dopant. Thus, it was inferred that the introduction of ZnO as a dopant can significantly improve the catalytic activity of C_{ZnO}-Dots and play a vital role in the photoreduction reaction on the catalyst surface.
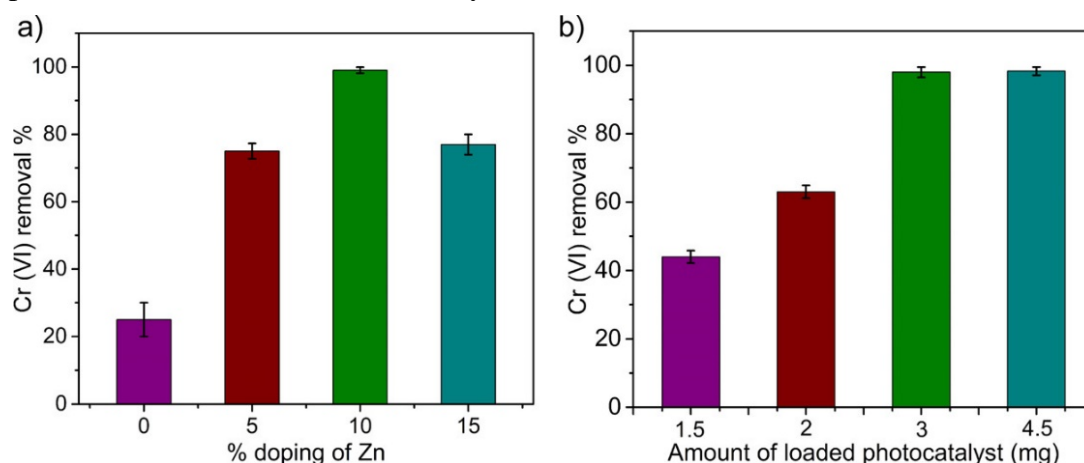

Figure 4.5: Effect of (a) % doping and (b) loading amount of the photocatalyst on the photoreduction of 100 ppm Cr(VI) in the presence of sunlight.

4.3.4. Photocatalytic Mechanism for Photoreduction

Figure 4.6a shows the plausible mechanism based on the experimental results. The electrons and holes in C_{ZnO}-Dots could be generated under sunlight illumination, as shown in equation (i). Then, the photogenerated hole in the valence band produced O_2 and H^+ as a result of reduction of H_2O, as shown in equation (ii) [60]. Afterward, the photogenerated electrons and H^+ approach Cr(VI) present in the surrounding of C_{ZnO}-Dots, for the photoreduction of Cr(VI) to Cr(III) as shown in equation (iii). Certainly, as expected, the solubility is enhanced because of the presence of defects in C_{ZnO}-Dots, which plays a critical role in the photoreduction process in approaching Cr(VI) to the active site of the C_{ZnO}-Dots surface for the

redox reaction. The valance state transformation of Cr or photoreduction of Cr(VI) to Cr(III) under the influence of sunlight irradiation using C_{ZnO}-Dots was supported by a CV study. The CV data presented in Figure 4.6b showed the cyclic voltammograms for the control and C_{ZnO}-Dots samples. The C_{ZnO}-Dots accelerate Cr(VI) to Cr(III) reduction under sunlight as observed from increase in the peak's current at ~ −0.11 V, however, such reduction did not occur under the dark condition. The increase in peaks current attributes to the decomposition of $Cr_2O_7^{-2}$ which normally did not occur, at such a low potential, but C_{ZnO}-Dots under conjugation may tune and enhance the overall process. On the other side in the case of the control sample (without doping) very insignificant reduction current occurred even under the influence of sunlight. The appearance of a single peak, broad in nature confirmed that the said reduction is a complex process for which a detailed electrochemical study is planned in the future. The reusability and stability of C_{ZnO}-Dots were also studied under sunlight irradiation, as shown in Figure 4.6c. The results indicate that the C_{ZnO}-Dots photocatalyst is stable up to seven cycles with the efficiency more than 90%.
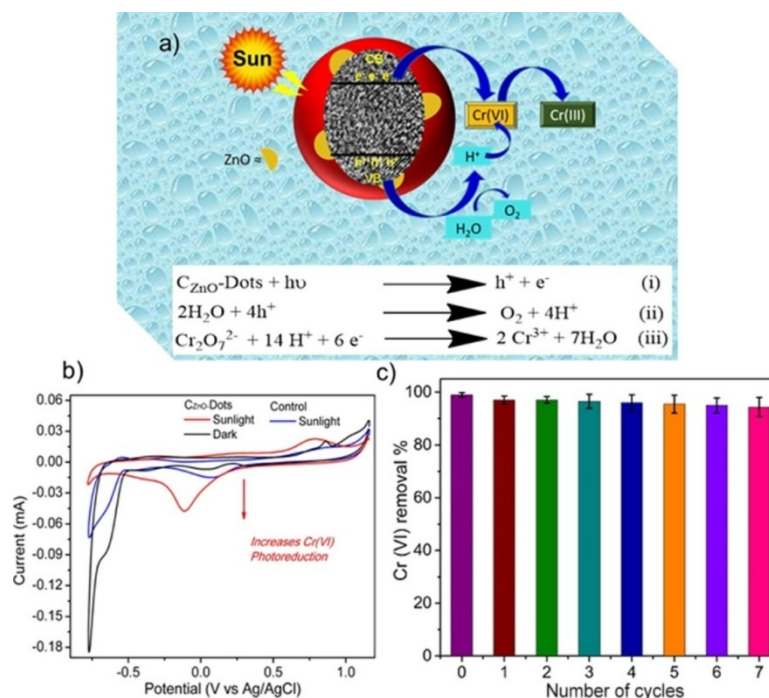
Figure 4.6: (a) Schematic representation of the plausible photoreduction mechanism of Cr(VI); (b) comparative CV response of the C_{ZnO}-Dot and control samples with a 100 ppm Cr(VI) solution in the dark and under sunlight irradiation; and (c) photocatalyst performance of C_{ZnO}-Dots up to seven cycles of recycling testing.

4.4   Conclusions

The doped-CD with inorganic salts can apparently form a newer platform among the existing class of fluorescent optical materials such as QD and organic dyes. The doped-soluble CD with a higher QY value can provide solutions to many newer emerging and existing problems. The aqueous solutions of red-emitting brightly fluorescent C_{ZnO}-Dots with excellent photostability could compete with the already existing commercially available QD and organic dyes for similar types of applications. Such as related to the deeper penetration ability of the fluorescent probe could directly relate the excellence of instructive image analysis. Beyond these, brightly fluorescent C_{ZnO}-Dots do have the potential for use as an excellent photocatalytic material because of their working window, which is situated in the lower wavelength region. Interestingly, further studies could reveal a vast prospective future of these soluble brightly fluorescent C_{ZnO}-Dots in the field of photocatalysis and water treatment.

4.5   References:

1.   Sun, Y.-P.; Zhou, B.; Lin, Y.; Wang, W.; Fernando, K. A. S.; Pathak, P.; Meziani, M. J.; Harruff, B. A.;Wang, X.; Wang, H.; Luo, P. G.; Yang, H.; Kose, M. E.; Chen, B.; Veca, L. M.; Xie, S.-Y. Quantum-Sized Carbon Dots for Bright and Colorful Photoluminescence. *J.Am.Chem. Soc.* **2006**, *128*, 7756– 7757.

2.   Shen, J.; Zhu, Y.; Yang, X.; Li, C. Graphene Quantum Dots: Emergent Nanolights For Bioimaging, Sensors, Catalysis and Photovoltaic Devices. *Chem. Commun.* **2012**, *48*, 3686– 3699.

3.   Li, X.; Rui, M.; Song, J.; Shen, Z.; Zeng, H. Carbon and Graphene Quantum Dots for Optoelectronic and Energy Devices: A Review. *Adv. Funct. Mater.* **2015**, *25* (31), 4929– 4947.

4.   Luo, P. G.; Sahu, S.; Yang, S.-T.; Sonkar, S. K.; Wang, J.; Wang, H.; LeCroy, G. E.; Cao, L.; Sun, Y.-P.Carbon "quantum" dots for optical bioimaging. *J. Mater. Chem. B* **2013**, *1* (16), 2116– 2127.

5.   Luo, P. G.; Yang, F.; Yang, S.-T.; Sonkar, S. K.; Yang, L.; Broglie, J. J.; Liu, Y.; Sun, Y.-P. Carbon-based quantum dots for fluorescence imaging of cells and tissues. *RSC Adv.* **2014**, *4* (21), 10791– 10807.

6.   Song, Y.; Zhu, S.; Yang, B. Bioimaging Based On Fluorescent Carbon Dots. *RSC Adv.* **2014**, *4*, 27184–27200.

7.   Wang, X.; Cao, L.; Yang, S.-T.; Lu, F.; Meziani, M. J.; Tian, L.; Sun, K. W.; Bloodgood, M. A.; Sun, Y.-P.Bandgap-Like Strong Fluorescence in Functionalized Carbon Nanoparticles. *Angew. Chem., Int. Ed.* **2010**,*122*, 5310– 5314.

8.   Cao, L.; Wang, X.; Meziani, M. J.; Lu, F.; Wang, H.; Luo, P. G.; Lin, Y.; Harruff, B. A.; Veca, L. M.; Murray, D.;Xie, S.-Y.; Sun, Y.-P. Carbon Dots for Multiphoton Bioimaging. *J. Am. Chem. Soc.* **2007**, *129* (37), 11318– 11319.

9.   Ali, H.; Bhunia, S. K.; Dalal, C.; Jana, N. R. Red Fluorescent Carbon Nanoparticle- Based Cell Imaging Probe. *ACS Appl. Mater. Interfaces* **2016**, *8*, 9305−9313.

10. Gao, T.; Wang, X.; Yang, L.-Y.; He, H.; Ba, X.-X.; Zhao, J.; Jiang, F.-L.; Liu, Y. Red, Yellow and Blue Luminescence by Graphene Quantum Dots: Syntheses, Mechanism and Cellular Imaging. *ACS Appl. Mater. Interfaces* **2017**, *9*, 24846– 24856.

11. Jiang, K.; Sun, S.; Zhang, L.; Lu, Y.; Wu, A.; Cai, C.; Lin, H. Red, Green and Blue Luminescence by Carbon Dots: Full-Color Emission Tuning and Multicolor Cellular Imaging. *Angew. Chem., Int. Ed.* **2015**, *54*, 5360–5363.

12. Kumawat, M. K.; Thakur, M.; Gurung, R. B.; Srivastava, R. Graphene Quantum Dots from Mangifera indica: Application in Near-Infrared Bioimaging and Intracellular Nanothermometry. *ACS Sustainable Chem. Eng.***2017**, *5*, 1382– 1391.

13. Liu, Y.; Duan, W.; Song, W.; Liu, J.; Ren, C.; Wu, J.; Liu, D.; Chen, H. Red Emission B, N, S-co-Doped Carbon Dots for Colorimetric and Fluorescent Dual Mode Detection of Fe3+ Ions in Complex Biological Fluids and Living Cells. *Angew. Chem., Int. Ed.* **2017**, *9*, 12663– 12672.

14. Amiot, C.; Xu, S.; Liang, S.; Pan, L.; Zhao, J. Near-Infrared Fluorescent Materials for Sensing of Biological Targets. *Sensors* **2008**, *8*, 3082.

15. .Hong, G.; Antaris, A. L.; Dai, H. Near-infrared Fluorophores for Biomedical Imaging. *Nat. Biomed. Eng.***2017**, *1*, 0010.

16. .Chen, J.; Wei, J.-S.; Zhang, P.; Niu, X.-Q.; Zhao, W.; Zhu, Z.-Y.; Ding, H.; Xiong, H.-M. Red-Emissive Carbon Dots for Fingerprints Detection by Spray Method: Coffee Ring Effect and Unquenched Fluorescence in Drying Process. *ACS Appl. Mater. Interfaces* **2017**, *9*, 18429– 18433.

17. Ding, H.; Yu, S.-B.; Wei, J.-S.; Xiong, H.-M. Full-Color Light-Emitting Carbon Dots with a Surface-State-Controlled Luminescence Mechanism. *ACS Nano* **2016**, *10*, 484– 491.

18. .Ding, H.; Ji, Y.; Wei, J.-S.; Gao, Q.-Y.; Zhou, Z.-Y.; Xiong, H.-M. Facile Synthesis of Red-Emitting Carbon Dots from Pulp-Free Lemon Juice for Bioimaging. *J. Mater. Chem. B* **2017**, *5*, 5272– 5277.

19. Sun, S.; Zhang, L.; Jiang, K.; Wu, A.; Lin, H. Toward High-Efficient Red Emissive Carbon Dots: Facile Preparation, Unique Properties and

Applications as Multifunctional Theranostic Agents. *Chem. Mater.* **2016**,*28*, 8659– 8668.

20. Wang, C.; Jiang, K.; Wu, Q.; Wu, J.; Zhang, C. Green Synthesis of Red-Emitting Carbon Nanodots as a Novel "Turn-on" Nanothermometer in Living Cells. *Chem.—Eur. J.* **2016**, *22*, 14475–14479.

21. Miao, X.; Yan, X.; Qu, D.; Li, D.; Tao, F. F.; Sun, Z. Red Emissive Sulfur, Nitrogen Codoped Carbon Dots and Their Application in Ion Detection and Theraonostics. *ACS Appl. Mater. Interfaces* **2017**, *9*, 18549– 18556.

22. Tripathi, S.; Sonkar, S. K.; Sarkar, S., Growth stimulation of gram (Cicer arietinum) plant by water soluble carbon nanotubes. *Nanoscale* **2011,** *3* (3), 1176-1181.

23. Sun, Y.-P.; Wang, X.; Lu, F.; Cao, L.; Meziani, M. J.; Luo, P. G.; Gu, L.; Veca, L. M. Doped Carbon Nanoparticles as a New Platform for Highly Photoluminescent Dots. *J. Phys. Chem. C* **2008**, *112*, 18295–18298.

24. Cheng, J.; Wang, C.-F.; Zhang, Y.; Yang, S.; Chen, S. Zinc ion-doped Carbon Dots with Strong Yellow Photoluminescence. *RSC Adv.* **2016**, *6* (43), 37189– 37194.

25. Xu, Q.; Liu, Y.; Su, R.; Cai, L.; Li, B.; Zhang, Y.; Zhang, L.; Wang, Y.; Wang, Y.; Li, N.; Gong, X.; Gu, Z.;Chen, Y.; Tan, Y.; Dong, C.; Sreeprasad, T. S. Highly Fluorescent Zn-Doped Carbon Dots as Fenton Reaction-Based Bio-Sensors: an Integrative Experimental-Theoretical Consideration. *Nanoscale* **2016**, *8*, 17919– 17927.

26. Son, D. I.; Kwon, B. W.; Park, D. H.; Seo, W.-S.; Yi, Y.; Angadi, B.; Lee, C.-L.; Choi, W. K. Emissive ZnO–graphene quantum dots for white-light-emitting diodes. *Nat. Nanotechnol.* **2012**, *7*, 465.

27. Wang, R.; Li, G.; Dong, Y.; Chi, Y.; Chen, G. Carbon Quantum Dot-Functionalized Aerogels for NO2 Gas Sensing. *Anal. Chem.* **2013**, *85*, 8065– 8069.

28. Zhu, A.; Qu, Q.; Shao, X.; Kong, B.; Tian, Y. Carbon-Dot-Based Dual-Emission Nanohybrid Produces a Ratiometric Fluorescent Sensor for In Vivo Imaging of Cellular Copper Ions. *Angew. Chem.* **2012**, *124*,7297– 7301.

29. Liu, S.; Tian, J.; Wang, L.; Zhang, Y.; Qin, X.; Luo, Y.; Asiri, A. M.; Al-Youbi, A. O.; Sun, X. Hydrothermal Treatment of Grass: A Low-Cost, Green Route to Nitrogen-Doped, Carbon-Rich, Photoluminescent Polymer Nanodots as an Effective Fluorescent Sensing Platform for Label-Free Detection of Cu(II) Ions. *Adv. Mater.* **2012**, *24*, 2037– 2041.

30. Zhang, J.; Yu, S.-H. Carbon Dots: Large-Scale Synthesis, Sensing and Bioimaging. *Mater. Today* **2016**, *19*, 382– 393.

31. Kong, B.; Zhu, A.; Ding, C.; Zhao, X.; Li, B.; Tian, Y. Carbon Dot-Based Inorganic–Organic Nanosystem for Two-Photon Imaging and Biosensing of pH Variation in Living Cells and Tissues. *Adv. Mater.* **2012**, *24*, 5844– 5848.

32. Baig, M. M. F.; Chen, Y.-C. Bright Carbon Dots as Fluorescence Sensing Agents for Bacteria and Curcumin. *J. Colloid Interface Sci.* **2017**, *501*, 341– 349.

33. Singh, A.; Khare, P.; Verma, S.; Bhati, A.; Sonker, A. K.; Tripathi, K. M.; Sonkar, S. K. Pollutant Soot for Pollutant Dye Degradation: Soluble Graphene Nanosheets for Visible Light Induced Photodegradation of Methylene Blue. *ACS Sustain. Chem. Eng.* **2017**, *5*, 8860– 8869.

34. Babar, D. G.; Sonkar, S. K.; Tripathi, K. M.; Sarkar, S. P2O5 Assisted Green Synthesis of Multicolor Fluorescent Water Soluble Carbon Dots. *J. Nanosci. Nanotechnol.* **2014**, *14*, 2334– 2342.

35. Saud, P. S.; Pant, B.; Alam, A.-M.; Ghouri, Z. K.; Park, M.; Kim, H.-Y. Carbon Quantum Dots Anchored TiO2 Nanofibers: Effective Photocatalyst for Waste Water Treatment. *Ceram. Int.* **2015**, *41*, 11953– 11959.

36. Yuan, X.; Jing, Q.; Chen, J.; Li, L. Photocatalytic Cr(VI) Reduction by Mixed Metal Oxide Derived from ZnAl Layered Double Hydroxide. *Appl. Clay Sci.* **2017**, *143*, 168– 174.

37. Bhati, A.; Singh, A.; Tripathi, K. M.; Sonkar, S. K. Sunlight-Induced Photochemical Degradation of Methylene Blue by Water-Soluble Carbon Nanorods. *Int. J. Photoenergy* **2016**, *2016*, 2583821.

38. Khare, P.; Singh, A.; Verma, S.; Bhati, A.; Sonker, A. K.; Tripathi, K. M.; Sonkar, S. K. Sunlight-Induced Selective Photocatalytic Degradation of

Methylene Blue in Bacterial Culture by Pollutant Soot Derived Nontoxic Graphene Nanosheets. *ACS Sustain. Chem. Eng.* **2018**, *6*, 579– 589.

39. Mishra, Y. K.; Modi, G.; Cretu, V.; Postica, V.; Lupan, O.; Reimer, T.; Paulowicz, I.; Hrkac, V.; Benecke, W.;Kienle, L.; Adelung, R. Direct Growth of Freestanding ZnO Tetrapod Networks for Multifunctional Applications in Photocatalysis, UV Photodetection and Gas Sensing. *ACS Appl. Mater. Interfaces* **2015**, *7*,14303– 14316.

40. Wen, T.; Fan, Q.; Tan, X.; Chen, Y.; Chen, C.; Xu, A.; Wang, X. A Core-Shell Structure of Polyaniline Coated Protonic Titanate Nanobelt Composites for Both Cr(VI) and Humic Acid Removal. *Polym. Chem.* **2016**, *7*,785– 794.

41. Zou, Y.; Wang, X.; Khan, A.; Wang, P.; Liu, Y.; Alsaedi, A.; Hayat, T.; Wang, X. Environmental Remediation and Application of Nanoscale Zero-Valent Iron and Its Composites for the Removal of Heavy Metal Ions: A Review. *Environ. Sci. Technol.* **2016**, *50*, 7290– 7304.

42. Santhosh, C.; Nivetha, R.; Kollu, P.; Srivastava, V.; Sillanpää, M.; Grace, A. N.; Bhatnagar, A. Removal Of Cationic And Anionic Heavy Metals From Water By 1D And 2D-Carbon Structures Decorated With Magnetic Nanoparticles. *Sci. Rep.* **2017**, *7*, 14107.

43. Khare, P.; Yadav, A.; Ramkumar, J.; Verma, N. Microchannel-Embedded Metal–Carbon–Polymer Nanocomposite As A Novel Support For Chitosan For Efficient Removal Of Hexavalent Chromium From Water Under Dynamic Conditions. *Chem. Eng. J.* **2016**, *293*, 44– 54.

44. Wen, T.; Wang, J.; Yu, S.; Chen, Z.; Hayat, T.; Wang, X. Magnetic Porous Carbonaceous Material Produced from Tea Waste for Efficient Removal of As(V), Cr(VI), Humic Acid and Dyes. *ACS Sustain. Chem. Eng.***2017**, *5*, 4371– 4380.

45. Resch-Genger, U.; Rurack, K. Determination of the photoluminescence quantum yield of dilute dye solutions (IUPAC Technical Report). *Pure Appl. Chem.* **2013**, *85*, 2005– 2013.

46. Sens, R.; Drexhage, K. H. Fluorescence quantum yield of Oxazine and Carbazine Laser Dyes. *J. Lumin.***1981**, *24–25*, 709– 712.

47. Verma, N. K.; Khare, P.; Verma, N. Synthesis Of Iron-Doped Resorcinol Formaldehyde-Based Aerogels For The Removal Of Cr(VI) From Water. *Green Process. Synth.* **2015**, *4*, 37– 46.

48. Tripathi, K. M.; Bhati, A.; Singh, A.; Sonker, A. K.; Sarkar, S.; Sonkar, S. K. Sustainable Changes in the Contents of Metallic Micronutrients in First Generation Gram Seeds Imposed by Carbon Nano-onions: Life Cycle Seed to Seed Study. *ACS Sustain. Chem. Eng.* **2017**, *5*, 2906–2916.

49. Tripathi, K. M.; Singh, A.; Bhati, A.; Sarkar, S.; Sonkar, S. K. Sustainable Feasibility of the Environmental Pollutant Soot to Few-Layer Photoluminescent Graphene Nanosheets for Multifunctional Applications. *ACS Sustain. Chem. Eng.* **2016**, *4*, 6399– 6408.

50. Tripathi, K. M.; Bhati, A.; Singh, A.; Gupta, N. R.; Verma, S.; Sarkar, S.; Sonkar, S. K. From The Traditional Way Of Pyrolysis To Tunable Photoluminescent Water Soluble Carbon Nano-Onions For Cells Imaging And Selective Sensing Of Glucose. *RSC Adv.* **2016**,*6*, 37319 – 37340.

51. Yang, C.; Zhu, S.; Li, Z.; Li, Z.; Chen, C.; Sun, L.; Tang, W.; Liu, R.; Sun, Y.; Yu, M. Nitrogen-doped Carbon Dots with Excitation-Independent Long-Wavelength Emission Produced by a Room-Temperature Reaction.*Chem. Commun.* **2016**, *52* (80), 11912– 11914.

52. Ke, C.-C.; Yang, Y.-C.; Tseng, W.-L. Synthesis of Blue-, Green-, Yellow- and Red-Emitting Graphene-Quantum-Dot-Based Nanomaterials with Excitation-Independent Emission. *Part. Part. Syst. Char.* **2016**, *33*,132– 139.

53. Karthik, P.; Vinoth, R.; Selvam, P.; Balaraman, E.; Navaneethan, M.; Hayakawa, Y.; Neppolian, B. A Visible-Light Active Catechol-Metal Oxide Carbonaceous Polymeric Material for Enhanced Photocatalytic Activity. *J. Mater. Chem. A* **2017**, *5*, 384– 396.

54. Neppolian, B.; Bruno, A.; Bianchi, C. L.; Ashokkumar, M. Graphene oxide based Pt–TiO2 photocatalyst: Ultrasound Assisted Synthesis, Characterization and Catalytic Efficiency. *Ultrason. Sonochem.* **2012**, *19*, 9– 15.

55. Chenthamarakshan, C. R.; Rajeshwar, K.; Wolfrum, E. J. Heterogeneous Photocatalytic Reduction of Cr(VI) in UV-Irradiated Titania Suspensions:

Effect of Protons, Ammonium Ions and Other Interfacial Aspects. *Langmuir* **2000**, *16*, 2715– 2721.

56. Pan, X.; Yi, Z. Graphene Oxide Regulated Tin Oxide Nanostructures: Engineering Composition, Morphology, Band Structure and Photocatalytic Properties. *ACS Appl. Mater. Interfaces* **2015**, *7*, 27167– 27175.

57. Zhao, Y.; Zhang, Y.; Liu, A.; Wei, Z.; Liu, S. Construction of Three-Dimensional Hemin-Functionalized Graphene Hydrogel with High Mechanical Stability and Adsorption Capacity for Enhancing Photodegradation of Methylene Blue. *ACS Appl. Mater. Interfaces* **2017**, *9*, 4006– 4014.

58. Umrao, S.; Sharma, P.; Bansal, A.; Sinha, R.; Singh, R. K.; Srivastava, A. Multi-layered graphene quantum dots derived photodegradation mechanism of methylene blue. *RSC Adv.* **2015**, *5*, 51790– 51798.

59. Yu, H.; Irie, H.; Hashimoto, K. Conduction Band Energy Level Control of Titanium Dioxide: Toward an Efficient Visible-Light-Sensitive Photocatalyst. *J. Am. Chem. Soc.* **2010**, *132*, 6898– 6899.

60. Wu, J.; Liu, B.; Ren, Z.; Ni, M.; Li, C.; Gong, Y.; Qin, W.; Huang, Y.; Sun, C. Q.; Liu, X. CuS/RGO Hybrid Photocatalyst for Full Solar Spectrum Photoreduction From UV/Vis to Near-Infrared Light. *J. Colloid Interface Sci.* **2018**, *517*, 80– 85.

Chapter-5

Water Soluble Carbon Nano-onions for Cell Imaging and Selective Sensing of Glucose
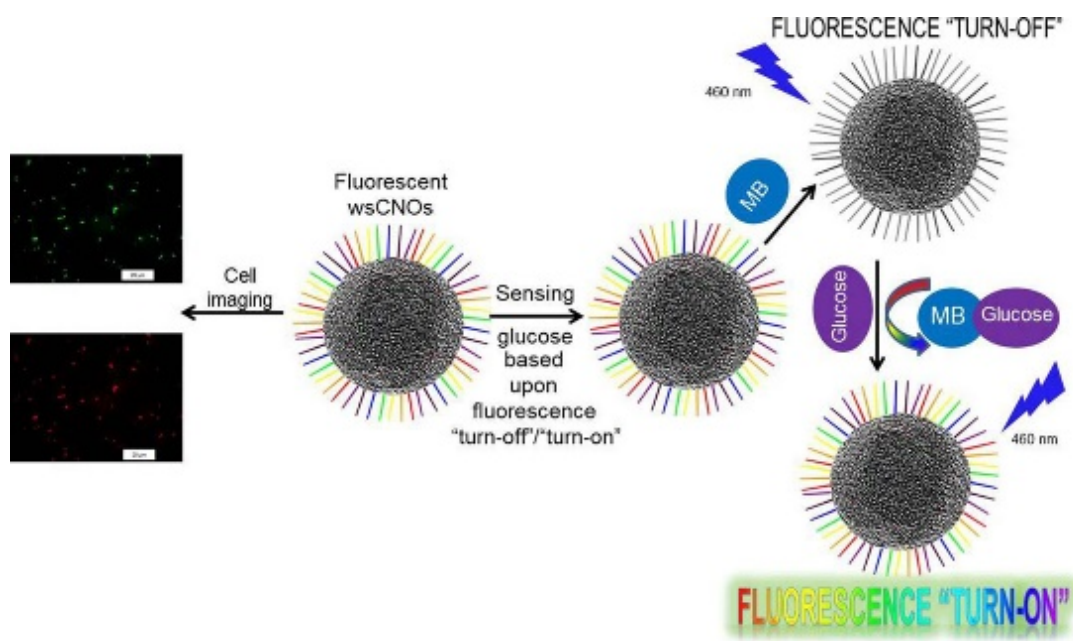
5.1   Introduction

Till now, only a few reports have been available on the investigation of biological applications of CNO and it is still necessary to understand in detail their non-toxic nature[1-6] and tunable PL properties [1,2,7,8]. To make these soluble in organic solvents various adducts of CNO were formed based upon simple organic chemistry [9,10]. Recently Giordani *et al.* investigated various routes for the modification of CNO surface using diverse functional groups for potential applications in biomedical imaging [7,8,11]. Low toxicity with biocompatibility and ease in cellular uptake with good penetration capability are the important aspects for bioimaging [1,2,5,12]. Readily achievable tunable PL in the green-red region with a slight extension in the NIR have added an additional advantage [7,13] in contrast to the blue-green emissions of other fluorescent nanocarbons. Imaging in the NIR region is of huge significance as it offers high biological transparency [14] because of low light scattering, deeper penetration and low background signal [15]. Sensing of blood glucose has gained extensive attention worldwide because diabetes mellitus is one of the major health problems [16]. It has become a global issue and according to the WHO, approximately 300 million people suffering from diabetes and this figure will increase up to 600 million by 2030 [17]. So glucose detection is highly significant in the clinical diagnosis and biochemical study of this illness. Most of the sensors used for glucose detection are either, based upon an electrochemical method, enzyme-based techniques (glucose oxidase) or microdialysis probes [17,18]. However, many of these methods suffer from instability, environmental sensitivity, cytotoxic effect of the probe and require sophisticated, expensive instrumentation, chemicals (enzymes) and the complex synthetic procedures are time consuming. In this chapter a traditional pyrolysis route was adopted for the synthesis of CNO using vegetable ghee as low cost available carbon source. To separate the most fluorescent fraction of wsCNO from the bulk as-produced wsCNO, gel filtration was done and this fraction was used for the imaging of *E. coli* and *P. putida* cells. The wsCNO possess a high density of carboxylic and hydroxyl groups on their surface making them a stable species in aqueous solution and thus, they can readily diffuse into the cell without causing any cell damage [1,2] and ultimately excreted from the body [1]. Furthermore, this most fluorescent fraction can be utilized as the non-enzymic

sensor for selective and immediate sensing of "glucose" via a fluorescent "turn-off"/"turn-on" [19] mechanism.

5.2.   Experimental section

5.2.1. Materials

All the experiments were performed in DI. Vegetable ghee (Dalda), was procured from a local market in Jaipur, India. All the chemicals and solvents were of analytical grade and used as-obtained without any further purification. MB, glucose, dopamine and amino acids were purchased from Sigma-Aldrich (India).

5.2.2. Instrumentation

TEM, fluorescence microscopy, XPS, FTIR, UV-Vis and fluorescence spectroscopy instrumentation were same as described in Chapter 2 and 3. Raman spectrometer with 532 nm laser excitation. TGA was conducted under a nitrogen atmosphere with a Mettler thermal analyzer at a heating rate of $10^{o}C$ min^{-1}. Weight loss versus temperature were recorded starting from room temperature up to $900^{o}C$. Surficial charge analysis for wsCNO in aqueous medium was done with zeta potential measurement on a Beckman Coulter Delsa™ Nano.

5.2.3. Synthesis of wsCNO

The CNO were synthesized using simple and traditional pyrolysis of vegetable ghee as a low cost source of carbon with a cotton wick. The soot was collected in an inverted borosilicate glass beaker to avoid any chance of metal impurities. The as-collected soot was purified using a Soxhlet extraction technique [12,21] in which soot was washed with different boiling solvents (acetone, methanol, acetonitrile and petroleum ether) to remove any unburnt hydrocarbons and impurities. The water solubility for the Soxhlet purified soot was achieved by refluxing it with 60% HNO_3 solution for 12 h and the excess nitrate was removed by repeatedly washing with DI in a water bath according to a previously reported method [22–24]. The yield of the water soluble product (as wsCNO) was 87% (based on the CNO used for oxidation). To isolate the most fluorescent fraction of wsCNO with a narrow size distribution, high-speed centrifugation was performed followed by a gel filtration separation method using a Sephadex G-100 column as

described earlier [25,26]. The overall yield of the light yellow colored fraction of wsCNO was 17% (based on the amount of CNO used for oxidation) having the QY value of 1.9% and this was used further for cell imaging and selective detection of glucose molecules.

5.2.4. Cell staining

Cells of the DH5α strain of *E. coli* and the MTCC 2445 strain of *P. putida* were incubated with the wsCNO (100 ppm) in 20 mL of freshly prepared food medium (Luria-Bertani media for *E. coli* and minimal media for *P. putida* cells), as described earlier [1,12,22,27]. Then, the cells with the remaining broth containing wsCNO, were washed thoroughly, three times, with phosphate buffered saline. The sample for cellular imaging was prepared by dropping a droplet of bacterial suspension (8–10 µL) on a glass slide.

5.2.5. Fluorescence detection of glucose

Glucose sensing was performed at room temperature in aqueous solution. Initially 1 mL of MB ($6.2*10^{-4}$ M) was added to an aqueous solution of wsCNO ($1.5*10^{-4}$ g mL^{-1}) by continuous addition of 0.1 mL MB solution in 10 steps. After adding MB, the fluorescence emission spectra were recorded immediately. DI was added to make the final volume up to 3 mL in each step. Glucose solution (0.1 mL; $1.8*10^{-2}$ M) was added to the MB–wsCNO solution to restore the fluorescence intensity. Interferences which originated from other protein, or amino acids were investigated individually. All the fluorescence spectral measurements were done at ambient conditions at the same excitation wavelength of 460 nm.

5.3. Results and discussion

The strong oxidizing nature of HNO$_3$ assists the incorporation of –COOH and –OH groups on to the surface of CNO. These groups impart its solubility in aqueous media with multi-colored emissive tunable photoluminescent properties, which represented the characteristic features of FNC [28,29]. Furthermore, the size selective separation was achieved using high-speed centrifugation followed by gel filtration to achieve the most fluorescent fraction of wsCNO having the QY value of 1.9%. Most importantly, the high-density surface of carboxylated wsCNO exhibited

a broad range of tunable PL emissions across a wide range of the visible spectrum with a very slight extension in the NIR region.

5.3.1. FTIR/Raman/XPS/powder XRD/TGA analysis

The FTIR spectra of CNO and wsCNO are shown in Figure 5.1(a). The FTIR spectrum of CNO (Figure 5.1(a)-solid line) shows a sharp peak around 2930 cm^{-1} which is because of the presence of sp^3 (C–H) stretching vibrations and a strong peak at around 1654 cm^{-1} shows the presence of (C=C) stretching vibrations. The FTIR spectrum of wsCNO (dotted line) as displayed in Figure 5.1(a) shows the characteristic peaks of –OH (broad) at 3402 cm^{-1}, –C=C– at 1578 cm^{-1} and –C=O at 1716 cm^{-1} (a sharp peak), which confirms the presence of surficial carboxylic and hydroxyl type hydrophilic groups [20,12]. It also shows the presence of sp^3 carbon because of the existence of a characteristic C–H peak at 2915 cm^{-1}. A peak at 1214 cm^{-1} showed the presence of a –C–O group in the wsCNO. To investigate the negative surface functionalities, zeta potential analysis was performed, which showed a high negative value of 40.04 mV, confirming the presence of high density negatively charged surface groups. [30] To quantify the sum of negative surface carboxyl groups present on the surface of wsCNO, a very simple acid–base titration was performed to calculate its weight percentage and was found to be in the range of 15–16.7% (varied batch-to-batch) [20,22,31]. This high density carboxylation leads to high solubility and stability of wsCNO in aqueous solution. As well as the solubility, high density "self-passivated" wsCNO generated by surface carboxylation will be useful for performing a huge range of functionalization chemistry of wsCNO with [4,32,33] or without biomolecules (such as oligomeric [25,32,33] and monomeric amines) [29] based upon the simple amide linkage chemistry. Raman spectra were used to understand the extent of derivatization concerning the ratio of intensities of the G and D bands (I$_G$/I$_D$) and for structural elucidation of graphitic materials regarding band positions[34]. Figure 5.1(b) shows the Raman graphs of Soxhlet purified CNO (solid line) and its water soluble version (dotted line). Both Soxhlet purified soot and wsCNO exhibited two prominent characteristic bands for carbon atoms present in the graphitic framework. The graphitic (G-band) at 1600 cm^{-1} and disordered (D-band) at 1349 cm^{-1} corresponds

to the E_2g mode of graphitic carbon in a two dimensional hexagonal lattice and a dangling bond in the disordered graphitic shells present in CNO, respectively [35]. Both D and G bands show the downward shift at ~1330 cm^{-1} (from 1349 cm^{-1}) and ~1582 cm^{-1} (from 1600 cm^{-1}), which corroborate the weakening of the graphitic structure in the form of bending and destructions of bonds influenced by the oxidative treatment [1,2,12,22,36], inferring the introduction of a high-density surface defect [1,2,12]. Incorporation of high-density defects in the outermost shell of the nano-onions containing higher number of shells resulted in a disordered like spectrum as reported by Choucair *et al* [34]. Incorporation of high-density surface functionalization is calculated using the I_G/I_D ratio. The wsCNO I_G/I_D ratio (0.18) was found to be much smaller in comparison with the Soxhlet purified CNO I_G/I_D ratio (0.43). The decrease in the values of I_G/I_D ratio for wsCNO strongly supports the formation of high degree of surface defects which arise from the transformation of sp^2 clusters of graphitic carbons in disordered functionalized sp^3 hybridized carbon atoms [37,22]. The presence of negative hydrophilic groups as surface elements and chemical composition was determined using XPS measurements. The XPS spectrum of wsCNO shown in Figure 5.1(c) clearly shows that carbon (C_{1s}) and oxygen (O_{1s}) are present on the surface of wsCNO at 286 eV and 535 eV, respectively. Figure 5.1(d) and (e) describes the high-resolution short scanned XPS spectra of C_{1s} and O_{1s}, respectively. Short scanned carbon, C_{1s} analysis as displayed in Figure 5.1(d) shows the presence of three different peaks located at 285.8 eV, 286.7 eV and 287.6 eV, which corresponds to the presence of C=C, C–O and C=O respectively and indicates the presence of carboxylic acid functionalities.[38] The short scan high-resolution XPS survey for the O_{1s} region shows the presence of three major peaks at 533.7 eV, 535.1 eV and 536.2 eV corresponding to the presence of C–O, C=O and COO^-, respectively [39]. The results of surface functionality analyses using XPS are in agreement with the results from FTIR analysis [40]. TGA analysis was carried out to understand the thermal stability of wsCNO [12]. The comparative TGA analysis for both the samples, Soxhlet purified CNO (solid line) and wsCNO (dotted line) are displayed in Figure 5.1(f). Both the samples show a gradual degradation in weight starting from 35°C. TGA analysis shows that wsCNO are thermally less stable in comparison with Soxhlet purified soot because of the

presence of a high degree of surficial oxygen species (–COOH/–OH) generated from the destruction of surficial graphitic framework of wsCNO during its oxidative process [22]. A weight loss of 24.1% was observed for wsCNO in comparison with a loss of 8.1% for Soxhlet purified CNO under the same temperature conditions. Figure 5.1(g) shows the XRD spectra of wsCNO having the characteristic peaks of graphitic carbon with an inter-planar distance of 0.32 nm [41].
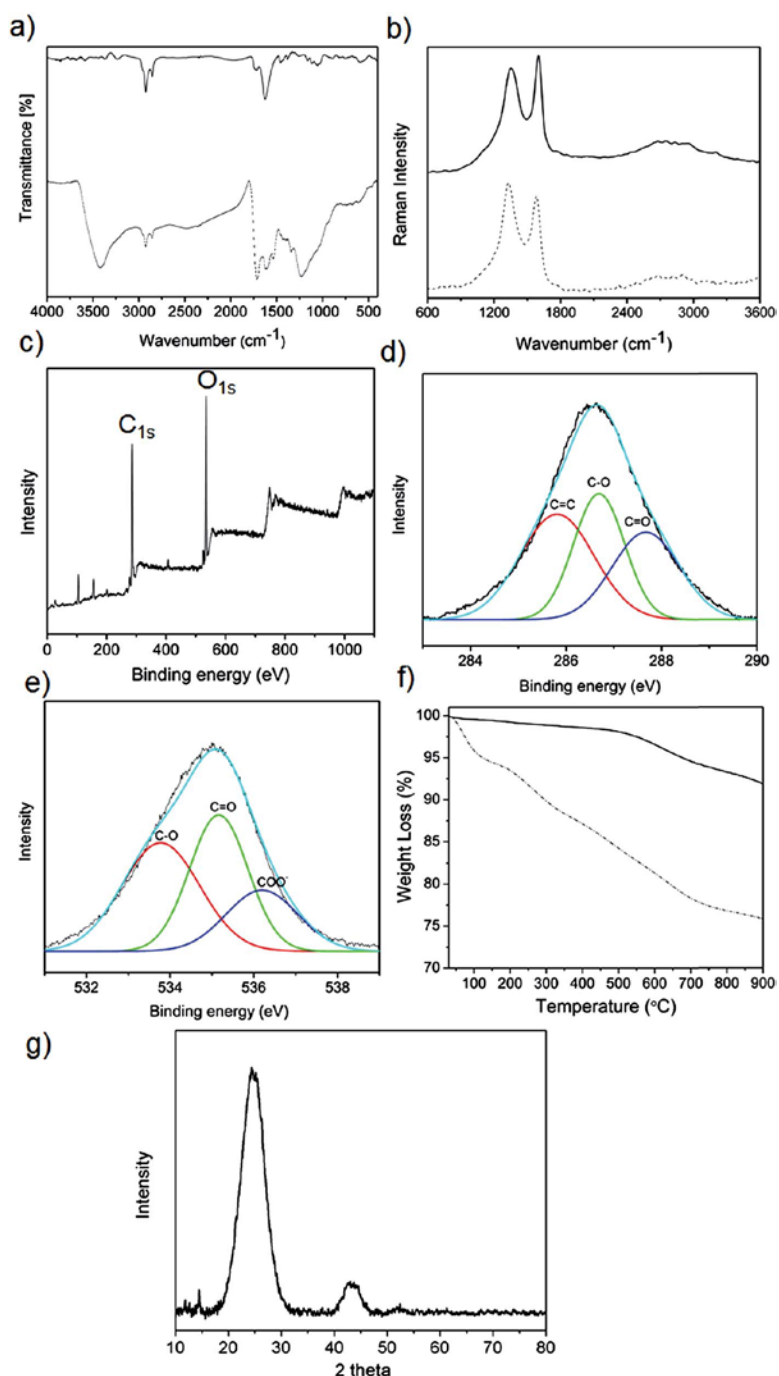
Figure 5.1: (a) FTIR spectra of CNO (solid line) and wsCNO (dotted line); (b) Raman spectra showing D and G band of Soxhlet purified soot (before derivatization solid line) and wsCNO (after derivatization, dotted line); (c) XPS spectrum showing elemental C and O in the wsCNO; (d and e) shortscan high-resolution XPS for carbon and oxygen; (f) TGA graphs of Soxhlet purified (solid line) and wsCNO (dotted line); (g) powder XRD showing two prominent peaks corresponding to the graphitic carbon in wsCNO.

5.3.2. Microscopic studies

The physical appearance and internal detailed microstructure characterization of soluble nano-onions were carried out using FESEM, TEM and HRTEM. Figure 5.2(a) shows a high magnification FESEM image, without presence of any amorphous type carbon. Figure 5.2(b) illustrates the well dispersed and spherical nature of wsCNO showing some opacity because of the overlapping of the nanoparticles. Based on Figure 5.2(b), the average size distribution of wsCNO was calculated statistically and the size distribution of wsCNO (diameter ranging from 10–50 nm) in the form of a histogram is shown in Figure5.2(c). The size range of the majority of the wsCNO were 20–40 nm. HRTEM images of nano-onions as shown in Figure 5.2(d) and (e) illustrate the presence of a closed quasi-spherical shape having graphitic inter-planer fringes with a lot of defects. HRTEM images show the presence of well-resolved lattice fringes with 0.32 nm lattice spacing, which is indicative of their graphitic nature [42]. HRTEM images clearly reveal the closed cage structure of well-defined concentric shells and their crystallized structure. Surficial defects as marked by black arrows are in good agreement with the Raman analysis regarding I_G/I_D ratio.
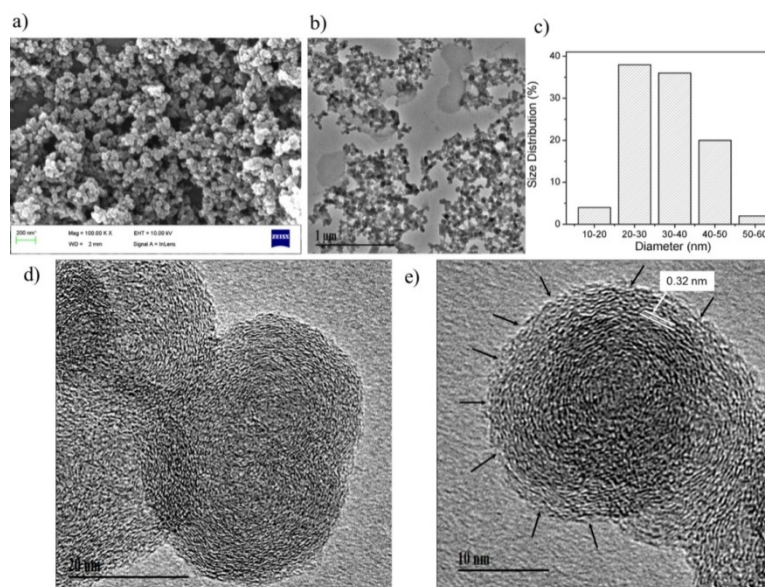
Figure 5.2: (a) High resolution FESEM image of wsCNO; (b) Low magnification TEM image showing the nearly monodispersed wsCNO; (c) Diameter distribution histogram**;** (d, e) HRTEM image of wsCNO and; (e) Shows the identified crystalline lattices planes of wsCNO with lot of surficial defects (marked by black arrows).

5.3.3. Absorption, PL emission–excitation study and photostability test under high ionic conditions:

The wsCNO are highly soluble in water and remain soluble for several months. The absorption spectrum as demonstrated in Figure 5.3(a) exhibits a characteristic absorption band which is attributed to the typical absorption of conjugated p-plasmons of sp^2 domains [12,43,22]. The excitation dependent tunable PL was studied at room temperature in an aqueous solution. wsCNO emits in a broader region of the visible spectrum with its extension to NIR (from 550 nm to 800 nm), as displayed in Figure 5.3(b), when excited from 400 to 660 nm with a progressive increment of 20 nm. The emission maximum is centered in the greener region of spectrum at about 550 nm (excitation at 400 nm) with the QY value of 1.9%. [18] Figure 5.3(c) shows the magnified image of Figure 5.3(b), revealing the tunable shifting of emissions towards the redder region of the spectrum with its NIR extension. The characteristics of the multi-colored tunable excitation dependent emission profiles of wsCNO continuously shifted towards the redder region of the spectrum which is the characteristic features of FNC [44,45]. The possible mechanism of a multi-colored tunable PL emissive profile from the single particle of

wsCNO involves the radiative recombination of quantum confinement effects of excitations [46,1,2,25,29,47], emissive surface traps, dipole emitted centers and the coupling of electron–phonons present over the defective surfaces of wsCNO [48,49]. Full width at half maximum measurements have the value of 65.23nm, showing the small size distribution of wsCNO. Figure 5.3(d) shows the excitation (PL) spectrum at 460 nm emission wavelengths for wsCNO with four absorptions centered at 220 nm (5.63 eV), 239 nm (5.18 eV) and 285 nm (4.35 eV) and 307 nm (4.0 eV) which confirms the presence of various types of light emitting centers [47,50]. Not only is the tunable PL important, but photostability is also another important issue related to its various uses in biological applications, because of the very different ionic environmental conditions of biological cells. To understand better the photostability, two different sets of experiment were performed: continuous photo-excitation and testing its stability in the presence of high ionic strength solutions. wsCNO exhibits excellent photostability and no sign of reduction in PL intensity was observed after 5h of continuous excitation with 400 nm wavelength as displayed in Figure 5.3(e). Additionally, the PL emission remains unaffected in the presence of high concentrated solutions of Na(I) and Ba(II) ions ($1*10^{-5}$ to 0.1 M) (Figure 5.3(f) and (g)), respectively. The fluorescence microscopic images of wsCNO under excitation at 488 nm and 562 nm are demonstrated in Figure 5.3(h) and (i), respectively. High photostability towards long-term continuous excitation and in a high ionic strength solution indicates its significant potential for fluorescent cell imaging and it could also be used for sensing purposes.
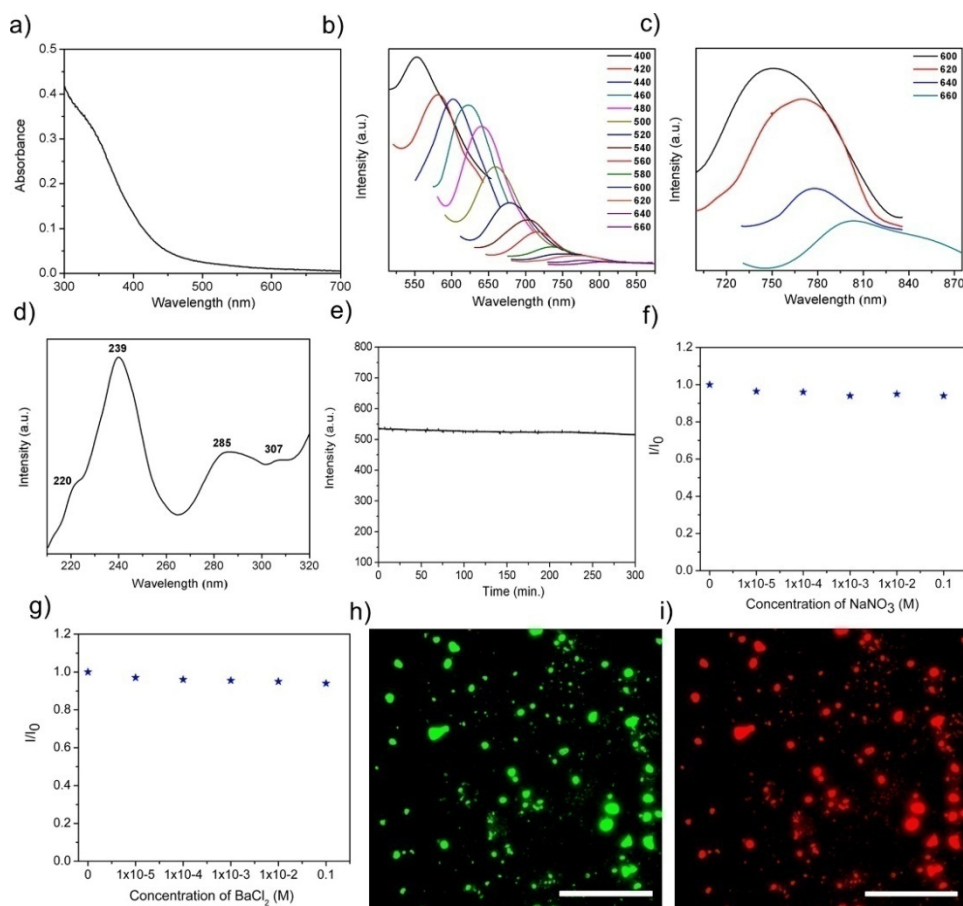
Figure 5.3: Multi-colored emissive tunable emissions profile of wsCNO; (a) Absorbance spectra of wsCNO in aqueous solution; (b) Excitation-dependent emission from 400-660 nm with the progressive increments of 20 nm; (c) Zoomed image of (b) showing NIR emission profiles; (d) PL excitation spectrum of wsCNO at 640 nm excitation wavelength; (e) Time dependence photostability test of wsCNO on continuous excitation with 400 nm wavelength for 5h; (f-g) Photostability test in the presence of high ionic strength of $NaNO_3$ and $BaCl_2$; (h) and (i) Fluorescence microscopic images of wsCNO under 488 nm (green) and 562 (red) nm bandpass filter respectively. Scale bar: 10 µm.

5.3.4. Fluorescence imaging of *E. coli* and *P. putida* cells

 E. coli and *P. putida* cells were used for the imaging purposes. A sample of wsCNO with a concentration of 100 ppm was mixed with 20 mL of the specific food media of *E. coli* and *P. putida,* in comparison with the control media (media without wsCNO). Cell imaging experiments were performed with three replicates each time, with and without the presence of wsCNO. Figure 5.4 shows the fluorescent images of

wsCNO labelled *E. coli* (a and b) and *P. putida* (c and d) under the green and red channel of fluorescence microscope, respectively. This simple and easy labelling of wsCNO via oral ingestion (mixing with food only) will be researched further for specified imaging of different parts of cell based upon the attachment of different surface functionalities which can selectively attach inside the different regions of cells.
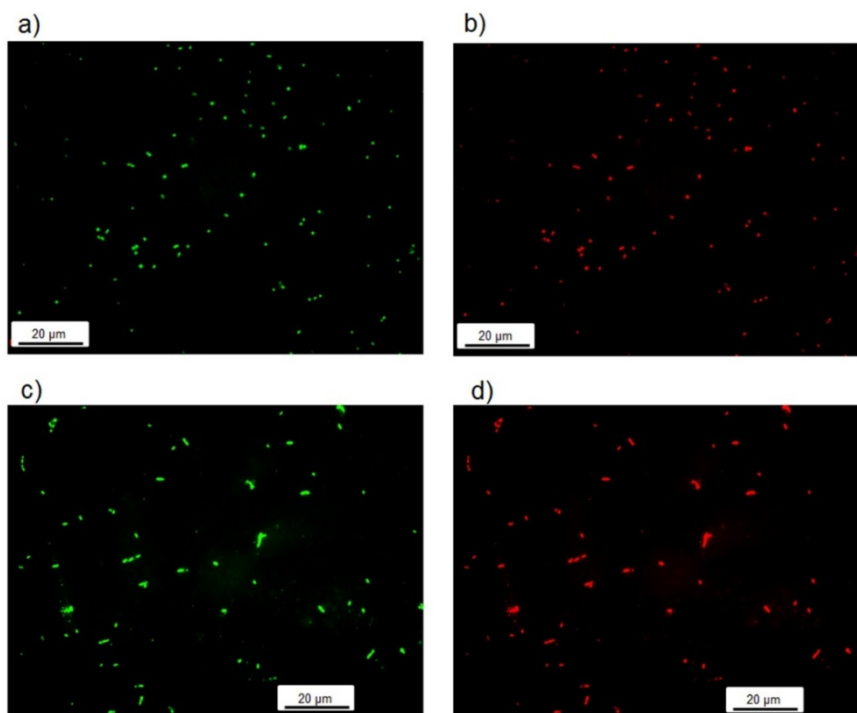
Figure 5.4: Fluorescence microscopy images of *E. coli* (a) and (b); *P. putida* (c) and (d) under 488 nm (green) and 562 nm (red) band pass filters respectively.

5.3.5. Glucose sensing

The most fluorescent fraction of "self-passivated" wsCNO, was used for the development of selective sensing of glucose based upon the simple fluorescence "turn-off/turn-on" mechanism [22]. Fluorescence intensity of wsCNO was efficiently quenched by MB to its maximum (fluorescent turn-off) and would be "turn on" after the addition of glucose. The mechanistic illustration for the development of wsCNO (fluorescence "turn-off/turn-on") based glucose biosensor is shown in Figure 5.5(a). When wsCNO interacted with MB, the fluorescent emission profiles of wsCNO were quenched to its maximum by the stepwise addition of MB. Because of the efficiency of high density, negatively charged wsCNO interacted with MB molecules via surficial charge transfer and hydrophilic interactions [22] that resulted in the fluorescence "turn off" for wsCNO as illustrated in Figure 5.5(b).

The intensity of the 623 nm center emission peak of wsCNO ($1.5 * 10^{-4}$ g mL^{-1}) was completely quenched by MB within 20 minutes by the gradual addition of 1 mL MB ($6.2 * 10^{-4}$M) in 10 steps (0.1 mL in each step) (Figure 5.5(b)). The maximally quenched fluorescence intensity of wsCNO (Figure 5.5(c) blue trace) was recovered by the addition of glucose (0.1 mL, $1.8*10^{-2}$ M). The photoluminescent emission in wsCNO occurred because of the recombination of the electron–hole pair via photo-generation on the surface [1,2,12,20,37,46]. After the adsorption of MB on the wsCNO surface, electron transfer from wsCNO to MB diminished the recombination of electron–hole pair and resulted in fluorescence quenching. The interaction of surficial hydrophilic groups with MB and better availability of the CNO surface for adsorption of MB act as the driving force for the fluorescence "turn off". The possible mechanism for the fluorescence "turn-on" could be because of H-bonding interaction between primary alcoholic group of glucose and nitrogen of the center ring of surface adsorbed MB. This causes the replacement of surface adsorbed MB molecules by glucose from the wsCNO and ultimately leads to its fluorescence restoration, termed as fluorescence "turn-on" as shown in Figure 5.5(c) (red trace) [51–55]. Glucose has two types of –OH groups, four similar types of secondary alcoholic groups and a single primary alcoholic group which is a bit more acidic in comparison with other four [52]. This primary alcoholic group has the tendency to bind with MB via H-bonding [51–55] and ultimately causes the reduction of MB. This simple reduction chemistry of MB by the protonation from glucose is very well known and is described in the literature [51–55]. The emission intensity continuously decreases with MB addition until a maximum is reached as shown by the Stern–Volmer plots in Figure 5.5(d). Also, wsCNO have a unique morphology and a significant number of defects in the forms of dangling bonds [56] which can also lower the activation energy of desorption of MB and selective sensing of glucose by fluorescence "turn-on". In addition to sensing, it is known that selectivity is a prime parameter for developing a sensor for biological applications in order to utilize its maximum potential inside very complicated cellular environments [57]. A non-enzymatic, wsCNO-based sensor was developed for the selective detection of glucose molecules. The selectivity of glucose, was explored with some common interferants, such as dopamine, uric acid and amino acids (cysteine, methionine, aspartic acid, tryptophan and valine; $2.4 * 10^{-2}$M) at identical experimental conditions. Figure 5.5(e), shows the selective detection of glucose by

comparison with other methods based on the fluorescence "turn-off"/"turn-on" mechanism of wsCNO. The comparison between wsCNO and various fluorescence sensors from the literature review for the detection of glucose are presented in Table 5.1. Although, a few materials have a lower detection limit than wsCNO ($1.3* 10^{-2}$ M) but the cost effective nature and simplicity of the detection process with wsCNO used here are advantageous in terms of immediate response time (restoration of maximally quenched fluorescence intensity) within a few seconds [17,58–61].
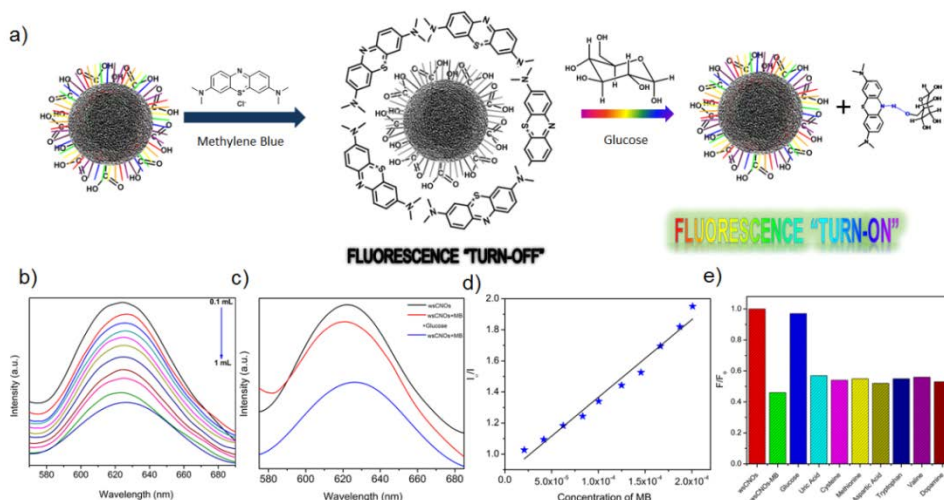
Figure 5.5: (a) A **s**chematic presentation depicted the mechanism based on fluorescence "turn-off" and "turn-on" method *via* the adsorption of MB and glucose molecules on wsCNO respectively for sensing glucose; (b) PL emission spectra from stepwise addition of 0.1 mL aqueous solutions of MB showing maximal quenched solution; (c) Fluorescence "turn on" after the replacement of MB molecules with glucose from wsCNO surface; (d) Relationship between the PL intensity of wsCNO and MB concentration and (e) Selectivity of wsCNO based fluorescence sensor for glucose.

Table 5.1 Performance comparison between various fluorescence sensors toward glucose molecule.

Methods	Response Time	Detection limits	Ref.
i-motif DNA	30 min.	4 µM	[58]
APBA-CuInS$_2$ QD	40 min.	1.2 µM	[17]
Optical fiber	10 min.	0.05 µg/ml	[62]
CdTe-QD	15 min.	50 nm	[59]
BSA-Au nanoclusters	60 min.	5.0×10^{-6}M	[60]
GOx immobilized on Bamboo inner cell membrane	5 min.	58µM	[61]
wsCNO	Immediate	1.3×10^{-2} M	this study

5.3.5.1 Calculation of detection limit(LD) of glucose

The detection limit of glucose was calculated with the help of following equation:

$$LD = \frac{3 * SD}{K}$$

K represents the slope of liner fit curve of the fluorescence turn on values (I/Io) *vs.* glucose concentration and SD denoted the the standard deviation. As demonstrated in Figure 5.6, the K value is obtained to be 234.46, whereas SD is 1.05. The LD was thus calculated to be 1.3×10^{-2} M.
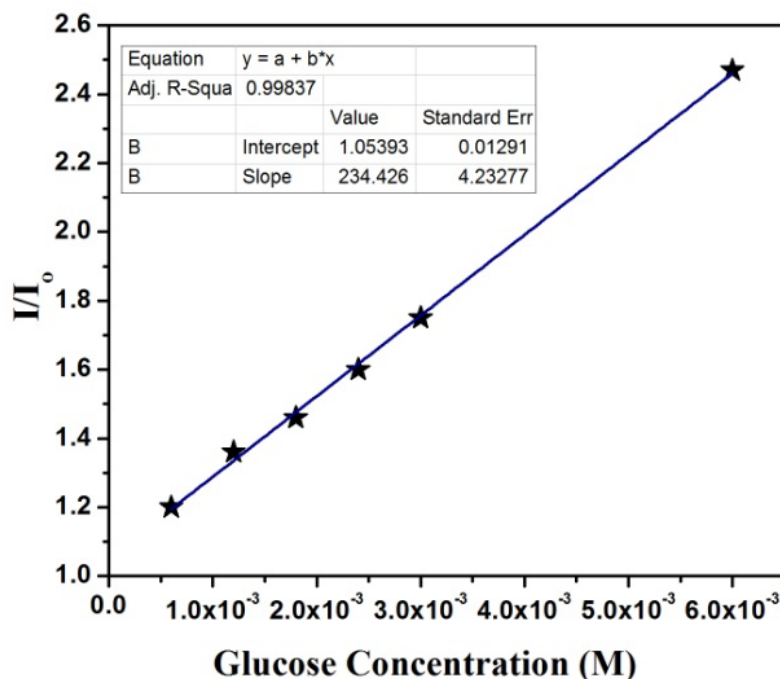
Figure 5.6: Calibration curve for fluorescence turn on by glucose

5.4.   Conclusion

Large-scale fabrication of pure wsCNO via a simple and convenient route is described in this chapter. The highly defective outer surfaces impart tunable PL properties to "self-passivated" wsCNO and make them a promising candidate for use in biological imaging and sensing applications. The most fluorescent fraction was separated using gel filtration and applied as the fluorescent probe for the imaging of *E. coli* and *P. putida* cells. Furthermore, the same fraction of wsCNO was used in this research for the selective and immediate sensing of glucose molecules, based upon the fluorescence "turn-off"/"turn-on" technique (detection limit = $1.3 * 10^{-2}$ M). The ease of synthesis of wsCNO by using vegetable ghee as a carbon precursor could lead the way for the fabrication of large scale, pure and NIR-emissive wsCNO for multi-functional applications.

5.5   References

1.   Ghosh, M., Sonkar, S. K., Saxena, M., Sarkar, S., Carbon Nano-Onions for Imaging the Life Cycle of Drosophila Melanogaster. *Small,* **2011,** *7* (22), 3170–3177.

2.   Sonkar, S. K., Ghosh, M., Roy, M., Begum, A., Sarkar, S., Carbon Nano-Onions as Nontoxic and High-Fluorescence Bioimaging Agent in Food Chain—an in Vivo Study from Unicellular E. Coli to Multicellular C. Elegans. *Mater. Express,* **2012,** *2* (2), 105-114.

3.   Bartelmess, J., Quinn, S. J., Giordani, S., Carbon Nanomaterials: Multi-Functional Agents for Biomedical Fluorescence and Raman Imaging. *Chem. Soc. Rev.,* **2015,** *44* (14), 4672-4698.

4.   Bartelmess, J., Giordani, S., Carbon Nano-Onions (Multi-Layer Fullerenes): Chemistry and Applications. *Beilstein J. Nanotechnol.,* **2014,** *5*, 1980-1998.

5.   Sonkar, S. K., Roy, M., Babar, D. G., Sarkar, S., Water Soluble Carbon Nano-Onions from Wood Wool as Growth Promoters for Gram Plants. *Nanoscale,* **2012,** *4* (24), 7670-7675.

6.   Luszczyn, J., Plonska-Brzezinska, M. E., Palkar, A., Dubis, A. T., Simionescu, A., Simionescu, D. T., Kalska-Szostko, B., Winkler, K., Echegoyen, L., Small Noncytotoxic Carbon Nano-Onions: First Covalent Functionalization with Biomolecules. *Chem. -Eur. J.,* **2010,** *16* (16), 4870-4880.

7.   Giordani, S., Bartelmess, J., Frasconi, M., Biondi, I., Cheung, S., Grossi, M., Wu, D., Echegoyen, L., O'Shea, D. F., Nir Fluorescence Labelled Carbon Nano-Onions: Synthesis, Analysis and Cellular Imaging. *J. Mater. Chem. B,* **2014,** *2* (42), 7459-7463.

8.   Bartelmess, J., De Luca, E., Signorelli, A., Baldrighi, M., Becce, M., Brescia, R., Nardone, V., Parisini, E., Echegoyen, L., Pompa, P. P., Giordani, S., Boron Dipyrromethene (Bodipy) Functionalized Carbon Nano-Onions for High Resolution Cellular Imaging. *Nanoscale,* **2014,** *6* (22), 13761-13769.

9.   Molina-Ontoria, A., Chaur, M. N., Plonska-Brzezinska, M. E., Echegoyen, L., Preparation and Characterization of Soluble Carbon Nano-Onions by

Covalent Functionalization, Employing a Na-K Alloy. *Chem. Commun.,* **2013,** *49* (24), 2406-2408.

10. Cioffi, C. T., Palkar, A., Melin, F., Kumbhar, A., Echegoyen, L., Melle-Franco, M., Zerbetto, F., Rahman, G. M. A., Ehli, C., Sgobba, V., Guldi, D. M., Prato, M., A Carbon Nano-Onion–Ferrocene Donor–Acceptor System: Synthesis, Characterization and Properties. *Chem. -Eur. J.,* **2009,** *15* (17), 4419-4427.

11. Bartelmess, J., Frasconi, M., Balakrishnan, P. B., Signorelli, A., Echegoyen, L., Pellegrino, T., Giordani, S., Non-Covalent Functionalization of Carbon Nano-Onions with Pyrene-Bodipy Dyads for Biological Imaging. *RSC Adv..* **2015,** *5* (62), 50253-50258.

12. Dubey, P., Tripathi, K. M., Sonkar, S. K., Gram Scale Synthesis of Green Fluorescent Watersoluble Onion-Like Carbon Nanoparticles from Camphor and Polystyrene Foam. *RSC Adv.,* **2014,** *4* (12), 5838-5844.

13. Bartelmess, J., Baldrighi, M., Nardone, V., Parisini, E., Buck, D., Echegoyen, L., Giordani, S., Synthesis and Characterization of Far-Red/Nir-Fluorescent Bodipy Dyes, Solid-State Fluorescence and Application as Fluorescent Tags Attached to Carbon Nano-Onions. *Chem.- Eur. J.,* **2015,** *21* (27), 9727-9732.

14. Kim, J.-W., Galanzha, E. I., Shashkov, E. V., Moon, H.-M., Zharov, V. P., Golden Carbon Nanotubes as Multimodal Photoacoustic and Photothermal High-Contrast Molecular Agents. *Nat Nanotechnol.,* **2009,** *4* (10), 688-694.

15. Wang, R., Zhang, F., Nir Luminescent Nanomaterials for Biomedical Imaging. *J. Mater. Chem. B,* **2012,** *2* (17), 2422-2443.

16. Zhong, X., Yuan, R., Chai, Y.-Q., Synthesis of Chitosan-Prussian Blue-Graphene Composite Nanosheets for Electrochemical Detection of Glucose Based on Pseudobienzyme Channeling. *Sens. Actuators, B,* **2012,** *162* (1), 334– 340.

17. Liu, Z., Liu, L., Sun, M., Su, X., A Novel and Convenient near-Infrared Fluorescence "Turn Off–on" Nanosensor for Detection of Glucose and Fluoride Anions. *Biosens. Bioelectron.,* **2015,** *65*, 145–151.

18. Saxl, T., Khan, F., Ferla, M., Birch, D., Pickup, J., A Fluorescence Lifetime-Based Fibre-Optic Glucose Sensor Using Glucose/ Galactose-Binding Protein. *Analyst,* **2010,** *136* (5), 968-972.

19. Pickup, J. C., Hussain, F., Evans, N. D., Rolinski, O. J., Birch, D. J. S., Fluorescence-Based Glucose Sensors. *Biosens. Bioelectron.,* **2004,** *20* (12), 2555–2565.

20. Tripathi, K. M., Sonker, A. K., Bhati, A., Bhuyan, J., Singh, A., Singh, A., Sarkar, S., Sonkar, S. K., Large-Scale Synthesis of Soluble Tunable-photoluminescence Graphitic Hollow Carbon Nano-Rods for Selective Fluorescent Detection of DNA. *New J. Chem.,* **2016,** *40* (2), 1571-1579.

21. Tripathi, S., Sonkar, S. K., Sarkar, S., Growth Stimulation of Gram (Cicer Arietinum) Plant by Water Soluble Carbon Nanotubes. *Nanoscale,* **2010,** *3* (3), 1176-1181.

22. Tripathi, K. M., Sonker, A. K., Sonkar, S. K., Sarkar, S., Pollutant Soot of Diesel Engine Exhaust Transformed to Carbon Dots for Multicoloured Imaging of E. Coli and Sensing Cholesterol. *RSC Adv.,* **2014,** *4* (57), 30100-30107.

23. Begum, A., Tripathi, K. M., Sarkar, S., Water-Induced Formation, Characterization and Photoluminescence of Carbon Nanotube-Based Composites of Gadolinium(Iii) and Platinum(Ii) Dithiolenes. *Chem. -Eur. J.,* **2014,** *20* (50), 16657-16661.

24. Sonkar, S. K., Saxena, M., Saha, M., Sarkar, S., Carbon Nanocubes and Nanobricks from Pyrolysis of Rice. *J. Nanosci. Nanotechnol.,* **2010,** *10* (6), 4064–4067.

25. Wang, X., Cao, L., Yang, S.-T., Lu, F., Meziani, M. J., Tian, L., Sun, K. W., Bloodgood, M. A., Sun, Y.-P., Bandgap-Like Strong Fluorescence in Functionalized Carbon Nanoparticles. *Angew. Chem. Int. Ed.,* **2010,** *49* (31), 5310–5314.

26. Andrews, P., Estimation of the Molecular Weights of Proteins by Sephadex Gel-Filtration. *Biochem. J.,* **1964,** *91* (2), 222-233.

27. Roy, M., Sonkar, S. K., Tripathi, S., Saxena, M., Sarkar, S., Non-Toxicity of Water Soluble Multi-Walled Carbon Nanotube on Escherichia-Coli Colonies. *J. Nanosci. Nanotechnol.,* **2012,** *12* (3), 1754–1759.

28. Babar, D. G., Sonkar, S. K., Tripathi, K. M., Sarkar, S., P₂O₅ Assisted Green Synthesis of Multicolor Fluorescent Water Soluble Carbon Dots. *J. Nanosci. Nanotechnol.,* **2014,** *14* (3), 2334–2342.

29. LeCroy, G. E., Sonkar, S. K., Yang, F., Veca, L. M., PingWang, Kenneth N. Tackett, I., Yu, J.-J., Vasile, E., Qian, H., Liu, Y., Luo, P. G., Sun, Y.-P., Toward Structurally Defined Carbon Dots as Ultracompact Fluorescent Probes. *ACS Nano,* **2014,** *8* (5), 4522.

30. White, B., Banerjee, S., O'Brien, S., Turro, N. J., Herman, I. P., Zeta-Potential Measurements of Surfactant-Wrapped Individual Single-Walled Carbon Nanotubes. *J. Phys. Chem. C,* **2007,** *111* (37), 13684–13690.

31. Hu, H., Bhowmik, P., Zhao, B., Hamon, M. A., Itkis, M. E., Haddon, R. C., Determination of the Acidic Sites of Purified Single-Walled Carbon Nanotubes by Acid–Base Titration. *Chem. Phys. Lett.,* **2001,** *345* (1–2), 25-28.

32. Kuznetsov, O. V., Pulikkathara, M. X., Lobo, R. F. M., Khabasheskua, V. N., Solubilization of Carbon Nanoparticles, Nanotubes, Nano-Onions and Nanodiamonds through Covalent Functionalization with Sucrose. *Russ. Chem. Bull.,* **2010,** *59* (8), 1495-1505.

33. Rettenbacher, A. S., Perpall, M. W., Echegoyen, L., Hudson, J., Smith, D. W., Radical Addition of a Conjugated Polymer to Multilayer Fullerenes (Carbon Nano-Onions). *Chem. Mater.,* **2007,** *19* (6), 1411-1417.

34. Choucair, M., Stride, J. A., The Gram-Scale Synthesis of Carbon Onions. *Carbon,* **2012,** *50* (3), 1109-1115.

35. Obraztsova, E. D., Fujii, M., Hayashi, S., Kuznetsov, V. L., Butenko, Y. V., Chuvilin, A. L., Raman Identification of Onion-Like Carbon. *Carbon,* **1998,** *36* (5–6), 821-826.

36. Tripathi, K. M., Begum, A., Sonkar, S. K., Sarkar, S., Nanospheres of Copper(Iii) 1,2-Dicarbomethoxy-1,2-Dithiolate and Its Composite with Water Soluble Carbon Nanotubes. *New J. Chem.,* **2013,** *37* (9), 2708-2715.

37.   Dubey, P., Tripathi, K. M., Mishra, R., Bhati, A., Singh, A., Sonkar, S. K., A Simple One-Step Hydrothermal Route Towards Water Solubilization of Carbon Quantum Dots from Soya-Nuggets for Imaging Applications. *RSC Adv.,* **2015,** *5* (106), 87528-87534.

38.   Wang, J., Wang, C.-F., Chen, S., Amphiphilic Egg-Derived Carbon Dots: Rapid Plasma Fabrication, Pyrolysis Process and Multicolor Printing Patterns. *Angew. Chem., Int. Ed.,* **2012,** *51* (37), 9297-9301.

39.   Zheng, B., Liu, T., Paau, M. C., Wang, M., Liu, Y., Liu, L., Wu, C., Du, J., Xiao, D., Choi, M. M. F., One Pot Selective Synthesis of Water and Organic Soluble Carbon Dots with Green Fluorescence Emission. *RSC Adv.* **2015,** *5* (15), 11667-11675.

40.   Hu, S., Guo, Y., Liu, W., Bai, P., Sun, J., Cao, S., Controllable Synthesis and Photoluminescence (Pl) of Amorphous and Crystalline Carbon Nanoparticles. *J. Phys. Chem. Solids,* **2011,** *72* (6), 749-754.

41.   Sonkar, S. K., Tripathi, K. M., Sarkar, S., Ferromagnetic Behaviour of Anthropogenic Multi-Walled Carbon Nanotubes Trapped in Spider Web Indoor. *J. Nanosci. Nanotechnol.,* **2014,** *14* (3), 2532-2538.

42.   Dubey, P., Sonkar, S. K., Majumder, S., Tripathi, K. M., Sarkar, S., Isolation of Water Soluble Carbon Nanotubes with Network Structure Possessing Multipodal Junctions and Its Magnetic Property. *RSC Adv.,* **2013,** *3* (20), 7306-7312.

43.   Portet, C., Yushin, G., Gogotsi, Y., Electrochemical Performance of Carbon Onions, Nanodiamonds, Carbon Black and Multiwalled Nanotubes in Electrical Double Layer Capacitors. *Carbon,* **2007,** *45* (13), 2511-2518.

44.   Das, S. K., Liu, Y., Yeom, S., Kim, D. Y., Richards, C. I., Single-Particle Fluorescence Intensity Fluctuations of Carbon Nanodots. *Nano Lett.,* **2014,** *14* (2), 620-625.

45.   Georgakilas, V., Guldi, D. M., Signorini, R., Bozio, R., Prato, M., Organic Functionalization and Optical Properties of Carbon Onions. *J. Am. Chem. Soc.,* **2003,** *125* (47), 14268-14269.

46.   Sun, Y.-P., Zhou, B., Lin, Y., Wang, W., Fernando, K. A. S., Pathak, P., Meziani, M. J., Harruff, B. A., Wang, X., Wang, H., Luo, P. G., Yang, H.,

Kose, M. E., Chen, B., Veca, L. M., Xie, S.-Y., Quantum-Sized Carbon Dots for Bright and Colorful Photoluminescence. *J. Am. Chem. Soc.,* **2006,** *128* (24), 7756–7757.

47. Wilson, W. L., Szajowski, P. F., Brus, L. E., Quantum Confinement in Size-Selected, Surface-Oxidized Silicon Nanocrystals. *Science,* **1993,** *262* (5137), 1242-1244.

48. Ghosh, S., Chizhik, A. M., Karedla, N., Dekaliuk, M. O., Gregor, I., Schuhmann, H., Seibt, M., Bodensiek, K., Schaap, I. A. T., Schulz, O., Demchenko, A. P., Enderlein, J., Chizhik, A. I., Photoluminescence of Carbon Nanodots: Dipole Emission Centers and Electron–Phonon Coupling. *Nano Lett.,* **2014,** *14* (10), 5656-5661.

49. Strauss, V., Margraf, J. T., Dolle, C., Butz, B., Nacken, T. J., Walter, J., Bauer, W., Peukert, W., Spiecker, E., Clark, T., Guldi, D. M., Carbon Nanodots: Toward a Comprehensive Understanding of Their Photoluminescence. *J. Am. Chem. Soc.,* **2014,** *136* (49), 17308-17316.

50. Dubey, P., Muthukumaran, D., Dash, S., Mukhopadhyay, R., Sarkar, S., Synthesis and Characterization of Water-Soluble Carbon Nanotubes from Mustard Soot. *Pramana,* **2005,** *65* (4), 681-697.

51. Adamčíková, L. u., Pavlíková, K., Ševčík, P., The Methylene Blue-D-Glucose-O2 System. Oxidation of D-Glucose by Methylene Blue in the Presence and the Absence of Oxygen. *Int. J. Chem. Kinet.,* **1999,** *31* (6), 463-468.

52. Feng, S., Bagia, C., Mpourmpakis, G., Determination of Proton Affinities and Acidity Constants of Sugars. *J. Phys. Chem. A,* **2013,** *117* (24), 5211-5219.

53. Campbell, J. A., Kinetics—Early and Often. *J. Chem. Educ.,* **1963,** *40* (11), 578-583.

54. Cook, A. G., Tolliver, R. M., Williams, J. E., The Blue Bottle Experiment Revisited: How Blue? How Sweet? *J. Chem. Educ.,* **1994,** *71* (2), 160-161.

55. Anderson, L., Wittkopp, S. M., Painter, C. J., Liegel, J. J., Schreiner, R., Bell, J. A., Shakhashiri, B. Z., What Is Happening When the Blue Bottle Bleaches: An Investigation of the Methylene Blue-Catalyzed Air Oxidation of Glucose. *J. Chem. Educ.,* **2012,** *89* (11), 1425-1431.

56. Zheng, Y., Ma, Y., Tao, Q., Li, Y., Ma, S., Cui, T., Wang, X., Dong, S., Zhu, P., Pressure Induced Structural Transition of Small Carbon Nano-Onions. *RSC Adv.,* **2016,** *6* (4), 2914-2919.

57. Baptista, F. R., Belhout, S. A., Giordani, S., Quinn, S. J., Recent Developments in Carbon Nanomaterial Sensors. *Chem. Soc. Rev.,* **2015,** *44* (13), 4433-4453.

58. Ke, Q., Zheng, Y., FanYang, Zhang, H., Yang, X., A Fluorescence Glucose Sensor Based on Ph Induced Conformational Switch of I-Motif DNA. *Talanta,* **2014,** *129*, 539–544.

59. Tang, B., Cao, L., Xu, K., Zhuo, L., Ge, J., Li, Q., Yu, L., A New Nanobiosensor for Glucose with High Sensitivity and Selectivity in Serum Based on Fluorescence Resonance Energy Transfer (Fret) between Cdte Quantum Dots and Au Nanoparticles. *Chem. -Eur. J.,* **2008,** *14* (12), 3637–3644.

60. Jin, L., Shang, L., Guo, S., Fang, Y., Wen, D., Wang, L., Yin, J., Dong, S., Biomolecule-Stabilized Au Nanoclusters as a Fluorescence Probe for Sensitive Detection of Glucose. *Biosens. Bioelectron.,* **2011,** *26* (5), 1965–1969.

61. Yang, X., Zhou, Z., Xiaoa, D., Cho, M. M. F., A Fluorescent Glucose Biosensor Based on Immobilized Glucose Oxidase on Bamboo Inner Shell Membrane. *Biosens. Bioelectron.,* **2006,** *21* (8), 1613–1620.

62. Meadows D L, Schultz J S. Design, manufacture and characterization of an optical fiber glucose affinity sensor based on an homogeneous fluorescence energy transfer assay system. *Analytica Chim Acta.* **1993**, *280* (1), 21–30.

Chapter-6

Water Soluble Carbon Nano-onions Imposed the Sustainable Changes in the Contents of Metallic Micronutrients in First Generation Gram Seeds: Life Cycle Seed to Seed Study

6.1   Introduction

Presently agricultural science need to adopt the sustainable strategies concerning the most serious global issue of continuously increasing food demand [1,2]. Related to boosting the crop productivity, along with preserving the nutritional values of food [1,3-5]. As a possible measure to increase the crop productivity, exploration of diverse nanoparticles as fertilizers/nanofertilizers in plants has increased in recent years [6-11]. To stimulate physiological and biochemical changes in plants. The long term and safer use of nanoparticles in agricultural science, requires the adaptation of sustainable strategies [3,12] precisely related with improved productivity. That directly depends on the nutrition's provided to the plants and can help to resolve the problem of increased food demand [7,13,14]. To be prepared in advance, we need to explore and optimize the use of advanced organic based fertilizers like sustainable nanocarbons [3,12,15-17] compared to synthetic chemical fertilizers. For increasing the productivity and nutrient contents in plants. Stimulating the healthier makeup of micronutrients contents in plants in an environmentally friendly manner could hold great future promises. Because of the significant role of micronutrients in all the metabolic and cellular functions of plants [18] such as in plant growth, production of chlorophyll, synthesis of growth hormones, gene expressions, cell division, photosynthetic activities, root development, N_2 and CO_2 fixation etc [19,20]. Deficiency of micronutrients in plant lead to retarded growth, deferred flowering, chlorosis of matured leaves, reduction in protein expressions, total protein synthesis and consequently, decrease in productivity [19-22]. However, the accumulation of nanoparticle/nanocarbons mainly in edible parts (seeds) of plants is a major concern and needs in-depth and detailed analysis [23].

Why the use of nanocarbons are very important to plant system? This idea is completely based on the age-old practice of charring crop wastes for the fabrication of biochar [24,25] just after harvesting and before sowing the next crop [21]. Biochar are scientifically explored carbon rich substances with porous structures, fabricated with biowaste, which provide sustainable benefits as fertilizers, possessing a high level of chemical and biological activity, capable of exchanging

various cations in the form of nutrients. Additionaly larger active surface area leads to increased adsorption capacity of biochar [26-30]. Likewise, nanocarbons as carbon nano-onion (CNO) have very high aspect ratio and tunable chemical and physical characteristics based on size and surface properties [31] that makes them very significant materials to be explored as nanofertilizers like biochar. Sarkar and co-workers reported the positive impact of biochar to increase the growth of wheat plants and control the flow of nutrients [16]. Several other reports are available to explore the positive prospects of plant–nanocarbon interactions [3,9,12,15-17,32-52]. SWCNT [15,47] and MWCNT [3,15,51] stimulated the overall growth of tomato plants by penetrating inside the thick seed coat in tomato seeds. wsCNT showed growth stimulating effects in gram [17] and wheat plants [44]. CSCNT were equated with the biosynthesis of lignin in *Arabidopsis thaliana* [49]. Recently, SWCNT in plant nanobionics are reported; which increase the total efficiency of photosynthetic machinery of chloroplasts in spinach [50]. Other reports discussed the use of nanocarbons with varied plants such as mustard [32], bitter melon [46], alfa-alfa [45], barley [39], cotton [34], maize [41], cucumber [48], onions [37], rice [36], grape [48] and soybean [39].

The aforementioned studies have focused on the short-term effects of nanocarbons in plants from the stage of seedlings to matured plants. Considering the numerous applications of nanocarbons in plants and lack of study related with the impact of stored nutrients for next (first) generation seeds, herein, we investigated the potential variations in micronutrients, protein and electrolytic contents of FGS obtained from wsCNO treated gram plants compared to control. Significant differences were observed in the stored contents of proteins, electrolytes and micronutrients in FGS obtained from wsCNO treated plants compared to the control plants. Our approach presented here is very basic and straightforward describing a simple finding, focused on the simple conversion of wood waste to wsCNO and utilizing these wsCNO for the long-term sustainable application in agricultural sciences as a nanofertilizer.

6.2   Experimental Section

6.2.1   Materials and Reagents

Wood wool is collected from the local market (free of cost). Common gram (*Cicer arietinum*) seeds were purchased from a local market. Sodium hypochlorite (4% (w/v) available chlorine), hydrogen peroxide (30%), nitric acid (65%) and hydrochloric acid (35%) were bought from Merk Chemicals India. Bradford reagents were purchased from the Sigma-Aldrich. All other chemical reagents were of analytical grade and used without further purification. DI water was used throughout, for the preparation of solutions and analysis, except watering of soil in the green house.

6.2.2   Instrumentation

TEM, fluorescence microscopy, XPS, FTIR, UV-Vis and fluorescence spectroscopy instrumentation were same as described in Chapter 2, 3 and 5. ICP-MS analysis of micronutrients was performed by PlasmaLab ICP-MS (Thermo Scientific, XSERIES 2) equipped with a one-piece quartz torch. The instrument for micronutrient analysis was operated under standard hot plasma conditions. The accuracy of ICP-MS instrument was found to be $\pm$ 0.1 mg L^{-1} with lower than 10% RSD precisions and spike recovery data was ~75–125%. Calibration was carried out with freshly prepared metal standard solutions prior to the analysis. AAS analysis was carried out by an Analyst 400 Autosampler model.

6.2.3   *Cicer arietinum* Seed Germination

The seeds of common gram plants were placed at a sterile place under normal conditions before use. The surface sterility of gram seeds was taken care by soaking those in 10% sodium hypochlorite solution for 10 min and consequently soaked in water for germination for 1 day and used afterward [17].

6.2.4   Synthesis of wsCNO

wsCNO were synthesized by a slightly modified method reported earlier from the pyrolysis of wood wool at 650°C [55] [wood wool is completely packed in covered quartz crucible to utilize minimum oxygen during pyrolysis) in a muffle furnace to obtain black powdered mass [12,54,55]. 10 g of wood-wool after pyrolysis lead to 7.5 g of carboneous materials as black powder. In a typical

synthetic procedure ~3 g of black powdered mass was placed in a Whatman thimble for subsequent washing with Soxhlet purification with acetone to remove unburnt organic contaminations. Here we used only acetone to minimize the use of various organic solvents [57,61]. Simple oxidation as described in earlier reports with nitric acid under reflux conditions for 12 h was performed to convert Soxhlet purified soot into its as prepared water-soluble version [69].

6.2.5 Exploration of wsCNO of Gram Plant for Obtaining the FGS

Different concentration of as prepared wsCNO ranges from 10, 20 and 30 µg mL^{-1} in comparison with control (0 µg mL^{-1} (without wsCNO) were used for the experiment. Sprouted seeds were placed (inverted) on the mouth of test tubes as reported earlier [17] (mouth of the test tubes were covered with paraffin film to prevent the seeds from falling down inside the test tube), for the initial 10 days to obtain the growth stimulating effects. Afterward, to complete their natural life cycle which is of ~4 months without adding any further extra doses of wsCNO. These 10 days old baby plants were transferred to natural soil under standard greenhouse conditions.

6.2.6 Statistical Analysis

Statistical study was performed to observe the significant changes in growth parameters (weight and dimensions) of FGS grown with wsCNO in comparison to control FGS. Moreover, similar study is performed to check remarkable changes in plant yield, protein concentration, electrical conductivity and micronutrient concentration values of FGS treated with wsCNO. The Tukey test in conjugation with analysis of variance (one-way ANOVA) was performed using Microsoft Excel software, on the basis of *p*-value measured at the 5% significance level [6,70].

6.2.7 Analysis of Protein Content in FGS

FGS were obtained from the parent plants after harvesting and used for the analysis of protein content. Samples for analysis of protein concentration were prepared using acid digestion. Quantification of total protein in treated and untreated gram seeds was done by using Bradford assay (λ_{max} 595 nm) [66]. The samples were diluted six times using DI water. A 40 µL portion of the Bradford reagents was added

in 160 μL of the sample and absorbance measurements were made after 20 min at 595 nm. For analyzing the protein contents, we perfomed the experiment in triplicate.

6.2.8   Conductivity Measurements of FGS

A simple electrical conductivity measurement [32] of the electrolytes that leached out from the FGS when placed in DI water for 24 h were done to analyze the impacts of wsCNO on stored electrolyte contents. FGS (15 in number) obtained from wsCNO treated and control plants were immersed in 25 mL DI water for 24 h. After the filtration, the electrical conductivity of the filtrate solutions containing leached electrolytes was measured by a conductivity meter (SensoDirect CD 24) in mS.

6.2.9   Sample Preparation for ICP-MS and AAS Analysis

The air-dried FGS were finally hand ground with a mortar and pestle. One gram of this powder sample was digested using 20 mL 1:1 HNO_3 and H_2O_2 and heated for 15 min at 95°C and was allowed to naturally cool down to room temperature [71]. In a second step 3 mL conc HNO_3 was added to it and heated until the volume of solution reduced to half and then allowed to cool at 80°C. Then 3 mL conc HCl was added to it and again heated for 15 min. In a third step, 10 mL H_2O_2 was dropwise added in solution until effervescence subsidized followed by the addition of 10 mL H_2O and was reflux for 15 min. Such prepared digested samples were filtered with 0.22 μm membrane and made up to 50 mL by adding DI water. Analysis of Fe was not possible by our ICP-MS instrument; so we analyzed the concentration of Fe by the AAS method.

6.2.10 FGS Sample Preparation for the Microscopic Analysis

The samples for TEM analysis of FGS were prepared as described in our earlier protocol [12]. FGS after harvesting were cut down into small pieces using surgical sharp blades. These small pieces were put into the sylgard coated petri dish and shifted in fixing solution (2.5% glutaraldehyde for 6 h at room temperature (in 0.1 M cacodylate buffer solution of pH 7.4)), followed by sequential washing with cacodylate buffer with 4% sucrose solution. Then small pieces of FGS were immersed in 1% osmium tetraoxide (aqueous) at pH 7.4 for 3 h at room temperature

and finally washed with buffer. The dehydration process was carried out in ascending order of ethanol series (70%, 90% and absolute ethanol) twice for 20 min. After the completion of the fixation process, small pieces of FGS were dewaxed in 100% xylene for a minute followed by incubating in 50:50 xylene:paraffin (40 min) [17]. Then FGS were transferred to 100% paraffin wax and allowed to stand for 15 h. After that, thin sections were cut down by using microtome (Leica microtome RM225). Thin sections were further washed with xylene followed by ethanol to remove the excess of wax from the sample. After complete drying, they were mounted on carbon film coated copper grids (200 mesh size) for TEM analysis.

6.3   Results and discussion

6.3.1   Spectroscopic characterization

A long known conventional oxidative treatment method was used for the water solubilization of Soxhlet purified soot under refluxing conditions (~12 h), that led to the introduction of negative functionalities like carboxylic and hydroxyl groups on the surface of CNO [53-56]. The aqueous solution of wsCNO was quite stable against an extended period even after the ~10 months from its initial solubility. Figure 6.1a shows the absorbance spectrum of wsCNO, with a band ~270 nm, that was attributed due to involvement of $\pi-\pi^*$ transitions. Comparative FTIR, TGA, Raman and XPS analyses were carried out to investigate the surface functionalities of wsCNO and Soxhlet purified soot. Figures 6.1 and 6.2 show the detailed comparative spectroscopic analysis regarding the nature and degree of functionalization of wsCNO. The FTIR spectrum of Soxhlet purified soot (blue line Figure 6.1b) shows the presence of vibrational bands associated with sp^2 and sp^3 carbon atoms and the emergence of additional negative surface functionalities in the case of wsCNO (black line) [57,58]. The Soxhlet purified soot (Figure 6.1b blue line) shows the stretching bands at 2924 cm^{-1} and 2853 cm^{-1} (weak, sp^3 −C–H), 1593 cm^{-1} (strong, C=C), 1384 cm^{-1} (medium, phenyl −C–H) and 1280 cm^{-1} (medium, −CH_2 bending). Oxidative treatment of the Soxhlet purified soot shows the additions of few new stretching bands ((black line Figure 6.1b), at 3428 cm^{-1} (broad, O–H), 2925 cm^{-1} (weak, C-H), 1721 cm^{-1} (strong C-O), 1606 cm^{-1} (strong, C=C), 1339 cm^{-1} (medium, phenyl C–H), 1242 cm^{-1} (medium, O–H bending) and 1130 cm^{-1} (weak, C–O).
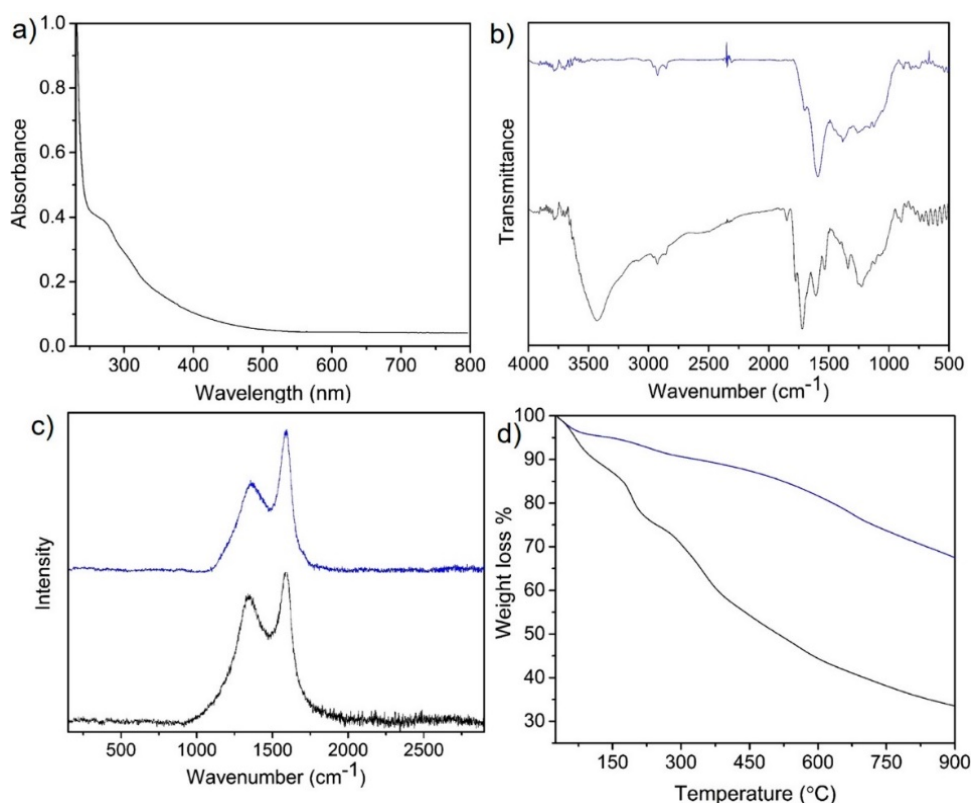
Figure 6.1: (a) Absorption spectrum of wsCNO. (b) FTIR spectra. (c) Raman and (d) TGA spectra of Soxhlet purified soot (blue line) and wsCNO (black line) respectively.

Raman spectroscopy is quite significant for the characterization of graphitic (G band) and disordered (D band) carbon structures in nanocarbons. G band attributed due to the first-order scattering of E_{2g} phonons by sp^2 carbon and D band results from the breathing mode of j-point phonons of A_{1g} symmetry [59]. Significant differences concerning peak positions and intensities were observed between Soxhlet purified soot (blue line) and wsCNO (black line) as illustrated in Figure 6.1c. The shifting of both D (1346 cm^{-1} from 1357 cm^{-1}) and G bands (1582 cm^{-1} from 1588 cm^{-1}) toward lower wavenumber, in wsCNO (in comparison with a Soxhlet purified soot) confirm weakening of the carbon framework during the oxidation process. The increase in surface defects concerning the number of sp^3 carbons during oxidation led to the increased D band area as compared with G band. The degree of functionalization can be quantified by a relative I_G/I_D intensity ratio. Decrease in I_G/I_D ratio from 0.52 (Soxhlet purified soot) to 0.44 (for wsCNO) was

attributed due to considerable augment in the active area of D-band (from the destruction of sp^{2}carbon clusters during oxidation) [60,61]. Surface defects in the form of sp^3 carbons in sp^2 islands of wsCNO were crucial regarding functionalization and further their water solubilization. Further, the Zeta potential measurements were performed to analyze the surface charge of wsCNO. The negative zeta potential value (~−56 mV) of wsCNO supporting the high degree of negative surface functionalization [62]. This negative zeta potential value can be extended upto ~−76 mV (for the most soluble fraction achieved by gel separation compare to the as prepared wsCNO) [63]. The extent of thermal stability of wsCNO compared to Soxhlet purified soot was analyzed with TGA measurements. Figure 6.1d shows the comparative weight loss versus temperature plots of Soxhlet purified soot and wsCNO. It is evident that wsCNO exhibited less thermal stability with a significant weight loss of ~67% in contrast to Soxhlet purified soot, which showed only ~32% weight loss at 900°C. Weight loss in the case of wsCNO was more prominent due to the decomposition of surface oxygen groups incorporated during oxidation along with weakening and destruction of the surface graphitic framework [61]. wsCNO showed 35% more weight loss than Soxhlet purified soot, which justifies the surfacial functionalization of thermally labile groups as evidenced by FTIR and Raman spectroscopy.

XPS analysis was performed to get a detailed analysis of wsCNO composition and the chemical nature of the negative surface functionalities of wsCNO. Figure 6.2a shows the full XPS survey scan of the wsCNO. Quantification of carbon (C_{1s}) and oxygen (O_{1s}) by XPS shows ~45% oxygen groups over the surface. The detailed analysis shows the presence of C_{1s} at 285.6 eV and O_{1s} at 534.5 eV in wsCNO. Over the deconvolution of the C_{1s} short scan, we can easily differentiate the four different modes of carbon binding with oxygen and carbon as −C–C– (284.4 eV), −C═C– (286.5 eV), −C–O– (287.2 eV) and −C═O (288.8 eV). Similarly, for O_{1s} deconvolution a short scan shows the differential binding of oxygen with carbon as −C–O– (531.1 eV), −C═O (533.1 eV) and COO$^-$ (534.2eV) [61,64,65].
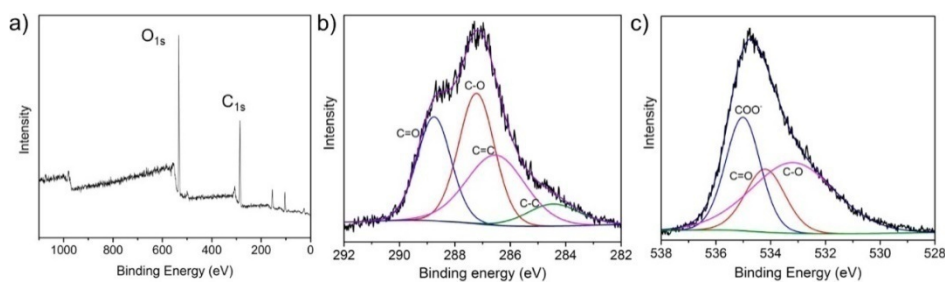
Figure 6.2: (a) XPS full scan of wsCNO and (b) its C_{1s} short scan. (c) O_{1s} short scan

6.3.2 Microscopic Studies

Morphological and microstructural characterization of wsCNO was carried out with FESEM, AFM, TEM and HRTEM analyses. FESEM and AFM (Figure 6.3a and b) images illustrate the spherical morphology of wsCNO, along with the AFM height profile (inset of Figure 6.3 b) of wsCNO. The low-resolution TEM image. Figure 6.4a confirms the spherical and homogeneous distribution of wsCNO without accompanying any other morphological impurities. The diameter distributions of wsCNO were mostly range from 20 to 40 nm and analyzed statistically as illustrated in Figure 6.4b.
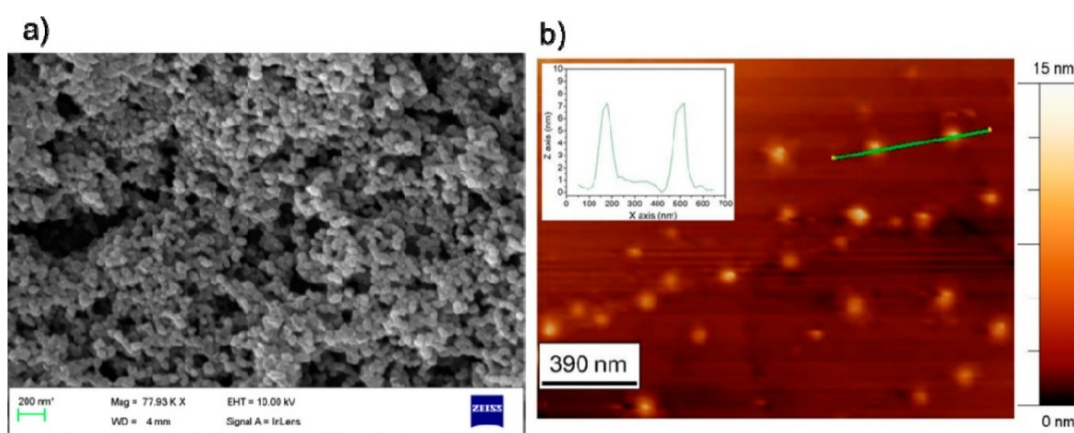
Figure 6.3: (a) FESEM image of wsCNO. (b) AFM image of wsCNO. (inset) Height profile analysis of wsCNO.
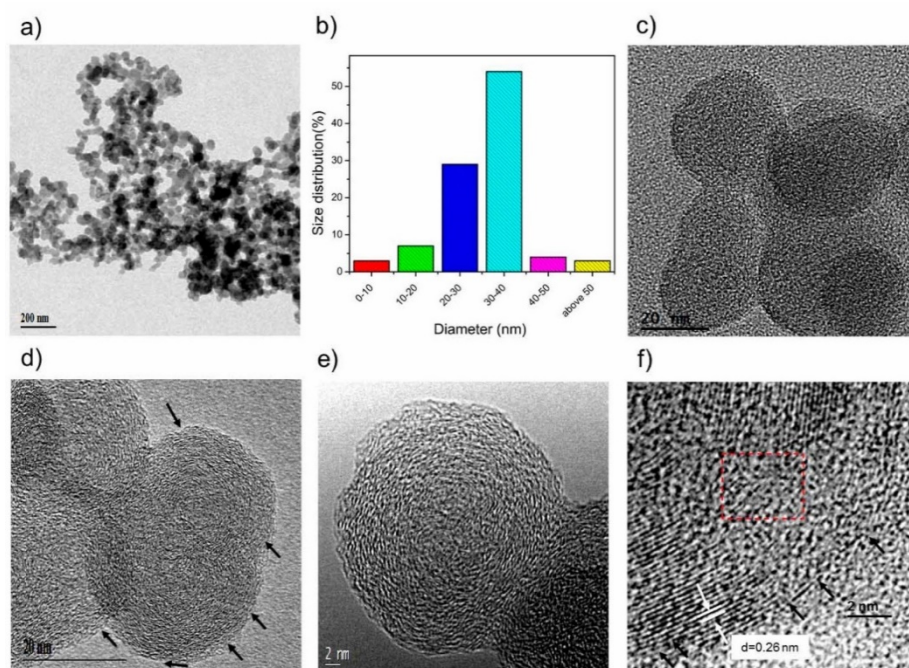
Figure 6.4: (a) TEM image of wsCNO corresponding to its (b) size distribution histogram. (c–e) HRTEM images of wsCNO. (f) HRTEM images of wsCNO showing an interlayer distance of 0.26 nm in the graphitic plane.

HRTEM images displayed in Figure 6.4(c–e) reveal the spherical onion like arrangements of concentric graphitic rings. Extensive surface derivatization via the impregnation of negative surface functionalities render the defective outer surface as shown in Figure 6.4d marked by black arrows. A red box in Figure 6.4f shows the missing graphitic planes in wsCNO and marked white arrows demonstrate the distance between interlayer graphitic planes (0.26 nm).

6.3.3 Effect of wsCNO on the Growth of FGS

Compared to the previous reports showing the accumulations of nanocarbons inside the fruits/flowers[3]. At present, we are concerned about the contamination of fresh fruits/seeds by the used nanocarbons. As the healthier seeds and fruits are the only medium that can store a sustainable future in agricultural sciences. In contrast to our previous finding that addressed the impact of wood wool derived wsCNO only on the phenotype of gram plants starting from the germination of seeds to harvesting of FGS, i.e. "seed to seed cycle". We deliberately attempt to restrict the accumulation of wsCNO inside the FGS and that can be possible by reducing the

dose. At the preliminary phase of our experiments we treated the seeds with wsCNO for 10 days only, under laboratory conditions in DI water (without using any growth medium) [12,17]. Subsequently, we placed the same 10 days old baby plants in soil under optimal conditions in a greenhouse to complete their life cycle [12,17] to yield FGS. The positive impact gained in our former work were again observed here in terms of the improved stored micronutrients, protein and the electrolytic contents of FGS harvested from wsCNO treated plants, compared to control plants. This can be related to the internalizations of wsCNO into the plants where they mostly works within water transport channels (xylem vessels) [12,17,40].

6.3.4 Phenotypical Analysis of FGS Obtained from wsCNO Treated and Control Plants

The phenotype of FGS was significantly affected by the interactions of wsCNO. Figure 6.5(a–d) illustrated the comparative digital camera images of FGS (20 in number) obtained from control 0,10,20 and 30 μg mL^{-1} wsCNO treated plants, just after the 15 days of harvesting. The weight and dimensions (length, width and height) of FGS obtained from control and treated plants were measured with microbalance and with a standard micrometer. It was observed that weight of FGS was remarkably increased by using wsCNO concentration of 10, 20 and 30 μg mL^{-1} which were significantly higher in comparison to control FGS (p-value < 0.05) (Figure 6.5e). Similarly, the dimensions of FGS obtained from wsCNO treated plants were found to be significantly higher than the FGS obtained from the control plants (p-value < 0.05) (Figure 6.5(f–h)). The maximum growth was observed from the plants treated to 30 μg mL^{-1} wsCNO that produced healthier seeds with an increase of ~35% in weight, ~24% in length, ~17% in diameter and ~16% in height over the control FGS. The as-obtained results are quite significant but the most important observation is that wsCNO exposure to plants, even for a shorter time period may follow the same trend in the form of increased growth rate, what they initially gained under laboratory conditions and that consequently led to the harvesting of healthier FGS.
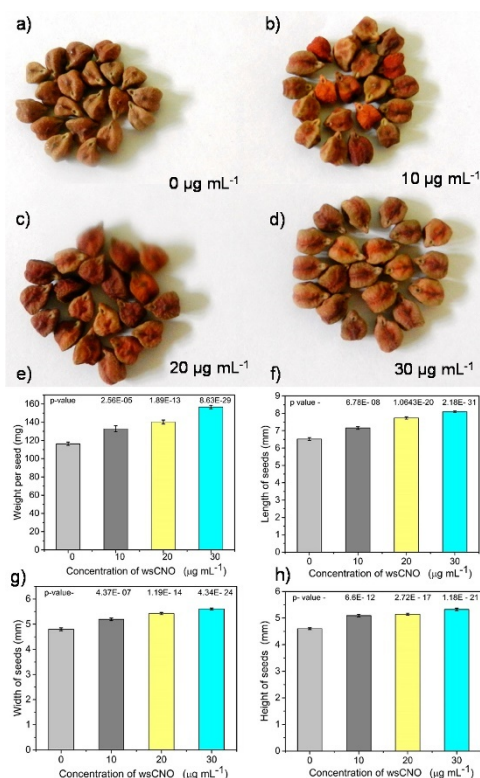
Figure 6.5: Digital camera images showing the visible difference in the phenotypes of FGS obtained from the plants treated with different concentration of wsCNO (a) 0 ; (b) 10; (c) 20; (d) 30 μg mL^{-1}. Histograms (e–h) showing significantly higher values for (e) weight per seed; (f) length; (g) width; (h) and height of individual seeds treated with different concentration of wsCNO in comparison to control FGS and presented with ± SE (number of seeds 50) along with significance (p-value < 0.05).

6.3.5   Effect on Yield Per Plant/Protein Content

FGS obtained from both control and wsCNO treated plants were sampled (15 days after harvesting) and analyzed for yield and stored protein contents. A comparative analysis of yield per plant is shown in Figure 6.6a that confirmed the significant increase in plant productivity. Plant treated to 30 μg mL^{-1} wsCNO produced ~1.7 times more seeds over control plants (*p*-value < 0.05). As we know, gram seeds have been used everywhere as an enriched energy source due to their high content of proteins. So we investigated the effect of wsCNO on the stored protein content of FGS and observed that wsCNO exposure considerably increased the stored protein content in FGS. Additionally, increase in protein concentration[3] in plants is a significant response toward wsCNO. Quantification of total protein content of FGS was determined by using Bradford assay (λ_{max} 595 nm)[66] to measure the physiological effect and is shown in Figure 6.6b. Plants treated with 10 and 20 μg mL^{-1} of wsCNO did not show significant differences (*p*-value < 0.05), but in the case of 30 μg mL^{-1} wsCNO, protein level was ~1.75 times higher than control FGS. Enrichment of FGS with higher protein content is a feasible, sustainable and a meaningful solution to meet the daily nutrient requirements of humans, especially in East Asian countries where protein-rich seeds and pulses supplement the vital nutrition. The mechanism for the increased protein concentration by wsCNO is still at an infant stage and requires a separate detailed investigation.
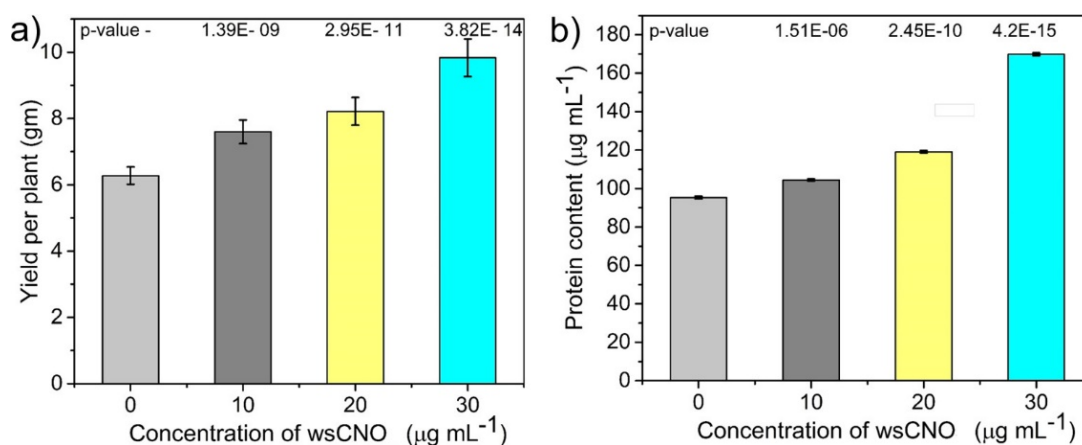
Figure 6.6: Histograms represent the effect of wsCNO concentration (a) on the yield of FGS per plant and (b) total protein contents of FGS with ± SE (number of seeds 25) along with the given significance (*p*-value < 0.05).

6.3.6 Effect on Electrical Conductivity of Stored Electrolytes

We performed a simple electrical conductivity test, to find out the effect of wsCNO on the stored electrolyte contents of FGS.[32] Conductivity of the solutions was measured to understand the contents of stored electrolytes within the FGS that leached out from them when placed in DI water. FGS (15 in number) from the control and wsCNO treated plants were placed in 25 mL of DI water for 24 h. Further the electrical conductivity of the solutions containing leached electrolytes was measured. The conductivity of the solution was found to be increased in ~1.5 times (p-value < 0.05) in case of FGS obtained from 30 μg mL^{-1} of wsCNO treated plants in comparison to control as shown in Figure 6.7
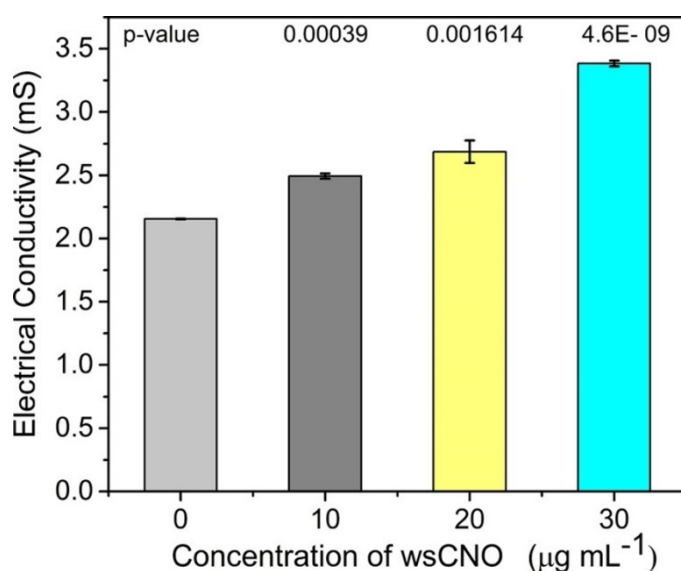
Figure 6.7: Histogram showing the electrical conductivity from stored electrolytes in FGS with ± SE (number of seeds 15) along with the given significance (p-value < 0.05).

6.3.7 Effect on the Concentration of Micronutrients

The significant increase in the protein and electrolyte contents in FGS insisted us to analyze the concentration of stored micronutrients in FGS with a real hope that their levels should increase. As an increase in micronutrient content can directly be associated with their critical functionalities needed for the physiochemical process, further growth and yield of seeds. The micronutrient levels were found to increase

for all the six tested metallic micronutrients (Mo, Cu, Mn, Ni, Zn and Fe) in the FGS obtained from the wsCNO treated plants as illustrated in the histograms, shown in Figure 6.8(a–f). From the all six micronutrient contents, Fe, Mn, Mo and Ni in FGS were more affected than Cu and Zn. Fe content in FGS was increased by ~3 times in the case of 30 μg mL^{-1} wsCNO treated plant than control (p-value < 0.05). Similarly, the contents of Mo, Mn and Ni experienced many fold increases for the FGS obtained from 30 μg mL^{-1} wsCNO treated plant in comparison with control (p-value < 0.05). We observed increase in the Mo level in FGS, which is related to plant productivity and a shortage of which effected the size of seeds, seeds per plant and the total protein synthesis [18]. Similary, a shortage of Ni depresses the grain growth [67]. Fe and Mn are the critical components of various enzymatic systems and are significantly required for protein synthesis; their deficiency causes decreased growth of plants [68]. Mn is required for germination and maturity. Zn is required for healthy flowering and fruiting. Cu is essential for the fertilization purposes that ultimately lead to plant productivity [17,18]. After analyzing the histogram plots shown in Figure 6.8 we can easily conclude the positive impacts of wsCNO on FGS of gram plants and could try to optimize these interactions more precisely in our future studies with different seeds, flowers and crops.
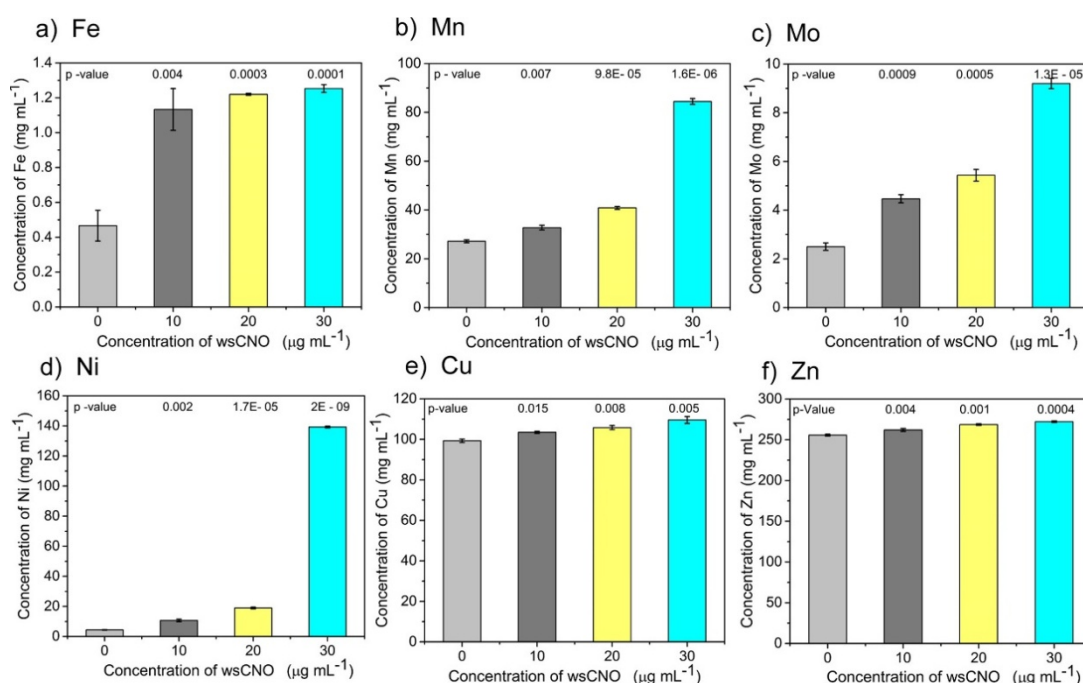
Figure 6.8: Histogram showing the effect of wsCNO on micronutrient concentration present inside the FGS in terms of ± SE, along with the given significance (*p*-value < 0.05) (Fe samples were analyzed by AAS and the rest, all by ICP-MS).

6.3.8   Raman and TEM Investigations of FGS

There have been conflicting reports related to the contamination of nanocarbons on the next generation's flowers and edible parts of plants based on their continuous dose [3,15,23]. Khodakovskaya *et al.* showed that tomato plants treated with MWCNT demonstrated a significant increase in the overall growth of plants [3]. That included an increase in plant height, number of leafs/flowers/fruits and also the overall size of the fresh fruits. But the next generation flowers got contaminated with MWCNT because of continuous dosing. The presence of MWCNT was detected by the presence of Raman G-band (~1587 cm^{-1}) in treated plants. Nalwade *et al.* showed almost similar results with cotton plants when interacting with oxidized MWCNT [34]. It was proposed that plants reproductive systems were activated by the use of MWCNT, which ultimately resulted in overall increased productivity. These increases in yield have been correlated with the increased uptake of water [12] nutrients and physiological environmental stress[35]. To avoid the accumulations of nanocarbons in next generation fruits[15], flowers[3] or seeds[23], we decided to reduce the dose. We used wsCNO for initial 10 days only and subsequently discontinued the dose and transferred these 10 days olds baby plants in soil to complete their natural life cycle. To better examine the precised information related to the accumulations of any wsCNO inside FGS, Raman and TEM analyses were performed to explore the presence or absence of wsCNO. Raman spectroscopy is one of the best detection methods for analyzing the wsCNO inside the desired plant parts, based on the unique spectroscopic signature of nanocarbons associated with D (~1350 cm^{-1}) and G bands (~1600 cm^{-1}). We did a comparative Raman analysis of the seed in two separate parts: cotyledon and the seed coat, associated with the 10 days old baby plants (Figure 6.9a) versus the cotyledon and seed coat of FGS (Figure 6.9b and c). Raman analysis of the seed (cotyledon and the seed coat) of 10 days old baby plants treated with wsCNO showed the D and G bands associated with the presence of wsCNO and the same

was absent in the case of the control seed (cotyledon and the seed coat) as presented in Figure 6.9a. Likewise, Raman analysis on FGS as illustrated in Figure 9b and c did not exhibit any characteristic D and G band signature peaks for all the four tested FGS (seed coats and cotyledons) and supported the absence of wsCNO. Similarly, the search of wsCNO as a contaminant inside the FGS was performed by TEM analysis. Samples were prepared according to the earlier reported prescribed protocols [12,17]. A clear TEM image of FGS obtained from the control (Figure 6.9d) versus wsCNO treated (Figure 6.9(e–g)) plants without having any characteristic image [12,17] of wsCNO, confirming the complete absence of wsCNO.
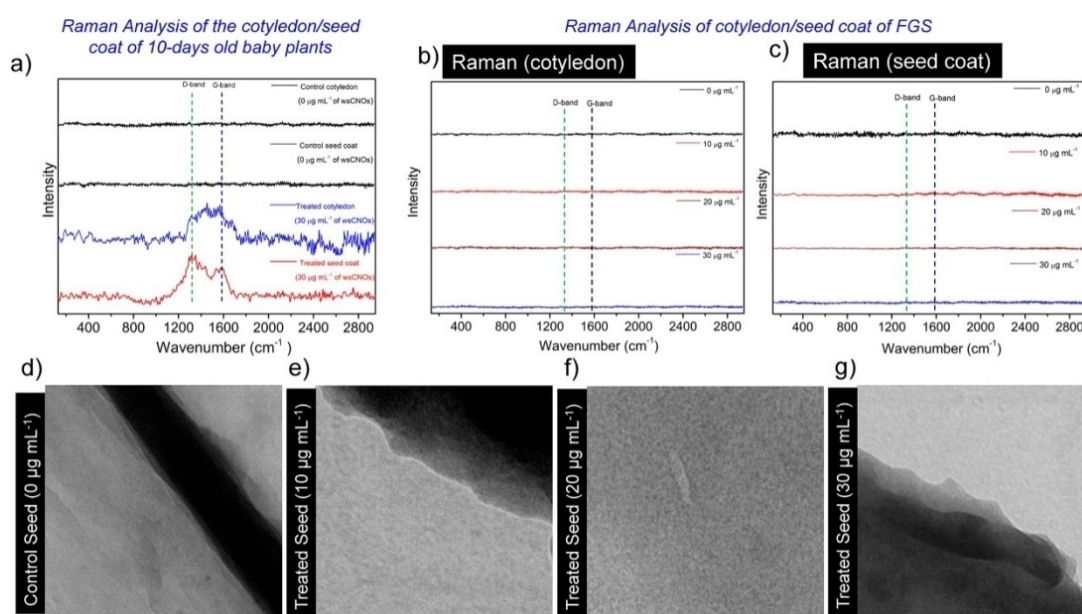
Figure 6.9: Comparative Raman spectra of (a) the seed (cotyledon and the seed coat) associated with 10 day old baby plants, control (0 μg mL^{-1}) versus the wsCNO (30 μg mL^{-1}) treated plants, showing the presence of D and G bands (marked with green line (for D band) and blue line (for G band) in FGS seeds obtained from wsCNO treated plants which were absent in control FGS. (b and c) Raman analysis of FGS: (b) cotyledon; (c) seed coat. These show the absence of wsCNO in FGS based on the absence of D and G bands. (d–g) TEM image of FGS from the control (0 μg mL^{-1}) (d) and treated (10; 20; and 30 μg mL^{-1} (e–g) plants, respectively, confirming the complete absence of wsCNO inside the FGS.

Raman and TEM analysis of FGS are in excellent agreement with a possible sustainable approach and need to explore more precisely for their practical and real-world applications. Initial findings confirm the absence of any wsCNO accumulation inside the FGS. Other parts of plants were excluded for now; this could involve the detailed analysis of roots, shoot and leaves and remains an intriguing question in the future of what could be the fate of these FGS when they would be planted in soil.

6.4. Conclusion

A primary plant/wsCNO interaction study based on the simpler experiments for the isolation of the healthier FGS obtained from the wsCNO treated plants compared to control plants under natural soil conditions was investigated. The positive effects of the exposure of wsCNO (at different concentration) were described, which showed the significant increase in the stored contents of FGS as protein, electrolytes and metallic micronutrients. As well, wsCNO treated plants yielded a greater quantity of FGS with improvement in overall seed size and weight. Thus wsCNO can be used as nanofertilizers based on their small quantites needed for stimulating the growth effects. The most meaningful and sustainable impact of the present finding is the exposure of limited amounts of wsCNO with plants, for the initial 10 days only just for the stimulating the positive growth of seedlings. These 10 days old baby plants were transferred to natural conditions to complete their life-cycle, seed to seed. We exclusively focused on the plant productivity, but not at the cost of next generation seed contamination with nanocarbons. This is being confirmed by Raman and TEM analysis. Moreover, large scale and precise field studies are of future concern to determine a more realistic approach concerning nanocarbon exposure for plants, with a positive note related to the age-old technique of charring biowaste, or using different versions of functionalized nanocarbons for the betterment of plant productivity.

6.5   References

1.   Ditta, A.; Arshad, M. Applications And Perspectives Of Using Nanomaterials For Sustainable Plant Nutrition*Nanotechnol. Rev.* **2016**, *5*(2) 209– 229.

2.   Ruttan, V. W. Productivity Growth in World Agriculture: Sources and Constraints *J. Econ. Perspect* **2002**, *16*(4) 161– 184.

3.   Khodakovskaya, M. V.; Kim, B.-S.; Kim, J. N.;Alimohammadi , M.; Dervishi, E.; Mustafa, T.; Cernigla, C. E.Carbon Nanotubes As Plant Growth Regulators: Effects On Tomato Growth, Reproductive System and Soil Microbial Community *Small* **2013**, *9*(1) 115–123.

4.   Mukherjee, A.; Majumdar, S.; Servin, A. D.; Pagano, L.; Dhankher, O. P.; White, J. C. Carbon Nanomaterial in Agriculture: A Critical Review *Front Front. Plant Sci.* **2016**, *7*, 1–16.

5.   Rico, C. M.; Majumdar, S.; Duarte-Gardea, M.; Peralta-Videa, J. R.; Gardea-Torresdey, J. L. Interaction of Nanoparticles with Edible Plants and Their Possible Implications in the Food Chain *J. Agric. Food Chem.***2011**, *59*, 3485– 3498.

6.   Ashfaq, M.; Verma, N.; Khan, S. Carbon Nanofibers as a Micronutrient Carrier In Plants: Efficient Translocation And Controlled Release Of Cu Nanoparticles *Environ. Sci.: Nano* **2017**, *4*, 138– 148.

7.   Cifuentes, Z.; Custardoy, L.; de la Fuente, J. M.; Marquina, C.; Ibarra, M. R.; Rubiales, D.;Pérez-de-Luque, A. Absorption And Translocation To The Aerial Part Of Magnetic Carbon-Coated Nanoparticles Through The Root Of Different Crop Plants *J. Nanobiotechnol.* **2010**, *8*, 26– 33.

8.   Hong, F.; Zhou, J.; Liu, C.; Yang, F.; Wu, C.; Zheng, L.; Yang, P. Effect Of Nano-TiO$_2$ On Photochemical Reaction Of Chloroplasts Of Spinach *Biol. Trace Elem. Res.* **2005**, *105*, 269– 279.

9.   Liang, T.-b.; Yin, Q.-s.; Zhang, Y.-l.; Wang, B.-l.; Guo, W.-m.; Wang, J.-w.; Xie, J. Effects Of Carbon Nanoparticles Application On The Growth, Physiological Characteristics And Nutrient Accumulation In Tobacco Plants *J. Food Agric Environ* **2013**, *11*(3-4) 954– 958.

10. Peralta-Videa, J. R.; Hernandez-Viezcas, J. A.; Zhao, L.; Diaz, B. C.; Ge, Y.; Priester, J. H.; Holden, P. A.;Gardea-Torresdey, J. L. Cerium Dioxide And Zinc Oxide Nanoparticles Alter The Nutritional Value Of Soil Cultivated Soybean Plants *Plant Physiol. Biochem.* **2014**, *80* (2) 128– 135.

11. Srivastava, G.; Das, C. K.; Das, A.; Singh, S. K.; Roy, M.; Kim, H.; Sethy, N.; Kumar, A.; Sharma, R. K.;Singh, S. K.; Philip, D.; Das, M. Seed Treatment With Iron Pyrite (FeS$_2$) Nanoparticles Increases The Production Of Spinach *RSC Adv.* **2014**, *4*, 58495– 58504.

12. Sonkar, S. K.; Roy, M.; Babar, D. G.; Sarkar, S. Water Soluble Carbon Nano-Onions From Wood Wool As Growth Promoters For Gram Plants *Nanoscale* **2012**, *4* (24) 7670– 7675.

13. Chakravarthi, V. P.; Balaji, N. Applications of Nanotechnology in Veterinary Medicine *Vet. World* **2009**, *3* (10), 477– 480.

14. Jacobsen, S.-E.; Sørensen, M.; Pedersen, S. M.; Weiner, J. Feeding The World: Genetically Modified Crops Versus Agricultural Biodiversity *Agron. Sustainable Dev.* **2013**, *33*, 651– 662.

15. Lin, S.; Reppert, J.; Hu, Q.; Hudson, J. S.; Reid, M. L.; Ratnikova, T. A.; Rao, A. M.; Luo, H.; Ke, P. C.Uptake, Translocation and Transmission of Carbon Nanomaterials in Rice Plants *Small* **2009**, *5* (10) 1128–1132.

16. Saxena, M.; Maity, S.; Sarkar, S. Carbon Nanoparticles In 'Biochar' Boost Wheat (Triticum Aestivum) Plant Growth *RSC Adv.* **2014**, *4* (75) 399948– 399954.

17. Tripathi, S.; Sonkar, S. K.; Sarkar, S. Growth Stimulation Of Gram (Cicer Arietinum) Plant By Water Soluble Carbon Nanotubes *Nanoscale* **2011**, 3, 1176–1181.

18. Bouis, H. E. Micronutrient Fortification Of Plants Through Plant Breeding: Can It Improve Nutrition In Man At Low Cost? *Proc. Nutr. Soc.* **2003**, *62* (2) 403– 411.

19. Fageria, N. K. *The Use Of Nutrients In Crop Plants*; Taylor and Fransis group: CRC Press, **2009**.

20. Monreal, C. M.; DeRosa, M.; Mallubhotla, S. C.; Bindraban, S.; Dimkpa, C. *The Application of Nanotechnology for Micronutrients in Soil-Plant System*; Virtual Fertilizer Research Center, **2015**.

21. Tan, Y.; O'Toole, N.; Taylor, N. L.; Millar, A. H. Divalent Metal Ions in Plant Mitochondria and Their Role inInteractions with Proteins and Oxidative StressInduced Damage to Respiratory Function *Plant Physiol.***2010**, *152* (2) 747– 761.

22. Yruela, I. Copper In Plants: Acquisition, Transport And Interactions *Funct. Plant Biol.* **2009**, *36*, 409– 430.

23. Khodakovskaya, M. V.; de Silva, K.; Nedosekin, D. A.; Dervishi, E.; Biris, A. S.; Shashkov, E. V.;Galanzha, E. I.; Zharov, V. P. Complex Genetic, Photothermal and Photoacoustic Analysis Of Nanoparticle-Plant Interactions *Proc. Natl. Acad. Sci. U. S. A.* **2011**, *108* (3) 1028– 1033.

24. Calderón, F. J.; Benjamin, J.; Vigil, M. F. A Comparison of Corn (Zea mays L.) Residue and its Biochar on Soil C and Plant growth *PLoS One* **2015**, *10*, e0121006

25. Boardman, S.; Jones, G. Experiments on the Effects of Charring on Cereal Plant Components *J. Archaeol. Sci.* **1990**, *17* (1) 1– 11

26. Chen, Z.; Xiao, X.; Chen, B.; Zhu, L. Quantification of Chemical States, Dissociation Constants and Contents of Oxygen-containing Groups on the Surface of Biochars Produced at Different Temperatures*Environ. Sci. Technol.* **2015**, *49*, 309– 317.

27. Keiluweit, M.; Nico, P. S.; Johnson, M. G.; Kleber, M. Dynamic Molecular Structure of Plant Biomass-Derived Black Carbon (Biochar) *Environ. Sci. Technol.* **2010**, *44*, 1247– 1253.

28. Klüpfel, L.; Keiluweit, M.; Kleber, M.; Sander, M. Redox Properties of Plant Biomass-Derived Black Carbon (Biochar) *Environ. Sci. Technol.* **2014**, *48*, 5601– 5611.

29. Liu, W.-J.; Jiang, H.; Yu, H.-Q. Development of Biochar-Based Functional Materials: Toward a Sustainable Platform Carbon Material *Chem. Rev.* **2015**, *115*, 12251– 12285.

30.   Manya, J. J. Pyrolysis for Biochar Purposes: A Review to Establish Current Knowledge Gaps and Research Needs *Environ. Sci. Technol.* **2012**, *46*, 7939– 7954.

31.   Bartelmess, J.; Giordani, S. Carbon Nano Onions (Multi Layer Fullerenes): Chemistry and Applications *Beilstein J. Nanotechnol.* **2014**, *5*, 1980– 1998.

32.   Mondal, A.; Basu, R.; Das, S.; Nandy, P. Beneficial Role of Carbon Nanotubes on Mustard Plant Growth: An Agricultural Prospect *J. Nanopart. Res.* **2011**, *13*, 4519– 4528.

33.   Liu, Q.; Chen, B.; Wang, Q.; Shi, X.; Xiao, Z.; Lin, J.; Fang, X. Carbon Nanotubes as Molecular Transporters for Walled Plant Cells *Nano Lett.* **2009**, *9* (3) 1007– 1010.

34.   Nalwade, A. R.; Neharkar, S. B. Carbon Nanotubes Enhance The Growth And Yield Of Hybrid Bt Cotton *Int. J. Adv. Sci. Technol. Res.* **2013**, *6* (3) 840– 846.

35.   Khodakovskaya, M. V.; de Silva, K.; Biris, A. S.; Dervishi, E.; Villagarcia, H. Carbon Nanotubes Induce Growth Enhancement of Tobacco Cells *ACS Nano* **2012**, *6* (3) 2128– 2135.

36.   Nair, R.; Mohamed, M. S.; Gao, W.; Maekawa, T.; Yoshida, Y.; Ajayan, P. M.; Kumar, D. S. Effect of Carbon Nanomaterials on the Germination and Growth of Rice Plants *J. Nanosci. Nanotechnol.* **2012**, *12* (3) 2212–2220.

37.   Canas, J.E.; Long, M.; Nations, S.; Vadan, R.; Dai, L.; Luo, M.; Ambikapathi, R.; Lee, H.; Olszyk, D. Effects of Functionalized and Nonfunctionalized Single-Walled Carbon Nanotubes on Root Elongation of Select Crop Species *Environ. Toxicol. Chem.* **2008**, *27* (9) 1922– 1931.

38.   Serag, M.F.; Kaji, N.; Venturelli, E.; Okamoto, Y.; Terasaka, K.; Tokeshi, M.; Mizukami, H.; Braeckmans, K.;Bianco, A.; Baba, Y. Functional Platform for Controlled Subcellular Distribution of Carbon Nanotubes *ACS Nano* **2011**, *5* (11) 9264– 9270.

39.   Lahiani, M. H.; Dervishi, E.; Chen, J.; Nima, Z.; Gaume, A.; Biris, A. S.; Khodakovskaya, M. V. Impact of Carbon Nanotube Exposure to Seeds of Valuable Crops *ACS Appl. Mater. Interfaces* **2013**, *5*, 7965– 7973.

40. Tripathi, S.; Sarkar, S. Influence of Water Soluble Carbon Dots On The Growth Of Wheat Plant *Appl. Nanosci.* **2015**, *5* (5) 609– 616.

41. Tiwari, D. K.; Dasgupta-Schubert, N.; Cendejas, L. M. V.; Villegas, J.; Montoya, L. C.; Garcıa, S. E. B.Interfacing Carbon Nanotubes (CNT) With Plants: Enhancement Of Growth, Water And Ionic Nutrient Uptake In Maize (Zea Mays) And Implications For Nanoagriculture *Appl. Nanosci.* **2014**, *4* (5) 577– 591.

42. Serag, M. F.; Kaji, N.; Tokeshi, M.; Baba, Y. Introducing Carbon Nanotubes Into Living Walled Plant Cells Through Cellulase-Induced Nanoholes *RSC Adv.* **2012**, *2*, 398– 400.

43. Torre-Roche,R.D. L.; Hawthorne, J.; Deng, Y.; Xing, B.; Cai, W.; Newman, L. A.; Wang, Q.; Ma, X.;Hamdi, H.; White, J. C. Multiwalled Carbon Nanotubes and C_{60} Fullerenes Differentially Impact the Accumulation of Weathered Pesticides in Four Agricultural Plants *Environ. Sci. Technol.* **2013**, *47*, 12539–12547.

44. Wang, X.; Gu, X.; Han, H.; Chen, K.; Liu, X.; Lu, D. Multi-Walled Carbon Nanotubes Can Enhance Root Elongation Of Wheat (*Triticum Aestivum*) Plants *J. Nanopart. Res.* **2012**, *14*, 841– 850.

45. Miralles, P.; Johnson, E.; Church, T. L.; Harris, A. T. Multiwalled Carbon Nanotubes In Alfalfa And Wheat: Toxicology And Uptake *J. R. Soc. Interface* **2012**, *9*, 3514– 3527.

46. Kole, C.; Kole, P.; Randunu, K. M.; Choudhary, P.; Podila, R.; Ke, P. C.; Rao, A. M.; Marcus, R. K.Nanobiotechnology Can Boost Crop Production And Quality: First Evidence From Increased Plant Biomass, Fruit Yield And Phytomedicine Content In Bitter Melon (Momordica Charantia) *BMC Biotechnol.* **2013**, *13*,37– 46.

47. Alimohammadi, M.; Xu, Y.; Wang, D. Y.; Biris, A. S.; Khodakovskaya, M. V. *Nanotechnology* **2011**, *22*(29), 295101– 295109.

48. Lin, D.; Xing, B. Phytotoxicity Of Nanoparticles: Inhibition Of Seed Germination And Root Growth *Environ. Pollut.* **2007**, *150*, 243– 250.

49. Serag, M. F.; Kaji, N.; Tokeshi, M.; Bianco, A.; Baba, Y. The Plant Cell Uses Carbon Nanotubes To Build Tracheary Elements *Integr. Biol.* **2012**, *4*, 127– 131.

50. Giraldo, J. P.; Landry, M. P.; Faltermeier, S. M.; McNicholas, T. P.; Iverson, N. M.; Boghossian, A. A.;Reuel, N. F.; Hilmer, A. J.; Sen, F.; Brew, J. A.; Strano, M. S. Plant Nanobionics Approach To Augment Photosynthesis And Biochemical Sensing *Nat. Mater.* **2014**, *13*, 400– 408.

51. Villagarcia, H.; Dervishi, E.; de Silva, K.; Biris, A. S.; Khodakovskaya, M. V. Surface Chemistry of Carbon Nanotubes Impacts the Growth and Expression of Water Channel Protein in Tomato Plants *Small* **2012**, *8*,2328– 2334.

52. Serag, M.F.; Kaji, N.; Gaillard, C.; Okamoto, Y.; Terasaka, K.; Jabasini, M.; Tokeshi, M.; Mizukami, H.;Bianco, A.; Baba, Y. Trafficking And Subcellular Localization Of Multiwalled Carbon Nanotubes In Plant Cells *ACS Nano* **2011**, *5* (1) 493– 499.

53. Tripathi, K. M.; Singh, A.; Bhati, A.; Sarkar, S.; Sonkar, S. K. Sustainable Feasibility of the Environmental Pollutant Soot to Few- Layer Photoluminescent Graphene Nanosheets for Multifunctional Applications *ACS Sustainable Chem. Eng.* **2016**, *4* (12) 6399– 6408.

54. Sonkar, S. K.; Ghosh, M.; Roy, M.; Begum, A.; Sarkar, S. Carbon Nano-Onions as Nontoxic and High-Fluorescence Bioimaging Agent in Food Chain—An In Vivo Study from Unicellular E. Coli to Multicellular C. elegans *Mater. Express* **2012**, *2* (2) 105– 114.

55. Ghosh, M.; Sonkar, S. K.; Saxena, M.; Sarkar, S. Carbon Nano-Onions For Imaging The Life Cycle Of Drosophila Melanogaster *Small* **2011**, *7*, 3170– 3177.

56. Dubey, P.; Tripathi, K. M.; Mishra, R.; Bhati, A.; Singh, A.; Sonkar, S. K. A Simple One-Step Hydrothermal Route Towards Water Solubilization Of Carbon Quantum Dots From Soya-Nuggets For Imaging Applications*RSC Adv.* **2015**, *5*, 87528– 87534.

57. Tripathi, K. M.; Sonker, A. K.; Sonkar, S. K.; Sarkar, S. Pollutant Soot Of Diesel Engine Exhaust Transformed To Carbon Dots For Multicoloured

Imaging Of E. Coli And Sensing Cholesterol *RSC Adv.***2014**, *4*, 30100– 30107.

58.   Babar, D. G.; Sonkar, S. K.; Tripathi, K. M.; Sarkar, S. P$_2$O$_5$ Assisted Green Synthesis of Multicolor FluorescentWater Soluble Carbon Dots *J. Nanosci. Nanotechnol.* **2014**, *14*, 2334– 2342.

59.   Choucair, M.; Stride, J. A. The Gram-Scale Synthesis Of Carbon Onions *Carbon* **2012**, 50, 1109– 1115.

60.   Dubey, P.; Tripathi, K. M.; Sonkar, S. K. Gram Scale Synthesis Of Green Fluorescent Water- Soluble Onion-Like Carbon Nanoparticles From Camphor And Polystyrene Foam *RSC Adv.* **2014**, 4, 5838– 5844.

61.   Tripathi, K. M.; Bhati, A.; Singh, A.; Gupta, N. R.; Verma, S.; Sarkar, S.; Sonkar, S. K. From The Traditional Way Of Pyrolysis To Tunable Photoluminescent Water Soluble Carbon Nano-Onions For Cells Imaging And Selective Sensing Of Glucose *RSC Adv.* **2016**, *6*, 37319– 37340.

62.   White, B.; Banerjee, S.; O'Brien, S.; Turro, N. J.; Herman, I. P. Zeta-Potential Measurements of Surfactant-Wrapped Individual Single-Walled Carbon Nanotubes *J. Phys. Chem. C* **2007**, *111*, 13684– 13690.

63.   Wang, X.; Cao, L.; Yang, S.-T.; Lu, F.; Meziani, M. J.; Tian, L.; Sun, K. W.; Bloodgood, M. A.; Sun, Y.-P.Bandgap-Like Strong Fluorescence in Functionalized Carbon Nanoparticles *Angew. Chem.* **2010**, *122*, 5438– 5442.

64.   Ray, S. C.; Saha, A.; Jana, N. R.; Sarkar, R. Fluorescent Carbon Nanoparticles: Synthesis, Characterization and Bioimaging Application *J. Phys. Chem. C* **2009**, *113*, 18546– 18551.

65.   Tripathi,K.M.; Sonker,A.K.; Bhati, A.; Bhuyan, J.; Singh, A.; Singh, A.; Sarkar, S.; Sonkar, S. K. Large-Scale Synthesis of Soluble Graphitic Hollow Carbon Nanorods with Tunable Photoluminescence For The Selective Fluorescent Detection of DNA *New J. Chem.* **2016**, *40*, 1571– 1579.

66.   Bradford, M. M. A Rapid and Sensitive Method for the Quantitation of Microgram Quantities of Protein Utilizing the Principle of Protein-Dye Binding *Anal. Biochem.* **1976**, *72*, 248– 254.

67.   Ghani, A.; Ali, Z.; Ishtiaq, M.; Maqbool, M.; Parvee, S. Estimation Of Macro And Micro Nutrients In Some Important Medicinal Plants Of Soon

Valley, District Khushab, Pakistan *Afr. J. Biotechnol.* **2012**, *11* (78), 14386– 14391.

68. Pacovsky, R. S. Micronutrient Uptake And Distribution In Mycorrhizal Or Phosphorus-Fertilized Soybeans*Plant Soil* **1986**, *95*, 379– 388.

69. Dubey, P.; Muthukumaran, D.; Dash, S.; Mukhopadhyay, R.; Sarkar, S. Synthesis And Characterization Of Water-Soluble Carbon Nanotubes From Mustard Soot *Pramana* **2005**, *65* (4), 681– 697.

70. Burklew, C. E.; Ashlock, J.; Winfrey, W. B.; Zhang, B. Effects of Aluminum Oxide Nanoparticles on the Growth, Development and microRNA Expression of Tobacco (Nicotiana tabacum) *PLoS One* **2012**, *7* (5), e34783.

71. Packer, A.P.; Larivière, D.; Li, C.; Chen, M.; Fawcett, A.; Nielsen, K.; Mattson, K.; Chatt, A.; Scriver, C.;Erhardt, L. S. Validation Of An Inductively Coupled Plasma Mass Spectrometry (ICP-MS) Method For The Determination Of Cerium, Strontium and Titanium In Ceramic Materials Used In Radiological Dispersal Devices (RDDs) *Anal. Chim. Acta* **2007**, *588*, 166– 172.

Chapter-7

Summary, Future Scope, Perspectives and Take Aways

7.1   Conclusion

This thesis presented a facile, cost effective methodology for the fabrication of fluorescent doped-CD and wsCNO and their multi-functional application in the field of photocatalysis, imaging, sensing and in agriculture as fertilizer material.

- In chapter 2 doped-CD show the strong affinity to work under the presence of natural sunlight towards the photoreduction of Cr(VI) to Cr(III), followed by its simpler removal via the precipitation method. Most significantly, it could reach up to the 2,000 ppm of Cr(VI). The doped-CD can work as an efficient photocatalyst as the regeneration ability shows that these doped-CD show a recyclability of more then 6 cycles with the efficiency more than 90%.

- In chpater 3 the red fluorescent doped-CD were first time used as a photocatalyst material and show photocatalytic degradation of pollutant dye MB. The red emitting fluorescent doped CD show a quantum yield of ~40%.

- In chapter 4 the use of doped-CD can play an essential role in the areas contaminated with heavy metal ions and the pollutant dyes. Additionally, the usage of the natural sunlight makes the whole process sustainable. The doped CD show enhanced quantum yield ~72%.

- In chapter 5 a simple non-invasive, fluorescence-based technique for imaging *Escherichia coli* (*E. coli*) and *Pseudomonas putida* (*P. putida*) cells using the wsCNO is described. The photoluminescent properties of wsCNO are being used for the selective sensing of glucose based on the fluorescence turn-off-on mechanisms.

- In chapter 6 wsCNO treated plants showed a significant increase in their yield and health with respect to their individual weight, overall dimensions, enhanced protein, stored electrolytes and metallic micronutrient contents in their first generation seeds.

7.2   Future Scope

- Doped-CD reported in chapter 2 can be further used for the removal of these other toxic metal ions like Hg(II), Pb(II), Cd(II) etc. Additionally these doped-CD can also be used as electrochemical sensor for the detection of heavy toxic metal ions. The photocatalytic ability and reusability makes these doped-CD a strong photocatalyst for purpose of water remediation.

- Doped-CD reported in chapter 3 can be used for degradation of other cationic and anionic dyes which was abundantly found in effluent waste water from the many industries/laboratories. The photocatalytic degradation of pollutant dye and reduction of metal ions by the doped-CD can act as a better alternative for the water remediation and the use of Sunlight makes the whole process more sustainable.

- The red fluorescent doped-CD reported in chapter 4 show a high QY ~72% after separating the most fluorescent fraction so these can be used for a better imaging probe with high resolution imaging for the safer in depth analysis of cells, tissues and organs.

- The treated wastewater (as described in chapter 2, 3 and 4) obtained from the degradation of pollutant dye or by the reduction of metal ions can be further used for watering the gardens, parks and playground.

- wsCNO reported in chapter 5 may load with specific drugs can be used for the drug transport in biomedical applications, and the whole delivery process could be monitored throughout the visible region by the mean of fluorescence.

- A sustainable approach based on the utilization of wood waste derived wsCNO (reported in chapter 6) as a nanofertilizer could provide a possible approach in agricultural science to overcome the shortage of stored nutrients inside the seeds and also to limit the excessive use of fertilizers.

- The PL properties of wsCNO can also be enhanced by the means of doping.

7.3   Perspectives and takeaways

After completed the research work, I have learned a lot of understanding, concerning the effective performance of the basic research in chemistry using the basic concept of natural science. As well, understand the importance of the teamwork to finish the time-bounded task and learned the positive insights from the failed experiment. How to answer to the quires raised by the expert reviewer, which always help me to understand the merits of our findings better. Being very much happy to be worked as a reflexive researcher, this is always a challenging, advantageous and rewarding.

Based on the presented findings, and the utilization of the sunlight, in future sunlight induced photocatalysis can be extended to real-world applications like moving from the batch reactions in small scale to the bulk reactor for treating the industrial waste. Additionally, the usage of the natural carbon sources like green bougainvillea leaves for the photocatalysts applications would be a sustainable approach for the removal of toxic heavy metal and dyes in large scale. These can directly mix with the industrial residual waste effluents and could work naturally in the presence of sunlight to obtain the treated wastewater (free from the toxic metal and dyes). In the preparation of CNOs waste wood wool is being used as an enhancer for the growth of gram plant and these CNO are absent in the first generation seeds, so our purpose of best out of waste is being fulfilled in the present work. In the future, these biocompatible CNO may prove to be a non-expensive, green nano-fertilizer for increasing the overall plant productivity in some other plants.

Annexure II

Permission of Figures

Copyright Clearance Center

RightsLink®

Home | Create Account | Help

ACS Publications
Most Trusted. Most Cited. Most Read.

Title: Quantum-Sized Carbon Dots for Bright and Colorful Photoluminescence

Author: Ya-Ping Sun, Bing Zhou, Yi Lin, et al

Publication: Journal of the American Chemical Society

Publisher: American Chemical Society

Date: Jun 1, 2006

Copyright © 2006, American Chemical Society

LOGIN

If you're a copyright.com user, you can login to RightsLink using your copyright.com credentials.

Already **a RightsLink user** or want to learn more?

PERMISSION/LICENSE IS GRANTED FOR YOUR ORDER AT NO CHARGE

This type of permission/license, instead of the standard Terms & Conditions, is sent to you because no fee is being charged for your order. Please note the following:

- Permission is granted for your request in both print and electronic formats, and translations.
- If figures and/or tables were requested, they may be adapted or used in part.
- Please print this page for your records and send a copy of it to your publisher/graduate school.
- Appropriate credit for the requested material should be given as follows: "Reprinted (adapted) with permission from (COMPLETE REFERENCE CITATION). Copyright (YEAR) American Chemical Society." Insert appropriate information in place of the capitalized words.
- One-time permission is granted only for the use specified in your request. No additional uses are granted (such as derivative works or other editions). For any other uses, please submit a new request.

If credit is given to another source for the material you requested, permission must be obtained from that source.

BACK | **CLOSE WINDOW**

Copyright Clearance Center

RightsLink®

Home | Create Account | Help

ACS Publications
Most Trusted. Most Cited. Most Read.

Title: Doped Carbon Nanoparticles as a New Platform for Highly Photoluminescent Dots

Author: Ya-Ping Sun, Xin Wang, Fushen Lu, et al

Publication: The Journal of Physical Chemistry C

Publisher: American Chemical Society

Date: Nov 1, 2008

Copyright © 2008, American Chemical Society

LOGIN

If you're a copyright.com user, you can login to RightsLink using your copyright.com credentials.

Already **a RightsLink user** or want to learn more?

PERMISSION/LICENSE IS GRANTED FOR YOUR ORDER AT NO CHARGE

This type of permission/license, instead of the standard Terms & Conditions, is sent to you because no fee is being charged for your order. Please note the following:

- Permission is granted for your request in both print and electronic formats, and translations.
- If figures and/or tables were requested, they may be adapted or used in part.
- Please print this page for your records and send a copy of it to your publisher/graduate school.
- Appropriate credit for the requested material should be given as follows: "Reprinted (adapted) with permission from (COMPLETE REFERENCE CITATION). Copyright (YEAR) American Chemical Society." Insert appropriate information in place of the capitalized words.
- One-time permission is granted only for the use specified in your request. No additional uses are granted (such as derivative works or other editions). For any other uses, please submit a new request.

If credit is given to another source for the material you requested, permission must be obtained from that source.

BACK | **CLOSE WINDOW**

Copyright
Clearance
Center

RightsLink®

Home | Account Info | Help | ✉

Title:	In Vivo NIR Fluorescence Imaging, Biodistribution, and Toxicology of Photoluminescent Carbon Dots Produced from Carbon Nanotubes and Graphite
Author:	Huiquan Tao, Kai Yang, Zhen Ma, et al
Publication:	Small
Publisher:	John Wiley and Sons
Date:	Nov 18, 2011
	© WILEY-VCH Verlag GmbH & Co. KGaA, Weinheim

Logged in as:
Sumit Sonkar
Account #:
3000944422

LOGOUT

Order Completed

Thank you for your order.

This Agreement between Sumit Sonkar ("You") and John Wiley and Sons ("John Wiley and Sons") consists of your license details and the terms and conditions provided by John Wiley and Sons and Copyright Clearance Center.

Your confirmation email will contain your order number for future reference.

printable details

License Number	4565230675216
License date	Apr 10, 2019
Licensed Content Publisher	John Wiley and Sons
Licensed Content Publication	Small
Licensed Content Title	In Vivo NIR Fluorescence Imaging, Biodistribution, and Toxicology of Photoluminescent Carbon Dots Produced from Carbon Nanotubes and Graphite
Licensed Content Author	Huiquan Tao, Kai Yang, Zhen Ma, et al
Licensed Content Date	Nov 18, 2011
Licensed Content Volume	8
Licensed Content Issue	2
Licensed Content Pages	10
Type of use	Dissertation/Thesis
Requestor type	University/Academic
Format	Print and electronic
Portion	Figure/table
Number of figures/tables	1
Original Wiley figure/table number(s)	Figure 4
Will you be translating?	No
Title of your thesis / dissertation	Fluorescent carbon dots and carbon nano onons synthesis and multifunctional application
Expected completion date	Apr 2019
Expected size (number of pages)	250
Requestor Location	Sumit Sonkar

4/10/2019   Rightslink® by Copyright Clearance Center

Copyright Clearance Center   **RightsLink®**   Home   Account Info   Help   Chat

Title:	Onion-like graphitic particles
Author:	D. Ugarte
Publication:	Carbon
Publisher:	Elsevier
Date:	1995

Copyright © 1995 Published by Elsevier Ltd.

Logged in as:
Sumit Sonkar
Account #:
3000944422

LOGOUT

Order Completed

Thank you for your order.

This Agreement between Sumit Sonkar ("You") and Elsevier ("Elsevier") consists of your license details and the terms and conditions provided by Elsevier and Copyright Clearance Center.

Your confirmation email will contain your order number for future reference.

printable details

License Number	4565231078527
License date	Apr 10, 2019
Licensed Content Publisher	Elsevier
Licensed Content Publication	Carbon
Licensed Content Title	Onion-like graphitic particles
Licensed Content Author	D. Ugarte
Licensed Content Date	Jan 1, 1995
Licensed Content Volume	33
Licensed Content Issue	7
Licensed Content Pages	5
Type of Use	reuse in a thesis/dissertation
Portion	figures/tables/illustrations
Number of figures/tables/illustrations	2
Format	both print and electronic
Are you the author of this Elsevier article?	No
Will you be translating?	No
Original figure numbers	Figure 2 and fIgure 4
Title of your thesis/dissertation	Fluorescent carbon dots and carbon nano onons synthesis and multifunctional application
Expected completion date	Apr 2019
Estimated size (number of pages)	250
Requestor Location	Sumit Sonkar Department of Chemistry, NIT Jaipur Jaipur, 302017 India Attn: Sumit Sonkar
Publisher Tax ID	GB 494 6272 12

https://s100.copyright.com/AppDispatchServlet   1/2

Copyright Clearance Center   **RightsLink®**   Home   Account Info   Help

ACS Publications
Most Trusted. Most Cited. Most Read.

Title: Green Fluorescent Onion-Like Carbon Nanoparticles from Flaxseed Oil for Visible Light Induced Photocatalytic Applications and Label-Free Detection of Al(III) Ions

Author: Kumud Malika Tripathi, Tuan Sang Tran, Yoon Jin Kim, et al

Publication: ACS Sustainable Chemistry & Engineering

Publisher: American Chemical Society

Date: May 1, 2017

Copyright © 2017, American Chemical Society

Logged in as:
Sumit Sonkar
Account #:
3000944422

LOGOUT

PERMISSION/LICENSE IS GRANTED FOR YOUR ORDER AT NO CHARGE

This type of permission/license, instead of the standard Terms & Conditions, is sent to you because no fee is being charged for your order. Please note the following:

- Permission is granted for your request in both print and electronic formats, and translations.
- If figures and/or tables were requested, they may be adapted or used in part.
- Please print this page for your records and send a copy of it to your publisher/graduate school.
- Appropriate credit for the requested material should be given as follows: "Reprinted (adapted) with permission from (COMPLETE REFERENCE CITATION). Copyright (YEAR) American Chemical Society." Insert appropriate information in place of the capitalized words.
- One-time permission is granted only for the use specified in your request. No additional uses are granted (such as derivative works or other editions). For any other uses, please submit a new request.

If credit is given to another source for the material you requested, permission must be obtained from that source.

BACK   CLOSE WINDOW

List of Publications

Research Paper Published:

1. **Bhati, A.;** Anand, S.R.;Saini, D.;Khare, P.; Sonkar, S.K. Sunlight-Facilaited Photoreduction of Cr(VI) to Cr(III) by Fluorescent Nitrogen Phosphorus Doped Carbon Dots. npj Clean Water, Nature. DOI/10.1038/s41545-019-0036-z

2. Anand, S. R**.; Bhati, A.**; Saini, D.; Gunture; Chauhan, N.; Khare, P.; Sonkar, S. K., Antibacterial Nitrogen-doped Carbon Dots as a Reversible "Fluorescent Nanoswitch" and Fluorescent Ink. *ACS Omega* 2019, *4* (1), 1581-1591.

3. Gunture; Singh, A.; **Bhati, A.;** Khare, P.; Tripathi, K. M.; Sonkar, S.K. Soluble Graphene Nanosheets for the Sunlight-Induced Photodegradation of the Mixture of Dyes and its Environmental Assessment. Sci. Rep., 2019, 9 (1), 2522..

4. **Bhati, A.;** Gunture; Tripathi, K. M.; Singh, A; Sarkar, S.; Sonkar, S. K., Exploration of Nano-carbons to Plant Science. New J. Chem. 2018, 42, 16411-16427.

5. **Bhati, A**.; Anand, S. R.; Saini, D.; Khare, P.; Dubey, P.; Sonkar, S. K., Self-doped nontoxic red-emitting Mg–N-embedded carbon dots for imaging, Cu(II) sensing and fluorescent ink. New J Chem 2018, 42 (24), 19548-19556**.**

6. **Bhati, A.**; Anand, S. R.; Gunture; Garg, A. K.; Khare, P.; Sonkar, S. K., Sunlight-Induced Photocatalytic Degradation of Pollutant Dye by Highly Fluorescent Red-Emitting Mg-N-Embedded Carbon Dots. *ACS Sustainable Chem. Eng.,* 2018, *6* (7), 9246–9256

7. Khare, P.;[†] **Bhati, A.**;[†] Anand, S. R.; Gunture; Sonkar, S. K., Brightly Fluorescent Zinc-Doped Red-Emitting Carbon Dots for the Sunlight-Induced Photoreduction of Cr(VI) to Cr(III). *ACS Omega* 2018, *3* (5), 5187-5194. (†= Equal contribution)

8. Khare, P.; Singh, A.; Verma, S.; **Bhati, A.**; Sonker, A. K.; Tripathi, K. M.; Sonkar, S. K., Sunlight-Induced Selective Photocatalytic Degradation of Methylene Blue in Bacterial Culture by Pollutant Soot Derived Nontoxic Graphene Nanosheets. *ACS Sustainable Chem. Eng.*, 2018, *6*, 579–589.

9. Singh, A.; Khare, P.; Verma, S.; **Bhati, A.**; Sonker, A. K.; Tripathi, K. M.; Sonkar, S. K. Pollutant Soot for Pollutant Dye Degradation: Soluble Graphene Nanosheets for Visible Light Induced Photodegradation of Methylene Blue. *ACS Sustainable Chem. Eng.*, 2017, 5, 8860−8869.

10. Tripathi, K. M.;[†] **Bhati, A.**; [†] Singh, A.; Sonker, A. K. Sarkar, S.; Sonkar, S. K. Sustainable Changes in the Contents of Metallic Micronutrients in First Generation Gram Seeds Imposed By Carbon Nano-Onions: Life Cycle Seed To Seed Study. *ACS Sustainable Chem. Eng.* 2017, 5, 2906-2916. (†= Equal contribution)

11. Tripathi, K. M.; Singh, A.; **Bhati, A.**; Sarkar, S.; Sonkar, S. K. Sustainable Feasibility Of The Environmental Pollutant Soot To Few-Layer Photoluminescent Graphene Nanosheets For Multifunctional Applications. *ACS Sustainable Chem. Eng.*, 2016, 4, 6399−6408.

12. **Bhati, A.**; Singh, A.; Tripathi, K. M.; Sonkar, S. K. Sunlight- Induced Photochemical Degradation of Methylene Blue by Water- Soluble Carbon Nanorods. *Int. J. Photoenergy*, 2016, 2016, 2583821.

13. Tripathi, K. M.; Sonker, A. K.; **Bhati, A.**; Bhuyan, J.; Singh, A.; Singh, A.; Sarkar, S.; Sonkar, S. K. Large-Scale Synthesis of Soluble Graphitic Hollow Carbon Nanorods with Tunable Photoluminescence for the Selective Fluorescent Detection of DNA. *New J. Chem.*, 2016, 40, 1571-1579.

14. Tripathi, K. M.; [†] **Bhati, A.**; [†] Singh, A.; Gupta, N. R.; Sarkar, S.; Sonkar, S. K. From The Traditional Way of Pyrolysis to Tunable Photoluminescent Water Soluble Carbon Nano-Onions for Cell Imaging and Selective Sensing of Glucose, *RSC Adv.*, 2016, 6, 37319-37329. (†= Equal contribution)

15. Dubey, P.; Tripathi, K. M.; Mishra, R.; **Bhati, A.**; Singh, A.; Sonkar, S. K. A Simple One-step Hydrothermal Route towards Water Solubilization of Carbon Quantum Dots from Soya-nuggets for Imaging Applications, *RSC Adv.*, 2015, 5, 87528–87534.

16. Singh, A.; **Bhati, A.**; Gunture, Tripathi, K. M.; Sonkar, S. K. Nano-carbons in Agricultural Plants: Can be a Potential Nano-Fertilizer? By Wiley-VCH Verlag GmbH & Co. KGaA. 2018.

Conferences, Seminar and Short-term course:
1. Participated in National Seminar on "Recent Trends & Advances in Chemical Science and their Impact on Environment" (RTACIE-2018) organized by department of chemistry, Amity University, Jaipur on 13th April 2018.
2. Five days short term course on "Nano Forms of Carbon" organized by Materials Research Centre, MNIT, Jaipur from 19th March-23rd March 2018.
3. Attended and participated in poster presentation in two days international conference on Condensed Matter & Applied Physics at Engineering College Bikaner, from 30[th-] 31st October 2015.
4. Attended and participated in poster presentation in three days "National Conference on Advanced Materials and Processing (CAMP-2015)" from 2nd- 4th December 2015 organized by physics, chemistry and metallurgy department, MNIT, Jaipur.
5. Attended and participated in poster presentation in three days National conference on "Recent Advancement in Chemical Sciences (RAICS-2015)" from 21st- 23rd August 2015 organized by department of chemistry, MNIT Jaipur and got the Best Poster Award.
6. Attended and participated in poster presentation in three days "National conference on Frontiers at the Chemistry – Allied Sciences Interface (FCASI-2015)" at Rajasthan University, Jaipur from 10th -12th March 2015.

ARTICLE   OPEN

Sunlight-induced photoreduction of Cr(VI) to Cr(III) in wastewater by nitrogen-phosphorus-doped carbon dots

Anshu Bhati [1], Satyesh Raj Anand[1], Deepika Saini[1], Gunture Kumar[1] and Sumit Kumar Sonkar [1]

Cr(VI) is a known toxic and non-biodegradable pollutant that results from multiple industrial processes, and can cause significant environmental damage if it is not removed from wastewater. However, it can be reduced to Cr(III), which is less toxic and can be readily precipitated out and removed. Here, a fast and facile single-step technique is reported for the synthesis of nitrogen–phosphorus doped fluorescent carbon dots (NP-CD) using a domestic microwave, as a potential photocatalytic material. Under natural sunlight, a simple photocatalytic experiment reveals that the NP-CD are highly efficient for the quantitative reduction of Cr(VI) to Cr(III) in synthetic contaminated water, in a linear range from 10 ppm (in approximately 10 min) to 2000 ppm (in approximately 320 min) by increasing the sunlight irradiation time followed by its removal by precipitation. NP-CD exhibit high recyclability of up to six cycles without any apparent loss in photocatalytic activity, demonstrating NP-CD as a potential photocatalyst material for Cr(VI) water treatment.

INTRODUCTION

Since their discovery, photoluminescent carbon dots (CD)[1] are being researched all over because of their sustainable-advantageous applications and ease of fabrication.[2,3] CD are presently offering a vast viable platform for many potential applications, such as bioimaging, sensing, photocatalysis, LED, and photovoltaic.[2,3] The elemental compositions of CD modified with the long-known method of "doping" that involves the use of heteroatoms and metallic salts as dopants. Doping is a well-established method for articulating the optical and electrical properties of semiconductor nanoparticles.[2,4] Many reports are available stating that the doped-CD show remarkable results in terms of better quantum yield over the blue-green[5] and red[6,7] region of the visible spectrum along with its novel applications. Few groups have reported the doping of nitrogen (N) and phosphorus (P) to form nitrogen-phosphorous doped carbon dots (NP-CD), using hydrothermal,[8–10] solvothermal,[11] and micro-wave[12–15] assisted methods with the different precursor materials. NP-CD used for several applications such as for sensing Hg^{2+},[10] as a nano-carrier of anticancer drug[16], imaging purpose[8,12–14,16], oxygen reduction,[17] intercellular Fe^{3+} sensor,[8] fluorescence sensing of living cells,[13] and in the flourescence sensing of reactive oxygen and nitrogen species.[9] Presently, the doping of the CD are used to articulate its potential properties, with a huge expectation of the exploration of its newer prospects. For instance, in the field of water treatment[18,19] via aqueous phase photo-catalysis,[6,7,20] which has been barely investigated. As per the general understanding, the heavy-metal-ion contamination in water is a severe threat, which indeed demands a viable, sustainable approach for its efficient sensing followed by its removal. For the same, sunlight-induced photocatalysis can be considered as a promising approach for the photodegradation of environmental pollutants.[21,22] The fabrication of novel nano-structured-materials with unique physical/chemical properties along with high efficiency towards the photocatalysis are the crucial step and required much attention.[6,7,18,23]

Beyond the conventional existing applications of CD, the present work investigate a newer perspective of NP-CD, using the natural sunlight for photoreduction of toxic Cr(VI) to Cr(III), followed by precipitation of Cr(III) salt. The toxic non-biodegradable[24] pollutant Cr(VI) is a well-known by-product of many industrial processes, like electroplating, paint making, leather tanning, and others, was discarded in the wastewater.[25] Cr(VI) is continuously damaging the aquatic system and shows devastating consequences.[26] Compared to the Cr(VI), Cr(III) is less toxic and can easily be precipitated out or adsorbed by the already existing methods.[27] So the conversion of Cr(VI) to Cr(III) followed by its simple precipitation is always in high demand. Nevertheless, it could be a sustainable approach, if the same can be performed under the presence of natural sunlight[6,7,18,23].

RESULTS AND DISCUSSION

A single-step process presented here describe the facile synthesis of the NP-CD from the pool of imidazole (source of nitrogen (N)), phosphoric acid (source of phosphorus (P)) and polyethylene glycol (source of carbon (C)), via the simplest method of microwave charring for ~4 min. The as-synthesized blue fluor-escent NP-CD utilized for the aqueous phase photoreduction of Cr(VI) to Cr(III) under the presence of natural sunlight. Compared to artificial light, natural sunlight shows its significant contribution towards the photoreduction of the Cr(VI) to Cr(III) concerning the time required for the photoreduction is shown in Table 1, which also includes synthesis time for the fabrication of nano-carbons in comparison with the existing reports. Furthermore, the Cr(III) was also precipitated out by the NaOH solution to get treated water from the synthetic contaminated water.

[1]Department of Chemistry, Malaviya National Institute of Technology, Jaipur 302017, India
Correspondence: Sumit Kumar Sonkar (sksonkar.chy@mnit.ac.in)

SCIENTIFIC REPORTS

OPEN

Soluble Graphene Nanosheets for the Sunlight-Induced Photodegradation of the Mixture of Dyes and its Environmental Assessment

Gunture[1], Anupriya Singh[1], Anshu Bhati[1], Prateek Khare[1], Kumud Malika Tripathi[2] & Sumit Kumar Sonkar[1]

Currently, the air and water pollutions are presenting the most serious global concerns. Despite the well known tremendous efforts, it could be a promising sustainability if the black carbon (BC) soot can be utilized for the practical and sustainable applications. For this, the almost complete aqueous phase photodegradation of the three well-known organic pollutant dyes as crystal violet (CV); rhodamine B (RhB); methylene blue (MB) and their mixture (CV + RhB + MB), by using water-soluble graphene nanosheets (wsGNS) isolated from the BC soot under the influence of natural sunlight is described. The plausible mechanism behind the photocatalytic degradation of dyes and their mixture has been critically analyzed via the trapping of active species and structural analysis of photodegraded products. The impact of diverse interfering ions like Ca^{2+}, Fe^{3+}, SO_4^{2-}, HPO_4^{2-}, NO_3^-, and Cl^- on the photodegradation efficiency of wsGNS was also investigated. Importantly, the environmental assessment of the whole process has been evaluated towards the growth of wheat plants using the treated wastewater. The initial studies for the fifteen days confirmed that growth of wheat plants was almost the same in the photodegraded wastewater as being noticed in the control sample, while in case of dyes contaminated water it showed the retarded growth. Using the natural sunlight, the overall sustainability of the presented work holds the potential for the utilization of pollutant soot in real-practical applications related to the wastewater remediation and further the practical uses of treated water.

The ever-growing desire to improve the quality of human lifestyle significantly promoted the rapid industrialization and urbanization[1–3]. Primarily, associated with the accelerating advancement of the automotive industrialization, which can directly link to the release of dirty-dangerous pollutant black soot as black carbon (BC)[4–7] particulate matter in the environment. BC is closely related with global warming and at present is continuously deteriorating the environmental and human health[7,8]. Along with air pollutions, industrialization have also brought the another important concern related to the water pollutions[9]. So, the most demanding aggravated concerns of the present world is to significantly reuse the waste products (it could also be the dangerous-dirty-BC)[10] and the treatment of wastewater[11,12]. From the standpoint of the overall environmental health, the discharge of the BC[7] in air and the effluents of industrial wastewater[13–15] (containing hazardous, carcinogenic and non-biodegradable organic dyes) in the water-bodies are unceasingly deteriorating the ecological balance[16,17], and causes many serious diseases[18–20]. At present, few groups have explored the recent-promising approaches related to the adaptation of pollutant soot as freely available carbon precursor for the synthesis/isolation of the value-added nano-carbons[21–29]. Such as carbon dots (CD)[23], graphene nanosheets (GNS)[24,25,27], single-walled carbon nanotubes (SWCNT)[26], carbon nanoparticles[22] used for the diverse applications[22,23,27] including the photodegradation of the pollutant dyes[24,25]. In the same context, the visible-light photocatalysis using the nano-carbons,

[1]Department of Chemistry, Malaviya National Institute of Technology, Jaipur, Jaipur, 302017, India. [2]Department of Bio-nanotechnology, Gachon University, Gyeonggi-do, South Korea. Gunture and Anupriya Singh contributed equally. Correspondence and requests for materials should be addressed to K.M.T. (email: kumud20010@gmail.com) or S.K.S. (email: sksonkar.chy@mnit.ac.in)

Article

Antibacterial Nitrogen-doped Carbon Dots as a Reversible "Fluorescent Nanoswitch" and Fluorescent Ink

Satyesh Raj Anand, Anshu Bhati, Deepika Saini, Gunture, Neetu Chauhan, Prateek Khare, and Sumit Kumar Sonkar*

Department of Chemistry, Malaviya National Institute of Technology, Jaipur, Jaipur 302017, India

ABSTRACT: The present finding describes an efficient facile approach for the fabrication of nitrogen-doped carbon dots (N-CDs) as a "fluorescent nanoswitch". Highly fluorescent blue-light-emitting N-CDs have been synthesized via a simpler hydrothermal method using 2,2′-(ethylenedioxy)-bis(ethylamine) and malic acid as the precursors. N-CDs showed excitation-dependent and pH-independent emission along with a quantum yield of ∼25%. The blue fluorescent emission of N-CDs has been selectively "turned off" (quenching of fluorescence (FL)) during the sensing of Cr(VI) with 0.02 μM limit of detection and further been selectively "turned on" (restoration of FL) on sensing ascorbic acid, compared with other metal cations and biomolecules tested. For testing the practical applicability of N-CDs, the switchable reversibility of the fluorescent nanoswitch has been tested for up to four cycles on the basis of FL "on−off−on". Furthermore, the toxicological test showed the antibacterial effect of the N-CDs on the tested Gram-positive *Staphylococcus aureus* and Gram-negative *Escherichia coli* cells. Additionally, these N-CDs can also be used as a fluorescent ink for imaging purposes.
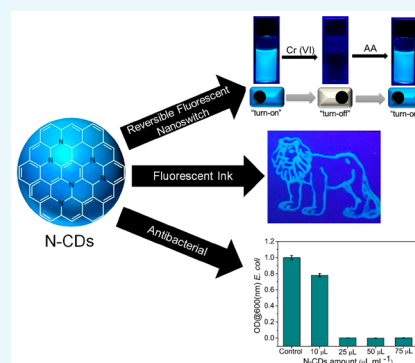
1. INTRODUCTION

Fluorescent carbon dots (CDs)[1−6] are zero-dimensional carbon materials consisting of variable composition of sp^2-/sp^3-hybridized carbon atoms with abundant functional groups over the shell, due to which they exhibit unique fluorescence (FL) properties.[1] Since their discovery,[2] CDs have triggered a great interest in a wide range of applications, from bioimaging,[3,7] sensing,[8,9] drug delivery,[10,11] photocatalysis,[12] energy storage,[13] and fluorescent ink[14,15] to disease diagnosis,[16,17] and also in the field of agriculture[18] because of their superior unique properties such as the biocompatibility, robust chemical inertness, nontoxicity,[19] and stability.[5,20−22] However, to accomplish more, presently the long-known method of doping has been articulating the optical properties of CDs as in the form of emergent doped-CDs.[7,23,24] The doping of heteroatoms significantly affects the physicochemical and photochemical properties of CDs.[7,24] Of all of the dopant materials, the doping of N has been a bit more feasible concerning its easier insertion in the carbonaceous matrix of CDs because of its comparable size to that of carbon along with the extra valence electron. Additionally, the emphasis on escaping the complicated synthesis methodologies also has been in demand, such as the exploration of newer sustainable approaches based on the hydrothermal,[25] solvothermal[26,27] and microwave-assisted[2,3,28] methodologies for the facile fabrication of doped CDs as these are easier and scalable methodologies with an extra advantage of ease in reproducibility. From the many potential applications, currently, N-CDs are being used for sensing the heavy metal ions like Cr(VI),[29] Hg(II),[9] Fe(III),[30] Cu(II),[31] Zn(II),[32] Cd(II),[33,34] and

Co(II)[35] especially because of their FL emission properties, "turn-off" and "turn-on".

Cr(VI) is highly toxic in nature as compared to its lower valent state Cr(III), causing several adverse impacts on the environment as well as on the human health.[36,37] Thus, their discharge into the environment through industrial and other anthropogenic activities needs to be monitored thoroughly. Therefore, it is essential to continuously observe the level of Cr(VI) in water media, which needs to be up to 0.9 μM, possibly via using simpler techniques with accuracy even at its lower level.[29] In addition, the detection of ascorbic acid (AA) (generally known as vitamin C) also has been important for human health as AA is protecting us from many diseases. Although a few reports have already been documented for the detection of Cr(VI) and AA in the literature,[38,39] the development of simpler and economic methodologies has always been in demand. For this, fluorescent properties of the CDs[2,3,40] and doped CDs like N-CDs have been explored on the basis of their abilities of FL sensing.

The present finding depicts a simpler methodology for the fabrication of N-CDs and their use as a reversible "fluorescent nanoswitch" for selective sensing of Cr(VI) and AA. N-CDs show excellent stability and solubility in aqueous medium, and their fluorescent properties do not change on addition of various other ions (interference study) and with the variation in the pH of the solution, which may offer the practical

PAPER

Self-doped nontoxic red-emitting Mg–N-embedded carbon dots for imaging, Cu(ii) sensing and fluorescent ink

Anshu Bhati, [ID] †[a] Satyesh Raj Anand, [ID] †[a] Deepika Saini,[a] Prateek Khare,[a] Prashant Dubey[b] and Sumit Kumar Sonkar [ID] *[a]

Presently, the doping of carbon dots (CD) with heteroatoms and metal-salts as external dopant is a common practice for enhancing its optical efficiency. This approach can involves the use of biomaterials such as plant leaves since they already possess metals inside as an essential element. In this study, the simple process of carbonization of a leaf extract yielded red-emitting magnesium–nitrogen embedded (self-doped) CD, which were denoted as r-Mg–N-CD, possessing a quantum yield value of ~41%. Importantly, r-Mg–N-CD was proven to be a biocompatible probe based on the bacteriological test performed on two different bacterial strains, *Escherichia coli* (*E. coli*) and *Proteus vulgaris* (*P. vulgaris*). In addition to the conventional imaging application, r-Mg–N-CD could also be used for the fluorescence-based selective sensing of Cu(ii) metal ions among various heavy metals with a detection limit as low as 50 nM and as red-emitting fluorescent ink.

1. Introduction

The advances in the field of optical bio-imaging[1–3] using the biocompatible fluorescent probes have increased tremendously over the past few years. In the search for biocompatible fluorescent probes, nanocarbon such as CD[4] and graphene quantum dots (GQD)[5] have been significantly used for several applications[6] and mostly explored for *in vivo* and *in vitro* imaging applications.[7–10] The increase in the number of reports on the wide exploration of CD[11–13] may be based on an economic viewpoint. Nanocarbons,[14–16] particularly CD,[2,7,17–19] are inexpensive sometimes free, and even can be isolated from waste materials. CD exhibit almost similar characteristic with the metal-based semiconductor quantum dots (QD) as the stable photoluminescence properties.[20,21] The ease of their availability and surface modification, which make them soluble in aqueous media, are the two most important characteristics of CD.[22,23] These characteristics significantly enhance their efficacy and make them better candidates compared to QD.[24,25] Presently, high-performance CD are being used as compatible bio-markers; however, their application is limited by their emissive profile, which is situated in the blue and green region.[26–31] This restricts their application in the

low energy wavelength region (red and near-infrared regions), particularly for imaging applications since the low energy wavelength is considered as the most suitable region for optical imaging applications in biological systems.[32,33] The deeper penetration of soluble fluorescent probes can directly combine the advantages of instructive image analysis (such as real-time visualization and differentiating between normal and abnormal cells) with minimal damage to living cells during *in vivo* studies. Several groups have reported red-emitting and near infra-red (NIR)-emitting CD for various applications, including imaging,[34–38] sensing,[39,40] fingerprint detection,[41] nano-thermometry,[38,42] theranostics,[40,43] photocatalytic degradation of dyes,[44] and photocatalytic reduction of toxic metal ions.[45] The important aspect observed while summarizing the above reports is that most reports are in the support of the well-known process of doping that can be performed by the addition of external materials as heteroatoms[46,47] or inorganic metal salts,[45] so that CD could function in the low-wavelength region for bioimaging applications.

Additionally, CD have also been explored for sensing applications based on their emissive fluorescence profiles, including the sensing of biomolecules, heavy metal ions, and organic pollutant dyes. Among the heavy metal ions, we focus on copper ions here. Sensing copper in aqueous media is important because it is the third most abundant trace element in the human body after iron and zinc,[48] and is responsible for participating in many enzymatic activities in biological systems. A deficiency and the deregulation of copper result in many severe diseases such as Alzheimer's, Menke's, Parkinson's, and Wilson's disease and

[a] *Department of Chemistry, Malaviya National Institute of Technology, Jaipur, Jaipur-302017, India. E-mail: sksonkar.chy@mnit.ac.in*

[b] *Centre of Material Sciences, Institute of Interdisciplinary Studies (IIDS), University of Allahabad, Allahabad, India*

† Anshu Bhati and Satyesh Raj Anand contributed equally to this work.

ROYAL SOCIETY OF CHEMISTRY

Check for updates

Exploration of nano carbons in relevance to plant systems

Anshu Bhati, [a] Gunture, [a] Kumud Malika Tripathi, [b] Anupriya Singh, [a] Sabyasachi Sarkar [c] and Sumit Kumar Sonkar *[a]

The effects of nano-carbon interactions on plant growth have recently been the subject of much scientific research. In the past, the use of insoluble nano-carbons on plants led to physical damage to the plant cells due to biochemical incompatibility; at present, the availability of dispersible or soluble forms of several nano-carbons avoids unnecessary physical damage, which could be a possible solution to the continuous increase in the demand for food. These interactions provide a feasible approach that is backed by the long-known results from age-old practices related to the simple addition of charred bio-waste as a carbon source, known as "biochar," to the soil as a promoter of nutrients. The purposeful use of biochar significantly increases the rate of development of the next generation crop along with the retention of soil fertility. It is known that biochar contains a significant amount of nano-carbons along with micro carbon with oxo-functionality; these are hydrophilic and are readily passed through the plant roots. As such, the potential application of charred carbons/biochar in the growth of plant systems is a time-tested process, and the same can be expected with the nano-carbons. This perspective article provides a summary of the recent advances in the agricultural applications of nano-carbons. In particular, the cellular uptake, translocation, and accumulation of nano-carbons inside the plant, and their significant impacts on the plant physiological parameters are studied. Like plant growth, water uptake and protein expression properties, increasing crop productivity and disease prevention are correlated. The present perspective article also addresses the negative aspects that arise, based on a few reports showing the toxicity of nano-carbons; most of these are physical in nature and care is needed to determine the quality of the nano-carbons, which should be biocompatible.

[a] Department of Chemistry, Malaviya National Institute of Technology, Jaipur, Jaipur-302017, India. E-mail: sksonkar.chy@mnit.ac.in
[b] Department of Chemistry, Indian Institute of Technology, Kanpur, Kanpur-208016, India
[c] Department of Chemistry, Indian Institute of Engineering Science and Technology, Shibpur, Howrah-711103, India

Anshu Bhati received her BSc degree (2005) from Maharani Girls College, Bikaner, and MSc Degree in Chemistry (2007) from Dr Tanveer Malawat College of Biosciences, Bikaner, Rajasthan, India. She is currently a PhD student in the Chemistry department, Malaviya National Institute of Technology, Jaipur, Rajasthan, India. She has been doing her research work under the supervision of Dr Sumit Kumar Sonkar. Her research

Anshu Bhati

work is focused on the synthesis of doped fluorescent nano-carbons for multifunctional uses like imaging, and sunlight induced-photocatalysis for water treatment.

Gunture is a PhD student at the Malaviya National Institute of Technology Jaipur, India, working under the supervision of Dr Sumit Kumar Sonkar, in the Chemistry department, Malaviya National Institute of Technology. He received his BSc degree (2011) from Raj Rishi College, Alwar, India, and obtained his MSc degree (2014) from University of Rajasthan, India. His research interest is focused on the fabrication of carbon nano-onions for bio-imaging, sensing and energy applications.

Gunture

Sunlight-Induced Photocatalytic Degradation of Pollutant Dye by Highly Fluorescent Red-Emitting Mg-N-Embedded Carbon Dots

Anshu Bhati,[†] Satyesh Raj Anand,[†] Gunture,[†] Anjali Kumari Garg,[†] Prateek Khare,*[,†] and Sumit Kumar Sonkar*[,†] [ID]

[†]Department of Chemistry, Malaviya National Institute of Technology, Jaipur, Jaipur 302017, India

ABSTRACT: A straightforward and simpler use of an age-old technique was utilized for the fabrication of "red-emitting magnesium-nitrogen-embedded carbon dots" (r-Mg-N-CD) from the leaves extract of *Bougainvillea* plant as a natural source of carbon. This technique is similar to the solvent-based technique, which is used for the extraction of fragrances and essential oils from flowers and leaves. The as-derived leaves extract was further carbonized using a simple domestic microwave to obtain the small-sized red-emitting carbonaceous material as r-Mg-N-CD. The r-Mg-N-CD showed excitation-independent emissions at ∼678 nm with excellent photo-stability and a high quantum yield value (∼40%). Moreover, the important perspective of the present finding is to use this r-Mg-N-CD as a potential photocatalyst material for the degradation of pollutant dye (methylene blue) under the presence of sunlight. To infer the significant influence of using natural sunlight in the process of dye degradation, a comparative analysis was performed, demonstrating the higher rate of photodegradation (∼6 times faster) under the influence of sunlight compared to the artificial visible-light from a 100 W tungsten bulb.

KEYWORDS: Carbon dots, Red-emitting carbon dots, Quantum yield, Pollutant dye, Photodegradation, Methylene blue
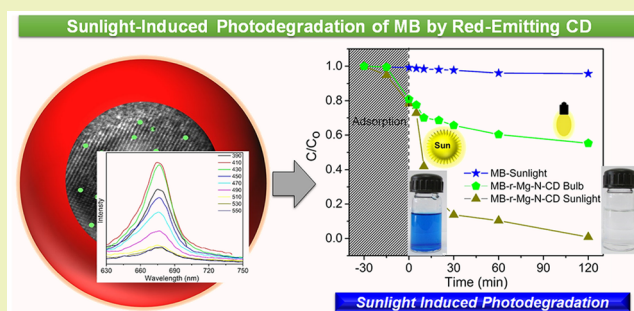
INTRODUCTION

Presently, advances to explore the nontoxic-biocompatible probes working in the long-wavelength region of the spectrum (red and near-infrared (NIR)) for the *in vivo* photoluminescent imaging have gained a lot of interest.[1] These probes are expected to enable safer in-depth imaging of cells, tissues, and organs. The red and the NIR regions constitutes the most suitable part of the spectrum that showed minimally intrusive absorption and self-fluorescence from the biological samples.[2,3] For this, significant efforts are already being taken for developing the highly fluorescent semiconductor quantum dots (QD) and organic dyes as a fluorescent probe for bioimaging applications.[4,5] However, the long-known biological constraint for the use of QD is its lower solubility and toxicity as well as the photobleaching effects associated with the fluorescent organic dyes, which certainly limit their long-term uses for biological applications.[6,7] Concerning the biocompat-ibility, photostability, and the high competitive quantum yield values of highly photoluminescent probes, carbon dots (CD)[8,9] and graphene quantum dots (GQD)[10,11] can be a better alternative. Since their discovery,[12,13] they have worked as an excellent alternative candidate[14,15] to the QD and organic dyes. They can be widely used and have a lower cost[16−19] (compared with QD/organic dyes). Additionally, the most important characteristic is its ease in surface functionalization, which imparts higher solubility-stability in aqueous media and tunable photoluminescence of CD,[15] which makes them a promising

material for multiple applications.[20−28] Nevertheless, being explored everywhere, including the few reports on its photocatalytic applications.[25,29−39] The tunable emissive profiles of CD and the other fluorescent nanocarbons are mostly limited between the blue and green regions. This emissive limit of blue and green CD makes them a limited probe for imaging in the lower wavelength region. The red and NIR emission of CD/GQD can be further explored on the basis of surface modifications and choosing a different carbon precursor.[40−44] A few groups have investigated the synthesis of red emitting CD/GQD, based on hydrothermal,[45−47] solvo-thermal,[48] and microwave[49−51] assisted methods using different synthetic precursor materials. These precursor materials have included o-phenyldiamine and phosphorous acid,[52] thiourea and citric acid,[53] lemon pulp,[46] mango leaves,[49] and they have been used these red-emitting CD/GQD for the multipurpose applications.[46−51,53−55] The most common observation noted for the emission in the higher-wavelength region in the published reports[40,45−49,51,53−57] was the influence of the incorporation/doping of heteroatoms.[48,51−54,57]

The present finding describes an easier approach for the fabrication of water-soluble "red-emitting magnesium-nitrogen-embedded carbon dots (r-Mg-N-CD)" from the leaves of a
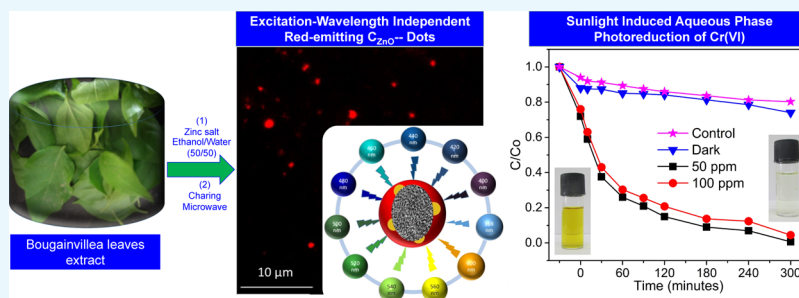
Brightly Fluorescent Zinc-Doped Red-Emitting Carbon Dots for the Sunlight-Induced Photoreduction of Cr(VI) to Cr(III)

Prateek Khare,[†] Anshu Bhati,[†] Satyesh Raj Anand, Gunture, and Sumit Kumar Sonkar*[ID]

Department of Chemistry, Malaviya National Institute of Technology, Jaipur, Jaipur 302017, India

ABSTRACT: The present finding deals with a simple and low-cost fabrication of surface-passivated, brightly fluorescent zinc-oxide-decorated, red-emitting excitation-independent ultrafluorescent CDs, denoted as "C_{ZnO}-Dots". Surface doping of zinc oxide significantly improved the quantum yield by up to ∼72%, and these brightly fluorescent red-emitting C_{ZnO}-Dots have been employed for the aqueous-phase photoreduction of 100 ppm hexavalent chromium(VI) to trivalent chromium(III) under the influence of sunlight irradiation. The overall utility of the prepared C_{ZnO}-Dots can be ascertained by their recyclability over seven cycles.

INTRODUCTION

Since their discovery, carbon-based fluorescent materials as carbon dots (CDs)[1] and graphene quantum dots (GQDs)[2] have been explored a lot because of their wide range in the applicative sustainability.[3−6] Their biocompatibility with higher values of quantum yield[7] has made CDs/GQDs significantly better candidates when compared with the long-known quantum dots (QDs), especially in the field of bioimaging applications.[4,8] However, at present, they are facing a few issues because of the emissive profiles situated in the narrower region of the visible spectrum (in between the blue and green regions).[4,5,8] A limited number of reports state that their emission lies in the higher wavelength region [red and near-infrared (NIR) regions].[9−13] The energy associated with the red and NIR regions of the spectrum is less, which can directly relate to them being lesser harmful to biological systems.[14,15] Work is already in progress for the fabrication of red-emitting CDs/GQDs with higher quantum yield via the hydro-thermal,[16,17] solvothermal,[11,18] and microwave[12,19,20] methods using different precursors such as carbon[9,11−13,16,18−21] and the heteroatoms[22] (as the dopant material) to achieve red-imaging.[12,16] Sun et al. report the synthesis of metal-doped green fluorescent ZnO and ZnS-doped/-decorated CD by the doping of zinc acetate on the surface of CD via hydrolysis by NaOH and precipitation with Na₂S, respectively.[23] Cheng et al. report the synthesis of yellow fluorescent C_{ZnO}-Dots via a one-step hydrothermal synthesis by mixing citric acid and zinc chloride in toluene and used them in bifunctional photonic crystal films, fluorescent microfibers, and patterns.[24] Xu et al. synthesized blue-light-emitting C_{ZnO}-Dots by mixing sodium citrate and zinc chloride via the hydrothermal method and used them as a biosensor.[25] ZnO/graphene quasi-core shell QDs were synthesized by Son et al., who used them in white-light-emitting diodes.[26] Apart from the above-mentioned applications, CD and doped CD are used in the field of sensing (gas,[27] heavy metals,[28−30] microbes,[31,32] etc.), optical displays,[33] tunable photoluminescence,[4,34] biocompatibility,[33] and competitive quantum yield values[7] and in the field of bioimaging (presently being explored in the red and NIR regions).[9−13] Based on their vast levels of applicative sustainability CDs/doped CDs can be expected to show their potential toward world's most serious concern, that is, contamination of water[35] which increases at a very high rate because of the increase in world population and industrialization. A huge amount of wastewater is discharged routinely which contains a large amount of heavy inorganic metal ions and organic compounds generally known as dyes that subsequently degraded the overall environmental and human health. Few reports are available for the photodegradation of the organic dyes by the waste derived nano-carbons.[36−39] The removal of heavy metals from wastewater has been carried out by different techniques.[40−44] Red-emitting CDs can be a significant material, simply because of their lower working levels of energy which can be used for the applications related to water treatment.

Under the influence of sunlight, the present work describes a new prospect of using red-emitting C_{ZnO}-Dots apart from their

Edited by
Chaudhery Mustansar Hussain and Ajay Kumar Mishra

Nanotechnology in Environmental Science

Volume 1 & 2

6

Nanocarbons in Agricultural Plants: Can be a Potential Nanofertilizer?

Anupriya Singh,[1] Anshu Bhati,[1] Gunture,[1]
Kumud Malika Tripathi,[2] and Sumit Kumar Sonkar[1]

[1]*Malaviya National Institute of Technology, Department of Chemistry, Jaipur, Rajasthan 302017, India*
[2]*Gachon University, Department of Bionanotechnology, Seongnam, Gyeonggi-do 13120, South Korea*

6.1 Introduction

At present, the need of opting for sustainable materials such as organic-based fertilizers is of great interest because of their better efficiencies [1–8] and biocompatibility [9–11], which makes them suitable for long-term use in agricultural sciences, compared to synthetic fertilizers [12–18]. The present situation demands [19–26] sustainable and newer techniques [2,27–32] that can be employed for increasing crop/plant productivity to meet the future challenges of global food crises. Owing to concerns about the toxicity issues and the long-term sustainable uses, switching from the synthetic fertilizers [12–18] to organic [33,34], carbon-based [28,35–41], and nanocarbon-based fertilizers [2,42–48] could be a worthy option. The increase in productivity [2,29,43] associated with growing food requirements using environment-friendly and simpler methods should be free from toxicity issues. We have been using synthetic fertilizers for decades to increase agricultural production [12–18], but they have brought on us adverse outcomes in the long run [16–18,49–53], such as destruction of valuable microorganisms [12,13,54] (responsible for conversion of plant and animal remains into nutrient-rich organic matter), water pollution [49], methemoglobinemia [49], soil contaminations [50], and so on, and significantly disturbing the natural constitution of soil [50–53]. Among all other types of organic fertilizers, charred carbon-based fertilizers deal with both the classical (additions of black carbon as biochar) and the modern techniques (applications of nanocarbons) used for increasing the crop productivity. This is very simple to understand based on the important and precise information taken from the long-known ancient practice in agricultural sciences, concerned with the deliberate additions of biochar [7,8,35–37] to the soil for increasing fertility [55–57], sequestration [56–58], restoration [59] of soil

Sunlight-Induced Selective Photocatalytic Degradation of Methylene Blue in Bacterial Culture by Pollutant Soot Derived Nontoxic Graphene Nanosheets

Prateek Khare,[†] Anupriya Singh,[†] Sankalp Verma,[‡] Anshu Bhati,[†] Amit Kumar Sonker,[‡] Kumud Malika Tripathi,*[§] and Sumit Kumar Sonkar*[†]

[†]Department of Chemistry, Malaviya National Institute of Technology, Jaipur, Jaipur 302017, India
[‡]Department of Materials Science & Engineering, Indian Institute of Technology, Kanpur, Kanpur 208016, India
[§]Department of Bio-nanotechnology, Gachon University, Gyeonggi-do, South Korea

S *Supporting Information*
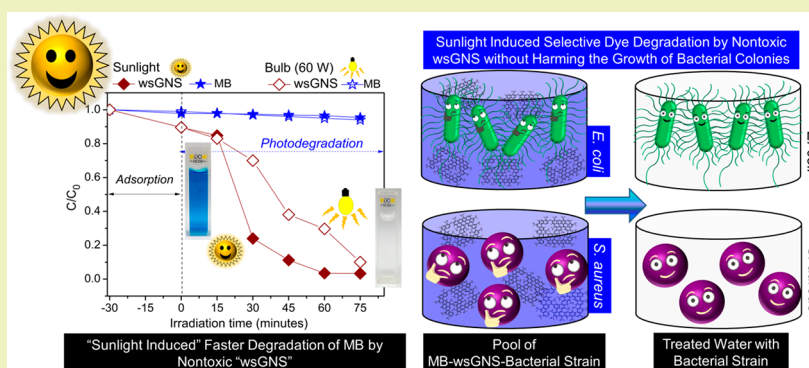
ABSTRACT: Herein, a potential approach is described for assessing the ecological importance of the graphitic nanocarbons isolated from dirty, dangerous black pollutant particulate material. A simple experiment of photodegradation and a toxicological test were done using the natural sunlight as a source of energy and the pollutant petrol soot derived water-soluble graphene nanosheets (wsGNS) as photocatalyst to achieve complete degradation of pollutant organic dye as methylene blue (MB). Compared to the artificial source of visible light (60W tungsten bulb), the sunlight-induced photodegradation using wsGNS show ~1.5 times higher rate of photodegradation. The toxicological test confirmed the nontoxic behavior of wsGNS against the two different types of bacterial strains: Gram-negative and Gram-positive cells, *Escherichia coli* and *Staphylococcus aureus*, respectively. Moreover, wsGNS are precisely used for the selective photodegradation of MB without harming the bacterial growth from the pool of MB-bacterial strains. Nontoxicity and selectivity along with the improved in photodegradation efficiencies by wsGNS under the influence of sunlight are the most significant and sustainable perspectives of the present finding.

KEYWORDS: *Pollutant soot, Toxic dye, Water-soluble graphene nanosheets, Methylene blue, Nontoxic, Selective photodegradation, Dye degradation*

INTRODUCTION

Advances in the field of light-induced photocatalysis,[1,2] particularly in aqueous-phase photocatalytic degradation[3,4] of various toxic and hazardous water-soluble organic pollutant dyes have shown tremendous development.[5,6] The prime focus for the aqueous-phase photodegradation of organic dyes is associated with their partial or complete degradation to relatively nontoxic constituents such as low molecular weight hydrocarbons that can ultimately end up to carbon dioxide and water.[7−10] Moreover, the use of sunlight as a freely available renewable light source under the natural conditions can offer an additional advantage for searching the newer sustainable alternatives of water remediation.[11,12] In the recent past years, the extent of the use of pollutant dyes like methylene blue (MB) in different industrial applications[13,14] followed by their

subsequent discharge as a waste in water stream is continuously increasing. Once released into the water bodies as contaminants, these were causing serious issues for both humans and the environment such as heart disease, lung and urinary bladder cancer, chromosomal fractures, mutagenesis, and respiratory toxicity in humans.[15−18] From the environmental perspective, organic dyes are well-known for their ability to significantly damage the aquatic biota of the water system.[19] So tremendous effort for the photodegradation of these pollutant dyes,[20] especially using metal-based nanomaterials, are gained a lot attention[21−23] because of their higher photodegradation

Pollutant Soot for Pollutant Dye Degradation: Soluble Graphene Nanosheets for Visible Light Induced Photodegradation of Methylene Blue

Anupriya Singh,[†] Prateek Khare,[†] Sankalp Verma,[‡] Anshu Bhati,[†] Amit Kumar Sonker,[‡] Kumud Malika Tripathi,*[,§] and Sumit Kumar Sonkar*[,†]

[†]Department of Chemistry, Malaviya National Institute of Technology Jaipur, Jaipur—302017, India

[‡]Department of Materials Science & Engineering and [§]Department of Chemistry, Indian Institute of Technology Kanpur, Kanpur—208016, India

S *Supporting Information*

ABSTRACT: The findings presented here offer a new approach for the environmental application of pollutant soot somewhat like utilizing a pollutant material for degrading the other pollutant material. Herein, a simpler approach is described for the isolation of two-dimensional graphitic materials as water-soluble graphene nanosheets (wsGNS) from the globally identified dirty—dangerous black pollutant particulate matter as black carbon (BC) from the petrol soot. The as-isolated wsGNS are further employed for the photocatalytic degradation of toxic dye such as methylene blue (MB) under the influence of visible light irradiation. The photodegradation performance of wsGNS compared to insoluble graphene nanosheets (GNS) showed ∼11 times faster degradation rate within ∼90 min of visible light exposure (60 W tungsten bulb). The insights of the aqueous phase photodegradation of MB by the system of MB-wsGNS were studied by different chemical characterization techniques including nuclear magnetic resonance spectroscopy, high-performance liquid chromatography, Raman, and fourier transform infrared spectroscopy. Furthermore, we have checked the regeneration efficiency of wsGNS, which was still at its higher value even after five cycles of recycling testing.

KEYWORDS: *Pollutant soot, Toxic dye, Water-soluble graphene nanosheets, Methylene Blue, Photodegradation, Dye degradation*
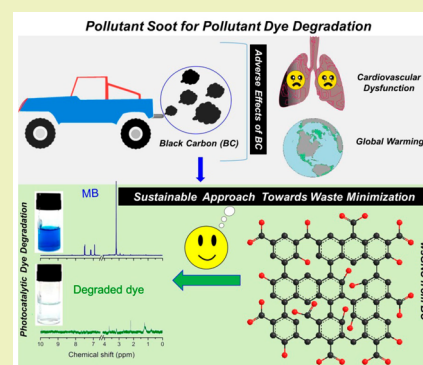
■ INTRODUCTION

The globally generated black particulate matter black carbon (BC) soot has, at present, shown dramatic negative impacts on human and environmental health. These include cancer,[1] dysfunctions of heart and lungs,[2] and mental retardation that are consequently responsible for the loss of millions of lives every year as well as significantly contributing toward global warming.[3] Similarly, like BC for air pollution, the contamination of water bodies arising from the discharge of water-soluble organic dyes[4] from various textiles and printing industries has also become a crucial environmental issue due to the fast growth in industrialization.[5] The considerable sources of nonaesthetic pollutants in water are potentially damaging the aquatic biota and life.[6] In reaction to the overall concern related to water pollution,[7] different techniques (adsorption, advanced oxidation process, flocculation, ultrafiltration, coagulation by chemical agents, etc.) have been employed in the past,[8] for the remediation of soluble toxic dyes.[9] From all the techniques, photocatalysis is very attractive and currently in high demand, since it provides a clean and cost-effective method for water purification. Additionally, visible light driven photocatalysis employs renewable and abundant energy to promote dye degradation under mild conditions. It can be a sustainable approach if we could utilize the nanocarbons derived from the pollutant BC[10−15] for the photocatalytic removal of organic dyes from wastewater via a single step that resolves two contaminant issues at the same time. The idea is very simple and purely based on the age-old practice of using carbon for water filtration because of its high adsorption efficiency.[16] The scientific insights about the conversion of pollutant soots into nanocarbons could open a new sustainable and potential window to mitigate climate change to some extent. Few groups have already been reported[11−15] the isolation (via the simplest processes from the bulk) of nanocarbons of different shapes from BC as carbon dots (CDs), single walled carbon nanotubes (SWCNT), and graphene nanosheets (GNS) for their multiple applications in the field of bioimaging,[11,15] sensing of heavy metal ions,[13] and sensing biomolecules.[11] Composition-wise (graphitic/amorphous structures) nanocarbons isolated from BC[11−15] and from other black charred carbonaceous materials[17−22] are similar to the nanocarbons fabricated from sophisticated instruments.[23−27]

Sustainable Feasibility of the Environmental Pollutant Soot to Few-Layer Photoluminescent Graphene Nanosheets for Multifunctional Applications

Kumud Malika Tripathi,[†] Anupriya Singh,[‡] Anshu Bhati,[‡] Sabyasachi Sarkar,[§] and Sumit Kumar Sonkar*,[‡]
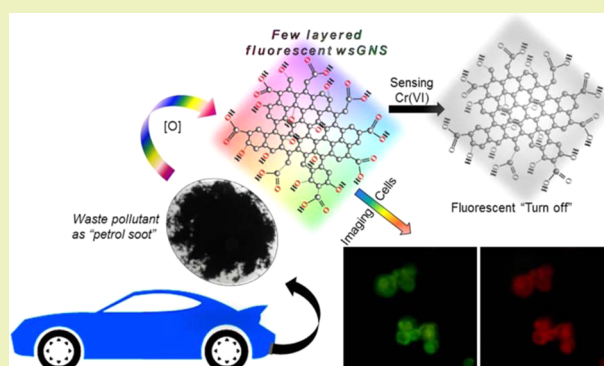
[†]Department of Chemistry, Indian Institute of Technology Kanpur, Kanpur 208016, India

[‡]Department of Chemistry, Malaviya National Institute of Technology, Jaipur, Jaipur 302017, India

[§]Department of Chemistry, Indian Institute of Engineering Science and Technology, Shibpur, Howrah 711103, India

S *Supporting Information*

ABSTRACT: A simple and realistic approach to the utilization of waste "black carbon particulates of petrol soot" for the fabrication of few-layer water-soluble photoluminescent graphene nanosheets (wsGNS) is described herein. Direct transformation of pollutant soot to fluorescent nanocarbons can be a promising approach for providing some economic benefits along with a clean atmosphere. Oxidation of petrol soot resulted in the isolation of the water-soluble version of graphene nanosheets (GNS). Oxidative treatment is a key step in preventing the aggregation of the GNS and rendering them water-soluble. A high degree of "self-passivation" on wsGNS provides evidence of the tunable photoluminescent emissions over a broad range of the visible spectrum with slight extension in the near-infrared region. The photoluminescent properties of wsGNS are used here for the selective detection of hexavalent chromium ions with a detection limit of 0.51 μM and for imaging HeLa cells.

KEYWORDS: *Pollutant soot, Water-soluble, Few-layer graphene nanosheets, Self-passivation, Photoluminescent, Chromium sensing*

1. INTRODUCTION

Globally generated black particulate matter, known as black carbon (BC), is recognized as a major air pollutant. Alternatively, this BC holds significant potential to be used as a free carbon precursor for the synthesis of valuable nanocarbons.[1−3] Considerable efforts and evidence of the role of air pollution caused by BC and its adverse impacts on the radiation budget of Earth have been documented.[4] To prevent its negative impacts, the quantity of BC should be decreased alternatively by its utilization in value-added products. To provide a clean environment along with some economic benefits, waste management of BC and identifying its second-life uses can be a possible approach to the synthesis of well-developed nanocarbons.[5−7] Recently, a few groups reported the presence of graphitic nanoparticles in the pollutant waste soot of diesel[5,6,8,9] and petrol engines,[7] along with the prospects of its application.[5,6,9] For example, Uchida et al. synthesized single-walled carbon nanotubes from diesel soot using a laser vaporization technique.[9] Tripathi et al. used diesel soot for the practical isolation of multiemissive water-soluble carbon dots (wsCD)[5] for multicolored imaging of *Escherichia coli* and sensing cholesterol. Wang et al. reported the synthesis of fluorescent water-soluble carbon nanoparticles (wsCNP)[6] for the selective sensing of Mn(II). Remarkably, Tripathi et al.[5] and Wang et al.[6] did not synthesize any nanocarbons. In contrast,

they synthesized only the soluble version of nanocarbons that was routinely manufactured during the burning process inside the engine chambers and discharged globally into the atmosphere as BC.[6,9,10] On the basis of these findings, we need to use these "freely available carbon precursors"[5−9] for the isolation of nanocarbons from pollutant soot. A few reports about the structural or nanostructural characterization of pollutant soot are also available.[7,11,12] The burning process in a diesel engine is very much similar to the burning of conventional hydrocarbon flames, whereas petrol engines typically need a "spark" for the ignition of fuel, which is premixed with atmospheric air.[7] Therefore, differences in morphologies of synthesized nanocarbons are expected.[5,6,8] Like diesel soot particulates, petrol soot particulates also cause environmental pollution,[10,13] but in comparison to diesel particulates, petrol soot particulates are a bit less harmful when they interact with the proteins of the cell membranes[10] but still cause several cardiopulmonary diseases.[14]

The findings presented in this paper are associated with the isolation of graphene nanosheets (GNS) from the petrol soot to provide some commercial and environmental benefits. GNS

Sustainable Changes in the Contents of Metallic Micronutrients in First Generation Gram Seeds Imposed by Carbon Nano-onions: Life Cycle Seed to Seed Study

Kumud Malika Tripathi,[†,‡] Anshu Bhati,[§,‡] Anupriya Singh,[§] Amit Kumar Sonker,[O] Sabyasachi Sarkar,[†,⊥] and Sumit Kumar Sonkar*[,§] [ID]
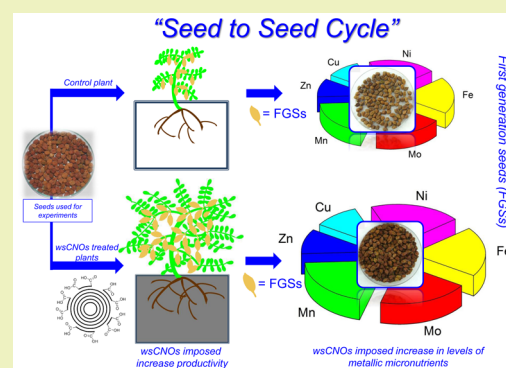
[†]Department of Chemistry and [O]Department of Materials Science & Engineering, Indian Institute of Technology, Kanpur, Kanpur—208016, India

[§]Department of Chemistry, Malaviya National Institute of Technology, Jaipur, Jaipur—302017, India

[⊥]Department of Chemistry, Indian Institute of Engineering Science and Technology, Shibpur, Howrah—711103, India

ABSTRACT: Plant−nanocarbon interactions have been mostly explored for enhanced germination, cell growth, and plant growth, with a limited study on the productivity of seeds under controlled conditions. The present finding reports the sustainable impacts of biowaste (wood wool) derived nanocarbons as carbon nano-onions (CNOs) on the entire life cycle of gram plants to obtain the first generation seeds (FGSs) as "seed to seed". A water-soluble version of CNOs as water-soluble carbon nano-onions (wsCNOs) at 0 (control), 10, 20, and 30 $\mu g\ mL^{-1}$ were used for the germination of gram seeds, for the initial 10 days only. Followed by transferring of 10 days old baby plants into the soil to complete their natural life cycle (∼4 months). FGSs harvested from the wsCNOs treated plants showed a significant increase in their yield and health with respect to their individual weight, overall dimensions, enhanced protein, stored electrolytes and metallic micronutrient contents. The protein content increased from 96 to 170 μg mL^{-1}, and the level of electrolytic conductivity increased from 2.2 to 3.4 mS in the FGSs, harvested from the plants treated with 0 (control) to 30 $\mu g\ mL^{-1}$ of wsCNOs, respectively. wsCNOs used here were presumably acting as a stimulant to increase the contents of metallic micronutrients (Mn, Mo, Cu, Zn, Fe, and Ni) in FGSs without showing its inside accumulations as a contaminant examined by transmission electron microscope (TEM) and Raman spectral analysis. In the future, a sustainable approach for the utilization of wood waste as a nanofertilizer could provide a possible approach in agricultural science to overcome the shortage of stored nutrients inside the seeds and also to limit the excessive use of fertilizers.

KEYWORDS: Waste wood wool, Water-soluble carbon nano-onions, First generation seeds, Micronutrients, Protein content, Conductivity, Enhanced productivity, Nanofertilizer

INTRODUCTION

Presently agricultural science need to adopt the sustainable strategies concerning the most serious global issue of continuously increasing food demand.[1,2] Related to boosting the crop productivity, along with preserving the nutritional values of food.[1,3−5] As a possible measure to increase the crop productivity, exploration of diverse nanoparticles as fertilizers/nanofertilizers in plants has increased in recent years.[6−11] To stimulate physiological and biochemical changes in plants. The long term and safer use of nanoparticles in agricultural science, requires the adaptation of sustainable strategies,[3,12] precisely related with improved productivity. That directly depends on the nutrition's provided to the plants and can help to resolve the problem of increased food demand.[7,13,14] To be prepared in advance, we need to explore and optimize the use of advanced organic based fertilizers like sustainable nanocarbons,[3,12,15−17] compared to synthetic chemical fertilizers. For increasing the productivity and nutrient contents in plants. Stimulating the

healthier makeup of micronutrients contents in plants in an environmentally friendly manner could hold great future promises. Because of the significant role of micronutrients in all the metabolic and cellular functions of plants.[18] Such as in plant growth, production of chlorophyll, synthesis of growth hormones, gene expressions, cell division, photosynthetic activities, root development, N_2 and CO_2 fixation, etc.[19,20] Deficiency of micronutrients in plant lead to retarded growth, deferred flowering, chlorosis of matured leaves, reduction in protein expressions, total protein synthesis, and, consequently, decrease in productivity.[19−22] However, the accumulation of nanoparticle/nanocarbons mainly in edible parts (seeds) of plants is a major concern and needs in-depth and detailed analysis.[23]

Research Article

Sunlight-Induced Photochemical Degradation of Methylene Blue by Water-Soluble Carbon Nanorods

Anshu Bhati,[1] Anupriya Singh,[1] Kumud Malika Tripathi,[2] and Sumit Kumar Sonkar[1]

[1]*Department of Chemistry, Malaviya National Institute of Technology Jaipur, Jawaharlal Nehru Marg, Jaipur 302017, India*
[2]*Department of Chemistry, Indian Institute of Technology Kanpur, Kanpur 208016, India*

Correspondence should be addressed to Kumud Malika Tripathi; kumud20010@gmail.com and
Sumit Kumar Sonkar; sksonkar.chy@mnit.ac.in

Water-soluble graphitic hollow carbon nanorods (wsCNRs) are exploited for their light-driven photochemical activities under outdoor sunlight. wsCNRs were synthesized by a simple pyrolysis method from castor seed oil, without using any metal catalyst or template. wsCNRs exhibited the light-induced photochemical degradation of methylene blue used as a model pollutant by the generation of singlet oxygen species. Herein, we described a possible degradation mechanism of methylene blue under the irradiation of visible photons via the singlet oxygen-superoxide anion pathway.

1. Introduction

Carbon nanorods (CNRs) [1, 2] are representing a unique class of one-dimensional carbon nanostructures, which may offer some advantageous properties in comparison with carbon nanotubes (CNTs) [3, 4] since CNRs offer straight, aligned, and hollow graphitic morphology [2]. CNRs are more or less similar to CNTs, except their straightness. Spaghetti type arrangements of CNTs restrict their many potential applications [5] that can be explored via the use of these CNRs. Till now, CNRs are the least explored in comparison with other members of nanocarbon family [3, 4, 6–17]. All these allotropic nanocarbons such as multiwalled CNTs [3]/ single-walled CNTs [4], fullerenes [6], carbon nanoonions [7–9], carbon nanodiamonds [10], graphene [11], graphene quantum dots [12], carbon dots [13–15], carbon nanofiber [16], and carbon nanocubes [17] have attracted a great concern in the diverse fields of science and technology because of their potential applications [5, 18–21]. Based on the few published reports, CNRs exhibited impressive electrical, thermal, and mechanical properties and are promising for field emission devices [22], energy storage devices [23], composite materials [24], and sensing applications [2]. The primary barrier for the successful commercialization of CNRs is its

typical synthetic procedures, such as chemical vapor deposition (CVD), arc discharge methods, solvothermal synthesis, electrodeposition, catalytic copyrolysis, and soft and hard template methods [2]. All these synthetic methods involve expensive instruments, metallic particles for growing the CNRs, high-temperature, multistep fabrication protocols, and sophisticated techniques that notably restrict their economic viability. A metal-catalyst-free synthesis of CNRs can be a significant approach.

Particularly for the biological application of CNRs [2], aqueous solubility is the most important parameter, which requires the surface modifications like chemical functionalization with electrophilic groups (oxygen-rich species) [25] and bioactive groups [26]. Tripathi et al. [2] described a new viable method for the catalyst-free synthesis of multicolored emissive wsCNRs from the pyrolysis of castor seed oil. The as-synthesized CNRs after Soxhlet purification were oxidized via simple oxidative method yielded photoluminescent water-soluble form as wsCNRs. The photoluminescent properties of wsCNRs were further utilized to construct a selective, specific, and active sensor for DNA sensing based upon fluorescent "turn-off/turn-on" technique [2]. The possible reasons for multicolored emissions from the single nanoparticle were attributed to the radiative recombination of photoinduced

CrossMark
click for updates

From the traditional way of pyrolysis to tunable photoluminescent water soluble carbon nano-onions for cell imaging and selective sensing of glucose†

Kumud Malika Tripathi,‡[a] Anshu Bhati,‡[b] Anupriya Singh,[b] Nidhi Rani Gupta,[c] Sankalp Verma,[d] Sabyasachi Sarkar*[e] and Sumit Kumar Sonkar*[b]

The traditional pyrolysis of vegetable ghee leads to the fabrication of graphitic photoluminescent, water soluble carbon nano-onions (wsCNO) with tunable photoluminescence without using any metal catalyst. Simple oxidative treatment by nitric acid fabricated a high density "self-passivated" water soluble version. As-synthesized wsCNO possessed tunable photoluminescence behavior from the visible-to-near infrared region. Further small sized wsCNO separated from the bulk as-synthesized wsCNO *via* gel filtration achieved a highly fluorescent colored fraction, used for cell imaging (*Escherichia coli* and *Pseudomonas putida*) and selective, immediate sensing of glucose molecules based upon a simple fluorescence "turn-off"/"turn-on" technique.

1. Introduction

Nano-sized fluorescent nanocrystals, generally referred as quantum dots (QDs), have attracted a lot of interest for imaging, especially in the biomedical sciences.[1,2] However, being metallic in nature their toxicity significantly challenges the excellent optical advantageous performances.[3–5] Tremendous efforts have been made to find a non-toxic alternative of QD-type photoluminescent probe with comparable optical properties. The outcome of these significant efforts has resulted in the discovery of a new class of fluorescent nano-carbons (FNCs),[6–12] referred as a non-toxic fluorescent probe, having optical properties comparable with QDs. FNCs predominantly consist of carbon dots (CD),[6,13,14] carbon nano-diamonds,[7] graphene quantum dots,[8,9,15] carbon nano rods[16,17] and carbon nano-onions (CNO).[10–12,18] Among all of these, the CD have been studied the most[6,14,19–24] as a fluorescent probe for non-toxic biological imaging purposes, whereas CNO have been

investigated least.[10,11,25–27] Because of the presence of a well-defined band gap, QDs shows quantum confinement effects as a result of which, its size dependent electronic and optical properties can easily be tuned. However, FNCs do not have any theoretically defined band gap based fluorescence color related size distributions of nanoparticles. Because of this, these are different from QDs and have the advantageous, significant properties of tunable photoluminescence from the single particle[10,11,28,29] together with high solubility, stability, and non-toxicity. Among the FNCs, CNO is an emerging class of quasi-spherical nano carbon, which typically consists of successive layer of graphene around a filled or hollow core and they offer a high aspect ratio and conductivity.[30] Morphologically, graphitic structures of CNO are in between fullerene and graphitic nanotubes having closed graphitic shells which are placed on one on another.[11,31,32] So far, less attention have been given to CNO even though the prospective applications have already discussed. CNO exhibited the characteristic, onion-like morphology and small domains of graphitic sp^2 carbons with localization of the π electrons and dangling bond defects in the periphery.[30] As a consequence, it could be envisioned as an enclosed graphitic shell with excellent optical and electro-chemical properties that render them a potential nanomaterial for industrial, biomedical and electronic applications.[33–36] From the time of their discovery[12] until the present date, only a limited number of synthetic methods for CNO have been available and it can be synthesized mainly by using high energy techniques. Such as the arc-discharge method, in which two graphite electrodes are arced under water for the synthesis of CNO on the water surface.[32] Annealing of nano-diamond for

[a]*Department of Chemistry, Indian Institute of Technology Kanpur, Kanpur-208016, India*

[b]*Department of Chemistry, Malaviya National Institute of Technology, Jaipur-302017, India. E-mail: sumitsonkar@gmail.com; Tel: +91-9415594017*

[c]*Department of Chemistry, GSSDGS Khalsa College, Patiala-147001, India*

[d]*Department of Materials Science & Engineering, Indian Institute of Technology Kanpur, Kanpur-208016, India*

[e]*Department of Chemistry, Indian Institute of Engineering Science and Technology, Shibpur, Howrah-711103, India. E-mail: abya@iitk.ac.in*

† Electronic supplementary information (ESI) available. See DOI: 10.1039/c6ra04030f

‡ Both the authors contributed equally.

A simple one-step hydrothermal route towards water solubilization of carbon quantum dots from soya-nuggets for imaging applications

Prashant Dubey,*[a] Kumud Malika Tripathi,[b] Ragini Mishra,[a] Anshu Bhati,[c] Anupriya Singh[c] and Sumit Kumar Sonkar*[c]

A simple and low-cost pyrolytic carbonization method has been performed for the easy synthesis of carbon quantum dots from soya-nuggets under an insufficient amount of oxygen. Furthermore, hydrothermal functionalization of the carbonized black material after Soxhlet purification with nitric acid leads to the formation of its quantum sized water soluble version. The hydrothermally functionalized, water soluble carbon quantum dots (wsCQDs) are highly fluorescent and self-passivated, having a quantum yield value of ~3%, with a small range of size distribution. High photostability with high solubility makes these potential candidates for imaging purposes, and we used these for the fluorescent labeling of *Escherichia coli* cells.

Introduction

In the past few years, fluorescent nano-carbons (FNCs),[1–9] comprising carbon dots (CDs),[1–4] carbon nano-diamonds (CNDs),[5] carbon nano-onions (CNOs),[6,7] and graphene quantum dots (GQDs),[8,9] have drawn immense interest, particularly for biological cell imaging[3,4,10–12] with several benefits in comparison with conventional metal-based quantum dots (QDs).[13–15] In terms of bio-compatibility (non-toxic nature),[4,12,16,17] their high values of quantum yield,[4,12,18] combined with their excellent solubility and stability,[1,3,4] make these QDs an effective fluorescent probe for long-term use for biological purposes.[3,4] FNCs are mostly composed of spherical nano-carbon possessing a high surface area to volume ratio, and have further been utilized for surface passivation purposes *via* simple surface modification (attaching surface functionalities). Surface modification is mainly achieved *via* the simple organic chemistry of oxidation, followed by the addition of polymeric[2,10] and monomeric amines[19] to achieve high quantum yield values[4,12,18] comparable with those of conventional metal-based QDs.[13–15] Metal-based QDs show classical quantum confinement effects[1] in their size-dependent multi-colored emission. Theoretically, in comparison with QDs, FNCs do not have any defined band gap for fluorescence emission,[19] and this is an advantageous property for multi-colored emission from the same nano-carbon.[20–22]

Among the FNCs, CDs are widely used fluorescent nano-carbons because of their simpler synthetic methodologies with easy reproducibility. It has been widely accepted that the presence of high density surfacial defects (defective centers) on FNCs is responsible for their tunable multi-colored emission profiles.[12] Emission from the defective centers of surfacial defects was first noticed from the surfacial defects of single-walled and multi-walled carbon nanotubes passivated with polymeric amines.[23,24] Since the first report of CDs from laser ablation of a graphitic target,[1] many more top-down[10–12,25–32] and bottom-up[33–40] synthetic techniques have been explored for their easy production. Along with exciting sophisticated techniques, such as arc-discharge,[41] abundant progress has been reported in the past few years for the cost-effective green synthesis of photoluminescent CDs by using bio-mass/waste bio-mass as a low-cost, compatible and easily available carbon precursor material, including ascorbic acid,[42] banana juice,[43] candle soot,[35] chicken eggs,[44] citrate,[45] chitosan,[46] diesel soot,[47] gelatin,[48] glucosamine,[49] saccharides,[50] juices (orange, sugar cane, and strawberry),[51–53] pomelo,[54] and watermelon peel.[55] Because of their simplicity and straightforward synthesis, most of the synthetic approaches involve either hydrothermal or microwave-assisted green methods. As synthesized, CDs and their functionalized versions have shown immense potential for a wide variety of applications, such as bio-imaging agents,[12,56] biosensors,[47,57] chemical sensors,[58] drug delivery,[59] electro-catalysts,[60] photo-catalysts,[61] and photodynamic therapy.[62] Low-cost synthetic protocols with easy reproducibility and bio-compatibility make these CDs best suited for imaging purposes.[3,12,62,63]

[a] Centre of Material Sciences, Institute of Interdisciplinary Studies (IIDS), University of Allahabad, Allahabad, 211002, India. E-mail: pdubey.au@gmail.com

[b] Laboratory of Materials Engineering of Brittany (LIMATB), University of South Brittany (UBS), 56321 Lorient Cedex, France

[c] Department of Chemistry, Malaviya National Institute of Technology (MNIT), Jaipur, 302016, India. E-mail: sksonkar.chy@mnit.ac.in

PAPER

Large-scale synthesis of soluble graphitic hollow carbon nanorods with tunable photoluminescence for the selective fluorescent detection of DNA†

Kumud Malika Tripathi,[a] Amit Kumar Sonker,[b] Anshu Bhati,[c] Jagannath Bhuyan,[a] Anupriya Singh,[c] Ajay Singh,[a] Sabyasachi Sarkar*[d] and Sumit Kumar Sonkar*[c]

Photoluminescent water-soluble hollow carbon nanorods were synthesized by the pyrolysis of castor oil seeds (*Ricinus communis*) without the use of a catalyst. Oxidation of the pyrolysed soot produced a water-soluble form of graphitic hollow carbon nanorods. These showed excitation-dependent multicoloured photoluminescent emission from the green to red region of the visible spectrum and extending to the near-infrared region. This photoluminescent behaviour was used to produce a fluorescent turn-off/turn-on sensor for the specific, sensitive and rapid determination of DNA with a detection limit of ~1.14 nM.

Introduction

Many different types of nanocarbon have been reported in recent years, such as fullerenes,[1] multiwalled carbon nanotubes,[2] single-walled carbon nanotubes,[3] carbon nano-onions,[4] carbon nanorods (CNRs),[5] carbon nanofibres,[6] graphene,[7] carbon nanodiamonds,[8] and the recently discovered photoluminescent carbon dots (CDs)[9,10] and graphene quantum dots.[11] These have attracted much interest as a result of their diverse applications.[11–25] Morphologically, CNRs are similar to 1D, multiwalled carbon nanotubes except they show less bundling and aggregation as a result of their linear shape and aligned graphitic inter-planar structure.[26–31] However, CNRs have not been studied very much because of the lack of a simple and reproducible method for synthesis. CNRs have potential applications in various field such as lithium ion batteries,[32] supercapacitors,[33] electrochemical applications[34,35] and in biologically important reactions like the electrocatalytic oxidation of NADH, uric acid[36] and dopamine.[37] Conventional synthetic procedures such as arc discharge,[38] chemical vapour deposition,[39–42] solvothermal methods,[32,43] template-assisted synthesis,[33,34,44,45] electrodeposition[46] and catalytic co-pyrolysis[47] have been used to obtain CNRs. Li *et al.*[38b] synthesized CNRs in an arc discharge experiment using an anode made from fullerene soot and iron particles. Wang *et al.*[39] fabricated plasma-enhanced CNRs with Au nanoparticles as a catalyst using hot filament chemical vapour deposition. Thién-Nga *et al.*[40] used BSYCO (Bi, Sr, Y, Cu, O) as a substrate for the synthesis of CNRs by chemical vapour deposition. Wang *et al.*[43] synthesized CNRs at low temperatures using tetrachloroethylene and potassium to obtain a C_2 infrastructure. An Ag catalyst has been used to synthesize CNRs *via* calcination.[43] Li *et al.*[44] synthesized CNRs using a soft template (a tri-block polymer) and phenolic resin by the combination of a hydrothermal method and annealing. Yu *et al.*[33] and Orikasa *et al.*[34] synthesized template-assisted CNRs using an Ni–hydrazine complex and aluminium substrate, respectively. Zou *et al.*[47] fabricated CNRs *via* pyrolysis using C_6H_6 and C_5H_6 with Fe and Mg catalysts in an autoclave. All these synthetic approaches required multi-step fabrication protocols, expensive instruments, high-temperature synthetic conditions, toxic chemicals, metallic particles and sophisticated techniques that restricted their economic viability. In contrast, the method reported here is an economically viable and catalyst-free process for the synthesis of CNRs in an almost quantitative yield.

We report the simple synthesis of CNRs at low cost without the use of a template or catalyst by the pyrolysis of castor seeds oil (*Ricinus communis*) used as a green carbon precursor. The method could be used on a large scale. Castor oil is composed ~87% fatty acid (ricinoleic acid) and is extensively used in medicine as an antiviral, antibacterial, antifungal and analgesic agent; it is also used in cosmetics.[48,49] The soot generated by burning castor oil in lamps was cleaned to remove any unburnt and volatile impurities. A simple nitric acid treatment of the

[a] *Department of Chemistry, Indian Institute of Technology Kanpur, Kanpur-208016, India*

[b] *Department of Materials Science & Engineering, Indian Institute of Technology Kanpur, Kanpur-208016, India*

[c] *Department of Chemistry, Malaviya National Institute of Technology, Jaipur, Jaipur-302017, India. E-mail: sksonkar.chy@mnit.ac.in*

[d] *Department of Chemistry, Indian Institute of Engineering Science and Technology, Shibpur, Howrah-711103, India. E-mail: abya@iitk.ac.in*

† Electronic supplementary information (ESI) available. See DOI: 10.1039/c5nj02037a

Curriculum VItae

CURRICULUM VITAE

Personal Information:

Name	:	Anshu Bhati
Date of Birth	:	26th July 1985
Sex	:	Female
Marital Status	:	Married
Nationality	:	Indian
Mobile No	:	+91-7877468980
Email	:	anshu.panwar.1985@gmail.com

Educational Qualifications:

Examination	Year	Percentage/ CGPA	Board/University
B.Sc.	2005	69%	Maharaja Ganga Singh University, Bikaner
M.Sc. -Chemistry	2007	66%	Maharaja Ganga Singh University, Bikaner
Ph.D.	2018	8.24 CGPA	Malaviya National Institute of Technology, Jaipur, Rajasthan

Professional Skill and Research Interest:

1. Synthesis, doping and characterization of carbon nanodots and carbon nano-onions through greener route and their wet applications.

2. Sensing of bio-molecules such as DNA, amino acids, glucose and cholesterol with fluorescence technique by carbon nano materials.

3. Synthesis and characterization of waste derived nano-carbons for visible light induced photocatalysis of pollutant dyes and reduction of toxic metal ions.

Working Hand:

1. SEM, TEM, HRTEM, AFM,

2. XRD, RAMAN, NMR, UV–Vis, FT-IR, TGA, AAS, XPS

3. Fluorescence spectroscopy, Cyclic Voltammetry

Research Paper Published:

1. **Bhati, A.;** Anand, S.R.;Saini, D.;Khare, P.; Sonkar, S.K. Sunlight-Facilaited Photoreduction of Cr(VI) to Cr(III) by Fluorescent Nitrogen Phosphorus Doped Carbon Dots. npj Clean Water, Nature. DOI/10.1038/s41545-019-0036-z

2. Anand, S. R.**; Bhati, A.**; Saini, D.; Gunture; Chauhan, N.; Khare, P.; Sonkar, S. K., Antibacterial Nitrogen-doped Carbon Dots as a Reversible

"Fluorescent Nanoswitch" and Fluorescent Ink. *ACS Omega* 2019, *4* (1), 1581-1591.

3. Gunture; Singh, A.; **Bhati, A.;** Khare, P.; Tripathi, K. M.; Sonkar, S.K. Soluble Graphene Nanosheets for the Sunlight-Induced Photodegradation of the Mixture of Dyes and its Environmental Assessment. Sci. Rep., 2019, 9 (1), 2522..

4. **Bhati, A.;** Gunture; Tripathi, K. M.; Singh, A; Sarkar, S.; Sonkar, S. K., Exploration of Nano-carbons to Plant Science. New J. Chem. 2018, 42, 16411-16427.

5. **Bhati, A**.; Anand, S. R.; Saini, D.; Khare, P.; Dubey, P.; Sonkar, S. K., Self-doped nontoxic red-emitting Mg–N-embedded carbon dots for imaging, Cu(II) sensing and fluorescent ink. New J Chem 2018, 42 (24), 19548-19556**.**

6. **Bhati, A**.; Anand, S. R.; Gunture; Garg, A. K.; Khare, P.; Sonkar, S. K., Sunlight-Induced Photocatalytic Degradation of Pollutant Dye by Highly Fluorescent Red-Emitting Mg-N-Embedded Carbon Dots. *ACS Sustainable Chem. Eng.,* 2018, *6* (7), 9246–9256

7. Khare, P.;[†] **Bhati, A.;**[†] Anand, S. R.; Gunture; Sonkar, S. K., Brightly Fluorescent Zinc-Doped Red-Emitting Carbon Dots for the Sunlight-Induced Photoreduction of Cr(VI) to Cr(III). *ACS Omega* 2018, *3* (5), 5187-5194. (†= Equal contribution)

8. Khare, P.; Singh, A.; Verma, S.; **Bhati, A.;** Sonker, A. K.; Tripathi, K. M.; Sonkar, S. K., Sunlight-Induced Selective Photocatalytic Degradation of Methylene Blue in Bacterial Culture by Pollutant Soot Derived Nontoxic Graphene Nanosheets. *ACS Sustainable Chem. Eng.*, 2018, *6*, 579–589.

9. Singh, A.; Khare, P.; Verma, S.; Bhati, A.; Sonker, A. K.; Tripathi, K. M.; Sonkar, S. K. Pollutant Soot for Pollutant Dye Degradation: Soluble Graphene Nanosheets for Visible Light Induced Photodegradation of Methylene Blue. *ACS Sustainable Chem. Eng.*, 2017, 5, 8860−8869.

10. Tripathi, K. M.;[†] Bhati, A.;[†] Singh, A.; Sonker, A. K. Sarkar, S.; Sonkar, S. K. Sustainable Changes in the Contents of Metallic Micronutrients in First Generation Gram Seeds Imposed By Carbon Nano-Onions: Life Cycle Seed To Seed Study. *ACS Sustainable Chem. Eng.* 2017, 5, 2906-2916. (†= Equal contribution)

11. Tripathi, K. M.; Singh, A.; Bhati, A.; Sarkar, S.; Sonkar, S. K. Sustainable Feasibility Of The Environmental Pollutant Soot To Few-Layer Photoluminescent Graphene Nanosheets For Multifunctional Applications. *ACS Sustainable Chem. Eng.*, 2016, 4, 6399−6408.

12. Bhati, A.; Singh, A.; Tripathi, K. M.; Sonkar, S. K. Sunlight- Induced Photochemical Degradation of Methylene Blue by Water- Soluble Carbon Nanorods. *Int. J. Photoenergy*, 2016, 2016, 2583821.

13. Tripathi, K. M.; Sonker, A. K.; Bhati, A.; Bhuyan, J.; Singh, A.; Singh, A.; Sarkar, S.; Sonkar, S. K. Large-Scale Synthesis of Soluble Graphitic Hollow

Carbon Nanorods with Tunable Photoluminescence for the Selective Fluorescent Detection of DNA. *New J. Chem.*, 2016, 40, 1571-1579.

14. Tripathi, K. M.; [†] Bhati, A.; [†] Singh, A.; Gupta, N. R.; Sarkar, S.; Sonkar, S. K. From The Traditional Way of Pyrolysis to Tunable Photoluminescent Water Soluble Carbon Nano-Onions for Cell Imaging and Selective Sensing of Glucose, *RSC Adv.*, 2016, 6, 37319-37329. (†= Equal contribution)

15. Dubey, P.; Tripathi, K. M.; Mishra, R.; Bhati, A.; Singh, A.; Sonkar, S. K. A Simple One-step Hydrothermal Route towards Water Solubilization of Carbon Quantum Dots from Soya-nuggets for Imaging Applications, *RSC Adv.*, 2015, 5, 87528–87534.

16. Singh, A.; Bhati, A.; Gunture, Tripathi, K. M.; Sonkar, S. K. Nano-carbons in Agricultural Plants: Can be a Potential Nano-Fertilizer? By Wiley-VCH Verlag GmbH & Co. KGaA. 2018.

Conferences, Seminar and Short-term course:

1. Participated in National Seminar on "Recent Trends & Advances in Chemical Science and their Impact on Environment" (RTACIE-2018) organized by department of chemistry, Amity University, Jaipur on 13th April 2018.

2. Five days short term course on "Nano Forms of Carbon" organized by Materials Research Centre, MNIT, Jaipur from 19th March-23rd March 2018.

3. Attended and participated in poster presentation in two days international conference on Condensed Matter & Applied Physics at Engineering College Bikaner, from 30th- 31st October 2015.

4. Attended and participated in poster presentation in three days "National Conference on Advanced Materials and Processing (CAMP-2015)" from 2nd- 4th December 2015 organized by physics, chemistry and metallurgy department, MNIT, Jaipur.

5. Attended and participated in poster presentation in three days National conference on "Recent Advancement in Chemical Sciences (RAICS-2015)" from 21st- 23rd August 2015 organized by department of chemistry, MNIT Jaipur and got the Best Poster Award.

6. Attended and participated in poster presentation in three days "National conference on Frontiers at the Chemistry – Allied Sciences Interface (FCASI-2015)" at Rajasthan University, Jaipur from 10th -12th March 2015.

I at this moment declare that the information given above is true to the best of my knowledge and belief.

Sincerely,

Anshu Bhati